BEILSTEIN JOURNAL OF ORGANIC CHEMISTRY

Antibacterials, bacterial small molecule interactions and quorum sensing

Edited by David R. Spring

Imprint

Beilstein Journal of Organic Chemistry
www.bjoc.org
ISSN 1860-5397
Email: journals-support@beilstein-institut.de

The *Beilstein Journal of Organic Chemistry* is published by the Beilstein-Institut zur Förderung der Chemischen Wissenschaften.

Beilstein-Institut zur Förderung der Chemischen Wissenschaften
Trakehner Straße 7–9
60487 Frankfurt am Main
Germany
www.beilstein-institut.de

BEILSTEIN JOURNAL OF ORGANIC CHEMISTRY

Natural and redesigned wasp venom peptides with selective antitumoral activity

Marcelo D. T. Torres[1,2], Gislaine P. Andrade[1], Roseli H. Sato[1], Cibele N. Pedron[1], Tania M. Manieri[1], Giselle Cerchiaro[1], Anderson O. Ribeiro[1], Cesar de la Fuente-Nunez[*2] and Vani X. Oliveira Jr.[*1]

Full Research Paper

Open Access

Address:
[1]Centro de Ciências Naturais e Humanas, Universidade Federal do ABC, Santo André, 09210580, SP, Brazil and [2]Synthetic Biology Group, MIT Synthetic Biology Center, Research Laboratory of Electronics, Department of Biological Engineering, and Department of Electrical Engineering and Computer Science, Massachusetts Institute of Technology; Broad Institute of MIT and Harvard, The Center for Microbiome Informatics and Therapeutics, Cambridge, 02139, MA, United States of America

Email:
Cesar de la Fuente-Nunez[*] - cfuente@mit.edu; Vani X. Oliveira Jr.[*] - vani.junior@ufabc.edu.br

* Corresponding author

Keywords:
breast cancer; decoralin; MCF-7 cells; peptide design; selective anticancer peptides; structure–activity relationships

Beilstein J. Org. Chem. **2018,** *14,* 1693–1703.
doi:10.3762/bjoc.14.144

Received: 08 March 2018
Accepted: 13 June 2018
Published: 06 July 2018

This article is part of the thematic issue "Antibacterials, bacterial small molecule interactions and quorum sensing".

Guest Editor: D. Spring

Abstract

About 1 in 8 U.S. women (≈12%) will develop invasive breast cancer over the course of their lifetime. Surgery, chemotherapy, radiotherapy, and hormone manipulation constitute the major treatment options for breast cancer. Here, we show that both a natural antimicrobial peptide (AMP) derived from wasp venom (decoralin, Dec-NH_2), and its synthetic variants generated via peptide design, display potent activity against cancer cells. We tested the derivatives at increasing doses and observed anticancer activity at concentrations as low as 12.5 μmol L^{-1} for the selective targeting of MCF-7 breast cancer cells. Flow cytometry assays further revealed that treatment with wild-type (WT) peptide Dec-NH_2 led to necrosis of MCF-7 cells. Additional atomic force microscopy (AFM) measurements indicated that the roughness of cancer cell membranes increased significantly when treated with lead peptides compared to controls. Biophysical features such as helicity, hydrophobicity, and net positive charge were identified to play an important role in the anticancer activity of the peptides. Indeed, abrupt changes in peptide hydrophobicity and conformational propensity led to peptide inactivation, whereas increasing the net positive charge of peptides enhanced their activity. We present peptide templates with selective activity towards breast cancer cells that leave normal cells unaffected. These templates represent excellent scaffolds for the design of selective anticancer peptide therapeutics.

Introduction

Approximately 12% of U.S. women develop breast cancer according to the U.S. Breast Cancer website (http://www.breastcancer.org/symptoms/understand_bc/statistics). The current treatment approaches, which include surgery, chemotherapy, radiotherapy, and hormone manipulation, are highly invasive and present numerous deleterious side effects. Therefore, alternative anticancer therapies are needed both to destroy cancer cells and to avoid toxicity towards normal host cells.

Antimicrobial peptides (AMPs) are produced by the innate immune system of virtually every organism on Earth. These agents represent promising anticancer candidates since, in addition to their activity vs bacteria [1], viruses, parasites [2-8], and fungi [1,9,10], they can kill cancer cells [11]. So far, >2,500 AMPs have been described in the literature and only ≈10% of those are known to exhibit anticancer activity, according to the Antimicrobial Peptide Database (http://aps.unmc.edu/AP/main.php). In total, there are around 600 anticancer/antitumoral peptides according to the Database of Anticancer Peptides and Proteins (http://crdd.osdd.net/raghava/cancerppd/). Those AMPs with anticancer activity have been termed anticancer peptides (ACPs). Since their initial discovery, ACPs have constituted a promising alternative to conventional chemotherapy [11,12]. ACPs are promising anticancer compounds as they offer advantages such as higher specificity and lower incidence of acquired resistance in comparison to existing therapies [12-14].

ACPs derive from various sources and consequently share low homology [15-18]. These peptides have similar characteristics such as a positive charge, amphipathic structure, defined secondary structures in hydrophobic environments, and rapid anticancer activity [12,19]. Helical structures are the most common structural motifs of ACPs. Their stable amphipathic structures tend to be key for their anticancer activity, as they enable membrane binding [20]. Their anticancer activity typically occurs at micromolar concentrations [21] and is not usually accompanied by hemolytic activity probably because there are structural differences between the membranes of red blood cells and cancer cells, which are zwitterionic and negatively charged, respectively. Structure–activity relationship studies have identified amphiphilicity and polar angle as the most important physicochemical properties required for ACPs to invade cancer cells or disturb their membranes [22,23].

In 2007, Konno et al. described decoralin (Dec-Ser-Leu-Leu-Ser-Leu-Ile-Arg-Lys-Leu-Ile-Thr), an α-helical AMP from *Oreumenes decoratus* wasp venom [24]. In addition, the authors described its amidated analog (Dec-NH_2), which displayed higher activity than its parent molecule against Gram-positive bacteria, Gram-negative bacteria, fungi, and protozoa. However, both peptides presented high hemolytic activity, which limited their use as potential therapies.

Torres et al. synthesized Dec-NH_2 analogs with single and double substitutions, which exhibited increased resistance to degradation and lower hemolytic activity [9,10]. The two Dec-NH_2 analogs designed to fit a leucine zipper (LZ) template [25,26] presented the lowest hemolytic activity against red blood cells and maintained the antimicrobial activity of the parent template molecule vs Gram-positive bacteria, Gram-negative bacteria, and fungi. The authors attributed these activities to the helical propensity of the designer peptides [9]. Another study further reengineered Dec-NH_2 to generate seven analogs containing single or double substitutions [10]. These derivatives were designed to preserve specific physicochemical features, such as net positive charge, hydrophobicity, and amphipathicity, which are known to be important for interacting with membranes, exerting bioactivity against microorganisms and cancer cells, and suppressing unwanted hemolytic activity [10].

Since the aforementioned peptides were designed to target negatively charged bacterial membranes, we reasoned that their activity would translate to cancer cells, whose membranes also possess a net negative charge. We hypothesized that their conformational tendency and physicochemical properties would enable interactions with tumor cell membranes, leading to subsequent death. In the present study, we investigated Dec-NH_2, its LZ template and single/double substituted derivatives for their ability to selectively kill MCF-7 breast cancer cells.

Results and Discussion

Peptide design, chemical synthesis, purification and physicochemical analyses

Dec-NH_2 is a cationic α-helical antimicrobial and antiparasitic peptide [9,10,24] that is rich in Leu residues. We took into account these characteristics and designed two of the analogs proposed here using to a leucine zipper template, on which Leu residues were present in both ‘a’ and ‘d’ positions of the heptad sequence. This template design favors helical stabilization via Leu-side chain interactions [25,27] (Figure 1 – $[Leu]^8$-Dec-NH_2 and $[Leu]^{10}$-Dec-NH_2). The remaining Dec-NH_2 derivatives were engineered by rationally introducing single and double substitution mutations (Figure 1). To introduce a net positive charge into the peptide sequences [28], we used Lys rather than Arg due to its superior flexibility, lower propensity in potentially toxic cell-penetrating peptides [29], and decreased hydrophobic side chain, which is associated with cytotoxicity [30]. Moreover, Lys residues are more frequent than Arg residues in

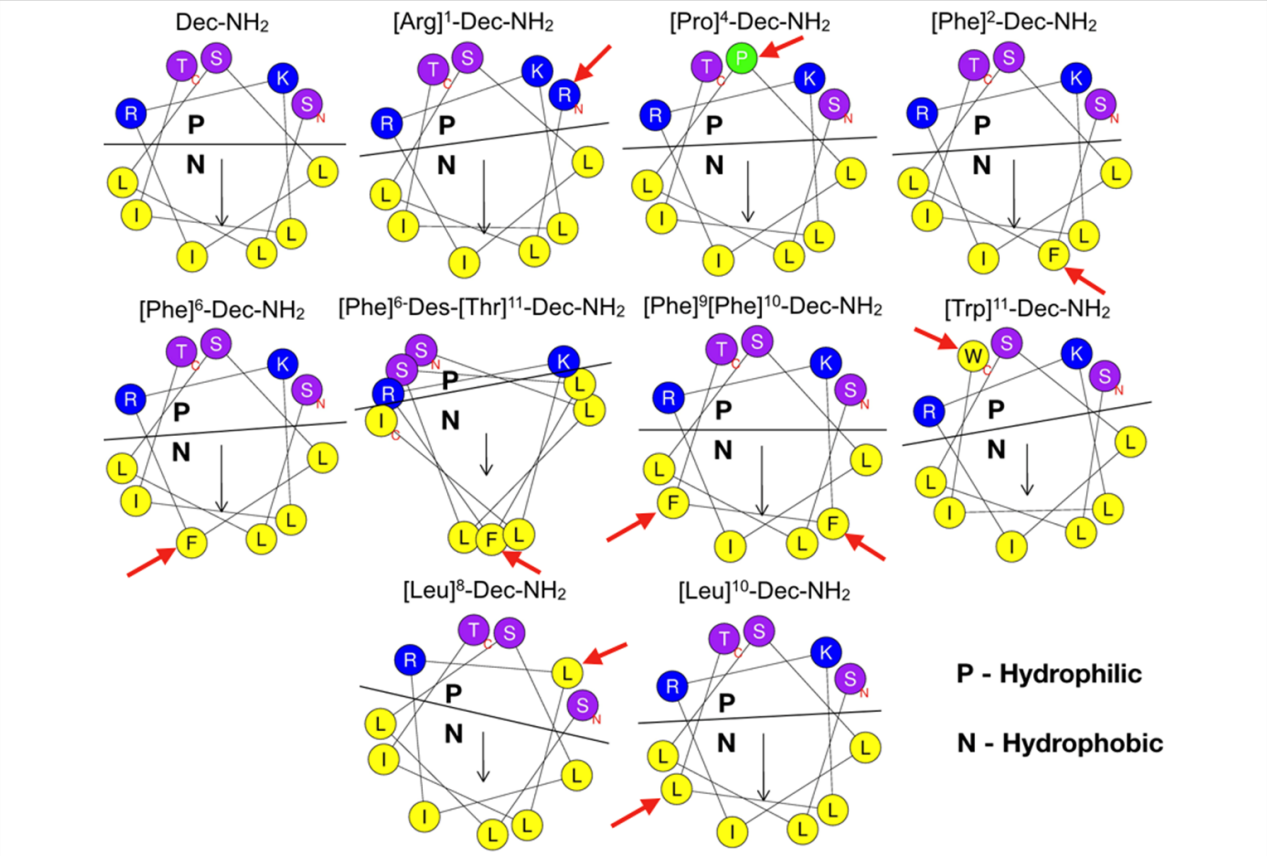

Figure 1: Helical wheel projections of Dec-NH_2 and its analogs, where the yellow circles refer to the hydrophobic amino acid residues, the blue ones to the cationic charged residues, the purple circles to the polar uncharged residues and the green circle to a proline residue. The black line denotes hydrophilic and hydrophobic faces of the amphipathic structures. Red arrows show the mutation positions.

naturally occurring wasp venom peptides [31]. Hydrophobicity was incorporated into the sequence via the substitution of residues from the wild-type sequence by Leu and Phe. Leu was chosen because a minimal amount of energy is required for it to adopt a helical structure [28], which favors antimicrobial activity, and it occurs at high frequency in wasp venom peptide sequences [31]. On the other hand, Phe was chosen because of its bulk and higher hydrophobicity values [30], making it possible to evaluate the effect of adding an aromatic residue to the hydrophobic face on structure and biological function. Additionally, unlike Trp, Phe residues are not major components of cell-penetrating peptides [32], which are typically cytotoxic, so we chose to synthesize a Trp-containing analog as well.

The changes in the designed analogs led to slight differences in specific physicochemical features (Table 1), such as hydrophobicity, hydrophobic moment, and net positive charge, characteristics that are known to be important for peptide–membrane interactions [10]. Some of these changes decreased the hemolytic activity against human red blood cells of Dec-NH_2, reported by Konno et al. [24], and retained the antimicrobial activity described by Torres et al. [9,10] and the conformational tendency of peptides. In addition, the modifications led to an increased charge [9,10], an important feature that correlates with the improved therapeutic index of the Dec-NH_2 derivatives and with the activity against microorganisms such as bacteria and fungi. Furthermore, Dec-NH_2 and its analogs were hemolytic at concentrations above their MIC values for the different microorganisms studied [9,10].

MTT cytotoxicity assays

MTT assays were performed to determine the toxicity of designer peptides against MCF-7 cancer cells and MCF-10A normal cells. MCF-10A cells were used as a control as they have the same genetic background as the MCF-7 cancerous cell line used here. Both cell types were treated with increasing concentrations of peptide for 2 and 24 h. ACPs are known to first interact with negatively charged membranes (i.e., cancer cell membranes) via electrostatic interactions, after which they tend to adopt helical conformations, which causes cell membrane permeabilization or even membrane disruption that may lead to necrosis [33]. These peptides may also be internalized into the cell, leading to the disruption of the mitochondrial membrane and causing apoptosis [33]. Torres et al. [9] described similar

Table 1: Theoretical physicochemical properties and hemolytic activity of decoralin and its synthetic analogs.[a]

peptide	sequence	H	μ_H	q	MHC (μmol L^{-1})[b]	IC_{50} (μmol L^{-1})[c]
Dec-NH_2	SLLSLIRKLIT-NH_2	0.78	0.65	+3	1.56	12.5
[Pro]^4-Dec-NH_2	SLL**P**LIRKLIT-NH_2	0.85	0.58	+3	12.50	25.0
[Arg]^1-Dec-NH_2	**R**LLSLIRKLIT-NH_2	0.69	0.70	+4	25.00	50.0
[Phe]^2-Dec-NH_2	S**F**LSLIRKLIT-NH_2	0.79	0.66	+3	3.12	50.0
[Phe]^6-Dec-NH_2	SLLSL**F**RKLIT-NH_2	0.78	0.65	+3	3.12	>50
[Phe]^6-Des[Thr]^{11}-Dec-NH_2	SLLSL**F**RKLI-NH_2	0.83	0.39	+3	12.50	50.0
[Trp]^{11}-Dec-NH_2	SLLSLIRKLI**W**-NH_2	0.96	0.49	+3	1.56	25.0
[Leu]^8-Dec-NH_2	SLLSLIR**L**LIT-NH_2	1.03	0.48	+2	50.00	>50
[Leu]^{10}-Dec-NH_2	SLLSLIRKL**L**T-NH_2	0.77	0.65	+3	25.00	12.5

[a]H (hydrophobicity), μ_H (hydrophobic moment), and q (charge) were calculated through heliquest freeware. MHC (maximal non-hemolytic concentration in μmol L^{-1}). [b]Maximal non-hemolytical concentration obtained by Torres et al. [9,10]. [c]IC_{50} values against MCF-7 in 24 h.

helical structure propensity and physicochemical properties for Dec-NH_2 and [Leu]^{10}-Dec-NH_2. The main difference between these two peptides in terms of their biological function was the substantially lower hemolytic activity of the [Leu]^{10}-Dec-NH_2 analog, which yielded a higher therapeutic index. The antimicrobial activity of these peptides was nearly equivalent (10^{-1} μmol L^{-1}). In contrast, the [Leu]^8-Dec-NH_2 analog presented a lower helical-structure tendency and almost no hemolytic activity vs human erythrocytes (Table 1), retained the antimicrobial activity of the WT, but was two orders of magnitude less active (10^1 μmol L^{-1}) than the [Leu]^{10}-Dec-NH_2 derivative. In Figure 2, it can be observed that, after 2 h, Dec-NH_2

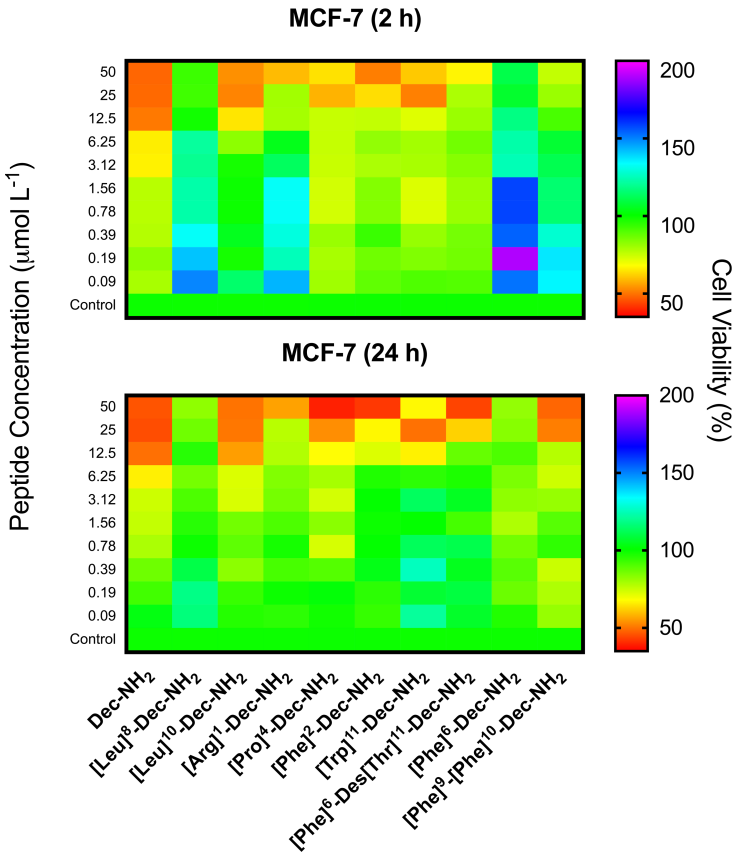

Figure 2: MTT assays using Dec-NH_2 and its synthetic analogs after 2 and 24 h of exposure to MCF-7 cancer cells. Experiments were done in triplicate.

caused lysis of more than 50% of the cancer cells at 3.12 μmol L^{-1}, and after 24 h, the LD_{50} value increased to 12.5 μmol L^{-1}. $[Leu]^{10}$-Dec-NH_2 behaves similarly to the template molecule, achieving >50% of cancer cell lysis at 25 μmol L^{-1} after 2 h of exposure and at 12.5 μmol L^{-1} after 24 h. Their cytotoxicity levels were similar when tested against MCF-10A normal cells (Figure 3), showing no significant cytotoxicity even at higher concentrations (≈100 μmol L^{-1}). On the other hand, $[Leu]^{8}$-Dec-NH_2 did not present significant activity against MCF-7 cells when compared to the negative control (Figure 2), and intriguingly was cytotoxic towards normal MCF-10A cells even at the lowest concentration tested (25 μmol L^{-1}, Figure 3). This cytotoxicity is due to large differences in the values of the $[Leu]^{8}$-Dec-NH_2 physicochemical parameters that were analyzed, e.g., hydrophobicity related features, and lower net positive charge, compared to either $[Leu]^{10}$-Dec-NH_2 or the wild-type molecule, since the Leu substitution was made at the hydrophilic face of the amphipathic helical structure.

All the other analogs were designed by tuning some of the physicochemical features that contribute to peptide–membrane interactions in order to preserve the activity of the native sequence. Some of these changes decreased the hemolytic activity of Dec-NH_2 towards human red blood cells reported by Konno et al. [24] and retained its antimicrobial activity. According to Torres et al. [10], the conformational tendency and increased charge are important contributors to improving the therapeutic index of Dec-NH_2 and its derivatives against microorganisms such as bacteria and fungi. Furthermore, Dec-NH_2 and its analogs were hemolytic at concentrations above their MIC vs the microorganisms tested. As observed in Figure 2, some of the peptides in this family showed promising results, causing substantial inhibition of cancer cell growth at a dose of ≈50 μmol L^{-1}, e.g., Dec-NH_2, $[Pro]^{4}$-Dec-NH_2, $[Arg]^{1}$-Dec-NH_2, $[Phe]^{2}$-Dec-NH_2 and $[Phe]^{6}$-Des$[Thr]^{11}$-Dec-NH_2.

The analogs presented similar antitumor activity in growth inhibition assays with MCF-7 breast cancer cells. Dec-NH_2, Trp- and Phe-substituted analogs were described as the most hemolytic peptides of their family [23]. Treatment with peptide $[Arg]^{1}$-Dec-NH_2 led to significant decreased cell viability 2 h post-exposure (Figure 2) but was not as effective vs MCF-7 cells as its parent peptide. This peptide was selected for cyto-

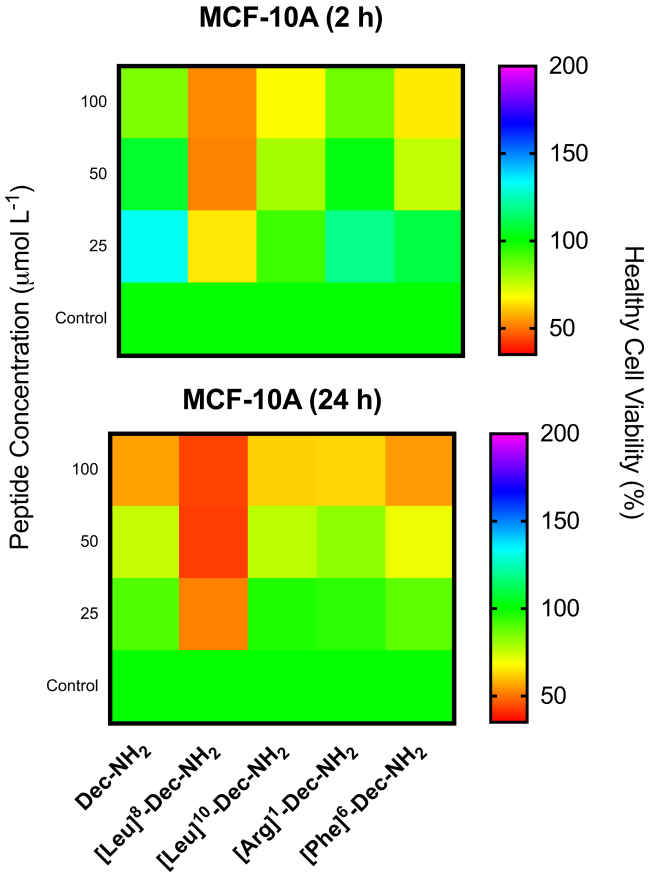

Figure 3: MTT assays evaluating the toxicity of Dec-NH_2 and its derivatives towards MCF-10A normal cells after 2 and 24 h. Experiments were performed in triplicate.

toxicity assays against normal cells because it was not as hemolytic as the wild-type and the other derivatives evaluated (Table 1) and presented higher antimicrobial activity when compared to the other analogs that also exhibited anticancer activity, such as [Pro]^4-Dec-NH_2 and [Phe]^6-Des[Thr]^{11}-Dec-NH_2 (Figure 2).

We also observed noticeable differences among the Phe-substituted peptides. For instance, [Phe]^2-Dec-NH_2 and [Phe]^6-Des[Thr]^{11}-Dec-NH_2 inhibited cell viability the most, at 50 μmol L^{-1} after 2 h (Figure 2). On the other hand, [Phe]^6-Dec-NH_2 did not show significant inhibition after 2 h and [Phe]^9-[Phe]^{10}-Dec-NH_2 did only show significant inhibition after 24 h (Figure 2). [Phe]^6-Des[Thr]^{11}-Dec-NH_2 did not present helical tendencies, as analyzed by Torres et al. [10], and was not as hemolytic as the other Phe-substituted analogs (Table 1).

[Pro]^4-Dec-NH_2 was described as an unstructured peptide even in helical promoter media [34,35] by Torres et al. [10] and was relatively hemolytic (Table 1) [10], but it decreased MCF-7 cancer cell viability more substantially after 24 h than after 2 h (Figure 2). [Trp]^{11}-Dec-NH_2, which had the highest hemolytic activity among the peptides of the Dec-NH_2 family (Table 1), significantly inhibited viability of MCF-7 cells at 25 μmol L^{-1} after 2 h (Figure 2).

Cell death assays

Flow cytometry experiments were performed in an attempt to obtain insight into the mechanism of peptide-mediated death of cancer cells. For these proof-of-concept assays, we focused on WT peptide Dec-NH_2. We utilized Annexin V labeling FITC (X axis) and propidium iodide (PI, Y axis). Under these conditions, (Annexin V+/PI+, right upper quadrant) were interpreted as necrotic cells and (Annexin V+/PI−, right lower quadrant) as apoptotic cells (Figure 4). As a positive control, we treated cells for 1 h with a solution of 2.0 μmol L^{-1} staurosporine (Figure 4).

Cells treated with 12.5 and 25 μmol L^{-1} of Dec-NH_2 showed approximately 16% of cells in the necrotic stage and around

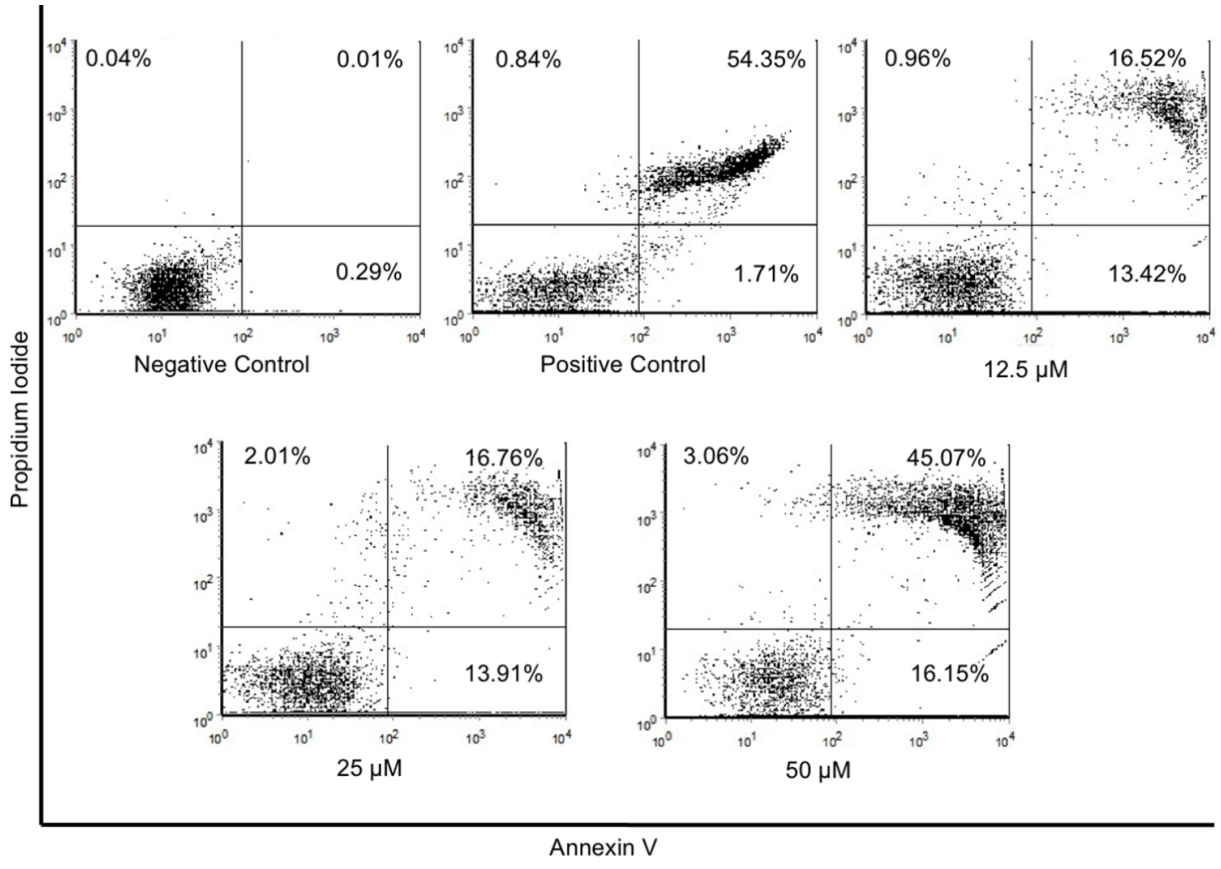

Figure 4: Cell death analysis using flow cytometry. Dot plot graphs from left to right, show cells treated with: (negative control) MCF-7 cells labeled with Annexin/PI, and (positive control) 2.0 μmol L^{-1} staurosporine labeled Annexin V-FITC and PI. Dot plot of MCF-7 cells after exposure to 12.5, 25 or 50 μmol L^{-1} of Dec-NH_2 for 24 h, and flow cytometry analysis with Annexin V-FITC versus PI. The divisions of the plots distinguish necrotic cells (Annexin V+/PI+, right upper quadrant) from apoptotic cells (Annexin V+/PI−, right lower quadrant).

14% of cells in the apoptotic stage after 24 h of incubation. However, the percentage of necrotic cells increased approximately three times (to 45%), when the concentration of Dec-NH_2 was increased to 50 μmol L^{-1}. This is consistent with the MTT assay results obtained with the same peptide (Figure 2), indicating that Dec-NH_2 triggers membrane disruption thus leading to cell death and necrosis of cancer cells.

AFM measurements

AFM was used to quantify the cellular structure (i.e., membrane roughness) of MCF-7 cells upon peptide treatment in order to determine whether cell topology was disturbed, as changes in topology would provide further insight into the mechanism of action of our lead peptides. Cantilevers in contact mode were used to obtain the topographic images from different areas of treated and untreated cell samples [36], and representative results are shown in Figure 5A–C. Peptides Dec-NH_2 and [Leu]^8-Dec-NH_2 were chosen as control peptides as they were the most and least potent, respectively, vs MCF-7 cells as determined by MTT assays (Figure 2).

Exposure of MCF-7 cells to positive control peptide Dec-NH_2 for 24 h increased cancer cell membrane roughness by approximately 100% compared with cells from the untreated control group (Figure 5D,E). Conversely, treatment with negative control peptide [Leu]^8-Dec-NH_2 did not significantly change membrane roughness (Figure 5D,E). Our data indicates that peptide treatment leading to membrane disruption and subsequent cell death is associated with changes in the membrane of cancer cells, specifically, greater roughness.

The AFM results are in line with the activity of the peptides obtained in MTT assays, which highlights the importance of certain physicochemical properties for the bioactivity of these two peptides, in line with previous work by Torres et al. [9]. Currently, there is no consensus on how the biophysical properties of peptides influence their antimicrobial and antitumoral activities. However, in the specific case of Dec-NH_2 and its analogs, helical propensity, having higher hydrophobicity, hydrophobic momentum, and displaying a net positive charge appeared to correlate with improved antitumoral activity. These

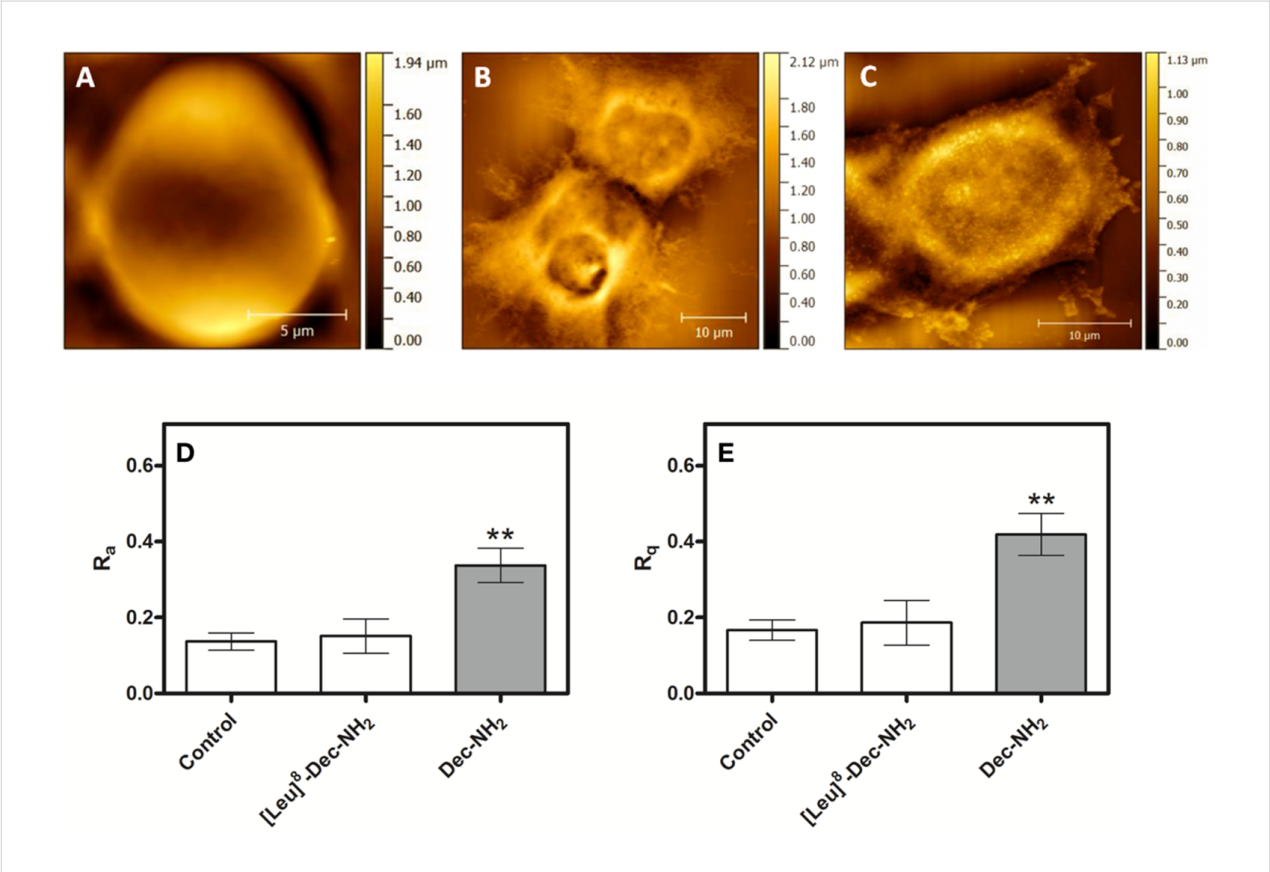

Figure 5: Topological images of untreated MCF-7 cells (A) and cells treated for 24 h with 50 μmol L^{-1} of Dec-NH_2 (B) or 50 μmol L^{-1} of [Leu]^8-Dec-NH_2 (C). Roughness values of membranes of untreated MCF-7 cells and of those cells treated with peptides. (D) Data represent the mean values of the surface relative to the center plane of measurements ± standard deviations (n = 5). (E) The root mean square of the values and the standard deviation of the area were analyzed. More than 5 points were measured per sample. Significant differences between peptide-treated and untreated cells are given by $p > 0.05$ (*).

results add to our current understanding of the structure–activity relationships of ACPs and may lead to novel insights about the innate immune system and to new peptide-based anticancer chemotherapies.

Conclusion

Current cancer treatments are associated with numerous harmful side effects, which warrants the discovery of novel forms of treatment. ACPs have been proposed as novel anticancer therapies because of their potential for selectively targeting cancer cells without harm to normal counterparts [37-39].

Membrane phospholipids confer permeability to the cell and regulate the flux of metabolites between the extracellular environment and the intracellular content [40]. The membrane of cancer cells is typically negatively charged due to a higher expression of anionic molecules such as phosphatidylserines, and negatively charged glycoproteins and glycosaminoglycans [22,23]. Here, we devised a strategy to exploit the negatively charged environment of cancer cells by targeting it with cationic peptides. This strategy is based on the electrostatic interaction of the peptides, through their cationic residues, with the anionic phospholipids present in the membrane [39,40]. The peptides accumulate in the membrane, leading to perturbation of membrane integrity and subsequent cell death [40-42].

We present results obtained with the naturally occurring peptide Dec-NH_2 derived from wasp venom and with its mutant analogs containing single and double substitutions. These peptides, which had been previously shown to display antimicrobial properties [9,10], exhibited anticancer activity against MCF-7 breast cancer cells at concentrations ranging from 12.5 to 50 μmol L^{-1} (Figure 2). The lead anticancer peptides were tested against healthy breast tissue from the same cell line background (MCF-10A) and were shown to selectively target cancer cells. The peptides' selectivity observed towards cancer cells versus normal cells is likely due to the acidic microenvironment that accompanies cancer cells, and the increased net negative charge of cancer cells versus normal cells, which display a net neutral charge [12,20].

The mechanism of peptide-mediated cell death was further analyzed using flow cytometry for the WT peptide (Dec-NH_2). Peptide treatment led to necrotic death of cancer cells. Additional AFM experiments revealed that the roughness of the cancer cell membrane increased significantly when treated with this peptide, when compared with untreated cells or cells treated with the negative control peptide [Leu]^8-Dec-NH_2. These results indicate that peptide treatment alters the ultrastructure of the cancer cell membrane, an alteration that is apparently part of the observed anticancer activity.

The biophysical features of peptides play an important role in peptide–membrane interactions. Here, we designed peptide variants derived from Dec-NH_2, taking into account key physicochemical properties of ACPs, such as hydrophobicity, amphipathicity, and positive net charge. Our results show that significant changes in amphipathicity, net charge, and hydrophobicity led to decreased activity against MCF-7 cancer cells ([Leu]^8-Dec-NH_2 and [Phe]^6-Dec-NH_2 analogs) and, in some cases, to unwanted effects, such as increased cytotoxicity against normal MCF-10A cells (e.g., [Leu]^8-Dec-NH_2). In addition, we identified [Leu]^{10}-Dec-NH_2 as an excellent candidate with which to pursue the use of ACPs for eventual clinical development, as it displayed reduced hemolytic activity than Dec-NH_2 and exhibited selective killing of cancer cells. The ACPs described here represent excellent scaffolds for the generation of potent, nontoxic, and selective anticancer agents.

Experimental

Peptide synthesis, purification and analysis

Peptides were synthesized by solid-phase peptide synthesis on Rink Amide resin, with a substitution degree of 0.52 mmol g^{-1} on a 0.1 mmol scale, using the Fmoc strategy on a peptide synthesizer (PS3 – Protein Technologies) as described by Torres et al. [9,10].

Dry-protected peptidyl-resin was exposed to TFA/anisole/water (95:2.5:2.5, v/v/v) for 2 h at room temperature. The crude deprotected peptides were precipitated with anhydrous diethyl ether, filtered from the ether-soluble products, extracted from the resin with 60% ACN (acetonitrile) in water and lyophilized.

The crude lyophilized peptides were then purified by preparative reversed-phase high-performance liquid chromatography (RP-HPLC) in 0.1% TFA/90% ACN in water (A/B) on a Delta Prep 600 (Waters Associates). Briefly, the peptides were loaded onto a Phenomenex C_{18} (21.2 mm × 250 mm, 15 μm particles, 300 Å pores) column at a flow rate of 10.0 mL min^{-1} and eluted using a linear gradient (0.33% B/min slope), with detection at 220 nm. Selected fractions containing the purified peptides were pooled and lyophilized. Purified peptides were characterized by liquid-chromatography electrospray-ionization mass spectrometry (LC/ESIMS).

LC/ESIMS data were obtained on a Model 6130 Infinity mass spectrometer coupled to a Model 1260 HPLC system (Agilent), using a Phenomenex Gemini C_{18} column (2.0 mm × 150 mm, 3.0 μm particles, 110 Å pores). Solvent A was 0.1% TFA in

water, and solvent B was 90% ACN in solvent A. Elution with a 5–95% B gradient was performed over 20 min, 0.2 mL min^{-1} flow and peptides were detected at 220 nm. Mass measurements were performed in a positive mode with the following conditions: mass range between 100 to 2500 *m/z*, ion energy of 5.0 V, nitrogen gas flow of 12 L min^{-1}, solvent heater of 250 °C, multiplier of 1.0, capillary of 3.0 kV and cone voltage of 35 V.

Cell culture and treatment

MCF-7 cells (ATCC) were maintained in RPMI 1640 medium supplemented with 10% heat inactivated FBS and 100 μg mL^{-1} penicillin/10 μg mL^{-1} streptomycin. One day before the assays, the cells were plated in 96-well microtiter plates with a density of 2.0×10^4 cells/well at 37 °C and 5% CO_2. On the next day, cells were treated with peptides serial dilutions (0.09–50 μmol L^{-1}), incubated in individual microtiter plates for 2 and 24 h and MTT assays were performed after treatment. Human breast epithelial cells MCF-10A (ATCC) were maintained in a mixture of Dulbecco's Modified Eagle's Medium and Ham's F12 nutrient mixture supplemented with 5% inactivated horse serum, 10 μg mL^{-1} insulin, 0.02 μg mL^{-1} human epidermal growth factor, 0.5 μg mL^{-1} hydrocortisone, 0.10 μg mL^{-1} choleric toxin, 100 U mL^{-1} penicillin, and 100 μg mL^{-1} streptomycin. The cells were preincubated for 24 h, plated in 96-well microtiter plates with a density of 2.0×10^4 cells/well at 37 °C and 5% CO_2. On the next day, cells were treated with peptides serial dilutions (25 to 100 μmol L^{-1}), incubated in individual microtiter plates for 4 and 24 h and MTT assay was performed after treatment. Experiments were performed in triplicate.

MTT assay

Briefly, MTT (Sigma-Aldrich) was dissolved in water and filtered to make up a 5 μg mL^{-1} solution. 30 μL of this solution were added to all the wells which already contained peptide-treated cells and kept at 37 °C for 45 minutes. Subsequently, the solution was discarded and replaced with 150 μL/well of DMSO and followed by gentle shaking for 15 minutes. Finally, the microplates were read on an ELISA reader at 570 nm. Experiments were performed in triplicate.

Cell death assay

The percentage of cells undergoing apoptosis and necrosis was determined by Annexin V/propidium Iodide staining using the ApopNexin™ FITC Apoptosis Detection Kit (Millipore) in a flow cytometer (BD Facs Canto II - BD). MCF-7 cells were seeded in 6-well plates and treated for 24 h with 12.5, 25 or 50 μmol L^{-1} Dec-NH_2 solution and 2.0 μmol L^{-1} staurosporine in water (positive control). The apoptosis assay was performed according to Matias et al. [36].

AFM measurements

The AFM imaging of MCF-7 cells untreated (control) and treated with peptide (50 μmol L^{-1} solutions of Dec-NH_2 and [Leu]^8-Dec-NH_2, which presented low activity when compared to other analogs and was used here as a treated control) was performed using an Agilent Technologies 5500 AFM/SPM microscope that was in contact mode and a Nanosensors™ PPP-CONT probe (NanoSensors; PPP-Cont-20, PointProbe-Plus Silicon-SPM-Sensor). The material properties and dimensions of the AFM tips used in this experiment were as follows: resonance frequency of 6–21 kHz, force constant of 0.02–0.77 N m^{-1}, cantilever length of 450 ± 10 μm, cantilever width of 50 ± 7.5 μm, cantilever thickness of 2 ± 1 μm, tip height of 10–15 μm and resistivity of 0.01–0.02 Ω cm. The assays were performed in triplicate; image processing and roughness determinations were performed with the aid of the Gwyddion software (http://gwyddion.net/download.php). In order to compare the cell surface, we used two roughness parameters, the mean roughness (R_a) and the mean square of Z data (R_q), where N is the difference between the highest and the lowest points in the analyzed area. These parameters should not be considered as absolute roughness values because they strictly depend on the tip used in the assays.

R_a is the mean value of the surface relative to the center plane of the measurements. This plane is defined by where the volumes enclosed by the image above and below are equal and it is given by Equation 1:

$$R_a = \frac{1}{L_x L_y} \int_0^{L_x} \int_0^{L_y} |f(x,y)| \, dxdy, \quad (1)$$

where $f(x,y)$ is the surface relative to the center plane and, L_x and L_y are the surface dimensions.

The root mean square of the Z values R_q is the standard deviation of the N values in the area analyzed and is given by Equation 2:

$$R_q = \sqrt{\sum_{n=1}^{N} \frac{(Z_n - Z_{avg})^2}{N}}, \quad (2)$$

where Z_{avg} is the average of the Z values in the given area, Z_n is the current value, and N is the number of points in this area [43].

Acknowledgements

This work was supported by Fundação de Amparo à Pesquisa do Estado de São Paulo (FAPESP VXO #2014/12938-6, AOR

#2014/18527-8, GC #2016/09652-9 and MDTT #2014/04507-5). Cesar de la Fuente-Nunez acknowledges funding from the Ramon Areces Foundation. The authors are grateful to the Multiuser Central Facilities (UFABC) for the experimental support.

ORCID® iDs

Marcelo D. T. Torres - https://orcid.org/0000-0002-6165-9138
Roseli H. Sato - https://orcid.org/0000-0002-9896-4072
Tania M. Manieri - https://orcid.org/0000-0003-1152-7425
Cesar de la Fuente-Nunez - https://orcid.org/0000-0002-2005-5629

References

1. Pedron, C. N.; Torres, M. D. T.; da Silva Lima, J. A.; Silva, P. I.; Silva, F. D.; Oliveira, V. X. *Eur. J. Med. Chem.* **2017,** *126,* 456–463. doi:10.1016/j.ejmech.2016.11.040
2. Torres, M. D. T.; Silva, A. F.; Alves, F. L.; Capurro, M. L.; Miranda, A.; Cordeiro, R. M.; Oliveira, V. X., Jr. *J. Pept. Sci.* **2016,** *22,* 132–142. doi:10.1002/psc.2849
3. Chamlian, M.; Bastos, E. L.; Maciel, C.; Capurro, M. L.; Miranda, A.; Silva, A. F.; Torres, M. D. T.; Oliveira, V. X., Jr. *J. Pept. Sci.* **2013,** *19,* 575–580. doi:10.1002/psc.2534
4. Torres, M. D. T.; Silva, A. F.; Alves, F. L.; Capurro, M. L.; Miranda, A.; Oliveira, V. X., Jr. *Int. J. Pept. Res. Ther.* **2014,** *20,* 277–287. doi:10.1007/s10989-014-9392-1
5. Ferreira, L. H. R.; Silva, A. F.; Torres, M. D. T.; Pedron, C. N.; Capurro, M. L.; Alves, F. L.; Miranda, A.; Oliveira, V. X., Jr. *Int. J. Pept. Res. Ther.* **2014,** *20,* 553–564. doi:10.1007/s10989-014-9425-9
6. Silva, A. F.; Bastos, E. L.; Torres, M. D. T.; Costa-Da-Silva, A. L.; Ioshino, R. S.; Capurro, M. L.; Alves, F. L.; Miranda, A.; De Freitas Fischer Vieira, R.; Oliveira, V. X., Jr. *J. Pept. Sci.* **2014,** *20,* 640–648. doi:10.1002/psc.2641
7. Silva, A. F.; Torres, M. D. T.; de Souza Silva, L.; Alves, F. L.; de Sá Pinheiro, A. A.; Miranda, A.; Capurro, M. L.; Oliveira, V. X. J., Jr. *Malar. J.* **2015,** *14,* No. 433. doi:10.1186/s12936-015-0974-y
8. Torres, M. D. T.; Silva, A. F.; De Souza Silva, L.; De Sá Pinheiro, A. A.; Oliveira, V. X., Jr. *J. Pept. Sci.* **2014,** *21,* 24–28. doi:10.1002/psc.2714
9. Torres, M. D. T.; Pedron, C. N.; da Silva Lima, J. A.; da Silva, P. I., Jr.; da Silva, F. D.; Oliveira, V. X., Jr. *J. Pept. Sci.* **2017,** *23,* 818. doi:10.1002/psc.3029
10. Torres, M. D. T.; Pedron, C. N.; Araújo, I.; Silva, P. I., Jr.; Silva, F. D.; Oliveira, V. X. *ChemistrySelect* **2017,** *2,* 18–23. doi:10.1002/slct.201601590
11. Baxter, A. A.; Lay, F. T.; Poon, I. K. H.; Kvansakul, M.; Hulett, M. D. *Cell. Mol. Life Sci.* **2017,** *74,* 3809–3825. doi:10.1007/s00018-017-2604-z
12. Hoskin, D. W.; Ramamoorthy, A. *Biochim. Biophys. Acta, Biomembr.* **2008,** *1778,* 357–375. doi:10.1016/j.bbamem.2007.11.008
13. Wang, K.-r.; Yan, J.-x.; Zhang, B.-z.; Song, J.-j.; Jia, P.-f.; Wang, R. *Cancer Lett.* **2009,** *278,* 65–72. doi:10.1016/j.canlet.2008.12.027
14. Deng, X.; Qiu, Q.; Wang, X.; Huang, W.; Qian, H. *Chem. Biol. Drug Des.* **2016,** *87,* 374–381. doi:10.1111/cbdd.12667
15. Suarez-Jimenez, G.-M.; Burgos-Hernandez, A.; Ezquerra-Brauer, J.-M. *Mar. Drugs* **2012,** *10,* 963–986. doi:10.3390/md10050963
16. Singh, B. P.; Vij, S.; Hati, S. *Peptides* **2014,** *54,* 171–179. doi:10.1016/j.peptides.2014.01.022
17. Dongol, Y.; Dhananjaya, B. L.; Shrestha, R. K.; Aryal, G. *Protein Pept. Lett.* **2016,** *23,* 688–698. doi:10.2174/0929866523666160511151039
18. Al-Benna, S.; Shai, Y.; Jacobsen, F.; Steinstraesser, L. *Int. J. Mol. Sci.* **2011,** *12,* 8027–8051. doi:10.3390/ijms12118027
19. Gomes, A.; Bhattacharjee, P.; Mishra, R.; Biswas, A. K.; Dasgupta, S. C.; Giri, B.; Debnath, A.; Gupta, S.; Das, T.; Gomes, A. *Indian J. Exp. Biol.* **2010,** *48,* 93–103.
20. Schweizer, F. *Eur. J. Pharmacol.* **2009,** *625,* 190–194. doi:10.1016/j.ejphar.2009.08.043
21. Hu, J.; Chen, C.; Zhang, S.; Zhao, X.; Xu, H.; Zhao, X.; Lu, J. R. *Biomacromolecules* **2011,** *12,* 3839–3843. doi:10.1021/bm201098j
22. Dennison, S.; Whittaker, M.; Harris, F.; Phoenix, D. A. *Curr. Protein Pept. Sci.* **2006,** *7,* 487–499. doi:10.2174/138920306779025611
23. Deslouches, B.; Di, Y. P. *Oncotarget* **2017,** *8,* 46635–46651. doi:10.18632/oncotarget.16743
24. Konno, K.; Rangel, M.; Oliveira, J. S.; dos Santos Cabrera, M. P.; Fontana, R.; Hirata, I. Y.; Hide, I.; Nakata, Y.; Mori, K.; Kawano, M.; Fuchino, H.; Sekita, S.; Neto, J. R. *Peptides* **2007,** *28,* 2320–2327. doi:10.1016/j.peptides.2007.09.017
25. Hakoshima, T. Leucine Zippers. *eLS;* John Wiley & Sons, Ltd, 2014. doi:10.1002/9780470015902.a0005049.pub2
26. Landschulz, W. H.; Johnson, P. F.; McKnight, S. L. *Science* **1988,** *240,* 1759–1764. doi:10.1126/science.3289117
27. Ahmad, A.; Azmi, S.; Srivastava, S.; Kumar, A.; Tripathi, J. K.; Mishra, N. N.; Shukla, P. K.; Ghosh, J. K. *Amino Acids* **2014,** *46,* 2531–2543. doi:10.1007/s00726-014-1802-3
28. Pace, C. N.; Scholtz, J. M. *Biophys. J.* **1998,** *75,* 422–427. doi:10.1016/S0006-3495(98)77529-0
29. Cutrona, K. J.; Kaufman, B. A.; Figueroa, D. M.; Elmore, D. E. *FEBS Lett.* **2015,** *589,* 3915–3920. doi:10.1016/j.febslet.2015.11.002
30. Eisenberg, D. *Annu. Rev. Biochem.* **1984,** *53,* 595–623. doi:10.1146/annurev.bi.53.070184.003115
31. Lee, S. H.; Baek, J. H.; Yoon, K. A. *Toxins* **2016,** *8,* No. 32. doi:10.3390/toxins8020032
32. Jin, J.; Bai, X.; Luan, N.; Yao, H.; Zhang, Z.; Liu, W.; Chen, Y.; Yan, X.; Rong, M.; Lai, R.; Lu, Q. *J. Med. Chem.* **2016,** *59,* 1791–1799. doi:10.1021/acs.jmedchem.5b01264
33. Lee, D. Y.; Noh, I.; Yoo, J.; Rejinold, N. S.; Kim, Y.-C. *Acta Biomater.* **2017,** *57,* 187–196. doi:10.1016/j.actbio.2017.05.040
34. Luo, P.; Baldwin, R. L. *Biochemistry* **1997,** *36,* 8413–8421. doi:10.1021/bi9707133
35. Buck, M. *Q. Rev. Biophys.* **1998,** *31,* 297–355. doi:10.1017/S003358359800345X
36. Matias, A. C.; Manieri, T. M.; Cerchiaro, G. *Oxid. Med. Cell. Longevity* **2016,** No. 6724585. doi:10.1155/2016/6724585
37. Hao, X.; Yan, Q.; Zhao, J.; Wang, W.; Huang, Y.; Chen, Y. *PLoS One* **2015,** *10,* e0138911. doi:10.1371/journal.pone.0138911
38. Zhao, J.; Hao, X.; Liu, D.; Huang, Y.; Chen, Y. *PLoS One* **2015,** *10,* e0139578. doi:10.1371/journal.pone.0139578
39. Tripathi, A. K.; Kumari, T.; Tandon, A.; Sayeed, M.; Afshan, T.; Kathuria, M.; Shukla, P. K.; Mitra, K.; Ghosh, J. K. *Acta Biomater.* **2017,** *57,* 170–186. doi:10.1016/j.actbio.2017.05.007
40. Trapella, C.; Voltan, R.; Melloni, E.; Tisato, V.; Celeghini, C.; Bianco, S.; Fantinati, A.; Salvadori, S.; Guerrini, R.; Secchiero, P.; Zauli, G. *J. Med. Chem.* **2016,** *59,* 147–156. doi:10.1021/acs.jmedchem.5b01165
41. Hecht, H.; Srebnik, S. *Biomacromolecules* **2016,** *17,* 2160–2167. doi:10.1021/acs.biomac.6b00378

42. Vagner, J.; Qu, H.; Hruby, V. J. *Curr. Opin. Chem. Biol.* **2008,** *12,* 292–296. doi:10.1016/j.cbpa.2008.03.009
43. Zhang, L.; Yang, F.; Cai, J.-Y.; Yang, P.-H.; Liang, Z.-H. *Biosens. Bioelectron.* **2014,** *56,* 271–277. doi:10.1016/j.bios.2014.01.024

License and Terms

BEILSTEIN JOURNAL OF ORGANIC CHEMISTRY

Defining the hydrophobic interactions that drive competence stimulating peptide (CSP)-ComD binding in *Streptococcus pneumoniae*

Bimal Koirala[1], Robert A. Hillman[2], Erin K. Tiwold[2], Michael A. Bertucci[*2] and Yftah Tal-Gan[*1]

Full Research Paper

Open Access

Address:
[1]Department of Chemistry, University of Nevada, Reno, 1664 North Virginia Street, Reno, Nevada, 89557, United States and [2]Department of Chemistry, Moravian College, 1200 Main Street, Bethlehem, Pennsylvania, 18018, United States

Email:
Michael A. Bertucci[*] - bertuccim@moravian.edu; Yftah Tal-Gan[*] - ytalgan@unr.edu

* Corresponding author

Keywords:
binding surface; competence stimulating peptide (CSP); protein–peptide interactions; quorum sensing; *Streptococcus pneumoniae*; structure–activity relationships (SAR)

Beilstein J. Org. Chem. **2018,** *14,* 1769–1777.
doi:10.3762/bjoc.14.151

Received: 03 May 2018
Accepted: 25 June 2018
Published: 16 July 2018

This article is part of the thematic issue "Antibacterials, bacterial small molecule interactions and quorum sensing".

Guest Editor: D. Spring

Abstract

Quorum sensing (QS) is a cell–cell communication mechanism that enables bacteria to assess their population density and alter their behavior upon reaching high cell number. Many bacterial pathogens utilize QS to initiate an attack on their host, thus QS has attracted significant attention as a potential antivirulence alternative to traditional antibiotics. *Streptococcus pneumoniae*, a notorious human pathogen responsible for a variety of acute and chronic infections, utilizes the competence regulon and its associated signaling peptide, the competence stimulating peptide (CSP), to acquire antibiotic resistance and establish an infection. In this work, we sought to define the binding pockets within the ComD1 receptor used for binding the hydrophobic side-chain residues in CSP1 through the introduction of highly-conservative point mutations within the peptide. Optimization of these binding interactions could lead to the development of highly potent CSP-based QS modulators while the inclusion of non-natural amino acids within the CSP sequence would confer resistance to protease degradation, a requirement for drug candidates.

Introduction

Quorum sensing (QS), a cell-density mechanism utilized by bacteria to assess their population density through the detection of diffusible signal molecules, enables bacterial species to synchronize their behavior and work as a multi-cellular organism at high cell numbers to achieve transformations that require population-wide efforts [1,2]. Many symbiotic and pathogenic phenotypes are regulated by QS, including bioluminescence, root nodulation, sporulation, swarming, biofilm formation, viru-

lence factor production and competence [3-5]. As such, QS has attracted significant attention as a means to control bacterial behaviors (i.e., promote productive processes while attenuating harmful traits). Extensive work aimed at developing small molecule-based QS modulators against a multitude of Gram-negative bacterial species, including *Pseudomonas aeruginosa*, *Vibrio fischeri*, *Vibrio harveyi*, *Vibrio cholerae*, and *Acinetobacter baumannii* has been conducted [6-10]. Contrary, with the exception of the accessory gene regulator (agr) QS circuitry in *Staphylococcus aureus* [11-16], Gram-positive QS systems are underrepresented in the literature. To address this issue, our research groups have been actively working to delineate the molecular mechanisms of several Gram-positive QS circuitries, including *Enterococcus faecalis* [17], *Streptococcus gallolyticus* subsp. *gallolyticus* [18], *Streptococcus pneumoniae* [19], and *Lactobacillus plantarum*. These circuitries are usually centered on a peptide signal, rather than a small molecule, and are fruitful ground for the development of peptide-based therapeutics.

S. pneumoniae is an opportunistic human pathogen that is responsible for a variety of acute and chronic infections, including pneumonia, bacteremia, sepsis, meningitis and otitis media, resulting in >22,000 deaths and direct medical costs totaling $3.5 billion a year in the United States alone [20,21]. The QS circuitry of *S. pneumoniae,* known as the competence regulon, is centered on the competence stimulating peptide (CSP, Figure 1). *S. pneumoniae* utilizes the regulon to become competent and acquire antibiotic resistance from the environment, initiate its attack on the human host through virulence factor production, and protect itself from the environment by forming biofilms [22-27]. The competence regulon in *S. pneumoniae* is therefore a major regulator of pathogenicity and thus a potential target for attenuating *S. pneumoniae* infections. *S. pneumoniae* strains can be divided into two main specificity groups based on the CSP signal that they produce (CSP1 and CSP2, Figure 1) and their cognate receptors (ComD1 and ComD2, respectively), with minimal cross-talk between the groups [28]. The two CSP signals share approximately 50% homology and differ mainly in hydrophobic residues in the central region of the peptides, suggesting that these residues are involved in receptor binding and specificity [29].

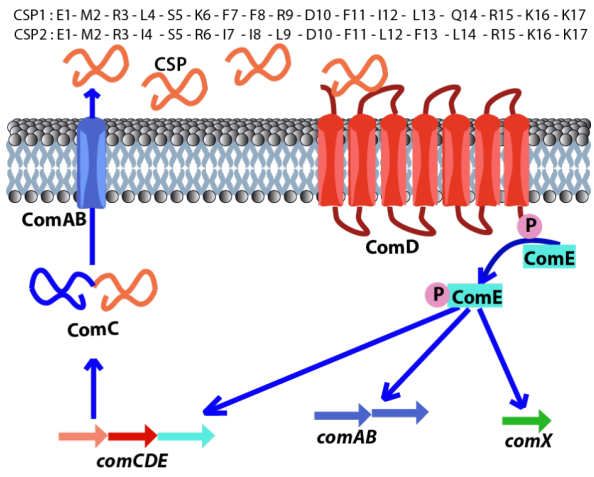

Figure 1: The competence regulon QS circuitry in *S. pneumoniae*. ComC is processed and secreted by ComAB as the mature CSP signal. Upon reaching a threshold concentration, CSP binds and activates the transmembrane histidine kinase receptor ComD. Upon activation, ComD phosphorylates ComE. Phosphorylated ComE then autoactivates the competence QS circuit and upregulates the expression of genes involved in virulence factor production, biofilm formation and attaining genetic competence through ComX. The sequences of the two CSP signals identified in *S. pneumoniae* are shown at the top.

Previously, Yang et al. conducted a systematic structure–activity relationship (SAR) analysis of the CSP1 scaffold and found that the hydrophobic residues in positions 4, 7, 8, 11, 12 and 13, along with Arg3, are important for ComD1 binding [19]. Moreover, three of these positions, 4, 7 and 8, were suggested by Johnsborg et al. to confer specificity between the ComD receptors [29]. Therefore, in this work, we aimed to define the hydrophobic pockets within the ComD1 receptor that are occupied by the hydrophobic residues in positions 4, 7, 8, 11, 12 and 13 as a means to enhance the binding interactions between CSP1 and ComD1. To this end, we utilized highly conservative mutations in these positions using both proteogenic and non-proteogenic amino acids and assessed the effects of these mutations on both receptor binding and specificity. Our analysis revealed that positions 4, 7, 8 and 11 are more resistant to modification than positions 12 and 13. Furthermore, it appears from our analysis that the side-chain residues do not occupy 100% of the binding pockets, thus these pockets can accommodate better elongated side-chain residues compared to truncated side-chains or those that introduce electrostatic effects. Finally, our results further correlated helicity with bioactivity. Combined, the results of this study can be used to design novel CSP-based QS modulators with improved pharmacological properties that could be applied to study QS in vivo.

Results and Discussion

Design and synthesis of CSP1 analogs

In this work, we aimed to define the binding pockets in ComD1 that accommodate the hydrophobic side-chain residues in CSP1 and determine their degree of occupancy as a means to optimize CSP1–ComD1 interactions and develop novel CSP-based QS modulators with improved activities. When optimizing protein–peptide interactions, it is important to determine which key side-chain residues within the peptide sequence fully occupy their binding pocket within the protein and which ones do not

optimally occupy their binding site, either by not occupying the entire binding pockets or by having some unfavorable steric clashes (Figure 2). To do so, one can either use computational models, when structural information of the protein/receptor is available [30], or utilize conservative point mutations within the ligand peptide to assess the occupancy level and degree of specificity. Since no structural information is available for the ComD receptors, we chose to assess the ComD1 binding pocket by synthesizing a set of CSP1 analogs bearing highly conservative point mutation in key hydrophobic positions (4, 7, 8, 11, 12 and 13). Aliphatic hydrophobic side-chains, namely Leu or Ile, were replaced with proteogenic and non-proteogenic aliphatic residues (Ile, Leu, Val, norleucine (Nle), or norvaline (Nva)), while aromatic hydrophobic residues (Phe) were replaced with other aromatic residues (phenylglycine (Phg), homophenylalanine (hPhe), or Tyr; Figure 3). The CSP1 analogs were constructed using standard solid-phase peptide synthesis (SPPS) protocols (see Materials and Methods for SPPS procedures), followed by purification to homogeneity by semipreparative RP-HPLC (see the Supporting Information File 1 for full characterization details).

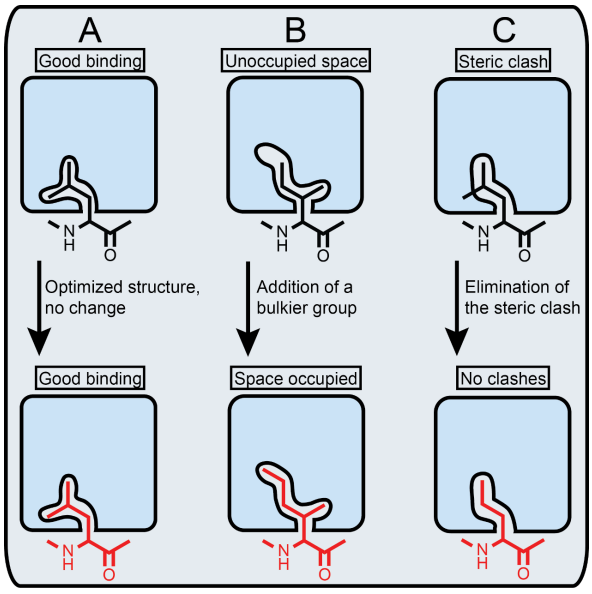

Figure 2: Assessment of protein–peptide binding pockets. Key side-chain residues (black) can either fully occupy their binding pocket (A), partially occupy their binding pocket (B), or have some unfavorable steric clashes (C). As such, no optimization (red) is required in (A), larger bulkier side-chain can be introduced to improve binding interactions in (B), while smaller side-chain residue can be introduced in (C) to eliminate steric clashes and improve binding.

Structure–activity relationships of CSP1 analogs

To assess QS modulation, we utilized the β-gal reporter strains, constructed by Lau and co-worker [31]. In these strains the *lacZ* gene is under the control of QS (pcomX). Thus, upon QS activation, ComE will bind pcomX and transcribe *lacZ* (in addition to upregulation of ComX). ComD modulation can therefore be quantified by measuring β-gal activity. The peptides were first screened for their ability to activate/inhibit the ComD1 and ComD2 receptors at high concentration (10 μM). Only analogs that exhibited greater than 75% activation compared to the

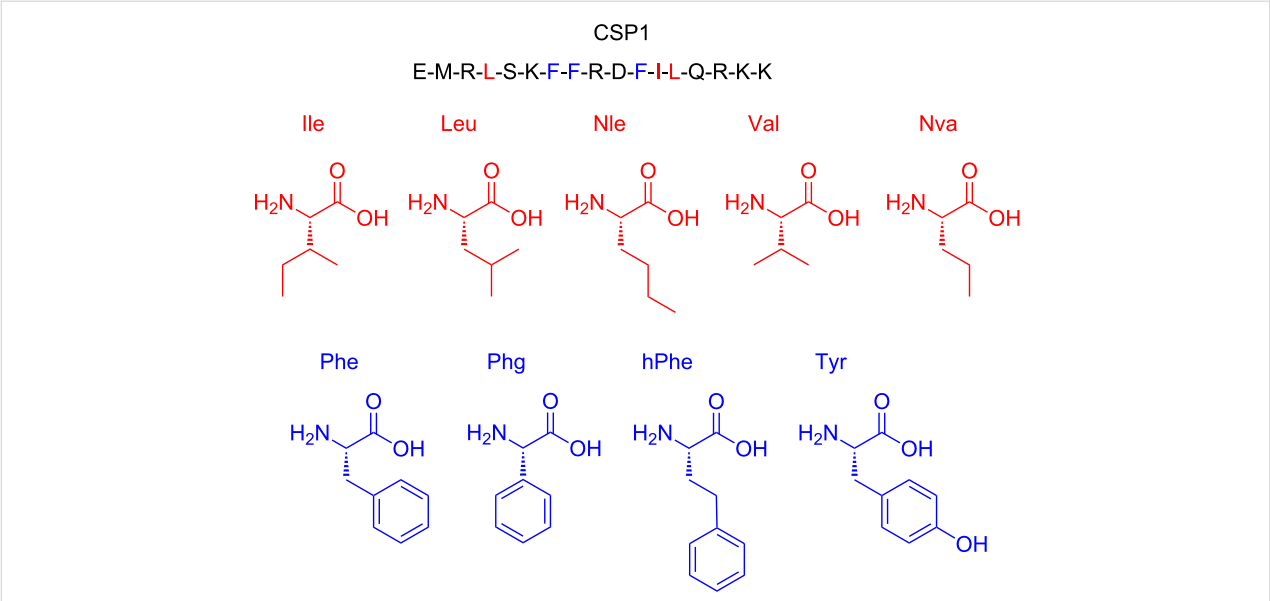

Figure 3: Design of CSP1 analogs. The CSP1 sequence is presented using the one-letter amino acid code. Residues in red were replaced by all the other red residues, while residues in blue were replaced by all the other blue residues. Nle, norleucine; Nva, norvaline; Phg, phenylglycine; hPhe, homophenylalanine.

native signal (CSP1 or CSP2) or greater than 50% inhibition of the maximal signal induced by the native peptide were further evaluated to determine their EC_{50}/IC_{50} values, respectively.

Starting with the ComD1 receptor, generally, it appears that the binding sites of the CSP1 aromatic residues are optimally occupied, leading to a more significant reduction in potency when the side-chain residue is changed compared to the aliphatic binding pockets (Table 1). Looking at the aliphatic residues in CSP1, the binding pocket for the fourth residue, leucine, can accommodate elongation of the aliphatic chain by one methylene (Leu → Nle) as well as movement or loss of chain-branching (Leu → Ile, Nle or Nva; Table 1). Contrary, truncation of the aliphatic chain by one carbon (Leu → Val) resulted in significant reduction in potency, suggesting that important binding interactions are occurring between the δ carbon of the Leu residue in CSP1 and the ComD1 binding pocket. Regarding the 12th position, Ile, it appears that the protein–peptide interface is more promiscuous, accommodating all types of modifications (Table 1). It seems that elongation by one carbon (Ile → Nle) as well as repositioning of branching (Ile → Leu) are slightly more tolerated than truncation (Ile → Val) or removal of branching (Ile → Nva). However, these changes were subtle (about 2-fold; Table 1). Overall, it appears from the results that the binding pocket of the 12th residue is not fully occupied by the side-chain residue and can be further optimized. Moving to the 13th position, Leu, this binding pocket also accommodated changes in carbon length and connectivity relatively well. In this case, relocation of branching (Leu → Ile) was most tolerated, followed by removal of branching, either with or without chain elongation (Leu → Nle or Nva; 2-fold reduction in potency). Truncation was least tolerable (Leu → Val; 3-fold decrease in potency). Combined, these results suggest that all three sites can be further optimized with an emphasis on utilizing longer, bulkier substituents. Moreover, the decreases in potency observed with the introduction of Val indicate that side chains containing δ carbons (at minimum) are required to preserve QS activity.

Turning to the aromatic residues, all of which are Phe, repositioning of the benzene ring at the seventh position (truncation or elongation, Phe → Phg or hPhe, respectively) led to an 8-fold reduction in potency. These results suggest that this ring sits in a relatively tight pocket (Table 1). Moreover, addition of a

Table 1: Biological and structural characterization of the CSP1 analogs[a].

Peptide name	ComD1		ComD2		Helicity (%)[d]
	EC_{50} (nM)[b]	95% CI[c]	EC_{50} (nM)	95% CI	
CSP1	10.3	6.27–16.8	526	498–556	20.1%
CSP1-L4I	10.2	6.74–15.4	>1000	–	34.8%
CSP1-L4NL	13.5	6.38–28.5	>1000	–	29.2%
CSP1-L4NV	5.74	2.94–11.2	627	332–1180	34.0%
CSP1-L4V	113	74.1–171	–[e]	–	30.1%
CSP1-F7FG	81.3	35.1–188	828	512–1340	26.3%
CSP1-F7HF	81.7	61.8–108	317	148–682	26.7%
CSP1-F7Y	344	155–764	–[e]	–	31.8%
CSP1-F8FG	884	514–1520	–[e]	–	13.4%
CSP1-F8HF	43.4	35.1–53.5	>1000	–	19.4%
CSP1-F8Y	85.0	72.2–100	–[e]	–	25.7%
CSP1-F11FG	>1000	–	>1000	–	15.9%
CSP1-F11HF	65.8	41.8–104	>1000	–	32.3%
CSP1-F11Y	95.6	59.4–154	–[e]		29.2%
CSP1-I12L	8.56	5.42–13.5	537	384–752	34.1%
CSP1-I12NL	6.68	3.52–12.6	>1000	–	24.7%
CSP1-I12NV	13.8	11.8–16.2	853	748–973	25.6%
CSP1-I12V	15.3	6.72–34.9	–[e]	–	29.0%
CSP1-L13I	9.12	5.96–13.9	705	426–1170	27.7%
CSP1-L13NL	18.6	7.95–43.3	>1000	–	17.3%
CSP1-L13NV	15.2	7.56–30.3	>1000	–	30.9%
CSP1-L13V	31.0	20.8–46.1	–[e]	–	25.8%

[a]See experimental section for details of reporter strains and methods. See Supporting Information File 1 for plots of agonism dose response curves and CD spectra. All bioassays were performed in triplicate. [b]EC_{50} values determined by testing peptides over a range of concentrations. [c]95% confidence interval. [d]Percent helicity determined from CD spectra in 20% TFE using the absorbance at 222 nm [32]. [e]EC_{50} not determined due to the analog's low induction in primary agonism screening assay.

hydroxy group (Phe → Tyr) resulted in a 33-fold reduction in potency, providing further support regarding the specificity of the binding pocket, specifically with regards to electronic/polar effects. The eighth position exhibited an interesting trend where truncation of the side-chain (Phe → Phg) was not tolerated (>80-fold reduction in potency) while elongation of the chain (Phe → hPhe) resulted in only a modest reduction in potency (4-fold change; Table 1). In this case, even the addition of a polar hydroxy moiety (Phe → Tyr) was relatively tolerated, resulting in an 8-fold reduction in potency. Together, these results suggest that the binding pocket for the eighth residue is not as optimally occupied as the one for the seventh residue. An identical trend to the 8th residue was also observed for the 11th residue, with only modest variations in potencies (Table 1). Combined, these results suggest that the binding pockets for the aromatic residues are mostly occupied and the benzene ring must be far enough from the CSP backbone in order to maintain helicity (see Structural Analysis below) and effectively interact with the binding pocket. Thus, pending no unexpected enhancement from isosteric substitutions (e.g., pyridylalanine, cyclohexylalanine, etc.), they are likely not ideal positions for further optimization.

With regards to the ComD2 receptor, since we performed highly-conservative mutations to the CSP1 scaffold, we did not expect significant changes in potencies against the ComD2 receptor, compared to CSP1. Indeed, most of the analogs exhibited similar activities to CSP1 against ComD2 (Table 1; <2-fold change). Interestingly, two mutations were not tolerable and resulted in significant loss of activity: These were Phe → Tyr for positions 7, 8 and 11, as well as Leu/Ile → Val for positions 4, 12 and 13. The valine substitution results are in agreement with the trend observed for the ComD1 receptor and further highlight the importance of the chain-length for effective binding, while the tyrosine substitution results suggest that the binding pockets within the ComD2 receptor cannot accommodate polar/electron-rich substituents.

Structural analysis of CSP1 analogs

Next, we wanted to assess the impact our modifications to the CSP1 scaffold had on its conformation. We utilized circular dichroism (CD) spectroscopy to evaluate the main structural motifs of the different analogs. Since only conserved modifications were introduced to the CSP1 sequence, we did not expect significant changes to the overall structural characteristics. Indeed, all the analogs exhibited α-helix CD spectra in membrane mimicking conditions (20% trifluoroethanol (TFE) in PBS buffer; Figure S4, Supporting Information File 1). Quantification of the helix content using both the mean residue ellipticity at 222 nm [32] and the BeStSel method [33] yielded similar trends (Table S2, Supporting Information File 1). Importantly, the two analogs that exhibited the lowest percent helicity, CSP1-F8FG and CSP1-F11FG, were the least active analogs against the ComD1 receptor (Table 1), supporting the hypothesis that an α-helix is required for effective ComD1 binding.

A helical wheel representation of the CSP1 sequence revealed that, with the exception of L13, all the residues discussed above (4, 7, 8, 11 and 12) occupy the same face of the helix (Figure 4). This result suggests that only one face of the CSP1 helix is directly interacting with the ComD1 receptor. Interestingly, L13 is predicted to be positioned on the opposite face of the helix, away from the proposed binding interface between CSP1 and ComD1. It is therefore not clear why this residue was found to be important for effective receptor binding. In-depth structural analysis of CSP1 in membrane mimicking conditions using NMR revealed that CSP1 adopts a kinked α-helix conformation, pointing the Leu13 side-chain more closely to the other hydrophobic side-chain residues than predicted by the helical wheel diagram (Yang et al. unpublished results). The kinked α-helix conformation may explain the importance of Leu13 in receptor binding. Alternatively, since the ComD receptors are predicted to dimerize upon activation, Leu13 may have a role in stabilizing the dimerization process prior to phosphorylating the response regulator, ComE. Lastly, it is possible that CSP1 interacts with the ComD1 receptor using more than just a single helical face. Additional structural studies are needed to test these hypotheses and conclusively determine the role of Leu13 in ComD1 binding and activation.

Conclusion

In conclusion, we incorporated highly conservative point mutations to the CSP1 sequence in order to define the hydrophobic binding pockets within the ComD1 receptor. Our analysis revealed that the binding pockets of the 4th, 12th and 13th positions in CSP1 are likely not optimally occupied by the current side-chain residues and can thus be the focus for optimization in order to obtain more potent CSP-based QS modulators. Our analysis also revealed that the binding pockets of the aromatic side-chains in CSP1 are likely optimally occupied by the current residues (Phe) and should thus be retained to maintain high affinity to the ComD1 receptor. Lastly, structural analysis using CD spectroscopy of the CSP1 analogs provided additional support that an α-helix conformation is required for effective ComD1 binding by CSP1. We believe that the insights revealed in this study are valuable to the development of highly potent CSP-based QS modulators with enhanced pharmacological properties.

Materials and Methods

Chemical reagents and instrumentation. All chemical reagents and solvents were purchased from Sigma-Aldrich and

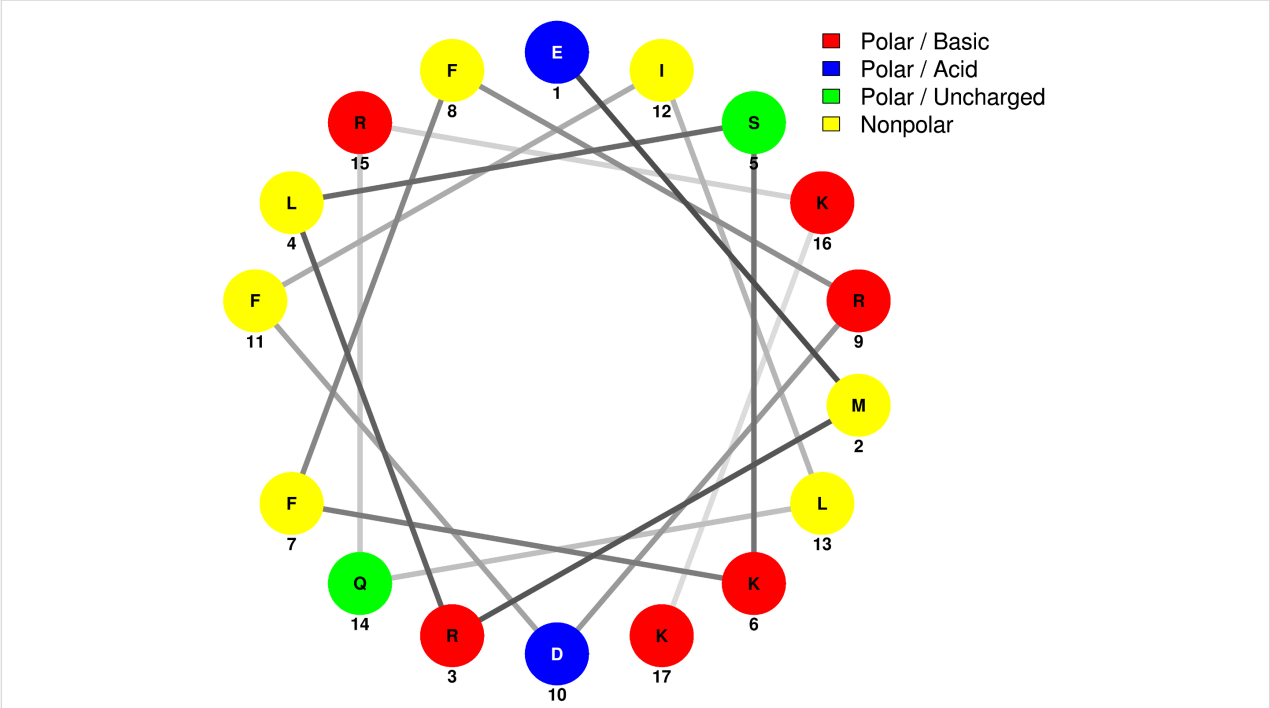

Figure 4: Helical wheel representation of CSP1. The CSP1 residues are presented using the one-letter amino acid code. The presentation reveals that, with the exception of L13, all the hydrophobic residues occupy the same face of the helix. Image produced using the NetWheels application (http://lbqp.unb.br/NetWheels/).

used without further purification. Water (18 MΩ) was purified using a Millipore Analyzer Feed System. Solid-phase resins were purchased from Chem-Impex or P3 Biosystems.

Reversed-phase high-performance liquid chromatography (RP-HPLC) was performed using two Shimadzu systems each equipped with a CBM-20A communications bus module, two LC-20AT pumps, an SIL-20A auto sampler, an SPD-20A UV–vis detector, a CTO-20A column oven, one with an FRC-10A fraction collector and one without. Matrix-assisted laser desorption ionization time-of-flight mass spectrometry (MALDI–TOF MS) data were obtained on either a Bruker Autoflex or Bruker Microflex spectrometer equipped with a 60 Hz nitrogen laser and a reflectron. In positive ion mode, the acceleration voltage on Ion Source 1 was 19.01 kV. Exact mass (EM) data were obtained on an Agilent Technologies 6230 TOF LC/MS spectrometer. The samples were sprayed with a capillary voltage of 3500 V and the electrospray ionization (ESI) source parameters were as follows: gas temperature of 325 °C at a drying gas flow rate of 3 L/min at a pressure of 25 psi.

Peptide synthesis. All the CSP1 analogs were synthesized on a 4-benzyloxybenzyl alcohol (Wang) resin (0.65 mmol/g) pre-loaded with Fmoc-L-Lys(Boc). With the exception of the phenylglycine and norvaline derivatives, the CSP1 analogs were synthesized using standard Fmoc-based solid-phase peptide synthesis (SPPS) procedures [34]. Phenylglycine and norvaline derivatives were prepared on a CEM Discover microwave synthesizer, with diisopropyl carbodiimide (DIC) as the coupling reagent along with Oxyma Pure. The ratio of DIC:Oxyma Pure:AA was 3.6:3:3 dissolved in *N*,*N*-dimethylformamide (DMF) for a final DIC concentration of 0.2 M. Reactions were run at 50 W at a temperature of 75 °C for 8 minutes, followed by 2 × 3 min deprotection with 20% piperidine in DMF.

Peptide purification. Crude peptides were purified with RP-HPLC. The crude peptide was dissolved in ACN/H_2O (1:4) and purified in 2.0–2.4 mL portions on either a Phenomenex Luna (5 µm, 10 mm, 150 mm, 100 Å) C18 column or a Phenomenex Kinetex (5 µm, 10 mm, 250 mm, 110 Å) C18 column with a flow rate of 5 mL/min; mobile phase A = 18 MΩ water + 0.1% TFA and mobile phase B = ACN + 0.1% TFA. The collected fraction was lyophilized overnight and dissolved again in ACN/H_2O (1:4) for a second prep run. Preparative HPLC methods were used to separate the crude peptide mixture to different chemical components using a linear gradient (first prep 15% B → 45% B over 30 min and second prep 25% B → 35% B over 30 min) as described in [19]. Then, either an analytical Phenomenex Luna C18 column (5 µm, 4.6 mm, 150 mm, 100 Å) or an analytical Phenomenex Kinetex C18 column (5 µm, 4.6 mm, 250 mm, 110 Å) was used to quantify the purity of the desired fraction using a linear gradient

(5% B → 95% B over 22 min or 27 min, respectively). Purities were determined by integration of peaks with UV detection at 220 nm. Only peptide fractions that were purified to homogeneity (>95%) were used for the biological assays. TOF-MS was used to validate the presence of synthesized peptides. The observed mass-to-charge (*m*/*z*) ratio of the peptide was compared to the expected *m*/*z* ratio for each peptide (see Table S1, Supporting Information File 1).

Biological reagents and strain information. All standard biological reagents were purchased from Sigma-Aldrich and used according to enclosed instructions. Donor horse serum (defibrinated) was purchased from Sigma-Aldrich and stored at 4 °C until use in bacterial growth conditions.

To examine the ability of the synthesized CSP analogs to modulate the ComD receptors, and thus the QS circuit in *S. pneumoniae*, β-galactosidase assays were performed using D39pcomX::lacZ (group I) and TIGR4pcomX::lacZ (group II) reporter strains as described in [19].

Bacterial growth conditions. Bacteria from a freezer stock were grown as described in [19]. Briefly, the bacteria were streaked into a THY agar plate supplemented with 5% donor horse serum and chloramphenicol at a final concentration of 4 μg/mL. The plate was incubated for 8 h in a CO_2 incubator (37 °C with 5% CO_2). Fresh colonies (single colony for D39pcomX::lacZ; multiple colonies for TIGR4pcomX::lacZ) were picked into sterilized cultural tubes containing 5 mL of THY broth supplemented with chloramphenicol at a final concentration of 4 μg/mL and the cultures were incubated in a CO_2 incubator overnight (15 h). Overnight cultures were then diluted (1:50 for D39pcomX::lacZ; 1:10 for TIGR4pcomX::lacZ) with THY and the resulting solution was incubated in a CO_2 incubator for 3–4 hours, until the bacteria reached early exponential stage (0.30–0.35 for D39pcomX::lacZ; 0.20–0.25 for TIGR4pcomX::lacZ) as determined by using a plate reader.

β-Galactosidase assay. Activation assays. The ability of synthetic CSP1 analogs to activate the expression of *comX* was determined using reporter strains grown in THY as described in [19]. Briefly, an initial activation screening was performed at high concentration (10 μM) for all CSP analogs. 2 μL of 1 mM solution of CSP analogs in dimethyl sulfoxide (DMSO) were added in triplicate to a clear 96-well microtiter plate. 2 μL of 20 μM solution of CSP1 were added in triplicate and served as the positive control for the group I strain (D39pcomX::lacZ), while 2 μL of 100 μM solution of CSP2 were added as the positive control for the group II strain (TIGR4pcomX::lacZ). These concentrations were chosen to afford full activation of the QS circuit, as determined from the dose-dependent curves created for the native CSPs. 2 μL of DMSO was added in triplicate and served as the negative control for both groups. Then, 198 μL of bacterial culture was added to each well containing CSP and analogs, the plate was incubated at 37 ºC for 30 minutes, and the OD_{600nm} was measured. In order to measure the β-galactosidase activity in the pneumococcal culture, the cells were lysed by incubating the culture for 30 minutes at 37 °C with 20 μL of 0.1% Triton X-100. In a new plate, 100 μL of Z-buffer solution (60.2 mM Na_2HPO_4, 45.8 mM NaH_2PO_4, 10 mM KCl, and 1.0 mM $MgSO_4$ in 18 MΩ H_2O; pH was adjusted to 7.0 and the buffer was sterilized before use) containing 2-nitrophenyl-β-D-galactopyranoside (ONPG) at a final concentration of 0.4 mg/mL was added, followed by 100 μL of lysate, and the plate was incubated for 3 hours at 37 ºC. The reaction was stopped by adding 50 μL of 1 M sodium carbonate solution, and the OD_{420nm} and OD_{550nm} were measured using a plate reader. The final results were reported as percent activation, which is the ratio between the Miller units of the analog and of the positive control. For calculation of Miller units, please see data analysis below. Analogs that exhibited high activity in the initial screening (see Figures S1 and S2, Supporting Information File 1) were further evaluated using a dose-dependent assay in which peptide stock solutions were diluted with DMSO in serial dilutions (either 1:2, 1:3, or 1:5) and assayed as described above. GraphPad Prism 5 was used to calculate the EC_{50} values, which are the concentration of a drug that gives half-maximal response.

Inhibition assays. Analogs that exhibited low *comX* activation in the initial screening (see Figure S2, Supporting Information File 1) were evaluated for competitive inhibition as described in [19]. Briefly, the ability of synthesized CSP analogs to inhibit the expression of *comX* by outcompeting CSP for the receptor binding site was evaluated using the same assay conditions as described above, except that in this case native CSP (for this purpose, CSP2) was added to every well in a set concentration (250 nM). This concentration was chosen to afford full activation of the QS circuit, as determined from the dose-dependent curves created for the native CSPs. 2 μL of a native CSP (25 μM solution) and 2 μL of a 1 mM solution of each CSP analog were added to the same well in triplicate in a clear 96-well microtiter plate. 2 μL of native CSP (25 μM solution) and 2 μL of DMSO were added to the same well in triplicate and served as the positive control. 4 μL of DMSO was added in triplicate and served as the negative control. Then, 196 μL of bacterial culture was added to the wells and the plate was incubated at 37 ºC for 30 minutes. The procedure for lysis, incubation with ONPG and all the measurements were as described in the activation assay. None of the analogs exhibited significant competitive inhibition in the initial screening (Figure S3, Supporting Information File 1).

Analysis of activation/inhibition data. Miller units were calculated using the following formula:

$$\text{Miller Unit} = 1000 \times \frac{\left[\text{Abs}_{420} - \left(1.75 \times \text{Abs}_{550}\right)\right]}{\left(t \times v \times \text{Abs}_{600}\right)}$$

Abs_{420} is the absorbance of *ortho*-nitrophenol (ONP). Abs_{550} is the scatter from cell debris, which, when multiplied by 1.75 approximates the scatter observed at 420 nm. t is the duration of incubation with ONPG in minutes, v is volume of lysate in milliliters, and Abs_{600} reflects cell density.

Circular dichroism (CD) spectroscopy. CD spectra were recorded with an Aviv Biomedical CD spectrometer (model 202-01) as described in [19]. Briefly, all the measurements were performed with a peptide concentration of 200 μM in PBS buffer (137 mM NaCl, 2.7 mM KCl, 10 mM Na_2HPO_4, 1.8 mM KH_2PO_4; pH was adjusted to 7.4) with 20% trifluoroethanol (TFE). Measurements were performed at 25 ºC with a quartz cuvette (science outlet) with a path length of 0.1 cm. Samples were scanned one time at 3 nm min^{-1} with a bandwidth of 1 nm and a response time of 20 s over a wavelength range (195 to 260 nm). Percent helicity (f_H) was calculated for all peptides using the following equation:

$$f_H = \frac{[\theta]_{222}}{[\theta_\infty]_{222}\left(1 - \frac{x}{n}\right)}$$

$[\theta]_{222}$ is the mean residue ellipticity of the sample peptide at 222 nm, $[\theta_\infty]_{222}$ is the mean residue ellipticity of an ideal peptide with 100% helicity (−44,000 deg cm^2 $dmol^{-1}$) [32], n is the number of residues in the potential helical region, and x is an empirical correction for end effects (2.5) [32]. Secondary structure contents were also calculated using the BeStSel (beta structure selection) method (http://bestsel.elte.hu/) [33].

Supporting Information

Supporting Information File 1

Full details of peptide characterization, initial screening results, dose response curves for CSP1 analogs, and CD spectra of all the CSP1 analogs.
[https://www.beilstein-journals.org/bjoc/content/supplementary/1860-5397-14-151-S1.pdf]

Acknowledgements

This work was supported by the Nevada INBRE through a grant from the National Institute of General Medical Sciences (GM103440) from the National Institutes of Health (NIH). *S. pneumoniae* D39pcomX::lacZ and TIGR4pcomX::lacZ reporter strains were generous gifts from G. W. Lau (University of Illinois at Urbana−Champaign). We would also like to thank M. J. Tucker (University of Nevada, Reno) for the use of the CD spectrometer and R. W. Mull for assistance with creating the figures in the paper.

ORCID® iDs

Bimal Koirala - https://orcid.org/0000-0003-1806-7935
Michael A. Bertucci - https://orcid.org/0000-0002-5421-7059
Yftah Tal-Gan - https://orcid.org/0000-0003-2052-6782

References

1. Bassler, B. L.; Losick, R. *Cell* **2006,** *125,* 237–246. doi:10.1016/j.cell.2006.04.001
2. Camilli, A.; Bassler, B. L. *Science* **2006,** *311,* 1113–1116. doi:10.1126/science.1121357
3. Ng, W.-L.; Bassler, B. L. *Annu. Rev. Genet.* **2009,** *43,* 197–222. doi:10.1146/annurev-genet-102108-134304
4. Parsek, M. R.; Greenberg, E. *Trends Microbiol.* **2005,** *13,* 27–33. doi:10.1016/j.tim.2004.11.007
5. Palmer, A. G.; Mukherjee, A.; Stacy, D. M.; Lazar, S.; Ané, J.-M.; Blackwell, H. E. *ChemBioChem* **2016,** *17,* 2199–2205. doi:10.1002/cbic.201600373
6. Rasko, D. A.; Sperandio, V. *Nat. Rev. Drug Discovery* **2010,** *9,* 117–128. doi:10.1038/nrd3013
7. Rutherford, S. T.; Bassler, B. L. *Cold Spring Harbor Perspect. Med.* **2012,** *2,* a012427. doi:10.1101/cshperspect.a012427
8. Welsh, M. A.; Blackwell, H. E. *FEMS Microbiol. Rev.* **2016,** *40,* 774–794. doi:10.1093/femsre/fuw009
9. Galloway, W. R. J. D.; Hodgkinson, J. T.; Bowden, S. D.; Welch, M.; Spring, D. R. *Chem. Rev.* **2011,** *111,* 28–67. doi:10.1021/cr100109t
10. Amara, N.; Krom, B. P.; Kaufmann, G. F.; Meijler, M. M. *Chem. Rev.* **2011,** *111,* 195–208. doi:10.1021/cr100101c
11. Wang, B.; Muir, T. *Cell Chem. Biol.* **2016,** *23,* 214–224. doi:10.1016/j.chembiol.2016.01.004
12. Tal-Gan, Y.; Stacy, D. M.; Foegen, M. K.; Koenig, D. W.; Blackwell, H. E. *J. Am. Chem. Soc.* **2013,** *135,* 7869–7882. doi:10.1021/ja3112115
13. Tal-Gan, Y.; Ivancic, M.; Cornilescu, G.; Yang, T.; Blackwell, H. E. *Angew. Chem., Int. Ed.* **2016,** *55,* 8913–8917. doi:10.1002/anie.201602974
14. Gordon, C. P.; Williams, P.; Chan, W. C. *J. Med. Chem.* **2013,** *56,* 1389–1404. doi:10.1021/jm3014635
15. Tal-Gan, Y.; Ivancic, M.; Cornilescu, G.; Cornilescu, C. C.; Blackwell, H. E. *J. Am. Chem. Soc.* **2013,** *135,* 18436–18444. doi:10.1021/ja407533e
16. Novick, R. P.; Geisinger, E. *Annu. Rev. Genet.* **2008,** *42,* 541–564. doi:10.1146/annurev.genet.42.110807.091640
17. McBrayer, D. N.; Gantman, B. K.; Cameron, C. D.; Tal-Gan, Y. *Org. Lett.* **2017,** *19,* 3295–3298. doi:10.1021/acs.orglett.7b01444
18. Harrington, A.; Tal-Gan, Y. *J. Bacteriol.* **2018,** *200,* e00709–17. doi:10.1128/jb.00709-17
19. Yang, Y.; Koirala, B.; Sanchez, L. A.; Phillips, N. R.; Hamry, S. R.; Tal-Gan, Y. *ACS Chem. Biol.* **2017,** *12,* 1141–1151. doi:10.1021/acschembio.7b00007

20. Mehr, S.; Wood, N. *Paediatr. Respir. Rev.* **2012,** *13,* 258–264. doi:10.1016/j.prrv.2011.12.001
21. Huang, S. S.; Johnson, K. M.; Ray, G. T.; Wroe, P.; Lieu, T. A.; Moore, M. R.; Zell, E. R.; Linder, J. A.; Grijalva, C. G.; Metlay, J. P.; Finkelstein, J. A. *Vaccine* **2011,** *29,* 3398–3412. doi:10.1016/j.vaccine.2011.02.088
22. Pestova, E. V.; Håvarstein, L. S.; Morrison, D. A. *Mol. Microbiol.* **1996,** *21,* 853–862. doi:10.1046/j.1365-2958.1996.501417.x
23. Håvarstein, L. S.; Coomaraswamy, G.; Morrison, D. A. *Proc. Natl. Acad. Sci. U. S. A.* **1995,** *92,* 11140–11144. doi:10.1073/pnas.92.24.11140
24. Lau, G. W.; Haataja, S.; Lonetto, M.; Kensit, S. E.; Marra, A.; Bryant, A. P.; McDevitt, D.; Morrison, D. A.; Holden, D. W. *Mol. Microbiol.* **2001,** *40,* 555–571. doi:10.1046/j.1365-2958.2001.02335.x
25. Hava, D. L.; Camilli, A. *Mol. Microbiol.* **2002,** *45,* 1389–1406. doi:10.1046/j.1365-2958.2002.03106.x
26. Oggioni, M. R.; Trappetti, C.; Kadioglu, A.; Cassone, M.; Iannelli, F.; Ricci, S.; Andrew, P. W.; Pozzi, G. *Mol. Microbiol.* **2006,** *61,* 1196–1210. doi:10.1111/j.1365-2958.2006.05310.x
27. Zhu, L.; Lin, J.; Kuang, Z.; Vidal, J. E.; Lau, G. W. *Mol. Microbiol.* **2015,** *97,* 151–165. doi:10.1111/mmi.13016
28. Pozzi, G.; Masala, L.; Iannelli, F.; Manganelli, R.; Havarstein, L. S.; Piccoli, L.; Simon, D.; Morrison, D. A. *J. Bacteriol.* **1996,** *178,* 6087–6090. doi:10.1128/jb.178.20.6087-6090.1996
29. Johnsborg, O.; Kristiansen, P. E.; Blomqvist, T.; Havarstein, L. S. *J. Bacteriol.* **2006,** *188,* 1744–1749. doi:10.1128/jb.188.5.1744-1749.2006
30. Rooklin, D.; Modell, A. E.; Li, H.; Berdan, V.; Arora, P. S.; Zhang, Y. *J. Am. Chem. Soc.* **2017,** *139,* 15560–15563. doi:10.1021/jacs.7b05960
31. Zhu, L.; Lau, G. W. *PLoS Pathog.* **2011,** *7,* e1002241. doi:10.1371/journal.ppat.1002241
32. Luo, P.; Baldwin, R. L. *Biochemistry* **1997,** *36,* 8413–8421. doi:10.1021/bi9707133
33. Micsonai, A.; Wien, F.; Kernya, L.; Lee, Y. H.; Goto, Y.; Réfrégiers, M.; Kardos, J. *Proc. Natl. Acad. Sci. U. S. A.* **2015,** *112,* E3095–E3103. doi:10.1073/pnas.1500851112
34. Chan, W. C.; White, P. D. *Fmoc Solid Phase Peptide Synthesis;* Oxford University Press: Oxford, United Kingdom, 2000.

License and Terms

BEILSTEIN JOURNAL OF ORGANIC CHEMISTRY

Synthesis of a leopolic acid-inspired tetramic acid with antimicrobial activity against multidrug-resistant bacteria

Luce Mattio[1], Loana Musso[1], Leonardo Scaglioni[1], Andrea Pinto[1], Piera Anna Martino[2] and Sabrina Dallavalle[*1,§]

Letter

Open Access

Address:
[1]Department of Food, Environmental and Nutritional Sciences, Università degli Studi di Milano, via Celoria 2, I-20133 Milano, Italy and [2]Department of Veterinary Medicine - Microbiology and Immunology, Università degli Studi di Milano, via Celoria 10, I-20133 Milano, Italy

Email:
Sabrina Dallavalle[*] - sabrina.dallavalle@unimi.it

* Corresponding author
§ Tel. +39 0250316818; Fax +39 0250316801

Keywords:
antimicrobial activity; multidrug-resistant bacteria; natural products; synthesis; tetramic acid

Beilstein J. Org. Chem. **2018,** *14,* 2482–2487.
doi:10.3762/bjoc.14.224

Received: 13 July 2018
Accepted: 04 September 2018
Published: 24 September 2018

This article is part of the thematic issue "Antibacterials, bacterial small molecule interactions and quorum sensing".

Guest Editor: D. Spring

Abstract

The increasing emergence of multidrug-resistant pathogens is one of the biggest threats to human health and food security. The discovery of new antibacterials, and in particular the finding of new scaffolds, is an imperative goal to stay ahead of the evolution of antibiotic resistance. Herein we report the synthesis of a 3-decyltetramic acid analogue of the ureido dipeptide natural antibiotic leopolic acid A. The key step in the synthetic strategy is an intramolecular Lacey–Dieckmann cyclization reaction of a linear precursor to obtain the desired 3-alkyl-substituted tetramic acid core. The synthesized analogue is more effective than the parent leopolic acid A against Gram-positive (*Staphylococcus pseudintermedius*) and Gram-negative (*E. coli*) bacteria (MIC 8 μg/mL and 64 μg/mL, respectively). Interestingly, the compound shows a significant activity against *Staphylococcus pseudintermedius* strains expressing a multidrug-resistant phenotype (average MIC 32 μg/mL on 30 strains tested). These results suggest that this molecule can be considered a promising starting point for the development of a novel class of antibacterial agents active also against resistant strains.

Introduction

The treatment of bacterial infections by antibiotics is widely regarded as one of the major achievements of the 20th century. However, the continued emergence of multidrug-resistant bacteria, mainly due to the abuse of antimicrobial molecules (e.g., for treatment of bacterial skin diseases [1]), emphasises the urgent need for novel antibiotic families. In this regard,

natural products are privileged compounds, as they possess biologically validated structures, which could become suitable leads in drug discovery [2].

Recently, our research group reported the first total synthesis of leopolic acid A (Figure 1), a fungal metabolite from a terrestrial-derived *Streptomyces sp*. isolated from the rhizosphere of the plant *Juniperus excelsa* [3,4]. Leopolic acid A is endowed with antibacterial activity against *Staphylococcus aureus* and *Staphylococcus pseudintermedius* with a MIC of 16 μg/mL, and against *Escherichia coli* with a MIC of 128 μg/mL [3,4]. In terms of structural features, this compound contains a 4-decyl-2,3-pyrrolidinedione ring linked to the ureido dipeptide L-Phe-L-Val. The 2,3-pyrrolidinedione ring is a quite unusual skeleton. A limited number of compounds containing this system have been synthesized so far [5-7] and, to the best of our knowledge, natural compounds with a 2,3-pyrrolidinedione nucleus are quite rare [8-11]. The lack of similar compounds may be due to the instability of the 2,3 pyrrolidinedione moiety [12]. Indeed, while developing the total synthesis of leopolic acid A, we encountered several difficulties in the construction of the ring, most of the intermediates being unstable [4].

In light of these results, we intended to investigate the role of the 2,3 pyrrolidinedione ring by replacing it with a more stable isomeric 2,4-pyrrolidinedione moiety. Actually, 2,4 pyrrolidinediones (tetramic acids) have recently attracted considerable attention for their antibacterial, antiviral, antifungal and anticancer activities [13]. More than one hundred of them have been isolated from a variety of natural sources and numerous analogues have been synthesized and studied for their multiple biological activities [13]. For this reason, we planned the synthesis of a leopolic acid A analogue containing the tetramic acid moiety in place of the 2,3-pyrrolidinone ring (compound **1**), while maintaining unchanged all the other structural features of the natural compound. The advantage of this substitution should be a higher stability of the heterocyclic ring, hopefully coupled with an increased activity due to the presence of the tetramic acid core.

In this paper we report the efforts made to develop a synthetic strategy to compound **1**, which may, in principle, have a value in the preparation of various analogues for structure–activity relationship (SAR) studies. The antibacterial activity of compound **1** was tested on *Staphylococcus pseudintermedius* and *Escherichia coli* strains chosen as representative of Gram-positive and Gram-negative bacteria. In particular, we demonstrated the ability of compound **1** to inhibit *Staphylococcus pseudintermedius* strains expressing a multidrug-resistant phenotype.

Results and Discussion

The instability of most of the *N*-unsubstituted 2,3-pyrrolidinediones prepared for the construction of leopolic acid A [4] forced us to develop a linear synthetic strategy consisting of 11 steps, not amenable for the preparation of analogues. Conversely, compound **1** appears well suited to a convergent synthetic approach based around two fragments, the ureido dipeptide L-Phe-L-Val and the 3-decyltetramic acid core (Figure 1).

Initially, we focused on the synthesis of the 2,4-pyrrolidinedione core. A review of the existing literature on tetramic acids syntheses revealed a considerable amount of papers regarding the preparation of 3-acyltetramic acids [14-18], whereas the synthesis of 3-alkyl-tetramic acids has been considerably less investigated [19-22]. We envisaged that the most straightforward route to the 2,4-pyrrolidinedione system could be a Lacey–Dieckmann cyclization starting from a *N*-acetoacetyl-α-amino ester. Interestingly, the biosynthetic pathways of the tetramic acid scaffold involves Lacey–Dieckmann cyclases [23] or a spontaneous intramolecular Claisen condensation, which occurs in the cytosol. To protect the α-amino ester nitrogen we chose the *p*-methoxybenzyl (PMB) group, easily removable by ceric ammonium nitrate (CAN). *N*-(4-Methoxybenzyl)glycine ethyl ester (**5**) was obtained in 87% yield by reacting 4-methoxybenzylamine (**3**) with bromoacetic acid ethyl ester (**4**) in THF (Scheme 1). The ester **5** was converted into compounds **6a** and **6b** by condensation with monoethyl malonate and monobenzyl malonate, in the presence of DCC and DMAP,

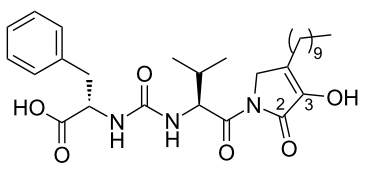

leopolic acid A

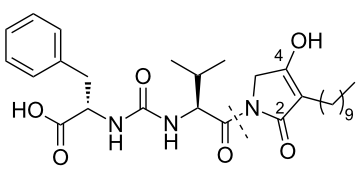

1

Figure 1: Structures of leopolic acid A and compound **1**.

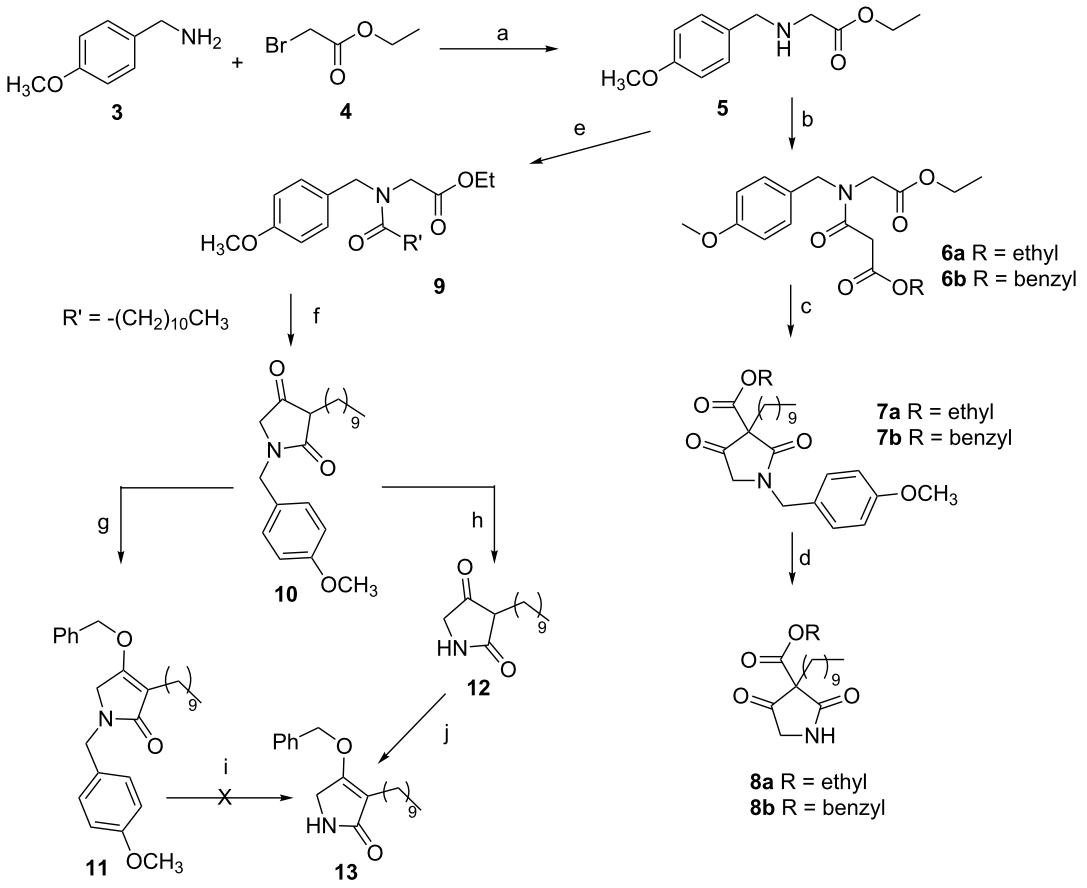

Scheme 1: Synthesis of 3-decyltetramic intermediate **13**. Reagent and conditions: a) TEA, THF, 0 °C to rt, 2.5 h, 87%; b) monoethyl malonate (for **6a**), monobenzyl malonate (for **6b**), DCC, DMAP, CH_2Cl_2, 0 °C to rt, 24 h (for **6a**), 12 h (for **6b**), **6a**: 80%, **6b**: 83%; c) TBAF, Et_2O, THF, 1-iododecane, rt, 24 h, **7a**: 22%, **7b**: 30%; d) CAN, CH_3CN/H_2O (3:1), 0 °C to rt, 1 h, **8a**: 81%, **8b**: 66%; e) dodecanoyl chloride, TEA, $CHCl_3$, 0 °C to rt, 3 h, 90%; f) *t*-BuOK 1 M in THF, THF, reflux, 1.5 h, 65%; g) benzyl tosylate, KHMDS 0.5 M in toluene, crown ether 18-crown-6, THF, 0 °C to rt, 3 h, 35%; h) TFA, 60 °C, 2h; i) CAN, CH_3CN/H_2O (3:1), 0 °C to rt, 1h; j) benzyl tosylate, KHMDS 0.5 M in toluene, crown ether 18-crown-6, THF, 0 °C to rt, 2.5 h, 30% over two steps.

in 80% and 83% yield, respectively. Starting from intermediates **6a** and **6b**, treatment with a tetrabutylammonium fluoride solution in diethyl ether at room temperature induced the cyclisation and the formation of an enolate, which was subsequently reacted with 1-iododecane and deprotected with ceric ammonium nitrate to afford derivatives **8a** and **8b**, respectively. Unfortunately, at this stage all attempts to decarboxylate compounds **8a** and **8b** failed [22]. To overcome the problem of decarboxylation, we planned to synthesize the alkyl-substituted tetramic core in one single step by Lacey–Dieckmann cyclisation of ethyl 2-(*N*-(4-methoxybenzyl)dodecanoylamino)acetate (**9**), although this compound does not contain an active methylene group. Thus, compound **5** was acylated with dodecanoyl chloride to obtain compound **9** in 90% yield. As expected, the cyclization reaction was found to be quite troublesome. Several attempts were made using different conditions (TBAF, Et_2O, rt; NaOEt, EtOH, reflux; NaH, THF, reflux; LDA, THF, −78 °C), but they all were unsuccessful. Finally, we succeeded in preparing intermediate **10** by treatment of compound **9** with potassium *tert*-butoxide (1 M in THF) in THF [24]. The optimisation of reaction conditions, work-up and purification, allowed us to obtain the desired compound in 65% yield.

Before removing the PMB group and installing the ureidodipeptide fragment, we needed to protect the oxygen at C-4 [15]. We selected a benzyl protecting group, as it could be cleaved by catalytic hydrogenation together with the benzyl ester of L-phenylalanine in the ureidodipeptide fragment (see synthesis of compound **20**) by a one-pot reaction. To increase the reaction rate toward *O*-alkylation, we used an aprotic polar solvent like DMF, which weakly solvates the enolates. However, treatment of compound **10** with benzyl bromide and K_2CO_3 in DMF gave exclusively the C-3 alkylated derivative. Thus, we considered that a hard leaving group such as a sulfonate should play a

key role in favouring *O*-alkylation. Moreover, we selected a base containing potassium as a metal cation, which provides a greater electron density to the nucleophilic enolate, thus favouring *O*-alkylation. Satisfyingly, O-selective alkylation of compound **10** was achieved by deprotonation with KHMDS followed by alkylation with benzyl tosylate in the presence of 18-crown-6 ether [15]. The synthesis of benzyl tosylate was accomplished using benzyl alcohol and freshly recrystallized *p*-toluenesulfonyl chloride in the presence of anhydrous trimethylamine and DMAP, in anhydrous dichloromethane [25].

At this stage, all attempts to obtain the key intermediate **13** removing the *p*-methoxybenzyl group [24,26-28] from **11** failed. Finally, compound **13** was successfully obtained by modifying the sequence of reactions. Deprotection of compound **10** with TFA [24], followed by selective alkylation with benzyl tosylate as previously described, afforded the desired *O*-alkyltetramic acid **13** in 30% yield.

The synthesis of the activated ureido fragment was achieved in four steps from suitably protected L-valine and L-phenylalanine. The benzyl protection of L-phenylalanine (**14**) was carried out with PTSA and benzyl alcohol in toluene and the ester **15** was isolated as its *p*-toluensulfonic acid salt by recrystallization with Et_2O in 70% yield (Scheme 2). L-valine (**16**) was protected as *tert*-butyl ester **17** by using perchloric acid in *t*-BuOAc in 75% yield. The unsymmetrical urea **18** was synthesized using triphosgene at room temperature in 50% yield. The *tert*-butyl ester was easily cleaved by trifluoroacetic acid in DCM at room temperature to furnish the corresponding acid **19** (yield 95%), which was activated by pentafluorophenol, DCC in EtOAc to give the pentafluorophenylester ureido-dipeptide **20** (60%, Scheme 2).

With both key fragments **13** and **20** in hand, we finally accomplished the *N*-acylation reaction using *n*-BuLi in THF at −60 °C [15] in 60% yield. Removal of both protecting groups by catalytic hydrogenation, gave the desired compound **1** in 72% yield (Scheme 3).

Compound **1** was subjected to a preliminary study to evaluate the antimicrobial activity against 80 strains of *Staphylococcus pseudintermedius* and 25 strains of *Escherichia coli*. Bacterial isolates of *S. pseudintermedius* and *E. coli*, previously identified using selective and differential cultural media (e.g., Mannitol Salt Agar; MacConkey Agar, Oxoid, Italy), were isolated on blood agar plates (Tryptic Soy Agar plus 5% defibrinated sheep blood, Microbiol, Italy) to obtain pure cultures [29]. The isolated colonies were used to assess the phenotypic profile of antimicrobial resistance. For this purpose, the Kirby Bauer disk diffusion method was used in accordance to Clinical Laboratory Standards Institute guidelines [30]. All the strains were treated with a panel of antimicrobial molecules belonging to five pharmacological categories: amoxicillin + clavulanic acid, cephalexin, cefovecin, clindamycin, doxycycline, enrofloxacin and marbofloxacin. Only for *S. pseudintermedius* strains,

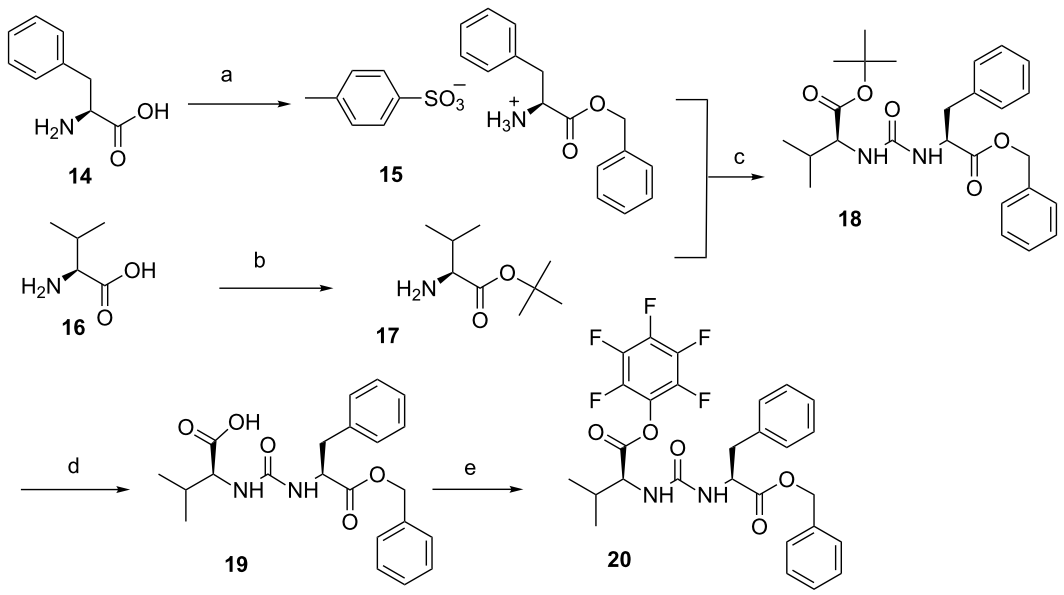

Scheme 2: Synthesis of dipeptide L-Phe-L-Val intermediate **20**. Reagents and conditions: a) PTSA·H_2O, benzyl alcohol, toluene, reflux, 10 h, 70%; b) $HClO_4$, *tert*-butyl acetate, 0 °C, 1 h, then rt, 20 h, 75%; c) triphosgene, DIEA, DCM, rt, 3 h, 50%; d) trifluoroacetic acid, DCM, rt, 3 h, 95%; e) pentafluorophenol, DCC, EtOAc, 0 °C, 1h, then rt, 3 h, 60%.

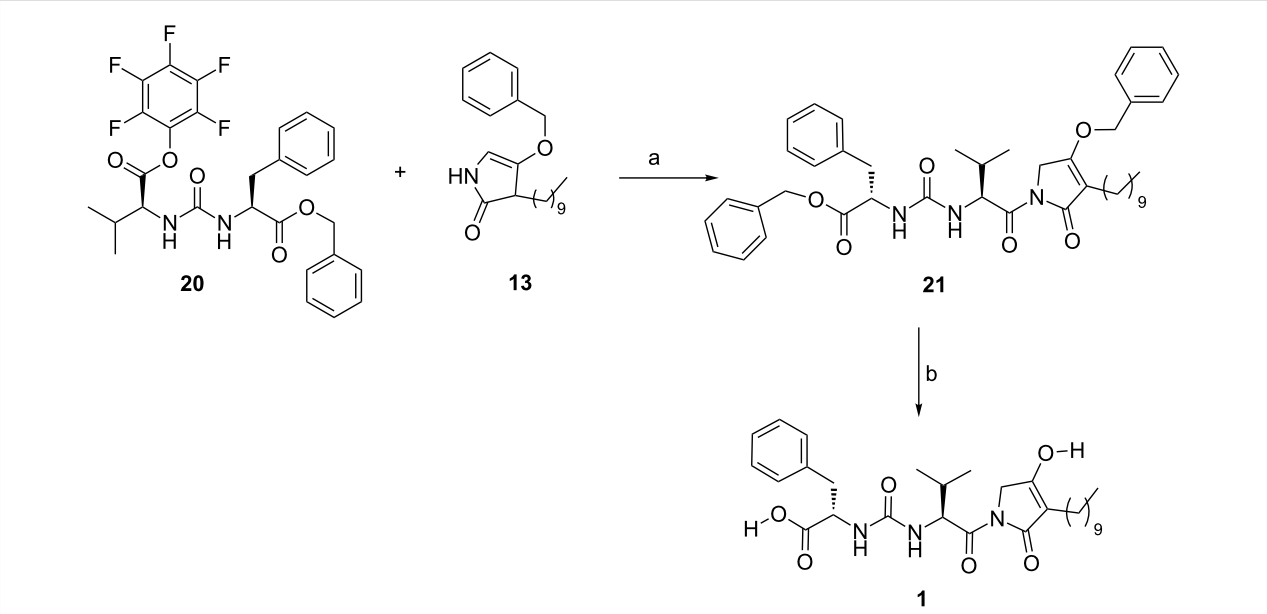

Scheme 3: Synthesis of compound **1**. Reagents and conditions: a) *n*-BuLi, THF, −60 °C, 220 min, 60%; b) H_2, Pd/C 10%, AcOEt, rt, 100 min, 72%.

oxacillin was also tested to assess methicillin-resistance (see Table S1, Supporting Information File 1, for details). After incubation, 30 strains of *S. pseudintermedius* revealed resistance phenoptype to three or more pharmacological categories and were considered multidrug resistant (MDR) [31]. MICs (minimum inhibitory concentrations) of compound **1** were evaluated on each bacterial strain (*E. coli* and *S. pseudintermedius* MDR or not) as reported by CLSI guidelines [30,32].

The average MIC values of **1** against 50 *Staphylococcus pseudintermedius* isolates were 8 μg/mL and versus *Escherichia coli* 64 μg/mL, lower than the MICs shown by the parent leopolic acid A (*Staphylococcus pseudintermedius* average MIC 16 μg/mL; *Escherichia coli* average MIC 128 μg/mL) [4]. Interestingly, compound **1** showed a significant activity also against *Staphylococcus pseudintermedius* strains expressing a multidrug-resistant phenotype (average MIC 32 μg/mL on 30 strains tested).

Conclusion

The development of novel strategies to fight bacterial infections is an imperative goal, mainly due to the increasing number of bacterial strains resistant to a wide spectrum of antibiotics. Aim of this work was the development of a synthetic strategy for obtaining new natural compound-derived scaffolds endowed with increased antimicrobial activity. Attention was focused on 2,4-pyrrolidinedione derivatives, so-called tetramic acids. As part of our search for new tetramic acid containing scaffolds, we have synthesized the 2,4-pyrrolidinone analogue of the natural compound leopolic acid A, by a convergent synthetic strategy. Compound **1** is more effective than the parent leopolic acid A against *Staphylococcus pseudintermedius* and *E. coli* strains (MIC 8 μg/mL and 64 μg/mL, respectively) and *Staphylococcus pseudintermedius* strains expressing a multidrug-resistant phenotype (average MIC 32 μg/mL on 30 strains tested). The results confirm that the replacement of the 2,3-pyrrolidinedione core with the tetramic acid nucleus leads to an increase of antimicrobial activity even on MDR strains, thus suggesting that the new scaffold can be considered as a promising candidate for further investigation. Efforts to synthesize analogues of compound **1** to deepen the structure–activity relationship (SAR) study of this novel class of antibacterial agents are underway.

Supporting Information

Supporting Information File 1

General experimental methods, synthetic procedures and analytical data for the reported compounds, antimicrobial activity evaluation procedures.
[https://www.beilstein-journals.org/bjoc/content/supplementary/1860-5397-14-224-S1.pdf]

Supporting Information File 2

^{1}H NMR and ^{13}C NMR spectra of the new compounds; COSY spectra of compounds **1**, **10**; HDMS spectra of compound **1**.
[https://www.beilstein-journals.org/bjoc/content/supplementary/1860-5397-14-224-S2.pdf]

ORCID® iDs

Luce Mattio - https://orcid.org/0000-0003-0955-3982
Loana Musso - https://orcid.org/0000-0002-6838-7753
Andrea Pinto - https://orcid.org/0000-0002-2501-3348
Piera Anna Martino - https://orcid.org/0000-0003-0108-638X
Sabrina Dallavalle - https://orcid.org/0000-0002-8813-8922

References

1. Zur, G.; Gurevich, B.; Elad, D. *Vet. Dermatol.* **2016,** *27,* 468–e125. doi:10.1111/vde.12382
2. Brown, D. G.; Lister, T.; May-Dracka, T. L. *Bioorg. Med. Chem. Lett.* **2014,** *24,* 413–418. doi:10.1016/j.bmcl.2013.12.059
3. Raju, R.; Gromyko, O.; Fedorenko, V.; Luzhetskyy, A.; Müller, R. *Tetrahedron Lett.* **2012,** *53,* 6300–6301. doi:10.1016/j.tetlet.2012.09.046
4. Dhavan, A. A.; Kaduskar, R. D.; Musso, L.; Scaglioni, L.; Martino, P. A.; Dallavalle, S. *Beilstein J. Org. Chem.* **2016,** *12,* 1624–1628. doi:10.3762/bjoc.12.159
5. Pace, P.; Spieser, S. A. H.; Summa, V. *Bioorg. Med. Chem. Lett.* **2008,** *18,* 3865–3869. doi:10.1016/j.bmcl.2008.06.056
6. Kawasuji, T.; Fuji, M.; Yoshinaga, T.; Sato, A.; Fujiwara, T.; Kiyama, R. *Bioorg. Med. Chem.* **2007,** *15,* 5487–5494. doi:10.1016/j.bmc.2007.05.052
7. Zhu, H.-L.; Ling, J.-B.; Xu, P.-F. *J. Org. Chem.* **2012,** *77,* 7737–7743. doi:10.1021/jo301192d
8. Tabussum, A.; Riaz, N.; Saleem, M.; Ashraf, M.; Ahmad, M.; Alam, U.; Jabeen, B.; Malik, A.; Jabbar, A. *Phytochem. Lett.* **2013,** *6,* 614–619. doi:10.1016/j.phytol.2013.08.005
9. Zuther, K.; Mayser, P.; Hettwer, U.; Wu, W.; Spiteller, P.; Kindler, B. L. J.; Karlovsky, P.; Basse, C. W.; Schirawski, J. *Mol. Microbiol.* **2008,** *68,* 152–172. doi:10.1111/j.1365-2958.2008.06144.x
10. El-Desouky, S. K.; Kim, K. H.; Ryu, S. Y.; Eweas, A. F.; Gamal-Eldeen, A. M.; Kim, Y.-K. *Arch. Pharmacal Res.* **2007,** *30,* 927–931. doi:10.1007/BF02993958
11. Badiola, E.; Olaizola, I.; Vázquez, A.; Vera, S.; Mielgo, A.; Palomo, C. *Chem. – Eur. J.* **2017,** *23,* 8185–8195. doi:10.1002/chem.201700464
12. Sundberg, R. J.; Pearce, B. C.; Laurino, J. P. *J. Heterocycl. Chem.* **1986,** *23,* 537–539. doi:10.1002/jhet.5570230245
13. Mo, X.; Li, Q.; Ju, J. *RSC Adv.* **2014,** *4,* 50566–50593. doi:10.1039/C4RA09047K
See for a recent review.
14. Jeong, Y.-C.; Moloney, M. G. *Synlett* **2009,** 2487–2491. doi:10.1055/s-0029-1217745
15. Hosseini, M.; Kringelum, H.; Murray, A.; Tønder, J. E. *Org. Lett.* **2006,** *8,* 2103–2106. doi:10.1021/ol060500i
16. Schobert, R. *Naturwissenschaften* **2007,** *94,* 1–11. doi:10.1007/s00114-006-0152-8
17. Detsi, A.; Micha-Screttas, M.; Ingglessi-Markopoulou, O. *J. Chem. Soc., Perkin Trans. 1* **1998,** 2443–2450. doi:10.1039/A801896K
18. Castellucci, N.; Gentilucci, L.; Tomasini, C. *Tetrahedron* **2012,** *68,* 4506–4512. doi:10.1016/j.tet.2011.11.006
19. Bai, W.-J.; Jackson, S. K.; Pettus, T. R. R. *Org. Lett.* **2012,** *15,* 3862–3865. doi:10.1021/ol301556a
20. Ishida, T.; Kobayashi, R.; Yamada, T. *Org. Lett.* **2014,** *16,* 2430–2433. doi:10.1021/ol500806u
21. Lan, H.-Q.; Ruan, Y.-P.; Huang, P.-Q. *Chem. Commun.* **2010,** *46,* 5319–5321. doi:10.1039/C0CC00452A
22. Page, P. C. B.; Hamzah, A. S.; Leach, D. C.; Allin, S. M.; Andrews, D. M.; Rassias, G. A. *Org. Lett.* **2003,** *5,* 353–355. doi:10.1021/ol027387q
23. Gui, C.; Li, Q.; Mo, X.; Qin, X.; Ma, J.; Ju, J. *Org. Lett.* **2015,** *17,* 628–631. doi:10.1021/ol5036497
24. Rostovskii, N. V.; Sakharov, P. A.; Novikov, M. S.; Khlebnikov, A. F.; Starova, G. L. *Org. Lett.* **2015,** *17,* 4148–4151. doi:10.1021/acs.orglett.5b01883
(ex 23).
25. Katakawa, K.; Yonenaga, D.; Terada, T.; Aida, N.; Sakamoto, A.; Hoshino, K.; Kumamoto, T. *Heterocycles* **2014,** *88,* 817–825. doi:10.3987/COM-13-S(S)66
26. Hunter, R.; Rees-Jones, S. C. M.; Su, H. *Beilstein J. Org. Chem.* **2007,** *3,* No. 38. doi:10.1186/1860-5397-3-38
27. Yoshimura, H.; Takahashi, K.; Ishihara, J.; Hatakeyama, S. *Chem. Commun.* **2015,** *51,* 17004–17007. doi:10.1039/C5CC07749D
28. Chen, M.; Roush, W. R. *Org. Lett.* **2012,** *14,* 426–428. doi:10.1021/ol203161u
29. Markey, B.; Leonard, F.; Archambault, M.; Cullinane, A.; Maguire, D. *Clinical Veterinary Microbiology,* 2nd ed.; Elsevier, 2013.
30. Clinical Laboratory and Standards Institute. *Performance Standard for Antimicrobial Disk and Dilution Susceptibility Tests for Bacteria Isolated from Animals CLSI VET01S,* 3rd ed.; Clinical and Laboratory Standards Institute: Wayne, Pennsylvania, 2015; Vol. 128.
31. Fitzgerald, J. R. *Vet. Dermatol.* **2009,** *20,* 490–495. doi:10.1111/j.1365-3164.2009.00828.x
32. Kawakami, T.; Shibata, S.; Murayama, N.; Nagata, M.; Nishifuji, K.; Iwasaki, T.; Fukata, T. *J. Vet. Med. Sci.* **2010,** *72,* 1615–1619. doi:10.1292/jvms.10-0172

License and Terms

BEILSTEIN JOURNAL OF ORGANIC CHEMISTRY

Impact of *Pseudomonas aeruginosa* quorum sensing signaling molecules on adhesion and inflammatory markers in endothelial cells

Carmen Curutiu[1,2], Florin Iordache[*3,4], Veronica Lazar[1,2], Aurelia Magdalena Pisoschi[3], Aneta Pop[3], Mariana Carmen Chifiriuc[1,2] and Alina Maria Hoban[1,2]

Full Research Paper

Open Access

Address:
[1]University of Bucharest, Faculty of Biology, Department of Microbiology-Immunology, Bucharest, Romania, [2]Research Institute of the University of Bucharest, Romania, [3]University of Agronomical Sciences and Veterinary Medicine, Faculty of Veterinary Medicine, Bucharest, Romania and [4]Institute of Cellular Biology and Pathology Nicolae Simionescu of Romanian Academy, Romania

Email:
Florin Iordache[*] - floriniordache84@yahoo.com

* Corresponding author

Keywords:
adhesion; host–pathogen interaction; inflammation; Pseudomonas; quorum sensing

Beilstein J. Org. Chem. **2018,** *14,* 2580–2588.
doi:10.3762/bjoc.14.235

Received: 02 August 2018
Accepted: 19 September 2018
Published: 05 October 2018

This article is part of the thematic issue "Antibacterials, bacterial small molecule interactions and quorum sensing".

Guest Editor: D. Spring

Abstract

Pseudomonas aeruginosa relies on the quorum sensing (QS) signaling system as a central regulator mechanism of virulence expression that contributes to the formation and maintenance of biofilms and tolerance to conventional antimicrobials. QS Signaling molecules (QSSMs) may be recognized and may function also within the host cells, being potentially involved in the progression of the infectious process. In this study we evaluate the expression of adhesion and inflammatory molecules in endothelial cells treated with *P. aeruginosa* QSSMs, in order to bring new insights on the mechanisms involved in the interaction of *P. aeruginosa* with host cells during the infectious process. Endothelial cells were stimulated with 20 μM of main *P. aeruginosa* QSSMs (OdDHL = *N*-(3-oxododecanoyl)-L-homoserine lactone, C4HSL = *N*-butyryl-L-homoserine lactone, PQS = 2-heptyl-3-hydroxy-4(1*H*)-quinolone and HHQ = 2-heptyl-4-quinolone). Adherence to endothelial cells, inert substratum and biofilm formation was evaluated. The expression of adhesion molecules (VE-cadherin, PECAM-1, ICAM-1, and P-selectin) and inflammatory response molecules (IL-1β, IL-6, TNFα, TGFβ, and eNOS) was assessed by qRT-PCR and flow cytometry. Our results showed that bacterial adherence to inert substratum and biofilm were decreased in the presence of all tested QSSMs. The adherence index of PAO1 laboratory strain to host cells was decreased between 10–40% in the presence of QSSMs, as compared to untreated control. Expression of eukaryotic cells adhesion molecules ICAM-1 and P-selectin was stimulated by QSSMs, whereas VE-cadherin and PECAM-1 levels were increased only by C4HSL. The inflammatory response of endothelial cells was also modulated, as observed by the modified expression of IL-1β (for C4HSL, PQS and HHQ), IL-6 (for C4HSL and HHQ), TNFα (for C4HSL and HHQ), TGFβ, and eNOS factors. Our

results demonstrate that the main pseudomonadal QSSMs differentially modulate endothelial cells adhesion and proinflammatory cytokine expression. These observations provide new insights in the mechanisms by which different QSSMs activate endothelial cells and modulate the infectious process, and support the importance of recent studies aiming to develop anti-QS therapeutic strategies to fight against *P. aeruginosa* infections.

Introduction

Pseudomonas (P.) aeruginosa is an opportunistic pathogen that causes severe and persistent infections in immune compromised individuals and in patients with bronchiectasis or cystic fibrosis. The infections become chronic, as *P. aeruginosa* develops resistance to conventional antibiotics due to its ability to produce virulence factors and modulate immune defenses by *quorum sensing* (QS) and biofilm production. *Pseudomonas aeruginosa* is recognized as the principal pathogen responsible of high morbidity and mortality in patients with cystic fibrosis, one of the most common life-threatening autosomal recessive genetic disease in Northwest European populations, determined by mutations in the cystic fibrosis transmembrane conductance regulator (CFTR) gene [1]. This mutation determines alteration of ion transport and subsequent dehydration of the airway surface liquid, resulting in a viscous mucus layer on the airway surface of cystic fibrosis patients that deteriorate the mucociliary clearance and enhance the infection, inflammation and respiratory insufficiency [2]. *P. aeruginosa* pathogenesis is multifactorial, as suggested by the large number and wide spectrum of bacterial virulence factors present either attached to the cell wall or extracellular virulence factors capable of producing massive tissue damage and blood dissemination of the infection [3]. The regulation of the virulence factors expression is coordinated by quorum sensing (QS), an intercellular communication system based on cell density dependent molecules with autoinductory properties that play a pivotal role in the pathogenesis of various infections. *P. aeruginosa* produce two types of quorum-sensing signaling molecules (QSSMs): *N*-acylhomoserine lactones (AHL) and 2-alkyl-4-quinolone (PQS) derivatives. The AHLs molecules described so far in *P. aeruginosa* belong at two quorum sensing (QS) systems: *las* and *rhl* systems whose autoinducer (AI) molecules are *N*-(3-oxododecanoyl)homoserine lactone (OdDHL, 3-oxo-C12-HSL), and *N*-butyryl-L-homoserine lactone (C4-HSL), respectively. AHL systems are interconnected by a third mechanism that uses signaling molecules such as 2-alkyl-4-quinolone (AQ), the most relevant one being 3-hydroxy-4-quinolone (PQS = Pseudomonas quinolone signal) and its immediate precursor 2-heptyl-4-quinolone (HHQ) [4,5]. QS systems modulate numerous microbial virulence features, such as bacterial adherence and biofilm formation. It was proved that QS signaling plays an important role in cell attachment, in the differentiation of Pseudomonas biofilms and even biofilm survival [6]. The *las* system is indispensable for the development of a normal biofilm, including the differentiation of biofilm-like structures (such as “mushrooms” and "columns") observed in biofilms developed in vitro [7]. Some studies have shown that QS-deficient mutant strains initially form biofilms with the same dense structure as wild strains. The mutant strains produce even "mushroom"-like structures similar to wild strains that have as carbon source, glucose, but compared to wild type, mature biofilms (10 or more days of development) produced by QS deficient strains differ in size and stability of the structure, being more flexible due to the production of QS-regulated extracellular DNA [8], which acts as a stabilizer of three-dimensional biofilm structure [8]. In patients with cystic fibrosis, the growth of bacteria in biofilm determines aggravation of the disease. Recent studies have found that the QS molecules interact with eukaryotic cells and modulate also host immune response [9]. But, although the roles of the *N*-acylhomoserine lactones in the modulation of immune response have been well studied, the results obtained until now were contradictory, depending on the cell line, the concentration and the time of action [10]. Moreover, the effects of AQs and other Pseudomonas molecules on the modulation of immune responses are poorly understood. The elucidation of the intimate QSSM mechanisms could contribute to the development of new anti-QS therapeutic strategies against *P. aeruginosa* infections, which are very difficult to treat.

The vascular endothelium is crucial for cell and tissue homeostasis and regulation of inflammatory response. The loss of its integrity causes plasma, proteins and cells to build up in the interstitial space, resulting in inflammation [11]. In order to avoid both chronic and acute inflammatory disease, e.g., atherosclerosis or loss of vascular volume, such as in septic shock, the soundness of the vascular permeability barrier is essential. The barrier function of the endothelium is strictly controlled by intercellular adherence junctions (AJ) and tight junctions (TJ), interconnected with cytoskeletal proteins. 3O-C12-HSL induces breaks in the epithelial barrier, disrupting cell junction and enhanced permeability by alterations in the phosphorylation status of TJ and AJ proteins [12]. The transmembrane protein vascular endothelial cadherin (VE-cadherin) is the major structural component of endothelial AJ with a pivotal role in endothelial barrier integrity. LasB protease released by *P. aeruginosa* during infection determines VE-cadherin cleavage and

facilitates type III secretion system toxicity in endothelial cells [13]. ICAM-1 (intercellular adhesion molecule 1) and PECAM-1 (platelet endothelial cell adhesion molecule 1) are endothelial- and leukocyte-associated transmembrane proteins that permit transmigration of leukocytes into tissues and are induced by interleukins (IL-1, IL-8), tumor necrosis factor (TNF), nitric oxide (NO), and other inflammatory and stress factors. The investigations of the role of QSSM produced by *P. aeruginosa* on vascular endothelial cells (EC) are poorly investigated. The aim of this study was to evaluate the expression of adhesion and inflammatory molecules in endothelial cells treated with *P. aeruginosa* quorum-sensing (QS) molecules, in order to elucidate their role in the occurrence of tissue damages, in which endothelial cells are involved, such as: wound healing, transepithelial migration of neutrophils, lung inflammation and permeability. Also, we highlighted the impact of QSSMs on microbial attachment at inert and cellular substrata and biofilm formation in vitro.

Results and Discussion

Adherence and biofilm development

Even though there are numerous recent studies about the influence of bacteria QSSMs on host cells, their results are chiefly about the effects of AHL molecules, whereas the interactions between host cells and PQS have remained largely unknown. As far as we know, this is the first publication showing how both *P. aeruginosa*-derived AHL and PQS impact adhesion and inflammatory parameters of endothelial cells. Also, the impact of the main *P. aeruginosa* QSSMs on key bacterial virulence factors such as attachment and biofilm formation was shown, as these behaviors are very important for the progression of the infectious process and represent the main host-pathogen interactions. Bacterial adherence to inert substrata and biofilms developed at different periods of time (24 h, 48 h and 72 h) were decreased in the presence of all tested QSSMs in PAO1 culture (Figure 1). Adherence to inert substratum was decreased with 37.4% for OdDHL, 32.2% for C4HSL, 32.4% for PQS and with 60% for HHQ compared with PAO1 control (Figure 1a). Biofilm formation was slightly inhibited by the presence of most of the tested OSSMs; only HHQ slightly increased the development of biofilm (21.7%) at 72 hours (Figure 1b).

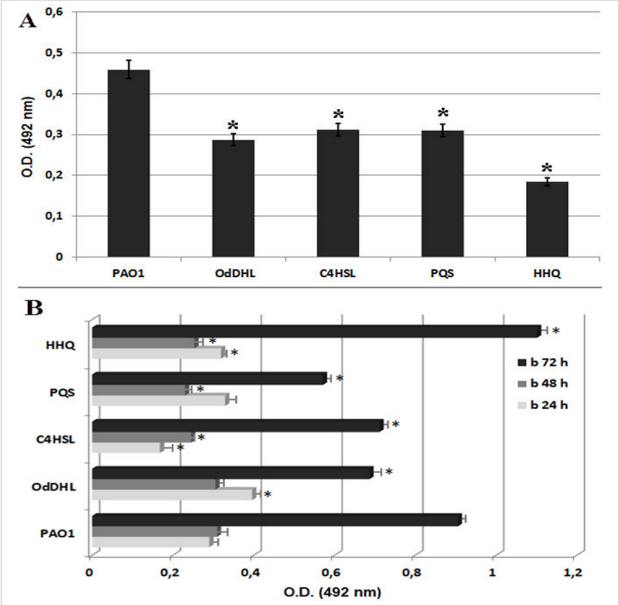

Figure 1: Graphic representation of the bacterial adherence to inert substrata (A) and biofilms developed after 24 h, 48 h and 72 h of incubation (B) in the presence of 20 µM purified QSSMs (*P < 0.05, based on ANOVA and Bonferroni post test of medians of 3 independent experiments performed in triplicate).

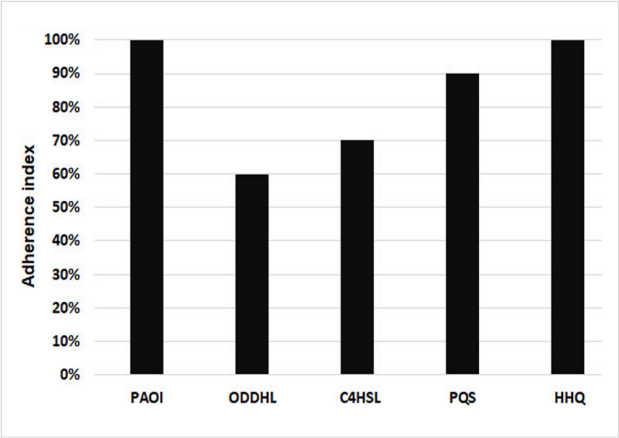

Figure 2: Graphic representation of the adherence index to cellular substrata of PAO1 strain treated with 20 µM of tested purified QSSMs.

The inhibitory effect of adherence was also observed for cellular substrate adherence. The adherence index of PAO1 strain to endothelial cells was decreased in the presence of 20 µM QSSMs compared to untreated control. The inhibitory effect was observed in the case of OdDHL (40% inhibition) and C4HSL (30% inhibition), and also a low inhibition (10%) was observed in the case of PQS (Figure 2). HHQ had no significant effect on the adherence index of *P. aeruginosa* to host endothelial cells, but a change in the adherence pattern of bacteria to the endothelial cells was registered, from aggregative (control PAO1) to diffuse aggregative. As seen in Table 1, changes in the adherence pattern were observed in the presence of all tested QSSMs. The main tendency of the tested QSSMs is to disperse microbial aggregates attached on the host cells, since it is clearly seen that the untreated PAO1 control has a higher aggregative potential, as compared to all other samples (Figure 3).

Flow cytometry analysis of endothelial cells adhesion molecules revealed that ICAM-1 and P-selectin production increased for all QSSMs treated samples, as compared with

Table 1: The adherence *patterns* to cellular substrate of PAO1 strain treated with 20 μM purified QQSMs.

sample	adherence pattern
control PAO1	aggregative
OdDHL	diffuse aggregative
C4HSL	localized aggregative
PQS	diffuse aggregative
HHQ	diffuse aggregative

control cells, the highest effect being observed in case of OdDHL and PQS. ICAM-1 showed an increased expression in endothelial cells treated with OdDHL (75.6% ± 0.48), C4HSL (21.7% ± 0.04), PQS (43.2% ± 0.011), HHQ (52.1 ± 0.019), as compared to control cells (13.7% ± 0.50). P-selectin expression was also increased for OdDHL (27.5% ± 0.03) and PQS (42.2% ± 0.04) treated cells, while C4HSL (6.5% ± 0.28) and HHQ (4.4% ± 0.02) treated samples provided lower values, comparable to untreated control cells (10% ± 0.19). The expression of PECAM-1 and VE-cadherin, were strongly positive for all QSSMs treated cells, as they are in untreated control endothelial cells (Figure 4). These results suggest an inflammatory/reactive response of endothelial cells, explained by the stimulation of ICAM-1 and P-selectin expression which correlate with an increased production of inflammatory cytokines (such as IL-1, IL-8, TNFα). These data are confirmed by recent literature showing the immunomodulatory effects of OdDHL and PQS signaling molecules [14]. It has been shown that OdDHL determines the overexpression of mRNA for IL-8 and stimulates the production of numerous active cytokines in fibroblasts and human epithelial cells in vitro. High concentrations (100 μM) of purified OdDHL activate the p42/44 MAPK signaling pathway and subsequently the NFκB transcription factor that stimulates the production of IL-8 proinflammatory cytokines [15] in human lung or fibroblast bronchial cells. 3-Oxo-C12-AHL also activates extracellular signal-regulated kinases (ERKs), which subsequently induces the activation of NFκB transcription factor. Thus, activation of NFκB is essential for maximal IL-8 production following stimulation of 3-oxo-C12-AHL cells [16]. In addition, the same group later demonstrated that *P. aeruginosa* can induce stimulation of prostaglandin E2 (PGE2) production via the COX-2 cyclooxygenase pathway. In vitro studies on human lung fibroblasts have shown that OdDHL causes overexpression of *cox-2* but not *cox-1*, and this effect appears to be related to NFκB activation. These autoinducers (AIs) stimulate the production of mem-

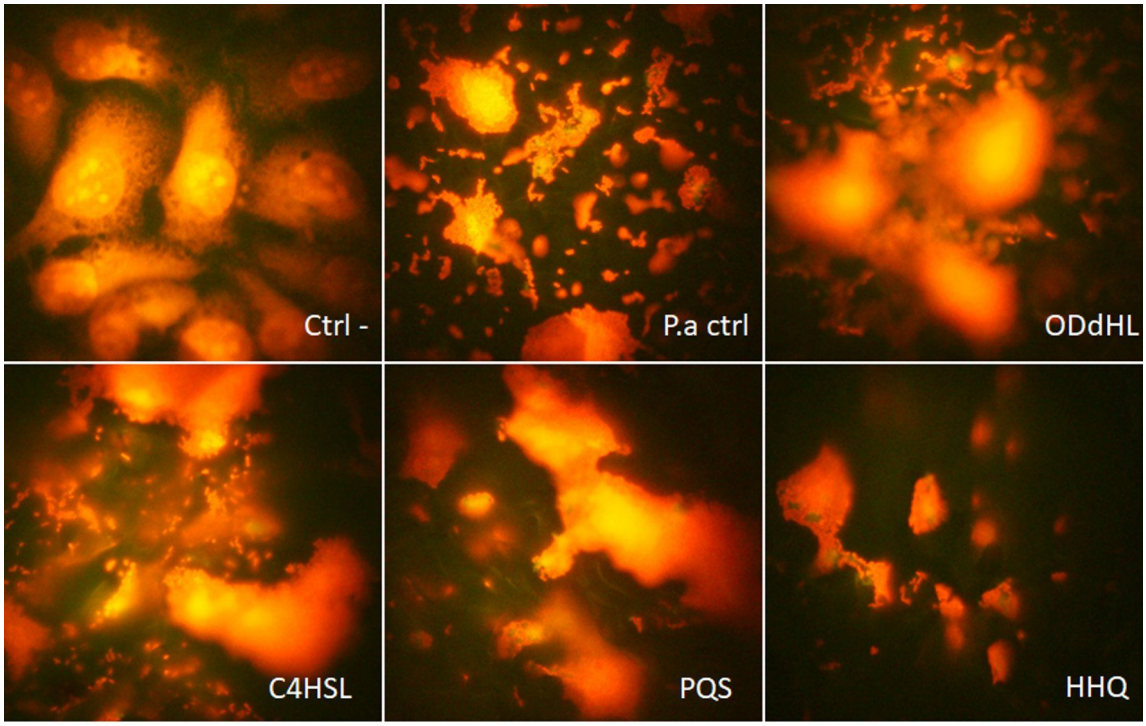

Figure 3: Fluorescence microscopy images of QSSMs treated euckariote cells, revealing attachment patterns. (Ctrl- = untreated control cells, P.a ctrl = *P. aeruginosa* control treated cells, ODdHL = *P. aeruginosa* + OddHL treated cells, C4HSL = *P. aeruginosa* + C4HSL treated cells, PQS = *P. aeruginosa* + PQS treated cells, HHQ = *P. aeruginosa* + HHQ treated cells, ob. 100×, immersion oil.

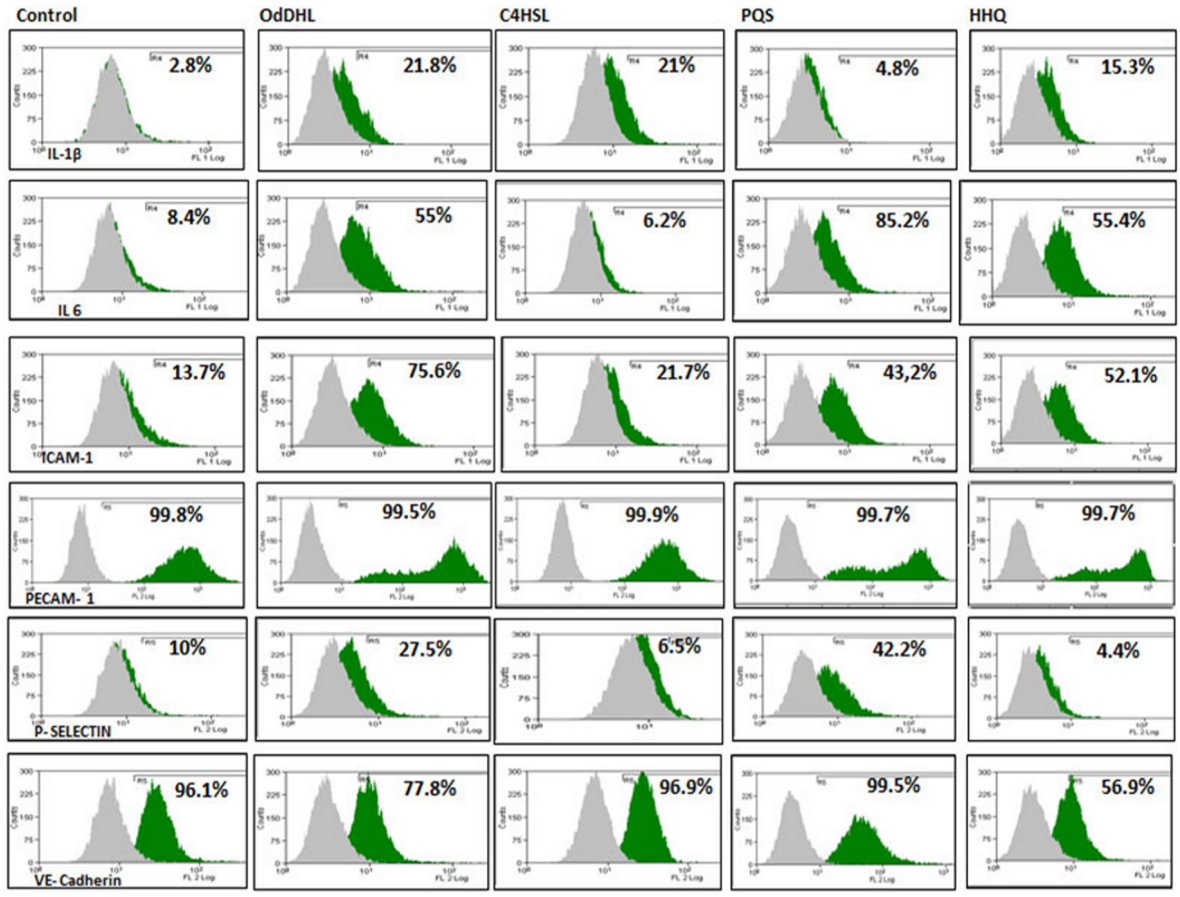

Figure 4: Flow cytometry assays for inflammatory (IL-1β, IL-6), and adhesion markers (ICAM-1, PECAM-1, P-selectin and VE-cadherin) in endothelial cells treated with PAO1 and QSSMs (*P < 0.05, Bonferroni post test of medians of 3 independent experiments performed in triplicate (n = 3)).

brane-associated prostaglandin E (PGE) and PGE2 but not PGE from cytosol. It is known that PGE2 plays a role in inducing mucus secretion, vasodilatation and edema, acting as a lipid mediator in immunomodulation [17]. These results indicate that OdDHL contributes to the induction of inflammation and pulmonary pathology in *P. aeruginosa* infections, which is mainly visible in cystic fibrosis patients. PGE2 and COX-2 have been shown to play an important role in suppressing the production of reactive oxygen species by diminishing the bacterial clearance process by macrophages. For these reasons, both PGE2 and COX-2 have been proposed as future therapeutic targets for the treatment of severe pneumonia produced by *P. aeruginosa* [18].

Another signaling molecule produced by *P. aeruginosa* has been shown to have immunomodulatory effects in the host cells [14,19]. PQS inhibits cellular proliferation without affecting IL-2 cytokine release when T cells are activated. PQS and OdDHL significantly reduce the ability of human peripheral mononuclear cells to respond to Con-A and to anti-CD3 and anti-CD28 antibodies. PQS does not affect cell viability while OdDHL inhibits cell proliferation and viability [20]. In addition, OdDHL inhibits the release of IL-2 and TNFα while PQS stimulates the release of these cytokines [21]. OdDHL can control PQS production, demonstrating that both molecules, while independent, with similar or different effects, act together [22]. The expression of adhesion molecules VE-cadherin and PECAM-1 was evaluated by qRT-PCR assay, and the obtained results sustained the flow cytometry data, suggesting the ability of QSSMs to modulate adhesion of host cells. An increased expression by 9 and 11 fold, respectively, was obtained when endothelial cells were treated with C4HSL (Figure 5). Migration of leukocytes from vessels into infected tissues involves interaction with endothelium through adhesion molecules. Adhesion molecules such as integrins (Cd11/Cd18) and ICAMs are usually involved in the inflammatory process during infection. *P. aeruginosa*-activated mast cells produce IL-1α and IL-1β, which stimulate the expression of ICAM-1 and

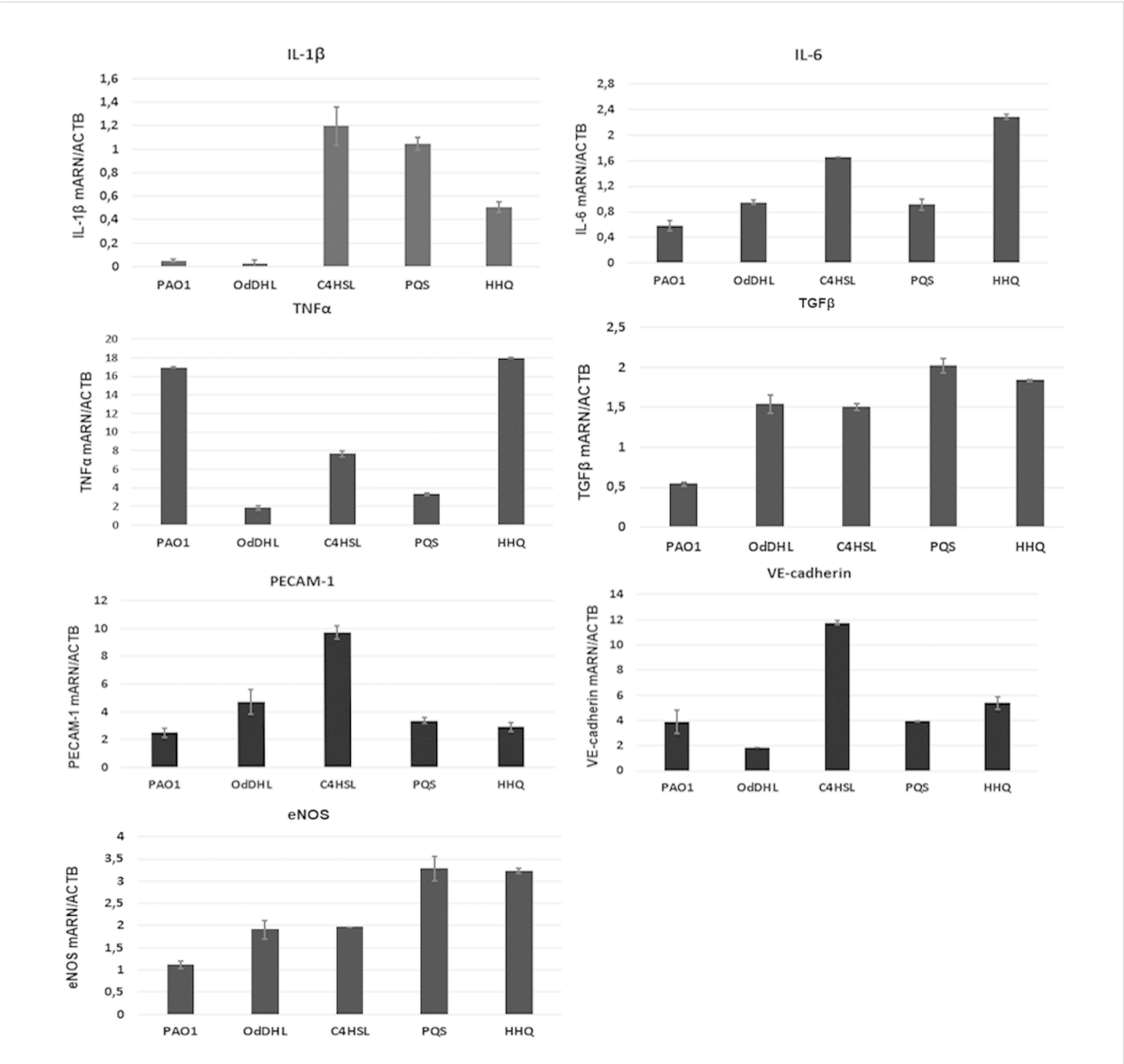

Figure 5: Expression levels (fold change) in qRT-PCR experiments for IL-1β, IL-6, TNFα, TGFβ, eNOS, VE-cadherin and PECAM-1 molecules performed on endothelial cells treated with PAO1 cultures and purified QSSMs ($P < 0.05$, based on ANOVA and Bonferroni post test of medians of 4 independent experiments performed in triplicate ($n = 3$)).

E-selectin in endothelial cell, this process being required for transendothelial migration [23]. Furthermore Lins et al. showed 2010 that ICAM-1 expression is modulated by ExoU cytotoxin injected via the type III secretion system, being involved in endothelial damage and bacterial dissemination [24].

Inflammatory markers

Proinflammatory cytokines and chemokines such as IL-1α, IL-1β, IL-6 and TNFα are produced by vascular cells such as endothelial cells and leucocytes within hours after *P. aeruginosa* infection. Flow cytometry assay showed elevated levels of IL-1β and IL-6. The level of IL-1β was increased after the stimulation with 20 μM QSSMs. The most significant IL-1β expression stimulation was observed in the sample treated with OdDHL (21.8% ± 0.09), as well C4HSL (21% ± 0.03), followed by HHQ (15.3% ± 0.3). PQS showed no effect in the production of IL-1β in endothelial cells (Figure 4). The expression of IL-6 was also increased after cellular treatment with OdDHL (55% ± 0.02), PQS (85.2% ± 0.015), HHQ (55% ± 0.02), while C4HSL showed no significant effect in the modulation of IL-6 expression (Figure 4). QRT-PCR results showed that the presence of C4HSL, PQS and HHQ molecules increased the expression level of IL-1β, while the PAO1 and OdDHL did not affect the level of IL-1β. IL-6 expression was slightly increased in the

presence of all QSSM (0.5–2.3 fold), the differences being more significant for C4HSL and HHQ. The expression of TGFβ, eNOS was significantly increased in the presence of all QSSMs, by 1.5–2.0 fold (TGFβ) and 1.2–3.2 fold (eNOS), respectively, suggesting an activated phenotype of endothelial cells. The expression levels of adhesion molecules such as VE-cadherin and PECAM-1 were stimulated by the QSSMs, high levels being observed in the cells grown in the presence of C4HSL (Figure 5). Though there are numerous recent studies focusing on the influence of bacteria QSSMs on host cells, they are chiefly about the effects of AHL molecules, whereas the interactions between host cells and PQS have remained largely unknown. As far as we know, this is the first publication showing how both *P. aeruginosa*-derived AHL and PQS impact adhesion and inflammatory parameters of endothelial cells.

Thomas et al. in 2006 tested the ability of natural 3-oxo-C12-AHL and 4 synthetic analogues to modulate cytokine production in the host cells and the results demonstrated that these soluble mediators stimulate the production of TNFα and nitric oxide (NO) in equine and murine macrophages [25]. The mechanism of action of QSSMs leads to the activation of NFκB signaling cascade, resulting in the upregulation of pro-inflammatory cytokines IL-6, IL-8, and TNFα. However, our results demonstrated that TNFα expression is inhibited by all tested QSSMs, excepting HHQ (Figure 5). The expression of inflammatory molecules is tissue dependent and seems to be influenced by soluble virulence factors produce by *P. aeruginosa* during infection. Previous studies showed that most *P. aeruginosa* QSSMs increases the level of IL-6 in vitro. While HHQ is significantly stimulating IL-10 secretion by more than 20-fold, PQS has no significant effect on IL-10 secretion in mesenchymal stem cells [10]. Bacterial lipopolysaccharides (LPS) and phospholipase C (PLC) induces high levels of TNFα, IL-1β, IFNγ, MIP-1 and MIP-2 in lung cells, but they do not affect IL-18 levels [26]. In the tracheal epithelium LPS stimulates TLR2 and TLR4, while flagellin stimulates TLR5 expression. Alveolar epithelial cells respond to *P. aeruginosa* by releasing IL-1β, IL-6, IL-8, MIP-2 while alveolar macrophages are producing IL-1β and IL-18 [27].

Conclusion

This is the first article about how *P. aeruginosa* derived QSSMs influence human endothelial cell adhesion and cytokine profile. Our findings demonstrate that the major pseudomonadal AHL and PQS auto-inducers differentially modulate bacteria adherence to inert and cellular substrata and biofilm formation, but also endothelial cells adhesion and pro-inflammatory cytokine expression. These observations may help in gaining insights into understanding host–pathogen interaction and communication and may have an impact on the development of new anti-QS therapeutic strategies to fight *P. aeruginosa* infections. Specifically, our results bring new information to help elucidating the mechanisms by which different QSSMs activate the host endothelial cells and promote epithelial lesions during *P. aeruginosa* infections.

Experimental

Adherence assay to inert substrate and biofilm formation was assessed by the adapted microtiter method [28]. Overnight PAO1 cultures were grown with QSSMs in 96 multi-well plates containing Tryptic Soy Broth (TSB) for 24 h, 48 h and 72 h at 37 °C. After each period of time, the plates were subsequently emptied and washed three times with phosphate buffered saline (PBS). The adherent cells were then fixed with cold methanol, stained with an alkaline 1% crystal violet solution for 15 minutes, washed with distilled water and resuspended in a 33% acetic acid solution. The intensity of the suspension was spectrophotometrically assessed, the amount of adhered biomass being proportional to the absorbance value read at 492 nm.

Adherence assay to cellular substrate

Cell culture. Endothelial cell line EA.hy926 was cultured in Dulbecco's Modified Eagle's Medium (DMEM, Sigma-Aldrich, St. Louis, MO, USA) containing 10% heat inactivated fetal bovine serum (FBS), 100 U/mL penicillin, 100 µg/mL streptomycin, and 50 µg/mL neomycin. Cell cultures were maintained at 37 °C in a humidified atmosphere containing 5% CO_2 and 21% O_2. To maintain optimal culture conditions, the medium was changed twice a week. Prior the infection with *P. aeruginosa* and adding QSSMs the endothelial cells were cultured in a medium without antibiotics. Endothelial cells were stimulated with *P. aeruginosa* PAO1 strain (control) and purifyed QSSMs (20µM) (OdDHL = *N*-(3-oxododecanoyl)-L-homoserine lactone; C4HSL = *N*-butyryl-L-homoserine lactone; PQS = 2-heptyl-3-hydroxy-4(1*H*)-quinolone; and HHQ = 2-heptyl-4-quinolone). For the adherence assay, Cravioto's adapted method was used [29]. Briefly, the endothelial cells monolayers were washed with PBS (phosphate buffered saline) and 1 mL of fresh medium without antibiotics was added to each well. Suspensions of *P. aeruginosa* were obtained from bacterial mid-logarithmic phase cultures grown in nutrient broth adjusted to 10^7 CFU/mL and 1 mL were used for the inoculation of each well in the presence of QSSMs. The inoculated plates were incubated for two hours at 37 °C. After incubation, endothelial cells were washed three times with PBS, fixed with cold methanol and stained with 5 µg/mL propidium iodide. The plates were washed, dried at room temperature and examined immediately with a fluorescent microscope (Eclipse TE300, with Digital Net Camera DN100, Nikon, Tokyo, Japan), by using the 100×, immersion oil objective.

The plates were examined microscopically to evaluate the adherence index and patterns. The adherence index was expressed as the ratio between the number of the eukaryotic cells with adhered bacteria and 100 eukaryotic cells counted on the microscopic field. The adherence patterns were defined as: localized adherence (LA) when tight clusters of microorganisms were noticed on the HeLa cell surface, aggregative adherence (AA) when a microbial stacked brick pattern characterizes the attachment, diffuse adherence (DA) when the bacteria adhered diffusely, covering the whole surface of the cell.

QRT-PCR assay

The gene expression level of adhesion and inflammatory molecules in endothelial cells treated with PAO1 cultures and QSSMs, was assessed by qRT-PCR. Total cellular RNA was isolated using RNeasy Mini kit (Qiagen, Hilden, Germany) and reverse-transcription reaction was performed using M-MLV polymerase (Thermo Fisher Scientific, Massachusetts, USA). The mRNA levels were quantified by amplification of cDNA using a real-time thermocycler (Viia7 Applied Biosystems thermalcycler, Thermo Fisher Scientific, Massachusetts, USA) and TaqMan chemistry using the following assays: IL-1β (Hs01555410_m1), IL-6 (Hs00174131_m1), TNFα (Hs00174128_m1), TGFβ (Hs01086000_m1), eNOS (Hs01574665_m1), VE-cadherin (Hs00975233_m1), PECAM-1 (Hs01065279_m1), GAPDH (Hs03929097_g1). PCR reaction had the following schedule: denaturation step at 95 °C for two minutes, 40 cycles of denaturation at 95 °C, 15 seconds and annealing at 60 °C, 40 seconds. The genes expression level was normalized to GAPDH. The relative quantification was done using the comparative CT method and expressed as arbitrary units.

Flow cytometry assay

Endothelial cells were stimulated with *P. aeruginosa* PAO1 strain and QSSMs (20 μM) for 20 hours and the expression of cell adhesion and inflammatory markers was assessed by flow cytometry (Gallios, Beckman-Coulter) using 1×10^5 endothelial cells stained with fluorochrome-conjugated (FITC - fluorescein-isothiocyanate and PE - phycoerythrin) primary antibodies against IL-1β, IL-6, ICAM-1 PECAM-1, P-selectin, VE-cadherin (Beckman-Coulter). Endothelial cells were detached using trypsin (Sigma-Aldrich, USA) and washed in PBS. Cells were then incubated with the primary antibodies at room temperature in the dark for 30 min. Further, the cells were washed twice and centrifuged at 400*g*, 10 min, in PBS suplemented with 1% BSA. For negative controls, endothelial cells were stained with the corresponding isotype-matched IgG antibodies (Beckman-Coulter). Flow cytometry data were analyzed using the Gallios software (Beckman-Coulter).

Statistical analysis

One way analysis of variance (ANOVA) was used to analyze the data (GraphPad software). Bonferroni post test was used when appropriate. P values < 0.05 were considered significant.

Acknowledgements

This work was supported by project No. 19/2018, PN-III-P1-1.1-PD-2016-1660, financed by the Executive Agency for Higher Education, Research, Development and Innovation Funding (UEFISCDI).

ORCID® iDs

Carmen Curutiu - https://orcid.org/0000-0002-4608-4487
Florin Iordache - https://orcid.org/0000-0002-5366-6792

References

1. Farkhooy, A.; Bodegård, J.; Erikssen, J. E.; Janson, C.; Hedenström, H.; Stavem, K.; Malinovschi, A. *BMC Pulm. Med.* **2018,** *18,* No. 118. doi:10.1186/s12890-018-0655-z
2. Buchanan, P. J.; Ernst, R. K.; Elborn, J. S.; Schock, B. *Biochem. Soc. Trans.* **2009,** *37,* 863–867. doi:10.1042/BST0370863
3. Lyczak, J. B.; Cannon, C. L.; Pier, G. B. *Microbes Infect.* **2000,** *2,* 1051–1060. doi:10.1016/S1286-4579(00)01259-4
4. Kim, K.; Kim, Y. U.; Koh, B. H.; Hwang, S. S.; Kim, S.-H.; Lépine, F.; Cho, Y.-H.; Lee, G. R. *Immunology* **2010,** *129,* 578–588. doi:10.1111/j.1365-2567.2009.03160.x
5. Williams, P.; Cámara, M. *Curr. Opin. Microbiol.* **2009,** *12,* 182–191. doi:10.1016/j.mib.2009.01.005
6. Jiménez-Gómez, P.; Pozuelo de Felipe, M. J.; Llinares Pinell, F.; García de los Ríos, J. E. Quorum-sensing in *Pseudomonas aeruginosa* and *Salmonella*: Active natural compounds as antagonists. In *Communicating Current Research and Educational Topics and Trends in Applied Microbiology;* Méndez-Vilas, A., Ed.; Formatex: Badajoz, Spain, 2007; pp 41–51.
7. Lazar, V. *Anaerobe* **2011,** *17,* 280–285. doi:10.1016/j.anaerobe.2011.03.023
8. Allesen-Holm, M.; Barken Bundvig, K.; Yang, L.; Klausen, M.; Webb, J. S.; Kjelleberg, S.; Molin, S.; Givskov, M.; Tolker-Nielsen, T. *Mol. Microbiol.* **2006,** *59,* 1114–1128. doi:10.1111/j.1365-2958.2005.05008.x
9. Feng, L.; Xiang, Q.; Ai, Q.; Wang, Z.; Zhang, Y.; Lu, Q. *Mediators Inflammation* **2016,** *16,* No. 4012912. doi:10.1155/2016/4012912
10. Holban, A.-M.; Bleotu, C.; Chifiriuc, M. C.; Bezirtzoglou, E.; Lazar, V. *Virulence* **2014,** *5,* 303–310. doi:10.4161/viru.27571
11. van Nieuw Amerongen, G. P. *Tissue Engineering and Biomaterials;* Springer: Berlin, Heidelberg, 2013; p 12.
12. Holm, A.; Vikström, E. *Front. Plant Sci.* **2014,** *5,* No. 309. doi:10.3389/fpls.2014.00309
13. Golovkine, G.; Faudry, E.; Bouillot, S.; Voulhoux, R.; Attrée, I.; Huber, P. *PLoS Pathog.* **2014,** *10,* e1003939. doi:10.1371/journal.ppat.1003939
14. Lin, J.; Cheng, J.; Wang, Y.; Shen, X. *Front. Cell. Infect. Microbiol.* **2018,** *8,* No. 230. doi:10.3389/fcimb.2018.00230

15. Gardères, J.; Henry, J.; Bernay, B.; Ritter, A.; Zatylny-Gaudin, C.; Wiens, M.; Müller, W. E. G.; Le Pennec, G. *PLoS One* **2014,** *9,* e97662. doi:10.1371/journal.pone.0097662
16. Smith, R. S.; Fedyk, E. R.; Springer, T. A.; Mukaida, N.; Iglewski, B. H.; Phipps, R. P. *J. Immunol.* **2001,** *167,* 366–374. doi:10.4049/jimmunol.167.1.366
17. Smith, R. S.; Rodney, K.; Iglewski, B. H.; Phipps, R. P. *J. Immunol.* **2002,** *169,* 2636–2642. doi:10.4049/jimmunol.169.5.2636
18. Sadikot, R. T.; Zeng, H.; Azim, A. C.; Joo, M.; Dey, S. K.; Breyer, R. M.; Peeble, R. S.; Blackwell, T. S.; Christman, J. W. *Eur. J. Immunol.* **2007,** *37,* 1001–1009. doi:10.1002/eji.200636636
19. Iordache, F.; Curutiu, C.; Holban, A.M.; Andrei, E.; Chifiriuc, C.; Lazar,V.; Ditu, L.M.; Constantinescu, A.; Maniu, H. *e-poster presented at ECCMID* 2015, topic Microbial Pathogenesis and Biofilms, Copenhagen, Denmark.
20. Skindersoe, M. E.; Zeuthen, L. H.; Brix, S.; Fink, L. N.; Lazenby, J.; Whittall, C.; Williams, P.; Diggle, S. P.; Froekiaer, H.; Cooley, M.; Givskov, M. *FEMS Immunol. Med. Microbiol.* **2009,** *55,* 335–345. doi:10.1111/j.1574-695X.2008.00533.x
21. Hooi, D. S. W.; Bycroft, B. W.; Chhabra, S. R.; Williams, P.; Pritchard, D. I. *Infect. Immun.* **2004,** *72,* 6463–6470. doi:10.1128/IAI.72.11.6463-6470.2004
22. Middleton, B.; Rodgers, H. C.; Cámara, M.; Knox, A. J.; Williams, P.; Hardman, A. *FEMS Microbiol. Lett.* **2002,** *202,* 1–7. doi:10.1111/j.1574-6968.2002.tb11019.x
23. Lin, T.-J.; Garduno, R.; Boudreau, R. T. M.; Issekutz, A. C. *J. Immunol.* **2002,** *169,* 4522–4530. doi:10.4049/jimmunol.169.8.4522
24. Lins, R. X.; de Assis, M. C.; Mallet de Lima, C. D.; Freitas, C.; Maciel Plotkowski, M. C.; Saliba, A. M. *Microbes Infect.* **2010,** *12,* 154–161. doi:10.1016/j.micinf.2009.11.005
25. Thomas, G. L.; Böhner, C. M.; Williams, H. E.; Walsh, C. M.; Ladlow, M.; Welch, M.; Bryant, C. E.; Spring, D. R. *Mol. BioSyst.* **2006,** *2,* 132–137. doi:10.1039/B517248A
26. Wieland, C. W.; Siegmund, B.; Senaldi, G.; Vasil, M. L.; Dinarello, C. A.; Fantuzzi, G. *Infect. Immun.* **2002,** *70,* 1352–1358. doi:10.1128/IAI.70.3.1352-1358.2002
27. Lin, C. K.; Kazmierczak, B. I. *J. Innate Immun.* **2017,** *9,* 250–261. doi:10.1159/000455857
28. Fleming, D.; Chahin, L.; Rumbaugh, K. *Antimicrob. Agents Chemother.* **2017,** *61,* No. e01998-16. doi:10.1128/AAC.01998-16
29. Holban, A. M.; Cotar, A. I.; Chifiriuc, M. C.; Bleotu, C.; Banu, O.; Lazar, V. *Afr. J. Microbiol. Res.* **2013,** *7,* 3453–3460.

License and Terms

BEILSTEIN JOURNAL OF ORGANIC CHEMISTRY

Targeting the *Pseudomonas* quinolone signal quorum sensing system for the discovery of novel anti-infective pathoblockers

Christian Schütz[1,2] and Martin Empting[*1,2,3]

Review

Open Access

Address:
[1]Helmholtz-Institute for Pharmaceutical Research Saarland (HIPS) - Helmholtz Centre for Infection Research (HZI), Department of Drug Design and Optimization (DDOP), Campus E8.1, 66123 Saarbrücken, Germany, [2]Department of Pharmacy, Saarland University, Campus E8.1, 66123 Saarbrücken, Germany and [3]German Centre for Infection Research (DZIF), Partner Site Hannover-Braunschweig, Saarbrücken, Germany

Email:
Martin Empting[*] - martin.empting@helmholtz-hzi.de

* Corresponding author

Keywords:
anti-infectives; pathoblockers; PQS; *Pseudomonas aeruginosa*; quorum sensing

Beilstein J. Org. Chem. **2018,** *14,* 2627–2645.
doi:10.3762/bjoc.14.241

Received: 31 July 2018
Accepted: 28 September 2018
Published: 15 October 2018

This article is part of the thematic issue "Antibacterials, bacterial small molecule interactions and quorum sensing".

Guest Editor: D. Spring

Abstract

The Gram-negative opportunistic pathogen *Pseudomonas aeruginosa* causes severe nosocomial infections. It uses quorum sensing (QS) to regulate and coordinate population-wide group behaviours in the infection process like concerted secretion of virulence factors. One very important signalling network is the *Pseudomonas* quinolone signal (PQS) QS. With the aim to devise novel and innovative anti-infectives, inhibitors have been designed to address the various potential drug targets present within pqs QS. These range from enzymes within the biosynthesis cascade of the signal molecules PqsABCDE to the receptor of these autoinducers PqsR (MvfR). This review shortly introduces *P. aeruginosa* and its pathogenicity traits regulated by the pqs system and highlights the published drug discovery efforts providing insights into the compound binding modes if available. Furthermore, suitability of the individual targets for pathoblocker design is discussed.

Introduction

In recent years, attempts to raise public awareness on antimicrobial resistance (AMR) and the large threat that it poses towards modern health standards have been made [1]. It is an alarming notion that at an increasing rate of available treatment options proves ineffective in eradicating bacterial infections [2]. Especially in the case of Gram-negative bacteria, an urgent need for novel medicines has been identified while the pipeline of drug candidates is literally running dry and a desirable renaissance of the golden age of antibiotic drug research in ‘big pharma’ is currently not to be seen on the horizon [3,4]. Nevertheless, some innovative strategies to be explored for their clinical applicability in combating bacterial infections have been devised

in the last decades mostly driven by academic research [5-7]. In contrast to addressing classical antibiotic drug targets involved in vital processes of the bacterial cell, 'antivirulence' strategies aim at abolishing pathogenic features without affecting cell viability, providing the basis for a lower drug-induced selection pressure [5,8,9]. Hence, a reduced rate of resistance development is expected [9]. A clinical proof-of-concept for this unconventional strategy has been provided recently by the approval of the toxin-neutralizing therapeutic antibody bezlotoxumab, which is henceforth in clinical use for pre-emptive treatment of recurring clostridial infections [10]. So, the potential of active principles, which do not kill the bacteria through bactericidal or bacteriostatic effects, but mediate their effect through pathogen-specific action on virulence mechanisms, has been unveiled. This short review focuses on the current knowledge of one particular antivirulence strategy against the important pathogen *Pseudomonas aeruginosa*, which is based on the disruption of the *Pseudomonas* quinolone signal quorum sensing system (pqs QS).

Review

Antimicrobial resistance and clinical relevance of *Pseudomonas aeruginosa*

P. aeruginosa is one of the threatening ESKAPE pathogens and has regularly been attributed with the label 'superbug' [11]. In 2017, the World Health Organization (WHO) has published a priority list for pathogens with urgent need for novel treatment options and carbapenem-resistant *P. aeruginosa* was ranked in the highest category 'critical' [12]. One of the main problems we face regarding this Gram-negative bacterium is that it shows a prominent ability to resist antibiotic treatment via several mechanisms. First and foremost, it possesses an intrinsic resistance to many antibiotics because of the low permeability of its cell wall and due to the action of a number of efflux pumps as well as β-lactamases. Efflux pumps in particular are nifty molecular machineries consisting of several protein components, which in total span from the inner to the outer side of the cell membrane. Their function is to expel a wide range of xenobiotics, among them antibiotics from the cephalosporin, carbapenem, fluroquinolone and aminoglycoside classes [13]. Through this mechanism, these drugs cannot reach their intracellular targets rendering them ineffective. β-Lactamases, on the other hand, act specifically on compounds which carry the eponymous cyclic moiety as the activity-driving motif and their genes are found to be encoded on the chromosomes of many *P. aeruginosa* strains. Hence, these antibiotic-inactivating enzymes provide resistance against penicillins and cephalosporins [14].

In addition to these intrinsic capabilities, *P. aeruginosa* is able to acquire resistances toward antibiotics it has come in contact with. These acquired resistances can be the result of spontaneous mutations in genes encoding for the target protein. For example, certain mutational changes within DNA gyrase will lead to lowered susceptibility for fluoroquinolones [15]. Other examples are mutants leading to efflux pump overexpression [15]. If the resistance determinant is located on a transferable plasmid, it can be efficiently spread among bacteria via horizontal gene transfer, which is probably the most frequent mechanism for the development of acquired resistances [15]. In these cases, the resistance determinant is inheritable and passed over to the next generation of bacteria.

Furthermore, a mechanism has been discovered, which is referred to as adaptive resistance and describes the observation that a persistent environmental stimulus can induce non-mutational resistances [15]. Under continuous treatment regimes, the antibiotic itself can of course be the stimulus. But, nutrient deprivation, pH, anaerobiosis, as well as biocides, polyamines, cations and carbon sources could also act as external triggers leading to adaptive resistance. The common effect of these stimuli seems to be an alteration in expression patterns ultimately impacting, e.g., efflux pump or enzymatic activity, as well as cell envelope properties or biofilm formation [15].

All the mechanisms described above help to explain the notion that established chronic *P. aeruginosa* infections are notoriously difficult to eradicate. This ubiquitous opportunistic pathogen is able to cause infections basically in every niche of the human body where it finds enough moisture [16]. Common sites of infection are the respiratory and urinary tracts, the eye and wounds, e.g., those resulting from burn injuries [17]. These occur frequently in hospitalized and especially immunocompromised individuals. Patients with chronic lung diseases like cystic fibrosis (CF) or bronchiectasis have a poor prognosis when *P. aeruginosa* colonisation is detected, as this is usually associated with loss of lung function, morbidity, and mortality [18]. In 2013, it has been estimated, that by the age of eighteen 80% of the CF patients are *Pseudomonas* positive. Recently, evidence has been provided that this ratio is reducing [19]. Nevertheless, with progression of age the majority of CF patients will become chronically infected with *P. aeruginosa* and this is still the major cause of death associated with this genetic disorder [20]. Importantly, it has been described that the amount of quinolone-based quorum sensing (pqs QS; vide infra) in those patients correlates with a negative prognosis and might function as a possible biomarker for the severity of the infection [21].

Quroum sensing (QS)

In general, the term quorum sensing describes a population-density-dependent cell-to-cell communication system making use

of small diffusible molecules as signalling agents. By this means, pathogenic bacteria can coordinate population-wide changes to expression patterns and regulate concerted group behaviours important in the infection process. Critical pathogenicity traits like the production of virulence factors or biofilm formation are under the control of these systems. Actually, title pathogen makes use of four intertwined QS systems, referred to as las, rhl, pqs, and iqs [22]. These subsystems influence each other establishing an intricate regulatory network with compensatory mechanisms ensuring environmental adaptability and fine-tuned control of associated virulence genes (Figure 1). All four have been studied in the pursuit of quorum sensing inhibitors (QSI) to be used as blockers of *P. aeruginosa* pathogenicity [11,23].

Typically, a QS system of Gram-negatives consists of a transcription regulator, the signal molecules and one or several enzymes involved in the synthesis of the latter. The regulator usually controls the transcription of the biosynthetic enzymes and also functions as a receptor for the signal molecules themselves. As these are actually autoinducers (AIs) and, hence, have an agonistic activity toward their receptor, a positive feedback loop is created. In *P. aeruginosa* three different chemotypes of AIs have been identified, to date: alkyl homoserine lactones (AHLs) used by the las and rhl systems, alkylquinolones (AQs) used by the pqs system and 2-(2-hydroxyphenyl)thiazole-4-carbaldehyde used by the iqs system (Figure 1). Strategies addressing las and rhl have been reviewed elsewhere [5,11], while to date one study on iqs inhibition has been reported [23]. Many drug discovery efforts towards effective pathoblockers have been published based on the design and optimisation of pqs targeting QSI, which is the topic of this review.

The biosynthetic cascade of the pqs QS system

PQS is the abbreviation for *Pseudomonas* quinolone signal and actually refers to the signal molecule 2-heptyl-3-hydroxyquinolin-4(1*H*)-one (Figure 2). This quinolone-based AI and its biosynthetic precursor HHQ (2-heptylquinolin-4(1*H*)-one) are ligands of a transcription factor called 'multiple virulence factor regulator' (MvfR), also referred to as PqsR. Through interaction with this receptor, HHQ and PQS induce the transcription of a variety of genes including their own biosynthetic enzyme cascade (PqsABCDE). Together with PqsH and PqsL, which are under the control of LasR from the las QS system, these enzymes manage to build up PQS and related molecules from anthranilic acid (Figure 2). This initial building block can be

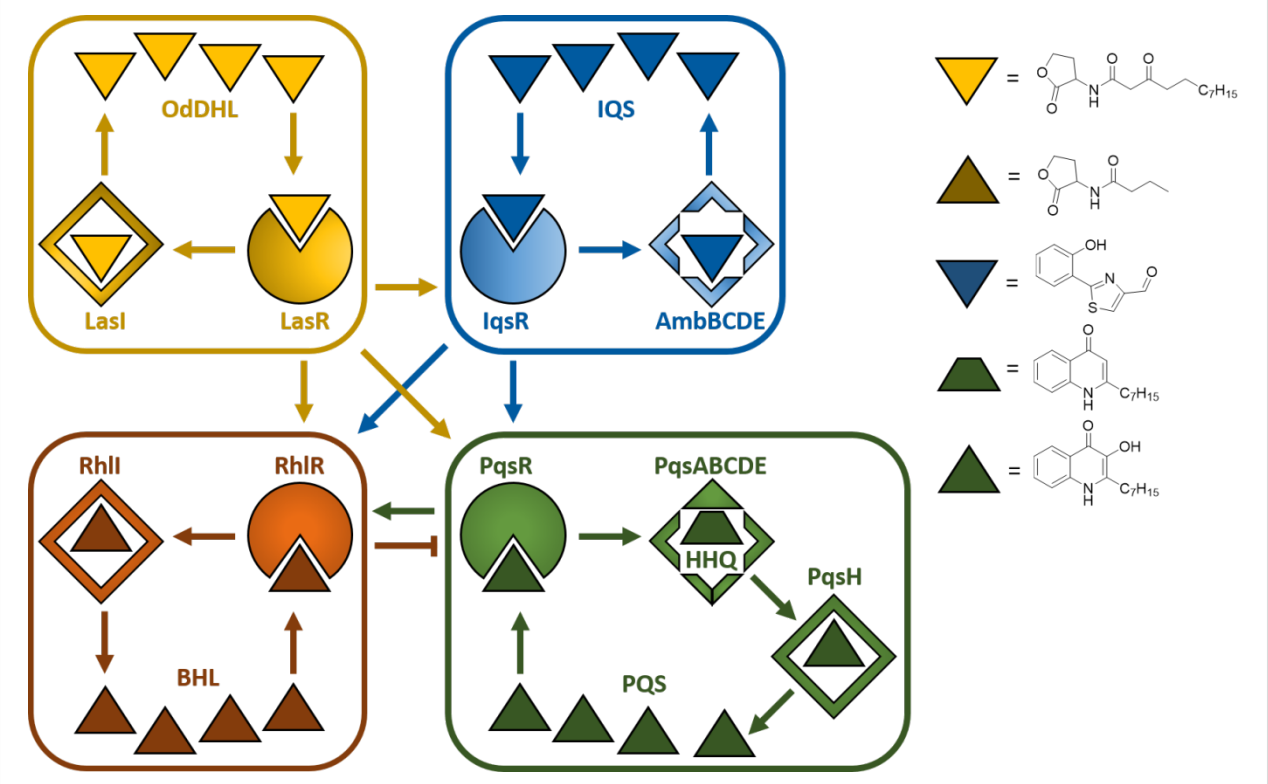

Figure 1: The four quorum sensing systems in *P. aeruginosa las, iqs*, *rhl*, and *pqs*. Abbreviations: OdDHL, *N*-(3-oxododecanoyl) homoserine lactone; IQS, integrating quorum sensing signal; BHL, *N*-butyryl-L-homoserine lactone; PQS, *Pseudomonas* quinolone signal. Positive control is represented by arrows, negative control by blunted arrow.

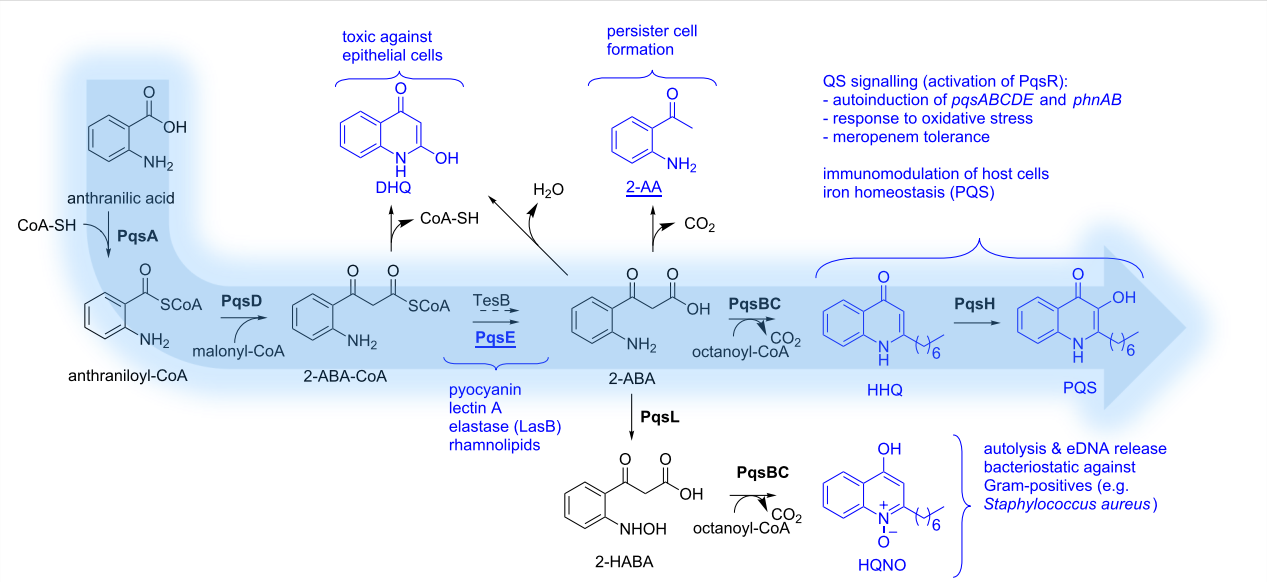

Figure 2: Schematic overview of the PQS biosynthesis and involvement of related metabolites and PqsE in virulence. Effector molecules are highlighted in blue. Enzymes are given in bold. Abbreviations: CoA, coenzyme A; 2-ABA-CoA, 2'-aminobenzoylacetyl-CoA; 2-ABA, 2'-aminobenzoylacetate; DHQ, dihydroxyquinoline; 2-AA, 2'-aminoacetophenone; 2-HABA, 2'-hydroxylaminobenzoylacetate; HHQ, 2-heptyl-4-(1*H*)-quinolone; HQNO, 4-hydroxy-2-heptylquinoline-*N*-oxide; PQS, *Pseudomonas* quinolone signal.

provided either through the kynurenine pathway starting from tryptophan or by anthranilate synthases from the PqsR-controlled phnAB operon starting using chorismic acid as a source [24]. Either way, the ligase PqsA starts PQS synthesis by condensing anthranilic acid with coenzyme A [25]. The resulting activated thioester (anthraniloyl-CoA) is then transferred to an active-site cysteine of the β-ketoacyl-ACP synthase III (FabH)-type enzyme PqsD [26,27]. Subsequently, another CoA-activated substrate comes into play. In analogy to fatty acid synthesis, malonyl-CoA is reacted with the enzyme-bound thioester to yield 2-aminobenzoylacetyl-CoA (2-ABA-CoA) under decarboxylation [28,29]. In a next step, the pathway-specific thioesterase PqsE generates 2-aminobenzoylacetate (2-ABA) [29]. It has been shown, that also the broad-specificity thioesterase TesB present in *P. aeruginosa* can catalyse this reaction [29]. The quinolone core is formed by action of the heterodimeric complex PqsBC. This time, CoA-activated octanoic acid is used to preload an active-site cysteine of PqsC with the fatty acid via a thioester linkage [30,31]. The previously produced 2-ABA is then consumed to from HHQ under decarboxylative condensation [30]. Finally, PQS is produced through hydroxylation of position 3 by the NADH-dependent flavin mono-oxygenase PqsH [32].

This biosynthetic cascade is also responsible for the generation of the pqs-related metabolites DHQ, 2-AA, and HQNO as well as other AQs having different lengths of the alkyl chain [29,30]. Aforementioned enzyme PqsL is needed for the production of HQNO, as it delivers the *N*-oxidised substrate 2-HABA for PqsBC-mediated condensation with octanoyl-CoA analogous to HHQ biosynthesis [27].

PQS-mediated pathogenicity traits and molecular targets

P. aeruginosa makes use of an arsenal of virulence factors and other pathogenicity traits to overwhelm and colonise the host in the infection process [5] and pqs QS plays a crucial role in the regulation of many of those. It is astonishing, that expression of 182 genes is altered in response to exogenous PQS [33]. Evidence has been gathered, that these effects are mediated either through direct PqsR-dependent action or by PqsR-independent mechanisms, which are most likely due to the iron-chelating as well as antioxidant properties of PQS [33]. Furthermore, it has been unravelled that the thioesterase PqsE, whose biosynthetic function is dispensable due to the presence of alternative thioesterases in *P. aeruginosa*, is actually also a major effector molecule of *pqs* QS [33]. Via a yet unknown mechanism, this enzyme regulates 145 genes, while only 30 of these overlap with the PQS regulon. It seems that these two are the main mediators of *pqs* QS response. In terms of pathogenicity traits, they are involved in the regulation of genes encoding for enzymes responsible for phenazine biosynthesis (pyocyanin production), hydrogen cyanide synthesis, Lectins LecA and LecB and additional genes involved in biofilm formation, enzymes for rhamnolipid synthesis, a Resistance-Nodulation-Cell division (RND) efflux pump encoded by *mexGHI-opmD* operon, components of Type 3 and Type 6 secretion as well as the exotoxin ExoS, and siderophore synthases [33].

In addition to virulence regulation, some remarkable secondary effects have been attributed to the PQS molecule [34]. This autoinducer has been described to mediate iron acquisition, cytotoxicity, outer-membrane vesicle biogenesis, and to exert host immune modulatory effects [34,35]. Interestingly, PQS as well as HHQ are able to interfere with nuclear transcription factor-κB and hypoxia-inducible factor 1 (HIF-1) signaling pathways and, thus, down-regulate host innate immune systems [36,37]. Other PQS-related metabolites have been shown to have additional effects. HQNO, for example, induces autolysis and release of extracellular DNA thereby promoting biofilm formation and increasing meropenem tolerance [38]. HQNO acts through inhibition of complex III in the respiratory chain of bacteria and mitochondria of eukaryotes and, hence, it can be considered a general cytotoxic agent. DHQ, a shunt product of the PQS biosynthetic pathway, is important for *P. aeruginosa* virulence in a *Caenorhabditis elegans* model and also excerts a growth inhibitory effect on epithelial cells [26,39]. Finally, 2-AA has been described to be important for persister cell formation, a very important tolerance mechanism against antibiotic treatment [40].

Among the virulence factors which are directly or indirectly controlled by pqs QS, pyocyanin is one of the most prominent. This redox-active pigment is responsible for the greenish-blueish colour of *P. aeruginosa* cultures. It seems that generation of reactive oxygen species is a major mechanism of pyocyanin cytotoxicity [41]. This tricyclic compound is known to induce apoptosis in neutrophils, but also to enhance neutrophil extracellular trap formation [42,43]. Both mechanisms impair neutrophil-mediated host defenses. Additionally, it has been hypothesised that pyocyanin functions as an extracellular electron shuttle, contributing to redox homeostasis of *P. aeruginosa* cells in biofilms with anaerobic conditions [44].

Due to these important virulence mechanisms, which are under direct or indirect control of pqs QS, targeting this master regulatory system with small molecular compounds, thereby blocking *P. aeruginosa* pathogenicity, is very attractive. However, this complex network of biosynthetic pathways and effector molecules renders selection of the perfect point for intervention difficult. Due to their rather peripheral role in AQ synthesis, PqsH and PqsL, have not been of significant interest for QSI discovery to date. However, all enzymes of the primary biosynthetic cascade pqsA–E as well as the signal molecule receptor PqsR might be valuable drug targets. Also, agents capable of modulating more than one target could be of interest. The question is, which of these targets and/or combinations asserts the most relevant virulence-attenuated phenotype after QSI treatment.

PqsA inhibitors

Anthranilic acid analogues

Since anthranilic acid (**1**) serves as a PqsA substrate, the first compound reported to inhibit PqsA is 6-FABA (**2**, Figure 3), which was able to block this enzyme and successfully suppressed the production of DHQ in PA14 strains at a rather high concentration of 1.5 mM. Moreover, it was shown that 6-FABA had no impact on the bacterial growth. Lépine et al. suggested that **2** competitively occupies the active site of PqsA [45] and therefore serves as a substrate analogue of AA (**1**). It was stated that the introduction of electron-withdrawing substituents could prevent activation of the carbonyl group as a CoA-ester.

In 2017, Witzgall et al. were able to co-crystallize 6-FABA-AMP within the *N*-terminal domain of PqsA (Figure 4) [46].

Key interactions involve a water-mediated hydrogen bond between the amino function of the compound and Q162, as in anthraniloyl-AMP. The reason why the fluorinated anthraniloyl-AMP shows good affinity is the formation of a hydrogen bond of the fluorine with the G279 backbone amide hydrogen and furthermore an interaction with the N7 position of the adenine moiety. Additionally a very typical fluorine/main-chain interaction with G302 could be observed.

Various halogenated derivatives of AA could also reduce HHQ and PQS levels. Especially 4- and 6-CABA (**3**, **4**) showed promising results in the suppression of signal molecules as well as in an in vivo mouse survival model at a concentration of 1.5 mM [47].

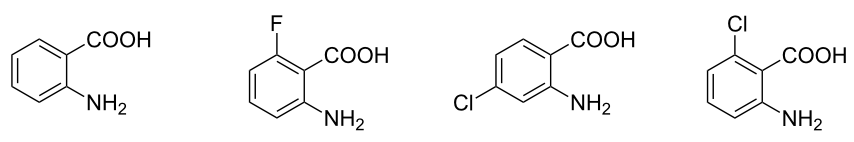

1 **2** **3** **4**

Figure 3: Anthranilic acid (**1**) and derivatives thereof (**2**–**4**).

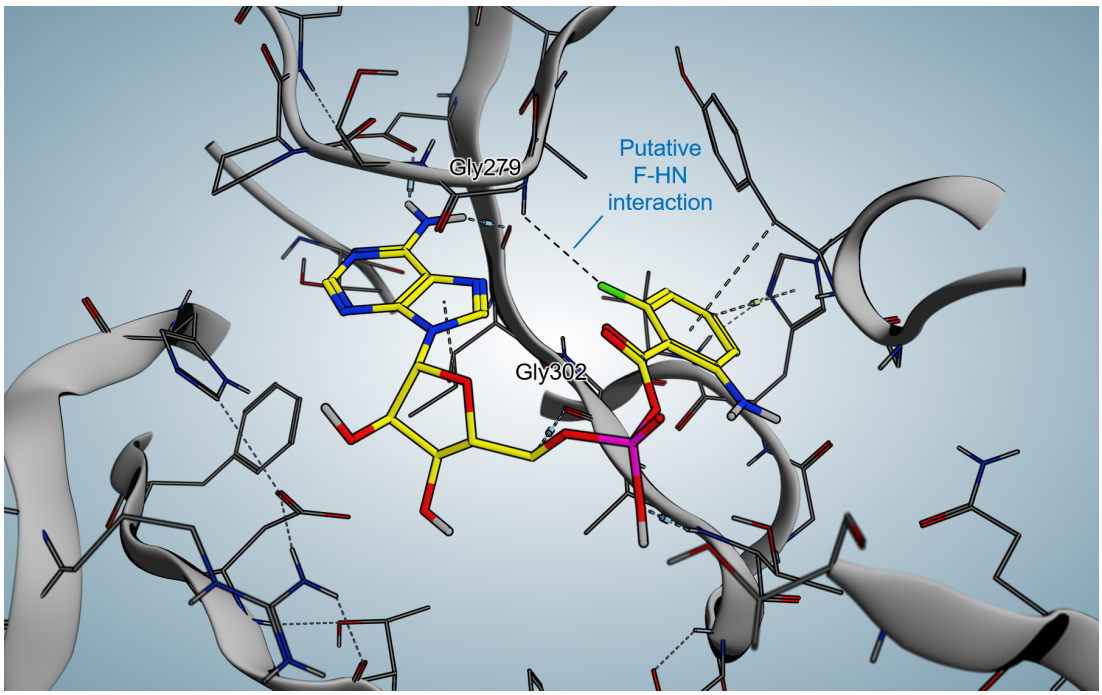

Figure 4: Crystal structure of 6-FABA-AMP in complex with PqsA.

Anthraniloyl-AMP mimetics

More recently, Ji et al. published two classes of sulfonyladenosine inhibitors, more precisely the sulfamate/sulfamide inhibitors **5**–**9** and the vinyl sulfonamide inhibitors **10** and **11** (Figure 5). While the latter showed very low affinity for the protein, the former displayed K_i values between 88 nM for compound **7** and 420 nM for compound **9**. Despite these promising results, the designed molecules were not able to reduce the signal molecules HHQ and PQS at satisfactory levels (300 µM < IC_{50} < 880 µM).

A plausible reason for this outcome might be low cell penetration and/or efflux pump mechanisms, which was supported by compound accumulation studies [48].

PqsD inhibitors

PqsD, the second enzyme in the biosynthetic cascade, has been studied intensely by the Hartmann group. Several design strategies have been pursued leading to diverse structural classes of inhibitors (Figure 6). Unfortunately, for none of these compounds an X-ray structure in complex with PqsD has been reported although the apoenzyme as well as a substrate-bound form has been successfully crystallized [49]. Using these coordinates, employing in silico methods allowed proposing plausible binding poses for prototypic analogues of the respective structural classes.

The first reported inhibitors of PqsD were 2-benzamidobenzoic acids [50]. In a pioneering study on the biosynthetic function of

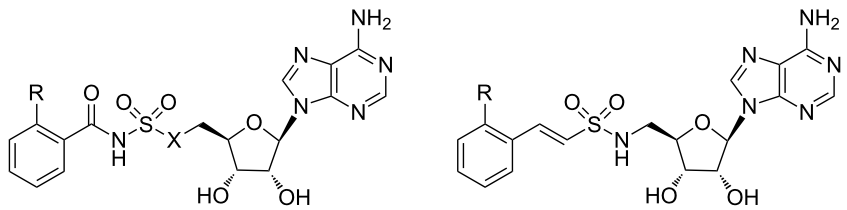

5 R = OH, X = O
6 R = OH, X = NH
7 R = NH_2, X = NH
8 R = NH_2, X = O
9 R = H, X = O

10 R = NH_2
11 R = OH

Figure 5: Structures of substrate mimetic PqsA inhibitors.

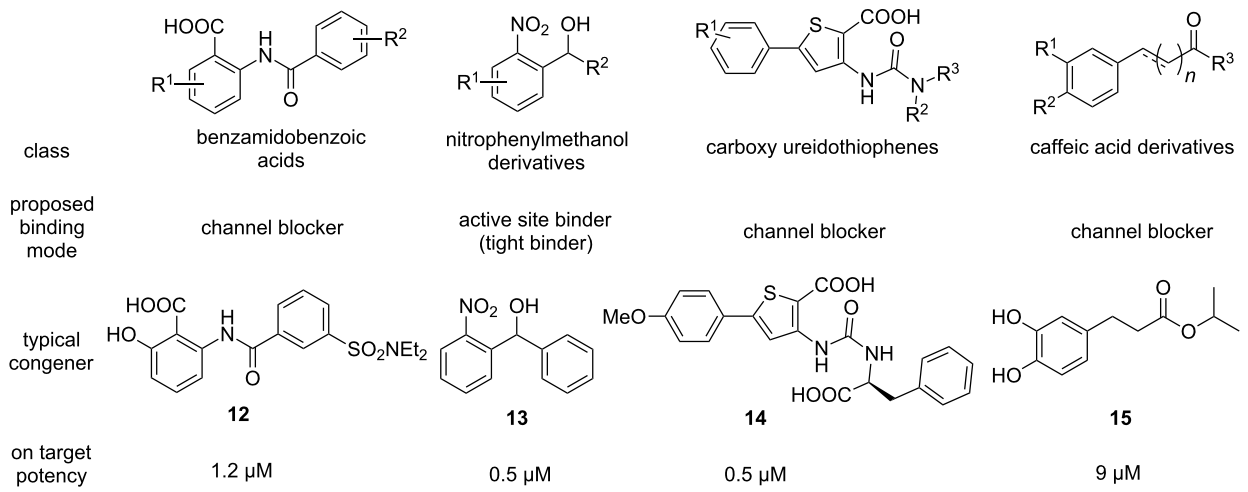

Figure 6: Structures and characteristics of prominent classes of PqsD inhibitors.

this β-ketoacyl-ACP synthase III (FabH)-type enzyme, known blockers of FabH were described to also inhibit this related target [50]. The claim that PqsD is directly responsible for HHQ production by using anthraniloyl-CoA and β-ketodecanoate as substrates, had to be revised later to also include PqsE and PqsBC as participants in AQ biosynthesis in *P. aeruginosa* (vide supra) [27]. Nevertheless, this conversion is indeed catalysed by PqsD in vitro and was successfully exploited for devising a valuable assay, which served as an SAR driver for most of the literature-known PqsD-directed projects. Further benzamidobenzoic acid derivatives were explored for their efficacy and a binding mode was proposed based on SPR- and STD-NMR-assisted docking [51]. These inhibitors appeared to bind in the substrate channel in a slightly remote position from the active site cysteine and, hence, termed channel blockers [51]. Optimised hits exhibited a potency in the single-digit micromolar range (**12**, Figure 6). However, it has been found that similar compounds also showed activity against RNA polymerase, a popular target for the development of new antibiotics [52,53]. Hitting such a target would jeopardise the principle of pathoblockers, which should only disarm the bacteria and not kill them. Hence, a follow-up study on PqsD/RNAP selectivity was conducted providing insights into motifs granting selective PqsD inhibition [52].

In a ligand-based approach, nitrophenylmethanol derivatives were identified as fragment-sized inhibitors of PqsD. Initially, these compounds where designed as transition state analogues mimicking the tetrahedral reaction intermediate between PqsD and anthraniloyl-CoA [54]. Upon simplification and rigidification through reduction in size as well as removal of rotatable bonds inhibitor **13** was obtained carrying the characteristic secondary alcohol of this class. Notably, both enantiomers of **13** show similar potency, but different thermodynamic profiles as measured via isothermal titration calorimetry (ITC) [55]. Despite its low molecular weight, **13** showed tight-binding kinetics and was able to reduce production of HHQ, as well as PQS. Furthermore, it was capable of attenuating biofilm production [54]. All the information gathered via site-directed mutagenesis combined with thermodynamic profiling, as well as surface plasmon resonance (SPR) experiments with and without covalent active site blockade, corroborated that the nitrophenylmethanol class directly binds to the active site near the reactive cysteine of PqsD [55]. This is in line with the initial transition state analogue design principle. Further structural exploration of this class showed that this fragment-like size helps to retain cellular activity [56]. While fragment growing could increase target activity to the nanomolar range, a complete loss of efficacy in the *P. aeruginosa* quorum quenching assays was observed [56]. This highlights a notable issue when addressing intracellular targets of this Gram-negative bacterium, as permeating the outer and inner membrane while escaping efflux and enzymatic deactivation may represent a true challenge.

The elucidation of the binding mode of the nitrophenylmethanol class was then exploited to gain insights into the interaction profile of another chemotype of PqsD inhibitors – the ureidothiophenes (Figure 6) [57,58]. An initial hit showing activity against the enzyme in the single-digit micromolar range was studied using a tailor-made SPR experiment including truncated and elongated derivatives as well as nitrophenylmethanol-based active-site blockers of different size as competitors. These experiments combined with molecular docking (Figure 7) led to the postulation of a plausible binding pose characterising the ureidothiophenes as channel blockers. This model was suc-

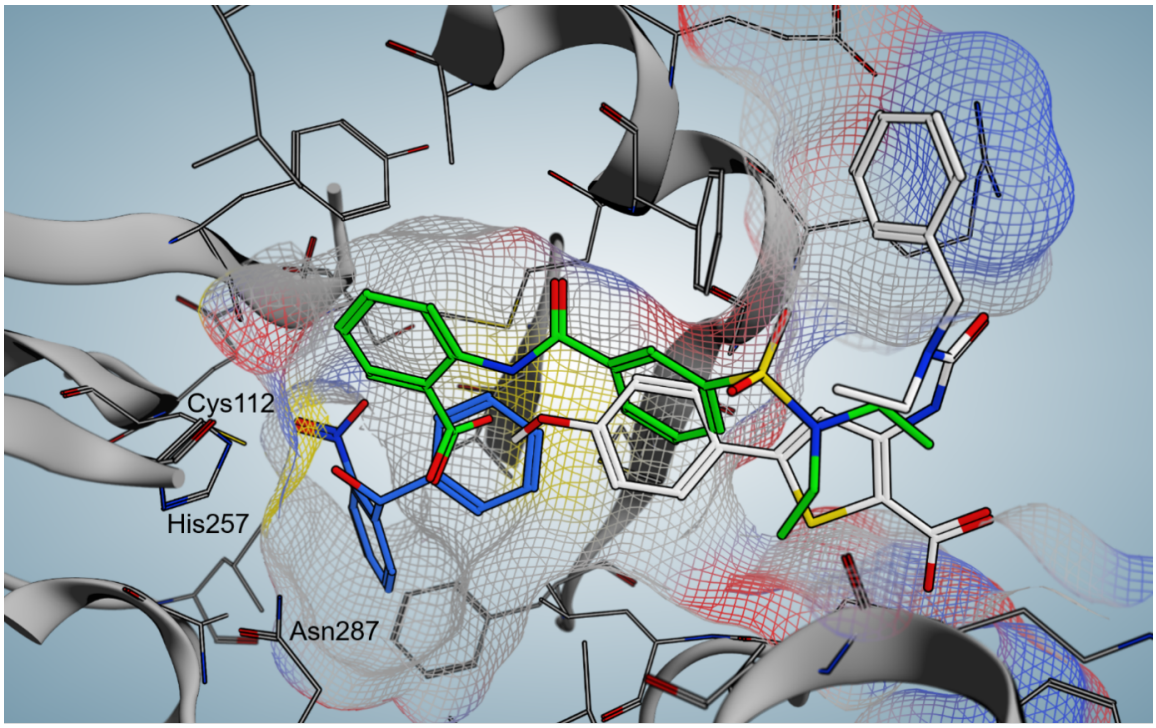

Figure 7: Comparison of docking poses of three prototypic PqsD inhibitors: benzamidobenzoic acid derivative **12** (green), nitrophenylmethanol derivative **13** (blue), carboxy ureidothiophene derivative **14** (white). Active site residues are labelled and the surface of the substrate tunnel is indicated by a mesh.

cessfully used for further optimisation attempts and nanomolar potency in the enzyme assay was achieved (**14**, Figure 6) [57,58]. Notably, a nucleophilic warhead could be introduced specifically reacting with the active-site cysteine through elongation into the substrate tunnel [57]. The binding models of the ureidothiophene and nitrophenylmethanol classes even allowed for the generation of a merged inhibitor [58]. One major liability of this class, however, was the general inefficacy in whole cell assays, which could not be improved, even through the attachment of a cell-penetrating peptide sequence [58].

One additional class, which did show cellular activity, was based on a catechol scaffold [59]. In analogy to the successful discovery of PqsD inhibitors starting from known FabH-targeting compounds (vide supra), ligands of another enzyme with high similarity to the signal molecule synthase were investigated. Here, substrates of chalcone synthase CHS2 from *Medicago sativa* were tested for their ability to block PqsD function. Indeed, caffeic acid analogues, such as **15**, were identified as hits and further characterized as channel blockers as described before [59].

Further interesting starting points for the discovery of PqsD inhibitors have been provided by a dedicated screening campaign involving fragment-based hit discovery, in silico screening and a similarity-guided approach starting from FabH inhibitors [60]. The most potent hit **16** of this study showed activity in the nanomolar range (Figure 8). Furthermore, a tetrazolopyrimidinone scaffold **19** has been reported to inhibit PqsD through a putative blockade of the CoA binding site [61].

The Böttcher group used a library of HHQ as well as PQS analogues to screen for PqsD inhibition [62]. To this end, a novel competition assay employing ‘clickable’ active-site-labelling probes was developed. These compounds contain terminal alkyne moieties, which can be exploited for straightforward decoration via copper(I)-catalyzed alkyne–azide cycloaddition (CuAAC), the prototypic click reaction. This facilitated the discovery of novel PqsD-targeting compounds through CuAAC-mediated conjugation of a fluorescent dye (Figure 9) [62].

Finally, Sangshetti et al. reported the discovery of linezolid-like Schiff bases, which showed promising anti-biofilm activity in the double-digit micromolar range [63]. Notably, their potency in attenuating biofilm formation was more pronounced than ciprofloxacin and linezolid itself. A docking study suggested PqsD to be the target of these compounds like **23** (Figure 10), although this remains speculative.

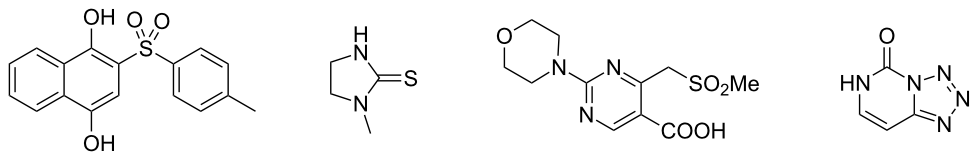

	16	17	18	19
hit identification method	target similarity (FabH inhibitor)	fragment screening	virtual screening	purine base mimic
proposed binding mode	channel blocker	channel blocker	channel blocker	channel blocker
on target potency	0.2 μM	4.7 μM	2.6 μM	9 μM

Figure 8: Structures and characteristics of hits against PqsD identified through different methods.

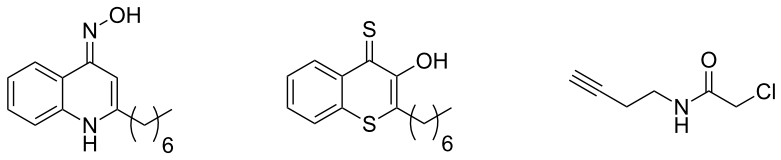

	20	21	22
type	HHQ derivative	PQS derivative	click probe used for competition assay
activity in competition assay	fully active at 240 μM	fully active at 24 μM	covalent active-site binder

Figure 9: HHQ and PQS analogues as PqsD inhibitors and chemical probe used for screening.

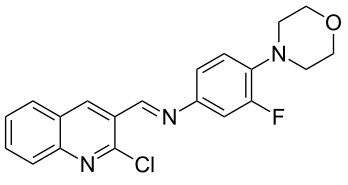

23
linezolid-like Schiff base

Figure 10: Structure of PqsD-targeting biofilm inhibitor derived from linezolid.

PqsE inhibitors

The pathway-specific thioesterase PqsE is not only responsible for hydrolyzing 2-ABA-CoA to form 2-ABA, but moreover also regulates bacterial virulence [29]. It has been shown that PqsE is a key effector of the *pqs* system and required for full *P. aeruginosa* virulence. One of its most prominent functions is the upregulation of pyocyanin, which is mediated through the *rhl* system. Notably, PqsE can still exert its function in absence of an active *pqs* QS [64,65]. Its important role in virulence regulation renders this enzyme an attractive target for pathoblockers.

In 2016, Zender et al. reported their attempt to inhibit PqsE through fragment-based screening. In order to block the thioesterase activity of the enzyme, a library of 500 fragments was screened via differential scanning fluorimetry (DSF) and the hit fragments **24**–**26** (Figure 11) were further validated using isothermal titration calorimetry (ITC) [66]. Binding to PqsE could be confirmed with K_D values of 0.9 ± 0.3 μM for **24** and 19.6 ± 3.7 μM for **26**.

The highly enthalpy-driven binding indicates a specific noncovalent interaction of **24** to the protein. To further investigate the binding mode of the hit fragments in the protein crystallization experiments were performed. Since the native substrate 2-ABA-

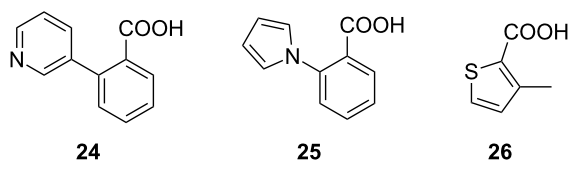

Figure 11: Fragment-based PqsE-inhibitors **24**–**26**.

CoA shows a short half-life, the reaction product 2-ABA was used as a surrogate to compare its binding mode with that of the hit fragments.

Even though the screening hits occupy the same binding site as the native cleavage product 2-ABA, the binding mode is different. The fragments bridge the two metal atoms in the binuclear active center via a water molecule in contrast to 2-ABA, where the carboxylate occupies this position (Figure 12). Moreover both, 2-ABA and the ligands **24**–**26** are stabilized by hydrophobic interactions. Additionally, compounds **24** and **25** are interacting with a histidine (His71) sidechain via π-stacking. For the thiophene-containing fragment **26** a π–π interaction of the sulfur with Phe195 can be observed.

In vitro evaluation was performed using a combined PqsDE assay due to the aforementioned instability of 2-ABA-CoA which in this scenario is generated in situ from anthraniloyl-CoA via PqsD-mediated condensation with malonyl-CoA. The hit fragments were able to block the thioesterase in the micromolar range (e.g., IC_{50} (**24**) = 25 ± 4 μM). When assessing the hits on *Pseudomonas* cultures, thioesterase inhibition remained, whereas none of the compounds had any impact on pyocyanin production at a concentration of 500 μM. This means that the regulatory function of PqsE is not linked to its hydrolase function. Since the regulatory function of the enzyme is not associated to its active site, it was hypothesized that it might be involved in a macromolecule–macromolecule interaction, e.g., protein–protein or protein–DNA/RNA interaction, while the exact molecular mechanism remains unclear. Even though Zender et al. were not able to attenuate PA virulence via blockage of PqsE, important new insights on this target were made. The discovery that pathoblockers targeting PqsE assumedly may not need to target the active site of the enzyme, but rather a different pocket or surface. To this end, further research on the exact molecular mechanism of the regulatory activity of PqsE is needed.

PqsBC

The small molecule 2-AA (**27**), which is also a secondary metabolite generated in the AQ biosynthesis pathway, was reported to inhibit PqsBC [31]. In a PqsBC-based biochemical assay it showed an IC_{50} in the micromolar range and was proven to reduce virulence in an acute mouse infection model [67].

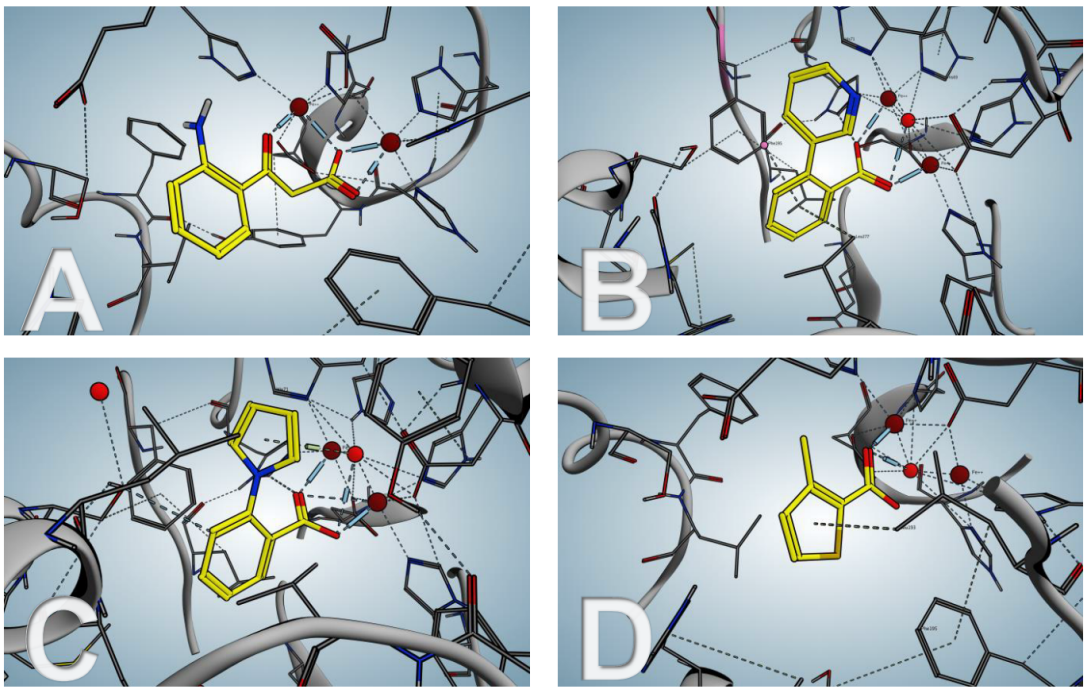

Figure 12: PqsE co-crystal structures. (A) native product 2-ABA; (B–D) hit fragments **24**–**26**.

In 2017, Maura et al. synthesized inhibitors based on a benzimidazole scaffold (Figure 13) [68]. Starting from a PqsR inhibitor, changes of the electronic properties on the benzimidazole by introducing an electron-donating group led to a higher PqsBC inhibitory activity, while decreasing the affinity to PqsR (compound **28**).

Nevertheless, it was shown that blockage of PqsBC leads to a reduction of HHQ but an accumulation of DHQ, which is reported to be toxic for epithelial cells, and 2-AA, which is involved in formation of persister cells [69]. In the same work, compounds **29** and **30** were evaluated. Compound **29** was first reported in a study aiming at the design of PqsD inhibitors, showing only very weak activity against this target. However, it showed surprisingly good effects on signal molecule production in cell-based assays. Later it was found that this compound actually gains its cellular activity through inhibition of PqsBC [56,70]. As already expected from previous results these compounds also showed a strong increase in 2-AA and DHQ production, while not affecting the overall production of AQ's.

PqsR

In 2017 Kamal et al. investigated the structure–functionality relationship of compounds targeting PqsR. They differentiated between agonists, neutral agonists, inverse agonists and agonistic/antagonistic mixed profile compounds. It was shown that only inverse agonists were able to reduce transcriptional levels below basal and with that the production of pyocyanin. This implies that the aim is to search rather for inverse agonists than for antagonists [71].

Ligand-based design

Following a ligand-based approach Lu et al. modified the native PqsR ligand HHQ (**31**) by introducing a strong electron-withdrawing nitro group in the 6-position (compound **33**) [72]. While displaying an IC_{50} of 51 nM in an *E. coli*-based reporter gene assay, **33** was also able to reduce pyocyanin production to 44% at 15 μM. Further investigations showed that when conducting the reporter gene assay in *P. aeruginosa* instead of using the heterologous *E. coli* system activity of **33** was drastically reduced (only 60% inhibition at 10 μM). The reason for this drop in activity was the cell-mediated oxidation of the 3-position of the quinolone core through action of the *P. aeruginosa* enzyme PqsH (Figure 14), turning the inverse agonist **33** into a strong agonist **34** (EC_{50} = 2.8 nM).

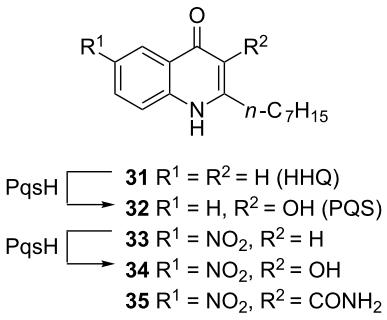

Figure 14: Native PqsR ligand HHQ (**31**) which is converted into PQS (**32**) by PqsH and synthetic inhibitors **33** and **35**, former is also converted by PqsH into the strong agonist **34**.

This phenomenon was overcome by blocking the metabolic susceptible 3-position with various functional groups resulting in **35** which showed good activity in both *E. coli* (IC_{50} = 35 nM) and *P. aeruginosa* (IC_{50} = 404 nM) based reporter gene assays. Furthermore, this compound was able to inhibit pyocyanin production with an IC_{50} of 2 μM and HHQ levels were reduced to 54% at a concentration of 15 μM. Additionally the Hartmann group demonstrated that **35** enables survival of PA14-infected *Galleria melonella* larvae [73]. Moreover, the optimised compound also benefited from a decreased clogP value compared to the parent compound **33**, which is reflected in an improved solubility [74]. In a recent publication by Kamal et al. the pharmacological profiles of several alkylquinolone compounds were investigated in a structure–functionality relationship manner, resulting in four different profiles: (a) agonists, (b) antagonists, (c) inverse agonists and (d) biphasic modulators. These studies revealed that pyocyanin production is only decreased significantly when the QS modulators are inverse agonists. It was hypothesized that the already mentioned 3-position is crucial for the functionality. Depending on the groups installed in this position and, hence, the different ligand–protein interactions they introduce, com-

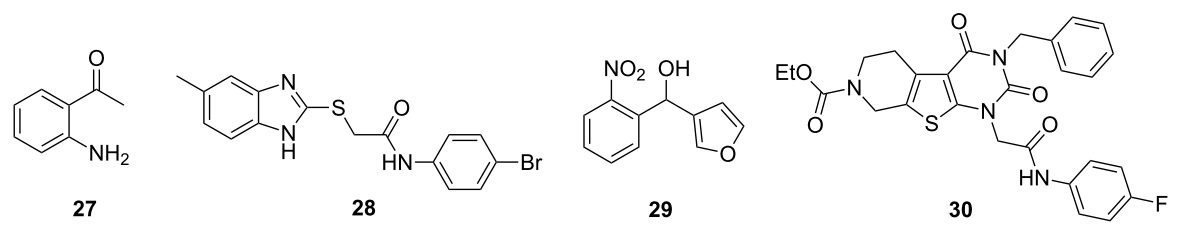

Figure 13: Structurally diverse PqsBC-inhibitors **27**–**30**.

pounds are either agonists, antagonists, or inverse agonists. This hypothesis was in accordance with a study made by Shanahan et al. who synthesized various other C-3 substituted analogs [75].

Ilangovan et al. discovered a quinazoline scaffold as another class of ligand-based hit compounds. Based on the C9-congener of HHQ several substituted 2-alkyl-4(*H*)-quinazolines were synthesized. The most potent compound **36** (Figure 15) showed micromolar inhibition in *P. aeruginosa* and was able to decrease pyocyanin levels down to less than 0.5 µg/mL at 100 µM. Furthermore, AQ signal molecules could also be suppressed. The crystal structure of the PqsR co-inducer binding site in complex with **36** was solved at 2.95 Å resolution (Figure 16), as well as a co-crystal structure of the native HHQ C9-congener NHQ [76] demonstrating a competitive binding mode.

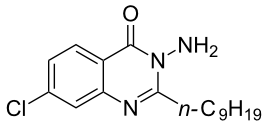

36

Figure 15: Quinazolinone inhibitor **36** (QZN).

When compared to the native ligand NHQ, **36** shows similar hydrophobic interactions (Figure 16). In addition, the chlorine is able to occupy a vacant sub pocket. A hydrogen bond is found between the backbone oxygen of L207 and the 3-NH_2 hydrogen atoms. Interestingly, adding the chlorine substituent in 7-position of PQS leads to a 135 times more potent agonist, indicating the importance of the vacant sub pocket next to T265. This also indicates that the quorum quenching activity of **36** depends on slight conformational changes. The L1 loop main chain and a rotation of the T265 side chain are hypothesized to be important for antagonistic/inverse agonistic functionality of PqsR-targeting QSIs.

More recently the same group used docking studies to select compounds from a quinolone-based compound library (Figure 17). The best fitting compounds **37**–**40** were then evaluated in a whole bacterial cell-based *P. aeruginosa* screening

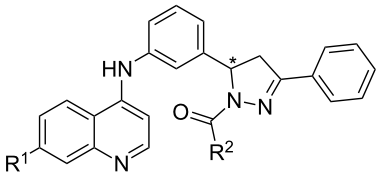

37 R^1 = Cl, R^2 = H
38 R^1 = Cl, R^2 = Me
39 R^1 = CF_3, R^2 = H
40 R^1 = CF_3, R^2 = Me

Figure 17: Structures of best fitting compounds **37**–**40** obtained from docking studies.

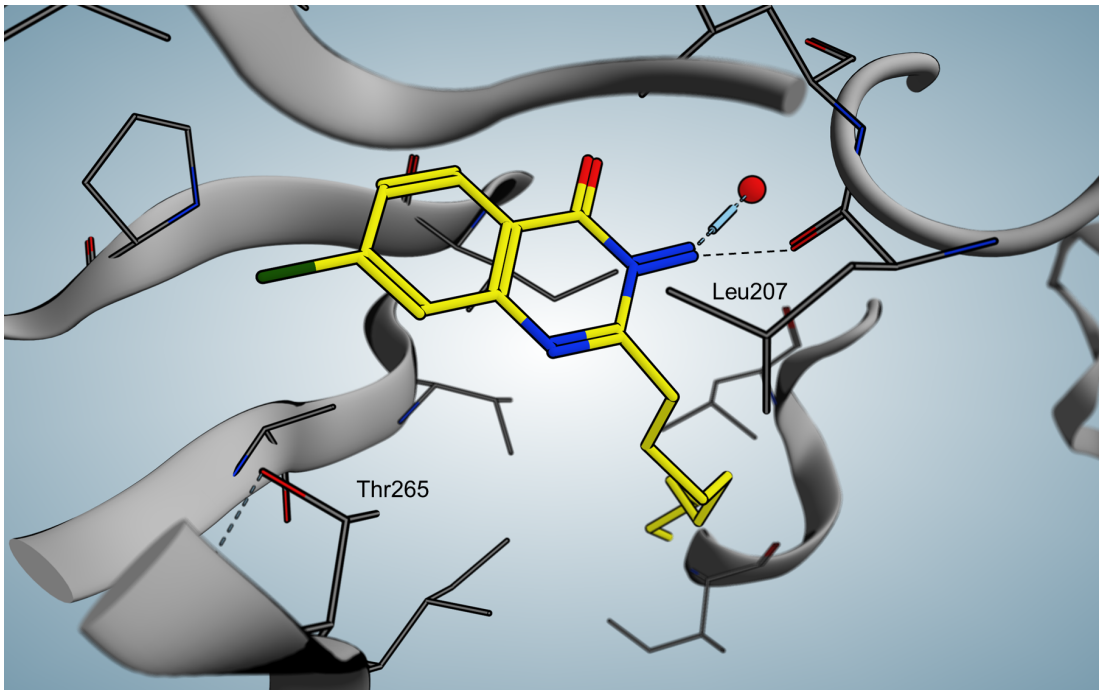

Figure 16: Crystal structure of QZN (**36**) in complex with $PqsR^{CBD}$.

with IC_{50} values in the low micromolar range. Additionally, they showed that compound **37** emerged as the most potent inhibitor of this series.

Compounds **37** and **39** furthermore exhibited inhibition of HHQ, PQS and HQNO production in PAO1 strains when treated with 3 × IC_{50}, whereas in PA14 a strong decrease in activity could be observed, especially for **39**.

Benzamide-benzimidazole (BB) series

In 2014, Starkey et al. performed a high-throughput whole-cell screening and identified the benzamide-benzimidazole (BB) motif as a promising scaffold for the inhibition of PqsR [77]. Starting from **41**, which was not only able to suppress expression of AQs but also completely blocked pyocyanin production at a concentration of 10 μM. Various analogues were synthesized resulting in compound **42** (M64), where similar as in the quinolones described by Lu et al., introduction of the electron-withdrawing nitro function led to very potent inverse agonist (Figure 18) [72]. M64 (**42**) proved a very potent inhibitor of HAQ and pyocyanin production at 1 μM.

Further investigations revealed that M64 (**42**) also reduces 2-AA levels leading to a decreased rate of persister cells. The compound also proved to be active in burn wound and lung infection models in mice and increased survival rates especially when applied in combination with sub-therapeutic doses of ciprofloxacin. In an analytics-driven study by Allegretta et al., the compound was further profiled regarding suppression of the PQS-related metabolites DHQ, 2-AA, HHQ, PQS and HQNO. In brief, this study demonstrated that PqsR is an excellent target for potent QSI compounds effectively suppressing AQ levels and 2-AA production at reasonable concentrations [69]. Lately, Maura and Rahme were able to demonstrate the effect of M64 (**42**) on biofilm formation [78]. Biofilm biomass was drastically reduced when treated with 1 and 10 μM of **42** compared to the untreated PA14 control. Function of PqsR is involved in regulation of HQNO-mediated autolysis and eDNA release, which has been reported to be important for antibiotic tolerance of biofilm-inheriting bacteria. Hence, Rahme and co-workers investigated the effect of their compound **42** on the ability to improve antibiofilm effects of two clinically relevant drugs. When growing biofilms for 48 h in presence or absence of M64 (**42**), followed by treatment of 10 μg/mL of meropenem or tobramycin for 24 h, the activity of the otherwise ineffective antibiotics could be restored. Especially in the case of meropenem, which did not have any effects at all on biofilm viable cells, **42** lead to remarkable results. In 2018, Kitao et al. solved the crystal structure for PqsR ligand binding domain in complex with M64 (**42**) with a resolution of 2.65 Å (Figure 19), unravelling the exact interactions of the compound with the protein [79].

Indicated key interactions are π-stacking of Y258 with the phenoxy moiety in the tail region and a hydrogen bond formed between the Q194 side chain and the carboxamide in the linker area. Furthermore the benzimidazole core shows hydrophobic contacts with isoleucins 149 and 236. More hydrophobic interactions were observed in the tail region, in particular with leucins 189 and 208 as well as Y258. Mutations at these specific residues indicated that the π–π interactions of Y258 are crucial for M64's full inhibition with respect to pyocyanin production, which was only weakly inhibited in an Y258M *P. aeruginosa* mutant strain. The importance of the phenoxy substitutent was further supported by a congener of M64 that lacks this motif and therefore is unable to be involved in π-stacking resulting in a nine-fold increased IC_{50} value compared to M64. Even though there is no specific interaction observed for the nitro function it is crucial for the activity and thus believed to form an instable H-bond with T265. The Rahme group already demonstrated in a former ITC assay that M64 is directly bound in the PqsR LBD [77]. However, they were also suggesting inverse agonistic effect of M64 based on mutation experiments [79]. Moreover an in vivo cross-linking assay of full-length PqsR and a corresponding I68F mutant was carried out leading to the suggestion that upon binding of M64 the protein stability might be increased. Based on these results it was proposed that M64 induces a change in conformation of the PqsR-DNA binding domain, whereas the LBD is not affected extensively.

Aryloxyacetindoles

Spero Therapeutics further optimized M64 (**42**), firstly by changing the phenoxyphenylamide into a carbonyl-linked

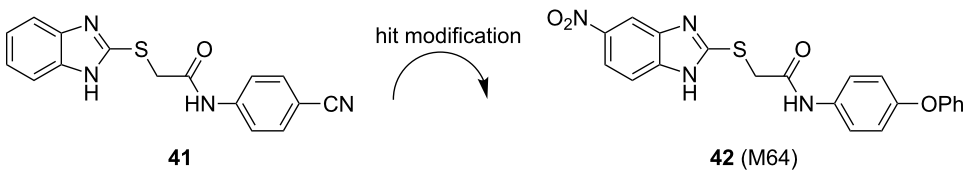

Figure 18: Initial hit **21** and optimized compound **42** (M64).

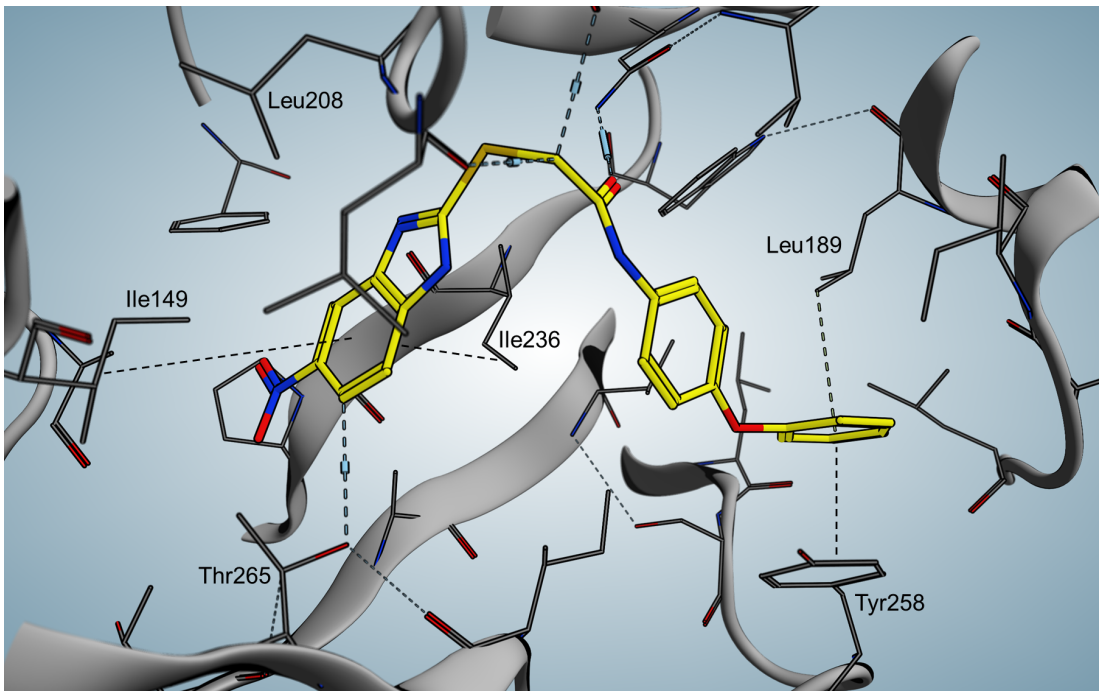

Figure 19: Co-crystal structure of M64 (**42**) with $PqsR^{LBD}$.

indole containing a hetarylether (**43**) [80]. Afterwards they varied the linkage of the benzimidazole moiety (compound not shown) [80]. In a follow-up patent they generated PqsR inhibitor **45** as a front-runner compound [81], in which the benzimidazole headgroup was replaced by a substituted naphthalene bearing a carboxamide, in analogy to a fragment **44** of Zender et al. [82] and similar to the carboxamide-decorated nitro-quinoline scaffold described by Lu et al. (Figure 20) [73].

Compound **45** was highly potent in inhibiting pyocyanin production (stated IC_{50} in a range of 50–250 nM) and was furthermore able to suppress PQS and HHQ production (50 nM < IC_{50} < 250 nM). In a murine thigh infection model using PA14, target engagement was demonstrated in vivo measuring PQS and HHQ levels from the corresponding tissues after treatment. Compound **45** was able to reduce PQS and HHQ levels to 50% and 40%, respectively, 12 hours post-infection. Up to now no further optimization or development of these compounds has been reported.

Fragment-based design

In 2012 Klein et al. obtained the benzamides **46** and **47**, as well as the hydroxamic acid **48** as hits within an SPR screening, which were further evaluated in ITC experiments in order to have a clearer view on the thermodynamic parameters (Figure 21). The antagonists displayed activity in a low double-digit µM range, but had only a marginal impact on the production of the virulence factor pyocyanin [83].

Further SPR screenings afforded hits **49**–**51** with EC_{50} between 7.5–17.8 µM. When compared to the benzamide class, compound **49** shows no significant increase in affinity to the target receptor but is able to inhibit pycocyanin formation by 46 ± 9% at a concentration of 250 µM, and is capable of reducing the AQ's HHQ and HQNO up to 43 ± 3% at the same concentration [82]. With these fragments in hand further growing and subsequent linking or merging may open new avenues for the generation of new drug-like PqsR inverse agonists.

Dual target QS inhibitors

PqsBC/PqsR

In an initial target assessment, Maura et al. found that compound **52** showed an ambiguous profile. This raised the question if this compound class could target additional targets of the PQS-system besides PqsR [68]. Experiments with a PqsR isogenic mutant strain revealed that **52** inhibits HHQ and PQS production, while raising 2-AA levels, pointing at PqsBC as a second target, which was corroborated via SPR studies. When exchanging the chlorine to bromine **53** a high PqsR activity was obtained while the affinity to PqsBC decreased (Figure 22).

The iodine-substituted derivative **54** showed both, a high PqsR, as well as a high PqsBC activity. Exchanging the electron-withdrawing nitro functionality with an electron-donating methyl group turned the PqsR antagonist **53** into a very potent PqsBC inhibitor while losing activity on the initial target PqsR. In addition to these mechanistic findings, it was also shown that the

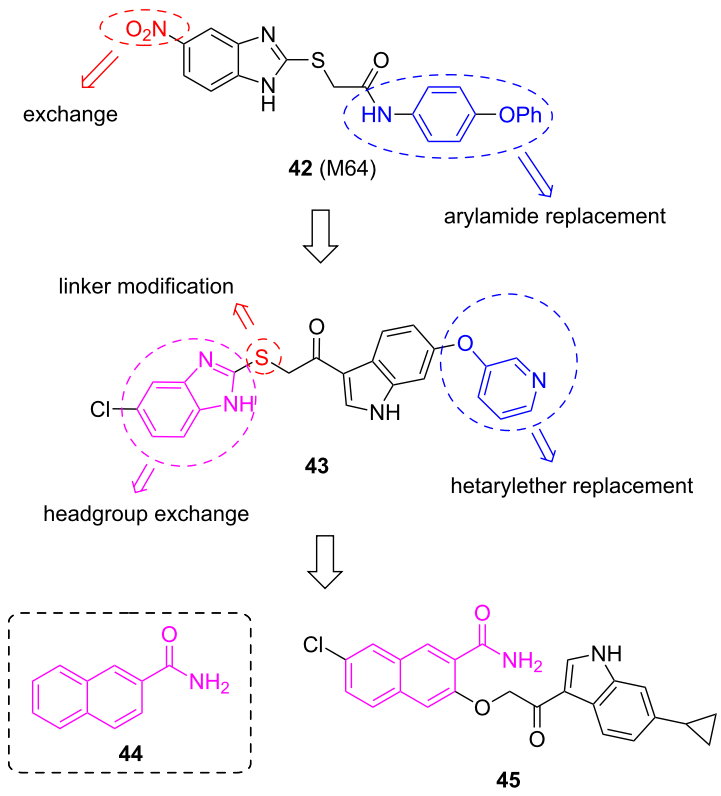

Figure 20: M64 (**42**) as the starting point for further optimization leading to **43**, which was further modified and merged with the fragment **44** to give compound **45**.

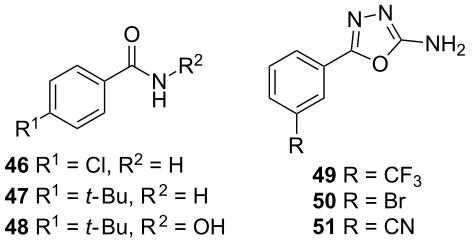

Figure 21: Hit fragments from the benzamide (**47**–**48**) and oxadiazole class (**49**–**51**).

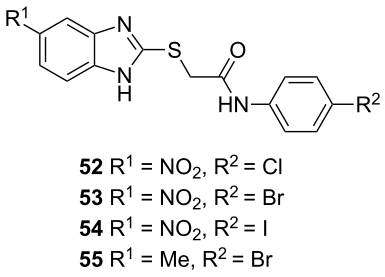

Figure 22: Structures of dual inhibitors **52**–**55**.

dual inhibitors are capable of rescuing human lung epithelial cells and macrophages at a concentration of 50 µM in cell-based infection models. Also antibiotic activity of meropenem (dose: 10 µg/mL) in presence of 10 µM of dual inhibitors could be partially reinstalled.

PqsD/PqsR

Thomann et al. showed that combining a PqsD and a PqsR activity synergistically affects pyocyanin production. Based on these results combining fragments from a PqsR and a PqsD inhibitor belonging to a sulfonyl-pyrimidine class, compound **56** was generated and its ability to reduce pyocyanin evaluated (Figure 23) [84]. While exhibiting IC_{50} values of 15 µM on PqsR and 21 µM on PqsD, the compound was able to inhibit the pyocyanin production with an IC_{50} of 86 µM. Moreover **56** also proved to be efficient in blocking pyoverdine production, another important *P.aeruginosa* virulence factor. When applied at a concentration of 500 µM less than 10% of pyoverdine production was remaining. At 100 µM the pyoverdine amount was cut to a half. Since also the levels of extracellular DNA could be reduced to a minimum with their dual inhibitor, the group investigated the effect of adding **56** to ciprofloxacin. The combination of this QSI together with the antibiotic significantly increased antibiofilm activity at the used concentrations

([CIPX] = 1 μM, [56] = 50 μM). The compound also proved to be active in a *Galleria melonella* survival assay being capable of ensuring survival up to more than 50% after 4.5 d post-infection at a dosage of 1.25 nmol compared to untreated PA14-infected larvae.

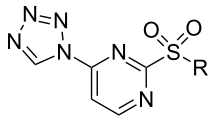

56 R = Me
57 R = *n*-Hex
58 R = 3,4-di-Cl-Ph

Figure 23: Sulfonyl pyrimidines **56**–**58** acting as dual PqsD/PqsR inhibitors.

Following the dual inhibitor concept, the class of sulfonylpyrimidines further afforded compounds **57** and **58** with promising activity. While PqsR activity slightly decreased (50 μM and 24 ± 5 μM, respectively) **57** exhibited an IC_{50} of 1.7 μM and **58** displayed sub-micromolar activity of 0.4 ± 0.1 μM. The effects on biofilm formation and eDNA release were evaluated at a concentration of 100 μM. Even if **57** was less potent on both PqsR and PqsD compared to **58**, it turned out to be more efficient in inhibiting biofilm production. When assessed on their ability to reduce extracellular DNA all three compounds were equally potent. Nevertheless compound **58** only showed a weak effect on the inhibition of pyocyanin (14% inhibition at 100 μM) [85].

Conclusion

In the past decade, the pqs QS system of *P. aeruginosa* has attracted increasing interest by academic researchers. This is certainly due to its prominent involvement in virulence regulation of this important Gram-negative pathogen. Among the various pathoblocker strategies, targeting a master regulator of pathogenicity traits appears to have huge translational potential. Hitting an array of virulence mechanisms at once instead of addressing just singular factor holds great promise for future discovery and development of pqs-targeting QSI. Compared to the other QS systems present in *P. aeruginosa* the pqs system is lacking some of the liabilities associated with the las and the rhl systems. The former AHL-dependent regulatory circuit has been described to be the first QS system to get lost upon chronification of *P. aeruginosa* infections [86]. However, chronic lung infections are one of the major indications with a very high medical need. In the case of addressing the rhl system, a non-unidirectional virulence modulatory effect is observed. Agonists of RhlR reduce pyocyanin, but induce rhamnolipid production, while antagonists have the inverted effect [87]. This raises some concerns about the applicability of RhlR as an effective 'stand-alone' pathoblocker target. A combination of rhl- and pqs-targeting QSI, however, seemed to provide promising and clear-cut antivirulence effects [88]. Finally, the potential of iqs-targeting approaches remains to be investigated as more insight in the function of this rather recently discovered regulator is needed. The pqs system is active in chronically infected cystic fibrosis patients and, according to the current knowledge, blockade of this master regulator delivers an unambiguous antivirulence effect.

In terms of published research, the most studied molecular targets within the pqs system are the signal molecule synthase PqsD and the receptor PqsR (MvfR), while in the latter case projects are currently in a clearly more advanced stage. When comparing the reported antivirulence effects of PqsD- and PqsR-targeting QSI, evidence is growing that hitting the transcriptional regulator results in more pronounced pathoblocking effects than addressing the biosynthetic enzyme cascade. However, a synergistic effect for dual-target inhibitors hitting PqsR and PqsD or PqsBC simultaneously has been described [68,84]. Additionally, the authors believe that attempts to effectively target PqsE are still worthwhile pursuing, given its prominent involvement in pqs virulence regulation. However, this would require elucidating the still unknown mechanism behind its regulatory function.

In order to translate the promising hit and lead compounds described above into the clinic, continuous discovery and development efforts are required. Especially the lead optimization stage is strongly dependent on integrated medicinal chemistry and biological profiling teams. In addition to potency considerations, drug-like properties aiming at favorable pharmacokinetics move into the focus [89]. Due to the complex nature of virulence phenotype assays as well as ADME/T testing cascades assembling the required teams, expertise, and resources might be a challenge especially for academic groups. Hence, often proclaimed drug discovery timelines for target-to-candidate projects of about 6 years or less [90] are quite unrealistic in this field. This actually underpins the urgency for current anti-infective discovery efforts to enable refilling the pipeline in due time before available treatment options run out. However, we believe the translational perspective for such pathoblockers is quite promising. Specifically, it has been shown that PqsR-targeting QSI are able to increase the susceptibility of *P. aeruginosa* biofilms against antibiotics [78]. Hence, adjunctive treatment approaches where a conventional backbone antibiotic therapy is potentiated by pathoblocking agents appears quite attractive. In analogy to current antiviral and anticancer strategies, more personalized pathogen-specific drug combinations should be pursued also in the bacterial infections

field. As a consequence, more advanced diagnostic tools have to be devised to enable fast and reliable analysis of the pathogen and its resistance profile. We are curious what future research will uncover in this important, yet underexploited, drug discovery field and believe exploring such strategies further will be a worthwhile endeavour.

Acknowledgements

We are grateful to Rolf W. Hartmann for his generous and persistent support and guiding expertise.

ORCID® iDs

Martin Empting - https://orcid.org/0000-0002-0503-5830

References

1. Price, L.; Gozdzielewska, L.; Young, M.; Smith, F.; MacDonald, J.; McParland, J.; Williams, L.; Langdridge, D.; Davis, M.; Flowers, P. *J. Antimicrob. Chemother.* **2018,** *73,* 1464–1478. doi:10.1093/jac/dky076
2. Ventola, L. C. *Pharm. Ther.* **2015,** *40,* 277–283.
3. Coates, A. R. M.; Halls, G.; Hu, Y. *Br. J. Pharmacol.* **2011,** *163,* 184–194. doi:10.1111/j.1476-5381.2011.01250.x
4. WHO. An analysis of the antibacterial clinical development pipeline, including tuberculosis. http://www.who.int/medicines/areas/rational_use/antibacterial_agents_clinical_development/en/ (accessed July 30, 2018).
5. Wagner, S.; Sommer, R.; Hinsberger, S.; Lu, C.; Hartmann, R. W.; Empting, M.; Titz, A. *J. Med. Chem.* **2016,** *59,* 5929–5969. doi:10.1021/acs.jmedchem.5b01698
6. Li, X.-H.; Lee, J.-H. *J. Microbiol. (Seoul, Repub. Korea)* **2017,** *55,* 753–766. doi:10.1007/s12275-017-7274-x
7. Żelechowska, P.; Agier, J.; Kozłowska, E.; Brzezińska-Błaszczyk, E. *Przegl. Lek.* **2016,** *73,* 334–339.
8. Mühlen, S.; Dersch, P. Anti-virulence Strategies to Target Bacterial Infections. In *How to Overcome the Antibiotic Crisis. Current Topics in Microbiology and Immunology;* Stadler, M.; Dersch, P., Eds.; Springer: Cham, 2015; Vol. 398, pp 147–183. doi:10.1007/82_2015_490
9. Dickey, S. W.; Cheung, G. Y. C.; Otto, M. *Nat. Rev. Drug Discovery* **2017,** *16,* 457–471. doi:10.1038/nrd.2017.23
10. Kufel, W. D.; Devanathan, A. S.; Marx, A. H.; Weber, D. J.; Daniels, L. M. *Pharmacotherapy* **2017,** *37,* 1298–1308. doi:10.1002/phar.1990
11. Soukarieh, F.; Williams, P.; Stocks, M. J.; Camara, M. *J. Med. Chem.* **2018,** in press. doi:10.1021/acs.jmedchem.8b00540
12. WHO. Global priority list of antibiotic-resistant bacteria to guide research, discovery, and development of new antibiotics. http://www.who.int/medicines/publications/global-priority-list-antibiotic-resistant-bacteria/en/ (accessed July 30, 2018).
13. Schweizer, H. P. *GMR, Genet. Mol. Res.* **2003,** *2,* 48–62.
14. Strateva, T.; Yordanov, D. *J. Med. Microbiol.* **2009,** *58,* 1133–1148. doi:10.1099/jmm.0.009142-0
15. Breidenstein, E. B. M.; de la Fuente-Núñez, C.; Hancock, R. E. W. *Trends Microbiol.* **2011,** *19,* 419–426. doi:10.1016/j.tim.2011.04.005
16. Golemi-Kotra, D. Pseudomonas Infections. *xPharm: The Comprehensive Pharmacology Reference;* Elsevier, 2008; pp 1–8.
17. Bodey, G. P.; Bolivar, R.; Fainstein, V.; Jadeja, L. *Rev. Infect. Dis.* **1983,** *5,* 279–313. doi:10.1093/clinids/5.2.279
18. da Silva Filho, L. V. R. F.; de Agujar Ferreira, F.; Reis, F. J. C.; de Britto, M. C. A.; Levy, C. E.; Clark, O.; Ribeiro, J. D. *J. Bras. Pneumol.* **2013,** *39,* 495–512. doi:10.1590/S1806-37132013000400015
19. Crull, M. R.; Ramos, K. J.; Caldwell, E.; Mayer-Hamblett, N.; Aitken, M. L.; Goss, C. H. *BMC Pulm. Med.* **2016,** *16,* 176. doi:10.1186/s12890-016-0333-y
20. Sordé, R.; Pahissa, A.; Rello, J. *Infect. Drug Resist.* **2011,** *4,* 31–41. doi:10.2147/IDR.S16263
21. Barr, H. L.; Halliday, N.; Barrett, D. A.; Williams, P.; Forrester, D. L.; Peckham, D.; Williams, K.; Smyth, A. R.; Honeybourne, D.; Whitehouse, J. L.; Nash, E. F.; Dewar, J.; Clayton, A.; Knox, A. J.; Cámara, M.; Fogarty, A. W. *J. Cystic Fibrosis* **2017,** *16,* 230–238. doi:10.1016/j.jcf.2016.10.005
22. Lee, J.; Zhang, L. *Protein Cell* **2015,** *6,* 26–41. doi:10.1007/s13238-014-0100-x
23. Li, S.; Chen, S.; Fan, J.; Cao, Z.; Ouyang, W.; Tong, N.; Hu, X.; Hu, J.; Li, P.; Feng, Z.; Huang, X.; Li, Y.; Xie, M.; He, R.; Jian, J.; Wu, B.; Xu, C.; Wu, W.; Guo, J.; Lin, J.; Sun, P. *Eur. J. Med. Chem.* **2018,** *145,* 64–73. doi:10.1016/j.ejmech.2017.12.076
24. Dubern, J.-F.; Diggle, S. P. *Mol. BioSyst.* **2008,** *4,* 882–888. doi:10.1039/b803796p
25. Coleman, J. P.; Hudson, L. L.; McKnight, S. L.; Farrow, J. M., III; Calfee, M. W.; Lindsey, C. A.; Pesci, E. C. *J. Bacteriol.* **2008,** *190,* 1247–1255. doi:10.1128/JB.01140-07
26. Zhang, Y.-M.; Frank, M. W.; Zhu, K.; Mayasundari, A.; Rock, C. O. *J. Biol. Chem.* **2008,** *283,* 28788–28794. doi:10.1074/jbc.M804555200
27. Dulcey, C. E.; Dekimpe, V.; Fauvelle, D.-A.; Milot, S.; Groleau, M.-C.; Doucet, N.; Rahme, L. G.; Lépine, F.; Déziel, E. *Chem. Biol.* **2013,** *20,* 1481–1491. doi:10.1016/j.chembiol.2013.09.021
28. Hutter, M. C.; Brengel, C.; Negri, M.; Henn, C.; Zimmer, C.; Hartmann, R. W.; Empting, M.; Steinbach, A. *J. Mol. Model.* **2014,** *20,* 2255. doi:10.1007/s00894-014-2255-z
29. Drees, S. L.; Fetzner, S. *Chem. Biol.* **2015,** *22,* 611–618. doi:10.1016/j.chembiol.2015.04.012
30. Witzgall, F.; Depke, T.; Hoffmann, M.; Empting, M.; Brönstrup, M.; Müller, R.; Blankenfeldt, W. *ChemBioChem* **2018,** *19,* 1531–1544. doi:10.1002/cbic.201800153
31. Drees, S. L.; Li, C.; Prasetya, F.; Saleem, M.; Dreveny, I.; Williams, P.; Hennecke, U.; Emsley, J.; Fetzner, S. *J. Biol. Chem.* **2016,** *291,* 6610–6624. doi:10.1074/jbc.M115.708453
32. Schertzer, J. W.; Brown, S. A.; Whiteley, M. *Mol. Microbiol.* **2010,** *77,* 1527–1538. doi:10.1111/j.1365-2958.2010.07303.x
33. Rampioni, G.; Falcone, M.; Heeb, S.; Frangipani, E.; Fletcher, M. P.; Dubern, J.-F.; Visca, P.; Leoni, L.; Cámara, M.; Williams, P. *PLoS Pathog.* **2016,** *12,* e1006029. doi:10.1371/journal.ppat.1006029
34. Lin, J.; Cheng, J.; Wang, Y.; Shen, X. *Front. Cell. Infect. Microbiol.* **2018,** *8,* No. 230. doi:10.3389/fcimb.2018.00230
35. Maura, D.; Hazan, R.; Kitao, T.; Ballok, A. E.; Rahme, L. G. *Sci. Rep.* **2016,** *6,* No. 34083. doi:10.1038/srep34083
36. Legendre, C.; Reen, F. J.; Mooij, M. J.; McGlacken, G. P.; Adams, C.; O'Gara, F. *Infect. Immun.* **2012,** *80,* 3985–3992. doi:10.1128/IAI.00554-12
37. Kim, K.; Kim, Y. U.; Koh, B. H.; Hwang, S. S.; Kim, S.-H.; Lépine, F.; Cho, Y.-H.; Lee, G. R. *Immunology* **2010,** *129,* 578–588. doi:10.1111/j.1365-2567.2009.03160.x
38. Hazan, R.; Que, Y. A.; Maura, D.; Strobel, B.; Majcherczyk, P. A.; Hopper, L. R.; Wilbur, D. J.; Hreha, T. N.; Barquera, B.; Rahme, L. G. *Curr. Biol.* **2016,** *26,* 195–206. doi:10.1016/j.cub.2015.11.056

39. Gruber, J. D.; Chen, W.; Parnham, S.; Beauchesne, K.; Moeller, P.; Flume, P. A.; Zhang, Y.-M. *PeerJ* **2016,** *4,* e1495. doi:10.7717/peerj.1495
40. Que, Y.-A.; Hazan, R.; Strobel, B.; Maura, D.; He, J.; Kesarwani, M.; Panopoulos, P.; Tsurumi, A.; Giddey, M.; Wilhelmy, J.; Mindrinos, M. N.; Rahme, L. G. *PLoS One* **2013,** *8,* e80140. doi:10.1371/journal.pone.0080140
41. Hall, S.; McDermott, C.; Anoopkumar-Dukie, S.; McFarland, A. J.; Forbes, A.; Perkins, A. V.; Davey, A. K.; Chess-Williams, R.; Kiefel, M. J.; Arora, D.; Grant, G. D. *Toxins* **2016,** *8,* No. 236. doi:10.3390/toxins8080236
42. Allen, L.; Dockrell, D. H.; Pattery, T.; Lee, D. G.; Cornelis, P.; Hellewell, P. G.; Whyte, M. K. B. *J. Immunol.* **2005,** *174,* 3643–3649. doi:10.4049/jimmunol.174.6.3643
43. Rada, B.; Jendrysik, M. A.; Pang, L.; Hayes, C. P.; Yoo, D.-G.; Park, J. J.; Moskowitz, S. M.; Malech, H. L.; Leto, T. L. *PLoS One* **2013,** *8,* e54205. doi:10.1371/journal.pone.0054205
44. Arai, H. *Front. Microbiol.* **2011,** *2,* No. 103. doi:10.3389/fmicb.2011.00103
45. Lépine, F.; Dekimpe, V.; Lesic, B.; Milot, S.; Lesimple, A.; Mamer, O. A.; Rahme, L. G.; Déziel, E. *Biol. Chem.* **2007,** *388,* 839–845. doi:10.1515/BC.2007.100
46. Witzgall, F.; Ewert, W.; Blankenfeldt, W. *ChemBioChem* **2017,** *18,* 2045–2055. doi:10.1002/cbic.201700374
47. Lesic, B.; Lépine, F.; Déziel, E.; Zhang, J.; Zhang, Q.; Padfield, K.; Castonguay, M.-H.; Milot, S.; Stachel, S.; Tzika, A. A.; Tompkins, R. G.; Rahme, L. G. *PLoS Pathog.* **2007,** *3,* 1229–1239. doi:10.1371/journal.ppat.0030126
48. Ji, C.; Sharma, I.; Pratihar, D.; Hudson, L. L.; Maura, D.; Guney, T.; Rahme, L. G.; Pesci, E. C.; Coleman, J. P.; Tan, D. S. *ACS Chem. Biol.* **2016,** *11,* 3061–3067. doi:10.1021/acschembio.6b00575
49. Bera, A. K.; Atanasova, V.; Robinson, H.; Eisenstein, E.; Coleman, J. P.; Pesci, E. C.; Parsons, J. F. *Biochemistry* **2009,** *48,* 8644–8655. doi:10.1021/bi9009055
50. Pistorius, D.; Ullrich, A.; Lucas, S.; Hartmann, R. W.; Kazmaier, U.; Müller, R. *ChemBioChem* **2011,** *12,* 850–853. doi:10.1002/cbic.201100014
51. Weidel, E.; de Jong, J. C.; Brengel, C.; Storz, M. P.; Braunshausen, A.; Negri, M.; Plaza, A.; Steinbach, A.; Müller, R.; Hartmann, R. W. *J. Med. Chem.* **2013,** *56,* 6146–6155. doi:10.1021/jm4006302
52. Hinsberger, S.; de Jong, J. C.; Groh, M.; Haupenthal, J.; Hartmann, R. W. *Eur. J. Med. Chem.* **2014,** *76,* 343–351. doi:10.1016/j.ejmech.2014.02.014
53. Hinsberger, S.; Hüsecken, K.; Groh, M.; Negri, M.; Haupenthal, J.; Hartmann, R. W. *J. Med. Chem.* **2013,** *56,* 8332–8338. doi:10.1021/jm400485e
54. Storz, M. P.; Maurer, C. K.; Zimmer, C.; Wagner, N.; Brengel, C.; de Jong, J. C.; Lucas, S.; Müsken, M.; Häussler, S.; Steinbach, A.; Hartmann, R. W. *J. Am. Chem. Soc.* **2012,** *134,* 16143–16146. doi:10.1021/ja3072397
55. Storz, M. P.; Brengel, C.; Weidel, E.; Hoffmann, M.; Hollemeyer, K.; Steinbach, A.; Müller, R.; Empting, M.; Hartmann, R. W. *ACS Chem. Biol.* **2013,** *8,* 2794–2801. doi:10.1021/cb400530d
56. Storz, M. P.; Allegretta, G.; Kirsch, B.; Empting, M.; Hartmann, R. W. *Org. Biomol. Chem.* **2014,** *12,* 6094–6104. doi:10.1039/c4ob00707g
57. Sahner, J. H.; Brengel, C.; Storz, M. P.; Groh, M.; Plaza, A.; Müller, R.; Hartmann, R. W. *J. Med. Chem.* **2013,** *56,* 8656–8664. doi:10.1021/jm401102e
58. Sahner, J. H.; Empting, M.; Kamal, A.; Weidel, E.; Groh, M.; Börger, C.; Hartmann, R. W. *Eur. J. Med. Chem.* **2015,** *96,* 14–21. doi:10.1016/j.ejmech.2015.04.007
59. Allegretta, G.; Weidel, E.; Empting, M.; Hartmann, R. W. *Eur. J. Med. Chem.* **2015,** *90,* 351–359. doi:10.1016/j.ejmech.2014.11.055
60. Weidel, E.; Negri, M.; Empting, M.; Hinsberger, S.; Hartmann, R. W. *Future Med. Chem.* **2014,** *6,* 2057–2072. doi:10.4155/fmc.14.142
61. Thomann, A.; Zapp, J.; Hutter, M.; Empting, M.; Hartmann, R. W. *Org. Biomol. Chem.* **2015,** *13,* 10620–10630. doi:10.1039/c5ob01006c
62. Prothiwa, M.; Szamosvári, D.; Glasmacher, S.; Böttcher, T. *Beilstein J. Org. Chem.* **2016,** *12,* 2784–2792. doi:10.3762/bjoc.12.277
63. Sangshetti, J. N.; Khan, F. A. K.; Patil, R. H.; Marathe, S. D.; Gade, W. N.; Shinde, D. B. *Bioorg. Med. Chem. Lett.* **2015,** *25,* 874–880. doi:10.1016/j.bmcl.2014.12.063
64. Farrow, J. M., III; Sund, Z. M.; Ellison, M. L.; Wade, D. S.; Coleman, J. P.; Pesci, E. C. *J. Bacteriol.* **2008,** *190,* 7043–7051. doi:10.1128/JB.00753-08
65. Rampioni, G.; Pustelny, C.; Fletcher, M. P.; Wright, V. J.; Bruce, M.; Rumbaugh, K. P.; Heeb, S.; Cámara, M.; Williams, P. *Environ. Microbiol.* **2010,** *12,* 1659–1673. doi:10.1111/j.1462-2920.2010.02214.x
66. Zender, M.; Witzgall, F.; Drees, S. L.; Weidel, E.; Maurer, C. K.; Fetzner, S.; Blankenfeldt, W.; Empting, M.; Hartmann, R. W. *ACS Chem. Biol.* **2016,** *11,* 1755–1763. doi:10.1021/acschembio.6b00156
67. Kesarwani, M.; Hazan, R.; He, J.; Que, Y.; Apidianakis, Y.; Lesic, B.; Xiao, G.; Dekimpe, V.; Milot, S.; Deziel, E.; Lépine, F.; Rahme, L. G. *PLoS Pathog.* **2011,** *7,* e1002192. doi:10.1371/journal.ppat.1002192
68. Maura, D.; Drees, S. L.; Bandyopadhaya, A.; Kitao, T.; Negri, M.; Starkey, M.; Lesic, B.; Milot, S.; Déziel, E.; Zahler, R.; Pucci, M.; Felici, A.; Fetzner, S.; Lépine, F.; Rahme, L. G. *ACS Chem. Biol.* **2017,** *12,* 1435–1443. doi:10.1021/acschembio.6b01139
69. Allegretta, G.; Maurer, C. K.; Eberhard, J.; Maura, D.; Hartmann, R. W.; Rahme, L.; Empting, M. *Front. Microbiol.* **2017,** *8,* No. 924. doi:10.3389/fmicb.2017.00924
70. Rahme, L.; Lepine, F.; Starkey, M.; Lesic-Arsic, B. Antibiotic tolerance inhibitors. WO Patent WO2012116010A3, Oct 26, 2012.
71. Kamal, A. A. M.; Petrera, L.; Eberhard, J.; Hartmann, R. W. *Org. Biomol. Chem.* **2017,** *15,* 4620–4630. doi:10.1039/c7ob00263g
72. Lu, C.; Kirsch, B.; Zimmer, C.; de Jong, J. C.; Henn, C.; Maurer, C. K.; Müsken, M.; Häussler, S.; Steinbach, A.; Hartmann, R. W. *Chem. Biol.* **2012,** *19,* 381–390. doi:10.1016/j.chembiol.2012.01.015
73. Lu, C.; Maurer, C. K.; Kirsch, B.; Steinbach, A.; Hartmann, R. W. *Angew. Chem., Int. Ed.* **2014,** *53,* 1109–1112. doi:10.1002/anie.201307547
74. Lu, C.; Kirsch, B.; Maurer, C. K.; de Jong, J. C.; Braunshausen, A.; Steinbach, A.; Hartmann, R. W. *Eur. J. Med. Chem.* **2014,** *79,* 173–183. doi:10.1016/j.ejmech.2014.04.016
75. Shanahan, R.; Reen, F. J.; Cano, R.; O'Gara, F.; McGlacken, G. P. *Org. Biomol. Chem.* **2017,** *15,* 306–310. doi:10.1039/c6ob01930g
76. Ilangovan, A.; Fletcher, M.; Rampioni, G.; Pustelny, C.; Rumbaugh, K.; Heeb, S.; Cámara, M.; Truman, A.; Chhabra, S. R.; Emsley, J.; Williams, P. *PLoS Pathog.* **2013,** *9,* e1003508. doi:10.1371/journal.ppat.1003508
77. Starkey, M.; Lepine, F.; Maura, D.; Bandyopadhaya, A.; Lesic, B.; He, J.; Kitao, T.; Righi, V.; Milot, S.; Tzika, A.; Rahme, L. *PLoS Pathog.* **2014,** *10,* e1004321. doi:10.1371/journal.ppat.1004321
78. Maura, D.; Rahme, L. G. *Antimicrob. Agents Chemother.* **2017,** *61,* e01362-17. doi:10.1128/AAC.01362-17

79. Kitao, T.; Lepine, F.; Babloudi, S.; Walte, F.; Steinbacher, S.; Maskos, K.; Blaesse, M.; Negri, M.; Pucci, M.; Zahler, B.; Felici, A.; Rahme, L. G. *mBio* **2018,** *9,* e02158-17. doi:10.1128/mBio.02158-17
80. Zahler, R.; Cui, D.; Zhou, D. Carbonyl linked bicyclic heteroaryl N-benzimidazoles and analogs as antibiotic tolerance inhibitors. WO Patent WO2016040764A1, March 17, 2016.
81. Zahler, R. Aryloxyacetylindoles and analogs as antibiotic tolerance inhibitors. WO Patent WO2016112088A1, July 14, 2016.
82. Zender, M.; Klein, T.; Henn, C.; Kirsch, B.; Maurer, C. K.; Kail, D.; Ritter, C.; Dolezal, O.; Steinbach, A.; Hartmann, R. W. *J. Med. Chem.* **2013,** *56,* 6761–6774. doi:10.1021/jm400830r
83. Klein, T.; Henn, C.; de Jong, J. C.; Zimmer, C.; Kirsch, B.; Maurer, C. K.; Pistorius, D.; Müller, R.; Steinbach, A.; Hartmann, R. W. *ACS Chem. Biol.* **2012,** *7,* 1496–1501. doi:10.1021/cb300208g
84. Thomann, A.; de Mello Martins, A. G. G.; Brengel, C.; Empting, M.; Hartmann, R. W. *ACS Chem. Biol.* **2016,** *11,* 1279–1286. doi:10.1021/acschembio.6b00117
85. Thomann, A.; Brengel, C.; Börger, C.; Kail, D.; Steinbach, A.; Empting, M.; Hartmann, R. W. *ChemMedChem* **2016,** *11,* 2522–2533. doi:10.1002/cmdc.201600419
86. Bjarnsholt, T.; Jensen, P. Ø.; Jakobsen, T. H.; Phipps, R.; Nielsen, A. K.; Rybtke, M. T.; Tolker-Nielsen, T.; Givskov, M.; Høiby, N.; Ciofu, O. *PLoS One* **2010,** *5,* e10115. doi:10.1371/journal.pone.0010115
87. Welsh, M. A.; Eibergen, N. R.; Moore, J. D.; Blackwell, H. E. *J. Am. Chem. Soc.* **2015,** *137,* 1510–1519. doi:10.1021/ja5110798
88. Welsh, M. A.; Blackwell, H. E. *Cell Chem. Biol.* **2016,** *23,* 361–369. doi:10.1016/j.chembiol.2016.01.006
89. Kerns, E. H.; Di, L. *Drug-like properties. Concepts, structure design and methods: from ADME to toxicity optimization;* Academic Press: Amsterdam, London, 2008.
90. Maqbool, F.; Abid, A.; Ahmed, I. *Int. J. Pharm.* **2017,** *13,* 773–784. doi:10.3923/ijp.2017.773.784

License and Terms

BEILSTEIN JOURNAL OF ORGANIC CHEMISTRY

The design and synthesis of an antibacterial phenothiazine–siderophore conjugate

Abed Tarapdar[1], James K. S. Norris[1], Oliver Sampson[2], Galina Mukamolova[2] and James T. Hodgkinson[*1]

Letter

Open Access

Address:
[1]Leicester Institute of Structural and Chemical Biology, and Department of Chemistry, University of Leicester, George Porter Building, University Road, Leicester, LE1 7RH, UK and [2]Leicester Tuberculosis Research Group, Department of Infection, Immunity and Inflammation, University of Leicester, Maurice Shock Medical Sciences Building, University Road, Leicester, LE1 9HN, UK

Email:
James T. Hodgkinson[*] - JTHodgkinson@le.ac.uk

* Corresponding author

Keywords:
NDH-2; phenothiazine; siderophore; siderophore–antibiotic; siderophore conjugate

Beilstein J. Org. Chem. **2018,** *14,* 2646–2650.
doi:10.3762/bjoc.14.242

Received: 21 August 2018
Accepted: 02 October 2018
Published: 16 October 2018

This article is part of the thematic issue "Antibacterials, bacterial small molecule interactions and quorum sensing".

Associate Editor: S. Flitsch

Abstract

Siderophore–antibiotic conjugates consist of an antibiotic covalently linked by a tether to a siderophore. Such conjugates can demonstrate enhanced uptake and internalisation to the bacterial cell resulting in significantly reduced MIC values and extended spectrum of activity. Phenothiazines are a class of small molecules that have been identified as a potential treatment for multidrug resistant tuberculosis and latent TB. Herein we report the design and synthesis of the first phenothiazine–siderophore conjugate. A convergent synthetic route was developed whereby the functionalised phenothiazine component was prepared in four steps and the siderophore component also prepared in four steps. In *M. smegmatis* the functionalised phenothiazine demonstrated an equipotent MIC value in direct comparison to the parent phenothiazine from which it was derived. The final conjugate was synthesised by amide bond formation between the two components and global deprotection of the PMB protecting groups to unmask the catechol iron chelating groups of the siderophore. The synthesis is readily amenable to the preparation of analogues whereby the siderophore component of the conjugate can be modified. The route will be used to prepare a library of siderophore–phenothiazine conjugates for full biological evaluation of much needed new antibacterial agents.

Introduction

One of the biggest challenges facing the modern society is antibiotic resistance and the prospect of current antibiotics becoming near redundant against previously treatable infections [1]. To meet this challenge there is a desperate need for new antibiotics, antibiotic targets and strategies to enhance the efficacy of current antibiotics [2]. One novel strategy which is receiving significant interest is the manipulation of bacterial iron transport pathways to deliver antibiotics to the bacterial

cell [3]. Iron is essential for bacterial survival and bacteria secrete high affinity iron chelating molecules to scavenge and solubilise Fe^{3+} from the extracellular environment [3]. The siderophore–Fe complex is recognised by specific receptor proteins on the outer membrane of the bacteria and internalised into the bacterium cell by active transport [4].

Siderophore–antibiotic conjugates consist of an antibiotic covalently linked by a 'tether' to a siderophore. Such conjugates overcome the bacterial membrane permeability barrier and facilitate active transport of the antibiotic to its internal target. Siderophore–antibiotic conjugates can demonstrate significantly enhanced bacterial killing potencies and an extended spectrum of activity [5,6]. Although there has been success reported with a number of antibiotics with differing targets the most success to date has been achieved with beta-lactam-based siderophore conjugates targeting membrane associated penicillin binding proteins (PBPs) [7]. Cefiderocol (S-649266) is a beta-lactam–siderophore conjugate currently in phase III clinical trials which demonstrates enhanced potency against Gram-negative bacteria including multidrug resistant (MDR) Gram-negative pathogens [8]. One hypothesis for the success of siderophore conjugates targeting PBPs, in comparison to other antibiotic targets, is that PBPs are membrane associated and it is not necessary for the siderophore conjugate to cross into the bacterial cytoplasm [7].

Phenothiazines are a privileged scaffold in drug discovery most noted for their use as antipsychotic drugs including chlorpromazine, trifluoperazine, and thioridazine. However, such drugs have also long been noted for their significant antimicrobial activity particularly against *Staphylococcus aureus* and *Mycobacterium tuberculosis* [9,10]. The emergence of MDR-TB has led to structure–activity studies to enhance the antitubercular activity of phenothiazines leading to the identification of chlorpromazine analogue **1** (Figure 1) which demonstrates MIC values comparable to first-line TB drugs in vitro [11]. However, the potency of such phenothiazines, including **1**, needs to be significantly increased to have more activity in vivo and direct clinical application [11]. A validated target of **1** has been identified as type II NADH dehydrogenase (NDH-2), a respiratory enzyme essential for growth in *M. tuberculosis* and other bacterial species [11]. NDH-2 is absent in mammalian cells and similar to PBPs is associated with the bacterial membrane [12]. Considering the significant antibacterial activity of phenothiazines, in particular the anti-TB activity of **1**, and their membrane-associated NDH-2 target we hypothesised **1** may be an interesting candidate for siderophore conjugation.

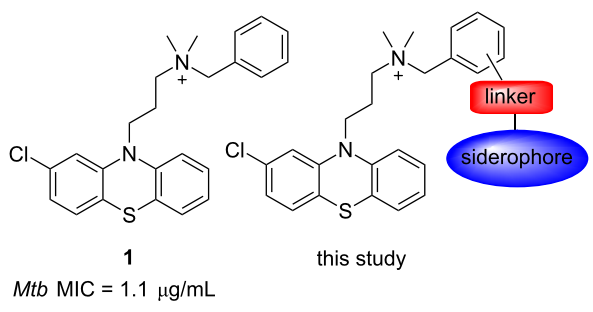

Figure 1: NDH-2 is a validated target for **1** with an MIC of 1.1 μg/mL against *M. tuberculosis*.

Results and Discussion

Typically siderophore–antibiotic conjugates consist of a linker joining the siderophore and antibiotic components. As the target is membrane-associated NDH-2 we decided to functionalise our conjugate with a non-cleavable linker. A polyethylene glycol (PEG) linker was selected as PEG linkers demonstrate enhanced water solubility in comparison to alkyl chain linkers. We then had to make a decision on the position of attachment for the PEG linker to compound **1**. For siderophore conjugates, it is crucial that the linker is attached to a position in **1** such that the antibacterial activity is not compromised. Based on previous structure–activity studies of **1** by Bate et al., whereby a methoxy group was positioned on the *para*-position of the phenyl ring of **1** without loss of activity, we hypothesised this may be a suitable position for PEG linker attachment [13].

From commercially available 2-(2-aminoethoxy)ethanol the amine functionality was Boc-protected under standard conditions to give compound **2** (Scheme 1). Under basic conditions **2** underwent an S_N2 reaction with commercially available *p*-xylylene dichloride to give **3**. Complete conversion of starting material was observed by ^{1}H NMR, however, the isolated yield of **3** was poor possibly due to competing N-alkylation of the Boc group. Isolation of the O-alkyl product **3** was confirmed by ^{13}C NMR. Despite the poor isolated yield of **3** the mass recovery was more than suitable to progress to the next steps. Initially, the reaction of **3** with chlorpromazine (free base) was attempted at room temperature; however, it was found refluxing was required to drive the reaction to completion to generate compound **4** in excellent yield. The final PEG-amine-functionalised phenothiazine **5** was isolated after removal of the Boc protecting group in TFA. Initial attempts at aqueous work-up conditions to isolate the free base resulted in lower isolated yields of **5** due to its high water solubility, and it was decided **5** would be progressed further as the TFA salt avoiding aqueous work-up.

To determine if the antibacterial activity of the derivatised phenothiazine was retained the MIC of compound **4** was determined in direct comparison to synthesised **1** against *Mycobac-*

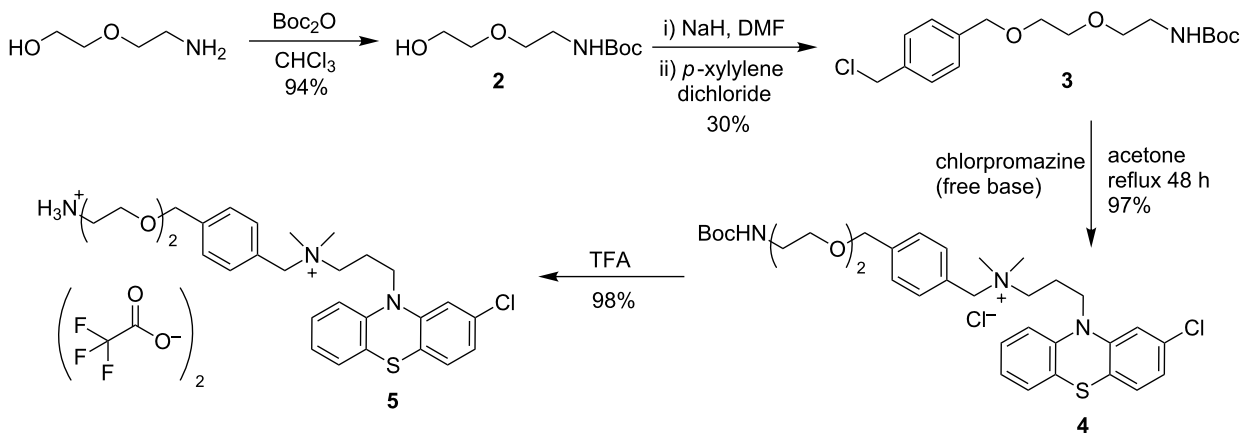

Scheme 1: Synthesis of phenothiazine-PEG-amine component.

terium smegmatis (see Supporting Information File 1). *M. smegmatis* is commonly used as a first assessment for antituberculosis activity. We were pleased to observe side by side compound **4** exhibited equimolar MIC values to **1** (6.25 μM, **1** and **4**) against *M. smegmatis*.

Next our attention turned to the siderophore component of the conjugate. In our proof of concept study we chose to synthesise the bis-catechol siderophore azotochelin. Catechol-based siderophores can act as xenosiderophores and be recognised for uptake by Gram-negative bacteria and *mycobacteria* [14,15]. Most commonly benzyl protecting groups are used in the synthesis of catechol siderophores and cleaved in the final step by palladium catalysed hydrogenation. However, as our final conjugate contains an aromatic halide we wanted to avoid hydrogenation as the final step and we instead chose to use the *para*-methoxybenzyl (PMB) protecting group which can be removed under acidic conditions.

PMB-protected benzoic acid building block **7** was prepared following a literature procedure in two steps (Scheme 2) [16]. Building block **7** was coupled to commercially available L-lysine methyl ester dihydrochloride to yield **8** in moderate yield. The majority of the dicyclohexylurea byproduct could be removed by cooling a solution of the residue dissolved in acetonitrile; however, column chromatography was required for analytical pure material. Ester hydrolysis proceeded smoothly in excellent yield to give the protected siderophore component **9**.

Finally the phenothiazine component **5** and siderophore component **9** where coupled together by amide bond formation using HATU (Scheme 3). Although the isolated yield of **10** is poor the reaction proceeded with good conversion to the desired product; however, on purification an unknown contaminant was challenging to separate from **9** and we wanted to progress with only analytically pure material for the final deprotection step. We were also surprised to observe compound **10** had undergone racemisation under these conditions. The exact cause of racemisation is unknown, but may possibly be due to the four equivalents of DIPEA used to ensure **5** is converted to its free base. This will be investigated further for the synthesis of future

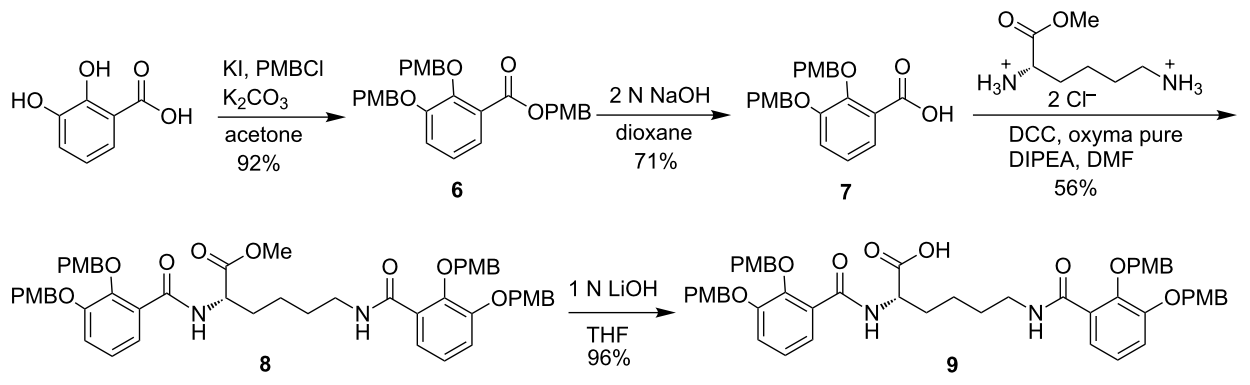

Scheme 2: Synthesis of the azotochelin siderophore component.

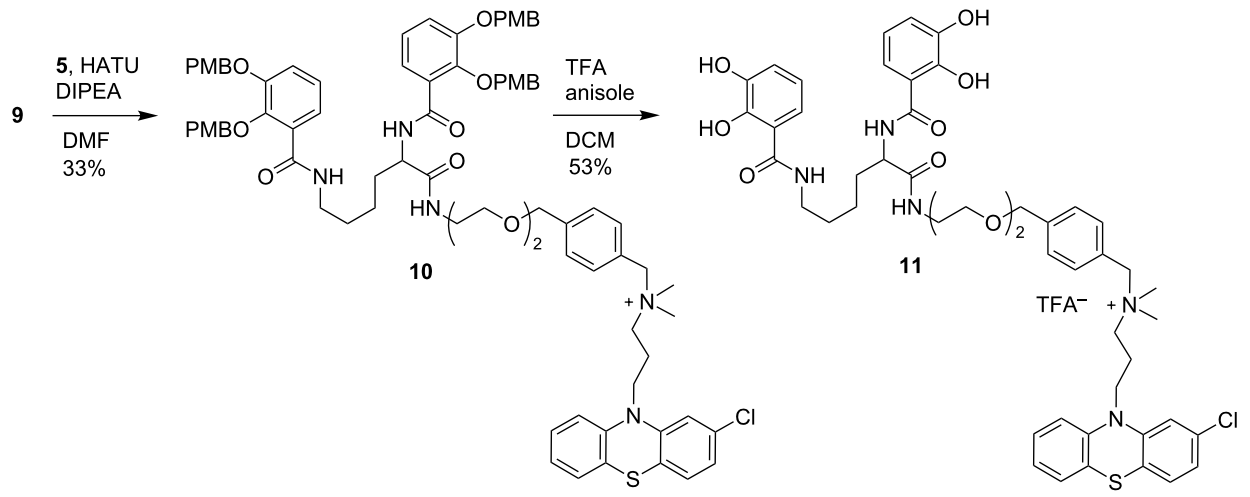

Scheme 3: Final conjugation and deprotection to yield a phenothiazine siderophore conjugate.

conjugates. In the final PMB global deprotection step we were pleased to observe the formation of our desired final phenothiazine–sideophore conjugate in moderate yield. The addition of anisole to the reaction mixture was found to be essential to inhibit competing electrophilic substitution side reactions. A number of techniques where investigated for purification including standard chromatography, recrystallization and trituration as the crude ^{1}H NMR revealed the majority of the desired product. However, purification by semi-preparative HPLC was required to obtain analytically pure material for biological evaluation.

Conclusion

In conclusion we have developed a novel synthetic route to the first phenothiazine–siderophore conjugate. This was achieved by a convergent two component synthesis in a total of ten synthetic steps. The work extends research into antibacterial phenothiazines and siderophore-mediated antibiotic delivery. A library of mono-, bis- and tris-catechol phenothiazine–siderophore conjugates are currently being prepared using this route. Their synthesis and MIC values against pathogenic mycobacteria, Gram-negative bacteria and Gram-positive bacteria, along with compound **11**, will be reported in due course.

Supporting Information

Supporting Information File 1

Full experiential protocols, characterisation of compounds including ^{1}H and ^{13}C NMR spectra, and biological evaluation of compound **4**.
[https://www.beilstein-journals.org/bjoc/content/supplementary/1860-5397-14-242-S1.pdf]

Acknowledgements

We thank the Royal Society for funding this research. We would also like to acknowledge Mick Lee for HRMS data of final compounds, Gerald Griffith and Vanessa Timmermann for aid in NMR spectroscopy experiments of final compounds. We would like to thank Professor Paul Cullis for proof reading the manuscript.

ORCID® iDs

Abed Tarapdar - https://orcid.org/0000-0001-9658-567X
James K. S. Norris - https://orcid.org/0000-0002-1224-2010
Oliver Sampson - https://orcid.org/0000-0001-8727-0588
James T. Hodgkinson - https://orcid.org/0000-0001-9978-7322

References

1. Prestinaci, F.; Pezzotti, P.; Pantosti, A. *Pathog. Global Health* **2015,** *109,* 309–318. doi:10.1179/2047773215Y.0000000030
2. O'Connell, K. M. G.; Hodgkinson, J. T.; Sore, H. F.; Welch, M.; Salmond, G. P. C.; Spring, D. R. *Angew. Chem., Int. Ed.* **2013,** *52,* 10706–10733. doi:10.1002/anie.201209979
3. Schalk, I. J. *J. Med. Chem.* **2018,** *61,* 3842–3844. doi:10.1021/acs.jmedchem.8b00522
4. Rainesa, D. J.; Moroz, O. V.; Blagovab, E. V.; Turkenburgb, J. P.; Wilson, K. S.; Duhme-Klair, A.-K. *Proc. Natl. Acad. Sci. U. S. A.* **2016,** *113,* 5850–5855. doi:10.1073/pnas.1520829113
5. Zheng, T.; Nolan, E. M. *J. Am. Chem. Soc.* **2014,** *136,* 9677–9691. doi:10.1021/ja503911p
6. Liu, R.; Miller, P. A.; Vakulenko, S. B.; Stewart, N. K.; Boggess, W. C.; Miller, M. J. *J. Med. Chem.* **2018,** *61,* 3845–3854. doi:10.1021/acs.jmedchem.8b00218
7. Schalk, I. J.; Mislin, G. L. A. *J. Med. Chem.* **2017,** *60,* 4573–4576. doi:10.1021/acs.jmedchem.7b00554
8. Choi, J. J.; McCarthy, M. W. *Expert Opin. Invest. Drugs* **2018,** *27,* 193–197. doi:10.1080/13543784.2018.1426745
9. Sharma, S.; Singh, A. *Expert Opin. Invest. Drugs* **2011,** *20,* 1665–1676. doi:10.1517/13543784.2011.628657

10. Schurig-Briccio, L. A.; Yano, T.; Rubin, H.; Gennis, R. B. *Biochim. Biophys. Acta* **2014,** *1837,* 954–963. doi:10.1016/j.bbabio.2014.03.017
11. Weinstein, E. A.; Yano, T.; Li, L.-S.; Avarbock, D.; Avarbock, A.; Helm, D.; McColm, A. A.; Duncan, K.; Lonsdale, J. T.; Rubin, H. *Proc. Natl. Acad. Sci. U. S. A.* **2005,** *102,* 4548–4553. doi:10.1073/pnas.0500469102
12. Sellamuthu, S.; Singh, M.; Kumar, A.; Singh, S. K. *Expert Opin. Ther. Targets* **2017,** *21,* 559–570. doi:10.1080/14728222.2017.1327577
13. Bate, A. B.; Kalin, J. H.; Fooksman, E. M.; Amorose, E. L.; Price, C. M.; Williams, H. M.; Rodig, M. J.; Mitchell, M. O.; Cho, S. H.; Wang, Y.; Franzblau, S. G. *Bioorg. Med. Chem. Lett.* **2007,** *17,* 1346–1348. doi:10.1016/j.bmcl.2006.11.091
14. Wittmann, S.; Heinisch, L.; Scherlitz-Hofmann, I.; Stoiber, T.; Ankel-Fuchs, D.; Möllmann, U. *BioMetals* **2004,** *17,* 53–64. doi:10.1023/A:1024409517626
15. Schumann, G.; Möllmann, U. *Antimicrob. Agents Chemother.* **2001,** *45,* 1317–1322. doi:10.1128/AAC.45.5.1317-1322.2001
16. Bergeron, R. J.; Bharti, N.; Singh, S.; McManis, J. S.; Wiegand, J.; Green, L. G. *J. Med. Chem.* **2009,** *52,* 3801–3813. doi:10.1021/jm900119q

License and Terms

BEILSTEIN JOURNAL OF ORGANIC CHEMISTRY

Non-native autoinducer analogs capable of modulating the SdiA quorum sensing receptor in *Salmonella enterica* serovar Typhimurium

Matthew J. Styles and Helen E. Blackwell*

Full Research Paper

Open Access

Address:
Department of Chemistry, University of Wisconsin–Madison, 1101 University Avenue, Madison, WI 53706, USA

Email:
Helen E. Blackwell* - blackwell@chem.wisc.edu

* Corresponding author

Keywords:
N-acyl L-homoserine lactone; LuxR-type receptor; Quorum sensing; *Salmonella enterica* serovar Typhimurium; SdiA

Beilstein J. Org. Chem. **2018,** *14,* 2651–2664.
doi:10.3762/bjoc.14.243

Received: 09 August 2018
Accepted: 26 September 2018
Published: 17 October 2018

This article is part of the thematic issue "Antibacterials, bacterial small molecule interactions and quorum sensing".

Guest Editor: D. Spring

Abstract

Quorum sensing (QS) allows many common bacterial pathogens to coordinate group behaviors such as virulence factor production, host colonization, and biofilm formation at high population densities. This cell–cell signaling process is regulated by *N*-acyl L-homoserine lactone (AHL) signals, or autoinducers, and LuxR-type receptors in Gram-negative bacteria. SdiA is an orphan LuxR-type receptor found in *Escherichia, Salmonella, Klebsiella, and Enterobacter* genera that responds to AHL signals produced by other species and regulates genes involved in several aspects of host colonization. The inhibition of QS using non-native small molecules that target LuxR-type receptors offers a non-biocidal approach for studying, and potentially controlling, virulence in these bacteria. To date, few studies have characterized the features of AHLs and other small molecules capable of SdiA agonism, and no SdiA antagonists have been reported. Herein, we report the screening of a set of AHL analogs to both uncover agonists and antagonists of SdiA and to start to delineate structure–activity relationships (SARs) for SdiA:AHL interactions. Using a cell-based reporter of SdiA in *Salmonella enterica* serovar Typhimurium, several non-natural SdiA agonists and the first set of SdiA antagonists were identified and characterized. These compounds represent new chemical probes for exploring the mechanisms by which SdiA functions during infection and its role in interspecies interactions. Moreover, as SdiA is highly stable when produced in vitro, these compounds could advance fundamental studies of LuxR-type receptor:ligand interactions that engender both agonism and antagonism.

Introduction

In the fight against bacterial infections, microbes have a decisive advantage over the medical community: evolution [1]. Using bacteriocidal or bacteriostatic chemotherapies to treat infection imposes evolutionary pressures that drive rapid resistance development and spread within and among bacterial populations [2,3]. Antibiotic resistant clinical isolates have been

observed for almost every known antibiotic, and the pace of new antibiotic discovery has lagged behind [4]. In recent years, non-bacteriocidal approaches have emerged as a new therapeutic strategy to treat infection with potentially a lesser propensity for resistance development and spread [4-6]. Interfering with the regulation of virulence phenotypes represents one such approach to complement antibiotics, and the interception of quorum sensing (QS) in bacteria has attracted considerable attention in this regard [7-9].

QS, a type of intra- and interspecies chemical communication, has been found to occur in many common bacterial pathogens [10,11]. These pathogens use QS to coordinate group beneficial behaviors such as virulence factor production, host colonization, and biofilm formation at high population densities [12]. Gram-negative bacteria typically use *N*-acyl L-homoserine lactone (AHL) signals for QS, which are produced by LuxI-type synthases and sensed by intracellular LuxR-type receptors (Figure 1A) [13]. The AHL signals are produced at a low, but constant basal level, and rapidly diffuse into the local environment. As the population grows, so does the concentration of AHL, and once it reaches a threshold intracellular level (and thus a "quorum" has been achieved), productive AHL:LuxR-type protein binding occurs that activates the transcription of genes involved in various group behaviors. SdiA is a LuxR-type receptor homolog found in *Salmonella*, *Escherichia, Klebsiella, Enterobacter*, and *Citrobacter* genera [14]. Interestingly, these species do not have LuxI-type synthases and do not produce

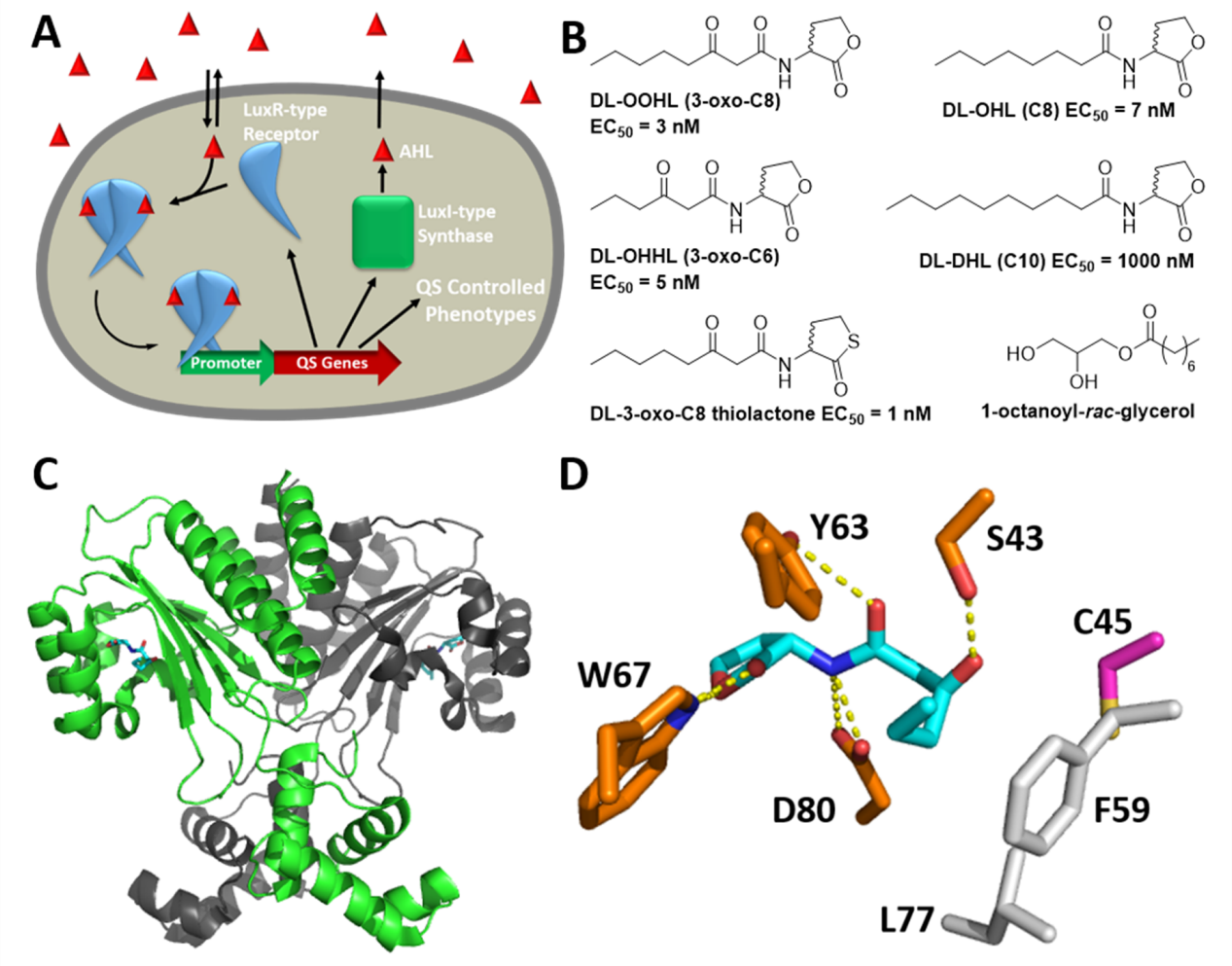

Figure 1: A) Overview of LuxI/LuxR-type QS. The LuxI-type protein produces the AHL signal. The AHL diffuses out of the cell and into the environment and other neighboring cells. At high population density, the intracellular concentration of AHL is sufficiently high to productively bind to the LuxR-type receptor protein. AHL binding typically promotes receptor homodimerization and binding to DNA at various promoters to activate transcription of QS-controlled genes, often including *luxI* and *luxR* (thereby autoinducing the QS system). B) Compounds previously reported to modulate SdiA (all examined as racemates) [20]. Their reported EC_{50} values in a *S.* Typhimurium SdiA reporter system are shown. L-OOHL (3-oxo-C8), L-OHHL (3-oxo-C6), L-OHL (C8), L-DHL (C10), and 1-octanoyl-*rac*-glycerol have been crystalized with SdiA from enterohemorrhagic *E. coli* (EHEC) [21,22]. C) The solid-state structure of the SdiA homodimer (PDB 4Y15; monomers shown in green and grey) bound to OOHL (cyan) [22]. D) Selected residues surrounding OOHL (cyan) in the SdiA ligand binding pocket (from PDB 4Y15 [22]): hydrogen bond acceptors/donors (orange), hydrophobic residues (grey), and a cysteine that potentially could be involved in inhibition (purple, see discussion below).

AHLs; thus, SdiA represents an orphan [14] or "solo" LuxR-type receptor, a class that is rapidly growing in number [15]. SdiA from the common foodborne pathogen, *S. enterica* serovar Typhimurium (*S.* Typhimurium hereafter), has been a target of research [16-19] and has high sequence identity with SdiA from other genera: for example, *S.* Typhimurium (GeneBank AAC08299.1) SdiA is 72% identical to *Escherichia coli* (GeneBank AWF10864.1) SdiA, 67% identical to *Klebsiella pneumoniae* (GeneBank CDO1572.1) SdiA, 71% identical to *Enterobacter clocae* (GeneBank AFN80302.1) SdiA, and 84% identical to *Citrobacter koseri* (GeneBank SQB29462.1) SdiA.

Early studies of SdiA in *S.* Typhimurium and *E. coli* identified low levels of AHL-independent SdiA activity by overexpressing SdiA from a plasmid [23-26]. However, once Michael et al. [16] discovered that SdiA in *S.* Typhimurium responds to exogenously supplied natural AHLs, AHL-dependent SdiA regulons were identified in both *S.* Typhimurium [27,28] and *E. coli* [14,29-31]. In *S.* Typhimurium, SdiA promotes transcription of *pefI*, *srgA*-*E*, and *rck* [28,32]. *pefI* and *srgA* are members of the plasmid encoded fimbriae (pef) operon; PefI negatively regulates the pef operon and SrgA is a disulfide oxidoreductase involved in correctly folding PefA, a fimbrial subunit [33]. The functions of SrgB-D are unknown [28]. SrgE is a type III secreted effector, but its target is unknown [19]. Lastly, rck (resistance to complement killing) has two known functions that are critical for infection: rck confers resistance to human complement and is responsible for the zipper mechanisms by which *S.* Typhimurium invades host cells [34,35].

AHLs produced by other species in the *Salmonella* and *E. coli* environment are believed to be critical to SdiA function. For example, SdiA in *S.* Typhimurium has been shown to be activated in the presence of AHL-producing pathogens in the digestive tract of mice (producing organism: *Yersinia enterocolitica*) [18] and turtles (producing organism: *Aeromonas hydrophila*) [17]. Further, the introduction of a LuxI-type synthase (via a plasmid) into *S.* Typhimurium provided the pathogen with a competitive advantage in colonizing mice over bacteria that lacked the plasmid [18]. Similarly, enterohemorrhagic *E. coli* (EHEC) requires SdiA and AHLs produced by other species in the bovine rumen in order to colonize cattle [19,36]. These results strongly indicate the importance of SdiA in the virulence of this family of pathogens. Despite these findings, however, the precise roles of SdiA in QS and in promoting survival and host colonization remain poorly understood.

What we lack in mechanistic understanding of SdiA's role in virulence is perhaps made up for by the ability to produce and manipulate SdiA in vitro. Indeed, SdiA appears to be far more stable and amenable to characterization in vitro relative to other LuxR-type receptors, and is poised for biophysical characterization [21,22,37]. LuxR-type proteins consist of two domains: a larger N-terminal ligand-binding domain (LBD) connected to a smaller C-terminal DNA-binding domain (DBD). In 2006, the structure of the EHEC SdiA LBD was solved by NMR in the presence and absence of AHL and demonstrated increased folding and structure upon ligand binding [37]. Recently, two groups reported X-ray crystal structures of full-length EHEC SdiA as a homodimer in the presence of four naturally occurring AHLs (shown in Figure 1B) [21,22]. These studies reveal a structure for the SdiA dimer that incorporates LBD and DBD domains comparable to those of the other reported full length LuxR-type proteins (i.e., TraR and QscR) [21,22], albeit with different interdomain interactions that likely direct the final assembly. Despite these reported structures, we still have a very poor understanding of non-native ligand–receptor interactions involved in LuxR-type receptor activation (or inactivation). Most LuxR-type proteins are highly unstable in vitro in the absence of an agonist ligand, and this instability is typically heightened in the presence of an antagonist [38]. As such, the observed stability of EHEC SdiA in vitro, both in the absence and presence of AHLs, provides a new and potentially powerful pathway to begin to delineate the AHL:LuxR-type receptor interactions that engender agonism, and possibly, antagonism [21,22]. Such studies will require AHL-type ligands capable of SdiA agonism and antagonism.

Non-native ligands that modulate the activity of many different LuxR-type receptors have been utilized to delineate the mechanism of various QS systems, to understand the roles of QS in infection, and to attenuate virulence phenotypes in wild-type bacteria in the absence and presence of their native hosts [38-50]. The majority of these compounds have been based on the AHL scaffold. The development of small molecule probes for SdiA has lagged relative to these prior studies. Indeed, to our knowledge, there have only been two reports of experimental studies of AHL-type ligand activity in SdiA in any bacterial species, and no antagonists have been reported. The first study involved the discovery by Michael et al. [16] that *S.* Typhimurium actually responds to exogenous natural AHLs (vide supra), demonstrated through the testing of the C4, C6, C8, C10, and C12 AHLs as well as their 3-oxo analogs. In 2007, Janssens et al. characterized the potency of a small set of AHLs (as racemic mixtures) in SdiA from *S.* Typhimurium with varied tail lengths (4–14 carbons), oxidation levels at the tail β-carbon, and lactone head group replacements [20]. One AHL, *N*-(3-oxooctanoyl) DL-homoserine lactone (DL-OOHL, shown in Figure 1B) was determined as the optimal natural AHL for SdiA (EC_{50} = 3 nM, as determined using a cell-based reporter for SdiA), and its homocysteine thiolactone analog (Figure 1B) was found to be three-fold more potent (EC_{50} = 1 nM). We

sought to build on these prior studies in the current work and identify an expanded range of synthetic ligands for SdiA.

Herein, we report the screening of a focused library of AHL analogs for activity in the SdiA receptor from *S.* Typhimurium. Compound efficacies and potencies were measured in agonism and antagonism assays using an SdiA luminescence reporter system, and follow-up studies were performed in an *E. coli* SdiA reporter. The results provide a broad picture of the types of AHL scaffolds that can agonize and antagonize *S.* Typhimurium SdiA, allowing for the definition of key structure–activity relationships (SARs) for the modulation of SdiA activity. These compounds represent new chemical tools for exploring the role of SdiA and QS in *S.* Typhimurium infections, for characterizing the mechanisms by which non-native AHLs interact with LuxR-type proteins, and for developing pathways toward novel antivirulence strategies targeting SdiA.

Results and Discussion

Selection of the AHL library for screening. We sought to examine a range of AHL-type scaffolds for activity in SdiA. We selected a series of sub-libraries from our in-house compound collections for analysis with demonstrated activities in other LuxR-type receptors, including TraR from *Agrobacterium tumefaciens* [45,51-54]; AbaR from *Acinetobacter baumannii* [47,55]; LasR [45,51-54,56], QscR [57], and RhlR [48,56] from *Pseudomonas aeruginosa*; ExpR1 and ExpR2 from *Pectobacterium carotovora* [46,58]; and LuxR from *Vibrio fischeri* [45,51-54]. The full set of 151 compounds tested is shown in Supporting Information File 1. An overview of the structures in each sub-library is provided below.

Sub-libraries A and H contained AHLs with differing acyl tail lengths and oxidation levels at the tail β-carbon, including many naturally occurring AHLs [51,55]. The B and D sub-libraries were designed to test the effects of lactone stereochemistry, substitution of a variety of more structurally diverse and non-native functional groups on the acyl tail (e.g., alkyl, cycloalkyl, and aryl), and alkyl linker length between the head group and these functional groups [51]. The C and E sub-libraries consisted of substituted phenylacetanoyl homoserine lactones (PHLs), phenylpropionyl homoserine lactones (PPHLs), and phenoxyacetyl homoserine lactones (POHLs), many of which we have previously found to be highly active in a range of LuxR-type receptors as both agonists and competitive antagonists [45,47,48,51,56]. The Q and R sub-libraries contain a related group of substituted benzoyl homoserine lactones (BHLs) [56]. Sub-library S probed the effects of branched alkyl groups on the acyl tail [56]. The F sub-library contained a variety of AHL analogs with alternative, often hydrolysis resistant head groups coupled to native-like alkyl tails, or aryl tails from known active PHLs or POHLs [53,54]. Notably, this sub-library contained a range of thiolactone analogs, including the L-OOHL thiolactone analog, for comparison to the work of Janssens et al. [20]. We also included a set of AHLs and non-AHL-derived compounds (termed "library **1**–**22**") that have been reported by our laboratory and others to be strong modulators of LasR in *P. aeruginosa* [59]. As these compounds represent some of the best-characterized LuxR-type receptor modulators reported, the examination of their activity profiles in SdiA was also of interest. Lastly, we included compound **23**, 1-octanoyl-*rac*-glycerol (Figure 1B), in our assays as X-ray crystallographic studies revealed it was present in the AHL binding site of SdiA (from EHEC) when purified in the absence of AHL (i.e., a complex that originally was thought to be "apo" SdiA [22]), and we sought to determine if it had any functional activity in SdiA.

Biological assays for SdiA activity. Cell-based reporter strains that rely on detecting the transcriptional activity of LuxR-type receptors are commonly used to assess the activity of exogenous ligands. We used the *S.* Typhimurium-pJNS25 reporter strain constructed by Smith and Ahmer [27] and also used by Janssens et al. [20] to examine SdiA activity. This strain naturally produces SdiA and contains a reporter plasmid with the promoter region for *srgE* fused to the *luxABCDE* operon of *V. fischeri* (see Experimental section for details of all strains and plasmids). SdiA activity is thus reported by the production of luciferase and resulting bioluminescence. We also prepared an SdiA reporter in *E. coli* (JLD271-pJN105SE-pSC11SE) to examine *S.* Typhimurium SdiA activity in an alternate background and with a different reporter gene output. *E. coli* JLD271 is the *sdiA* mutant of K-12 *E. coli* [60]. This reporter construct uses an arabinose inducible promoter to produce *S.* Typhimurium SdiA and the promoter region for *srgE* fused to *lacZ* to report SdiA activity. SdiA activity is then measured using standard β-galactosidase assays [61]. In both reporter strains, signal was normalized to the difference between the positive control (10 μM OOHL) and the negative control (1% DMSO; no compound).

We note that, due assumedly to its enhanced stability relative to other LuxR-type receptors, *S.* Typhimurium SdiA was observed to have activity in these reporter assays even in the absence of exogenous AHL, leading to a higher background signal from the negative control relative to that typically observed in LuxR-type receptor reporter assays [38,59]. For the *S.* Typhimurium reporter, the negative control was at 20% the level of the positive control based on raw luminescence. Further, for the *E. coli* JLD271 reporter, the negative control was at 50% the level of the positive control; we reason that this higher background relative to *S.* Typhimurium is due to the

overexpression of SdiA in this reporter. Conditions for both assays (length of incubation, temperature of incubation, and β-galactosidase substrate for developing the *E. coli* assay) were carefully optimized to maximize the signal-to-noise ratio between the positive and negative control in view of these high background levels (data not shown) [62].

Initial screening results in the *S.* Typhimurium SdiA reporter. All 151 compounds were screened for agonism (at 100 μM and 1 μM) and competitive antagonism (at 100 μM and 1 μM) in the *S.* Typhimurium SdiA reporter. The full assay results are tabulated in Supporting Information File 1, and an overview is provided in Figure 2. For agonism at 100 μM, 119 compounds (79% of the library), and at 1 μM, 71 compounds (47% of the library), activated SdiA by at least 50% (above the negative control). This level of promiscuity in terms of agonist ligands is high for a LuxR-type receptor. For comparison, RhlR and QscR were activated beyond 50% by only 23% [56] and 11% [57] of a comparable in-house library at 100 μM and 5 μM, respectively. General trends for SdiA agonism are listed here. All natural AHLs with acyl tail lengths of 4–12 carbons, regardless of the oxidation state at the β-carbon, were able to activate SdiA by greater than 50% at 100 μM. Most of the PHLs, PPHLs, and POHLs were able to activate SdiA more than 50% at 100 μM, but BHLs were not as well tolerated. The D sub-library results suggested that a wide range of functional groups and multiple ring systems could be tolerated on the acyl tail. Changing the head group to a phenyl or cyclohexane was not well tolerated; however, cyclopentane, thiolactones, and the alternative stereochemistry, D-lactone were generally tolerated. Interestingly, 1-octanoyl-*rac*-glycerol (**23**) showed no agonism in this reporter assay, suggesting it does not act as an AHL signal surrogate in SdiA [22]. At 1 μM, only 24 compounds (16% of the library) were able to activate SdiA greater than 80%. To narrow this study, these 24 compounds were selected for further characterization to determine their relative potencies.

For the SdiA antagonism assays, compounds (at 100 μM) were competed against the EC_{90} of (enantiopure) L-OOHL (10 nM). Only 4 compounds (3% of the library) were able to inhibit SdiA activity in *S.* Typhimurium by greater than 65% under these conditions (Figure 2). This is a lower percentage of inhibitors than we typically identify for this AHL analog library, even with the heightened stringency of testing against an agonist (here, L-OOHL) at its EC_{90} value. For reference, 24% and 12% of a comparable in-house library were found to inhibit QscR [57] (at 5 μM) and RhlR [56] (100 μM) by greater than 65%, respectively. Lowering our cut-off, we found 23 compounds that could inhibit SdiA by greater than 30%. These compounds could be classified as follows: long chain AHLs (12–16 carbons); BHLs, PHLs and PPHLs with large substituents on the aryl ring; glycine ethyl ester replacements for the lactone head group; and compound **11** (ITC-12), originally reported by the Meijler lab [44], which has an isothiocyanate (itc) at its acyl tail terminus installed for potential covalent capture in the AHL-binding site (vide infra). These 23 compounds were selected for further characterization to determine their relative inhibitory potencies in SdiA.

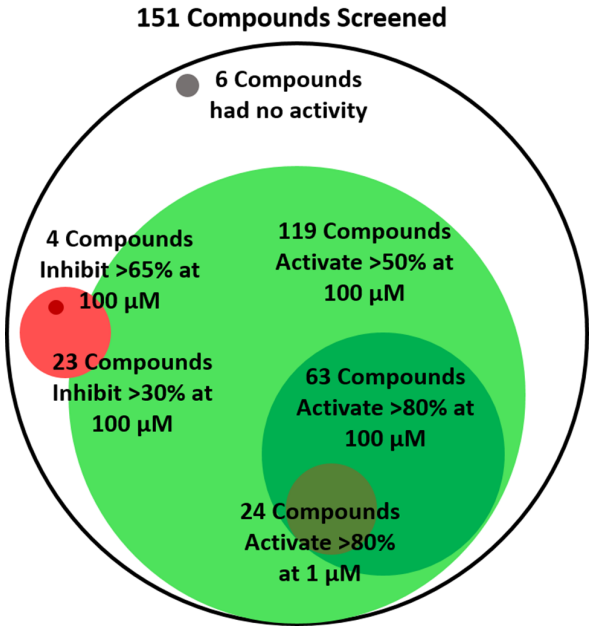

Figure 2: Overview of SdiA agonism and antagonism single-point screening results in the *S.* Typhimurium reporter. Agonists are indicated in green. Antagonists are indicated in red. Compounds with less than 10% agonism and antagonism (i.e., no activity) are indicated in grey. All circles are scaled to their proportion of the library. Overlaps largely indicative of overlapping compound sets.

Characterization of the efficacies and potencies of SdiA agonists. The lead agonists were subjected to dose–response analysis using the *S.* Typhimurium SdiA reporter as described in the Experimental section (see Supporting Information File 2 for the full dose–response curves). The structures of the agonist compounds are shown in Figure 3 and their maximal activities (i.e., efficacies) and EC_{50} values (i.e., potencies) are listed in Table 1.

Corroborating prior work by Michael et al. [16] and Janssens et al. [20], SdiA was found to be most strongly activated by natural AHLs with a six to eight carbon tail (**2**, **A2**; Figure 3). The PHL class was also highly active in SdiA; of the 36 PHLs tested, 30 showed greater than 75% activity at 100 μM. Based on potency, PHLs with a *meta* substitution were favored for SdiA agonism (**F11**, **C8**, **C11**, **E7**, **C14**, **C6**, **E5**, and **E1**), but

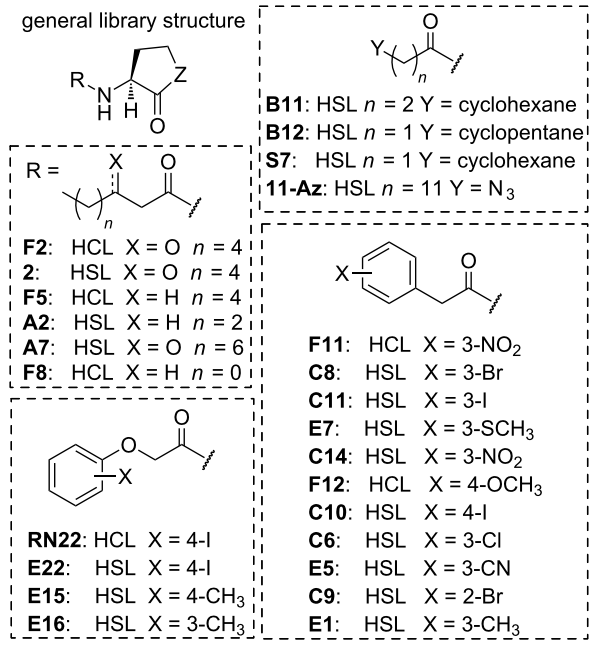

Figure 3: Chemical structures of the most potent SdiA agonists. Compound names (except for **11-Az**) match those reported in our prior publications. HSL = homoserine lactone, Z = O. HCL = homocysteine thiolactone, Z = S. Compound **2** = L-OOHL. Compounds within each cluster (indicated by hashed line box) are listed in order of highest to lowest potency.

Table 1: Characterization data for SdiA agonists (listed by potency).[a]

compound	activation (%)	EC_{50} (nM)	95% CI (nM)[b]
F2	119	0.70	0.39–1.25
2 (L-OOHL)	110	1.03	0.549–1.92
F5	79[c]	2.28	1.42–3.67
F11	97	2.47	1.49–4.08
RN22	93	6.08	3.89–9.49
E22	108	10.4	6.68–16.1
C8	96	19.1	13.8–26.3
C11	90	20.6	15.8–26.8
A2	81[c]	20.9	18.0–24.3
E7	91	26.0	17.8–38.0
A7[d]	85[c]	26.6	22.3–31.7
E15	98	33.0	20.6–52.9
F12	84	38.8	21.4–70.4
E16	100	43.3	33.1–56.8
C10	67[c]	47.2	35.7–62.3
B11	93	50.1	36.7–68.5
C6	95	51.9	38.8–69.6
B12	93	54.7	43.9–68.2
E5	73[c]	62.2	50.6–76.6
F8[d]	91	62.8	56.4–70.0
C9	103	63.5	50.4–80.1
E1	99	66.4	48.3–91.2
S7	89	106	60.7–185
11-Az	110	125	82.5–190

[a]All assays are biological triplicates of technical triplicates using the *S.* Thyphmurium-pJNS25 reporter strain (see Experimental section). [b]CI = confidence interval for the EC_{50} value. [c]Maximal activity was significantly (p = 0.05) different than the positive control, 10 μM L-OOHL (**2**). See ref. [62]. [d]Hill slope in dose response curve significantly different from 1 (p = 0.05). **A7** = 0.84 +/− 0.05 (SD); **F8** = 1.24 +/− 0.07 (SD).

certain *para* (**C10**, **F12**) and *ortho* (**C9**) substituted PHLs were also highly potent. The nature of the substituent at the *meta* position could vary, ranging from electron withdrawing (NO_2, **F11**) to electron donating (SCH_3, **E7**), but larger substituents were favored (e.g., I and Br over Cl). Many of these highly potent PHL agonists of SdiA are also potent antagonists of other LuxR-type receptors, most notably *para*-iodo-PHL **C10**, which inhibits RhlR [56], AbaR [47], LuxR [45], ExpR1 [58], ExpR2 [58], and TraR [45]. Strikingly, the top agonist PHL structures identified for SdiA are similar to those in RhlR; six of the eight PHL SdiA agonists characterized are also RhlR agonists [56]. This correlation is interesting because *sdiA* is the descendent of a horizontal gene transfer of *rhlR* [63]. Indeed, the sequence of SdiA from *Salmonella* is 45% identical to RhlR, more than it is to LasR (27%), QscR (33%), TraR (23%), LuxR (27%), or CviR (32%) [21]. In further support of a possible similarity between SdiA and RhlR, the cognate AHL signal of RhlR, butanoyl HL **A1**, is also a moderate agonist of SdiA, with 100% maximal activation and an EC_{50} of 578 nM (see Supporting Information File 2 for full dose–response curve).

The most intriguing class of SdiA agonists was the POHLs. All three of the POHLs tested (**E22**, **E15**, and **E16**) tested and one thiolactone POHL analog (**RN22**) activated SdiA by more than 75% at 1 μM. This finding is in stark contrast to our previous studies of POHLs in other LuxR-type receptors, as we have largely only found them to be antagonists. For instance, *para*-iodo **E22**, the most potent POHL agonist in SdiA, is an antagonist in RhlR [56], TraR, LuxR, and LasR [45]. POHL structures were not as well sampled in the assembled compound library as PHLs; these data suggest the screening of additional POHLs in SdiA in the future to better delineate SARs for this structure class. Overall, the agonism reporter assay data support SdiA as a less selective receptor for AHL-type agonists (assuming these non-native ligands target the AHL-binding site). Perhaps more interestingly, as SdiA appears to be activated strongly by non-native AHLs that typically inhibit other LuxR-type receptors, these data underscore the potential value of SdiA as a useful model system for investigating the interactions these ligands can have with LuxR-type receptors in vitro.

Only one class of alternate head group-containing compounds was present in the set of top SdiA agonists, the homocysteine thiolactone, corroborating prior work by Janssens et al. [20].

Because several thiolactone compounds (**F2**, **F5**, **F11**, **RN22**, **F12** and **F8**; structures shown in Figure 3) were quite potent (EC_{50} values ranging from 0.7–91 nM), we sought to characterize their lactone analogs (structures shown in Supporting Information File 1) to determine if the thiolactone substitution results in increased potency (comparison data in Table 2, see Supporting Information File 2 for full dose–response curves). While the potencies of thiolactones **F2** and **RN22** were not significantly different than their lactone analogs **2** and **E22**, the simple alkyl derivatives (thiolactones **F8** and **F5** vs lactones **A1** and **A3**) and the PHL-type derivatives (thiolactones **F11** and **F12** vs lactones **C14** and **C24**) were nearly an order of magnitude more potent. As thiolactone hydrolysis can occur more slowly than lactone hydrolysis in the AHL scaffold [53], these compounds may find utility as chemical probes due to their longer half-lives in biological media. These results suggest that this structural motif could be installed to potentially improve the potencies of other lactone-based SdiA agonists and antagonists.

Characterization of the efficacies and potencies of SdiA antagonists. The lead antagonists identified in the single point screens were subjected to dose–response analysis using the *S.* Typhimurium SdiA reporter as described in the Experimental section (see Supporting Information File 2 for the full dose–response curves). The structures of the lead SdiA antagonists are shown in Figure 4 and their maximal inhibition and IC_{50} values are listed in Table 3.

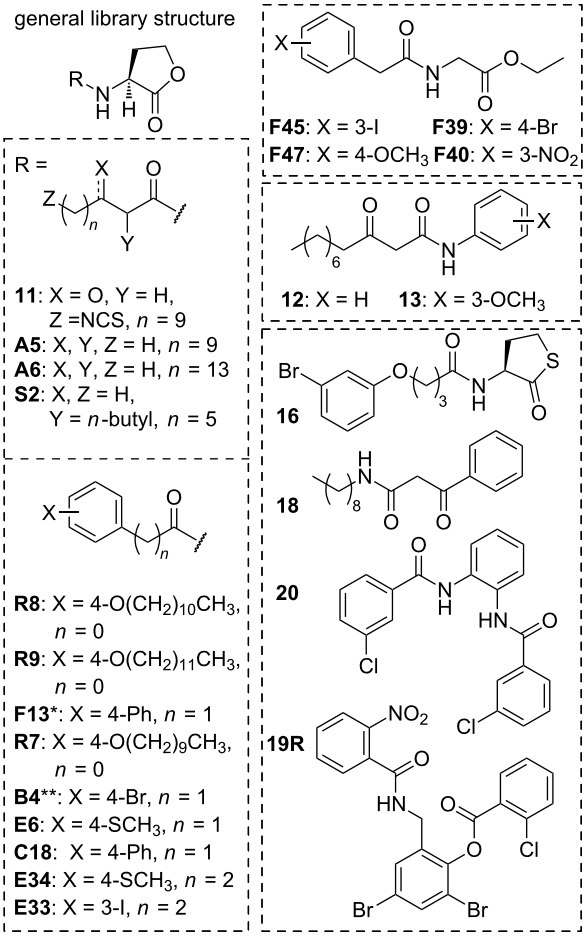

Figure 4: Chemical structures of the most potent SdiA antagonists. Compound names preceded by letters match those reported in our prior publications. * Indicates an L-thiolactone head group. ** Indicates a D-lactone head group. Compounds within each cluster (indicated by hashed line box) are listed in order of highest to lowest efficacy (maximal inhibition).

Several structural classes of SdiA antagonists emerged from this study (Figure 4): long alkyl tail AHLs (**A5**, and **A6**) long alkyl tail-functionalized BHLs (**R7**, **R8**, and **R9**) PHLs and PPHLs with large aryl substituents (**B4**, **C18**, **E6**, **E33**, **E34**, and **F13**), and PHL-type derivatives with glycine ethyl ester head groups (**F39**, **F40**, **F45**, and **F47**). In addition, an AHL with an electrophilic warhead for covalent modification (**11**, ITC-12) and various non-AHL compounds (**12**, **13**, **18**, **19R**, and **20**) were found to be SdiA antagonists. Most of the compounds that displayed antagonistic behavior were actually classical partial agonists of SdiA (i.e., capable of activating SdiA to a lower maximal level, and then inhibiting to that same level when competed against OOHL (**2**) [59]); maximal inhibition and maximal activation are both listed in Table 3 to underscore this activity profile. We note that **11** and **R8** were observed to

Table 2: Comparison of selected lactone and thiolactone analog EC_{50} values in SdiA.[a]

lactone	EC_{50} (nM)	95% CI (nM)[b]	corresponding thiolactone	EC_{50} (nM)	95% CI (nM)[b]	fold increase
2 (OOHL)	1.03	0.55–1.92	**F2**	0.700	0.39–1.25	1.47[c]
A1	578	482–693	**F8**	62.8	56.4–70.0	9.20
A3	18.1	7.44–43.8	**F5**	2.23	1.42–3.67	8.12
C14	28.3	24.0–33.3	**F11**	2.47	1.49–4.08	11.5
C24	252	194–327	**F12**	38.8	21.4–70.4	6.49
E22	10.4	6.68–16.1	**RN22**	6.08	3.89–9.49	1.71[c]

[a]All assays are biological triplicates of technical triplicates using the *S.* Thyphimurium-pJNS25 reporter strain (see Experimental section).
[b]CI = confidence interval for the EC_{50} value. [c]Not significantly different (p = 0.05).

Table 3: Characterization data for SdiA antagonists (listed by efficacy).[a]

compound	inhibition (%)	activation (%)	IC_{50} (μM)	95% CI (μM)[b]
11[c]	130[d]	−33	0.32	0.12–0.85
R8	120[d,e]	24	44.2	17.2–114
16[c]	89	48	44.6	11.7–17.0
F45	87	26	28.5	17.4–46.8
R9	63[e]	6	–[f]	–
A5	59[e]	57	–	–
F39	55[e]	50	–	–
20	53[e]	47	–	–
A6	52	20[e]	1.75	1.08–2.83
F13	51	59	2.35	0.781–7.08
R7	51	6[e]	3.10	1.57–4.18
B4	50[e]	52	–	–
E6	49[e]	74	–	–
19R[c]	44[e]	40	–	–
F47	42	61	–	–
C18	40[e]	48	–	–
12	39[e]	12	–	–
18	37[e]	53	–	–
F40	33	56	27.8	10.0–77.3
S2	32[e]	63	–	–
E34	30[e]	66	–	–
E33	19	67	9.64	3.25–28.6
13	19[e]	57	–	–

[a]All assays are biological triplicates of technical triplicates using the *S*. Thyphimurium-pJNS25 reporter strain (see Experimental section). [b]CI = confidence interval for the IC_{50} value. [c]Hill slope in dose response curve significantly different from −1 (p = 0.05). **11** = 0.40 +/− 0.08 (SD); **16** = −0.6 +/− 0.1 (SD); **19R** = −0.2 +/− 0.3 (SD). [d]Inhibition is listed as 100% minus the lowest % activity observed in the presence of 10 nM L-OOHL (**2**). Values >100% inhibition suggest that AHL-independent (background) SdiA activity is being inhibited. [e]Compound insolubility limited testing at higher concentrations; maximal observable activity reported. [f]– = Non-linear fit to the data could not be completed.

inhibit SdiA beyond 100% in these competitive antagonism assays. We speculate that this activity profile is due to the ability of these compounds to inhibit both AHL-dependent and AHL-independent SdiA activity, and return to this below.

Both C12 AHL **A5** and C16 AHL **A6** inhibited SdiA activity by greater than 50%. Interestingly, C14 AHL **H26** agonized SdiA to 39% (at 100 μM), but failed to inhibit SdiA (see Supporting Information File 1). Further, the 3-oxo analogues of **A5** and **A6** displayed SdiA agonism: **1** (3-oxo-C12) fully activated SdiA at 100 μM and **H25** (3-oxo-C16) activated SdiA to 57% at 100 μM, suggestive that contacts with the 3-keto group are important for receptor agonism. Antagonists **R7**, **R8**, and **R9** are all BHLs with long alkyl tails (10, 11, and 12 carbons, respectively) in the *para* position. Of these three compounds, **R8** displayed the greatest inhibitory activity in SdiA – inhibition to 120% with an IC_{50} of 44 μM. Interestingly, similar compounds with shorter tail lengths are potent inhibitors in other receptors: **R6**, with a 9-carbon tail, is a potent inhibitor of QscR and LasR, and **Q9**, with an 8-carbon tail, is a potent inhibitor of QscR [64]. A set of other compounds containing aryl tails with large substituents (such as Br, I, and SCH_3) also partially inhibit SdiA; specifically, thiolactone **16** (mBTL), which has a long (4 atom) linker between the amide and phenyl, inhibited SdiA activity by 89% with an IC_{50} of 45 μM. This compound was reported by the Bassler lab to also display partial agonism in RhlR in *P. aeruginosa* [50].

The defining features of these first three classes of SdiA antagonists are their relatively large tail groups. In the crystal structure of SdiA from EHEC bound to OOHL (**2**) [22], Nguyen et al. observed that two residues in the ligand-binding pocket, Phe59 and Leu77, were moved inward toward the alkyl tail of **2**, effectively closing the binding pocket relative to the "apo"-SdiA structure (bound to 1-octanoyl-*rac*-glycerol (**23**)). In *Salmonella* SdiA, these side chains are switched (Leu59 and Phe77), yet maintain bulky and hydrophobic character at these positions. We speculate that closing of this binding pocket on the AHL tail could differentiate the AHL-bound and highly active SdiA structure from the "apo" and less active SdiA structure. The sterically larger tails of the SdiA antagonists uncovered here could prevent the closing of the SdiA binding pocket

and the transition to the more active state. While additional studies are clearly necessary to support this hypothesis, it is congruent with the SdiA structural data, the observation that 1-octanoyl-*rac*-glycerol (**23**) has no activity in the SdiA reporter assay, and recently reported data for LasR suggestive of a closed ligand-binding site for maximal activation [65].

All of the glycine ethyl ester head group compounds tested exhibited SdiA antagonism despite varying between a range of PHL- and PPHL-type tails with differing aryl substituents (Figure 4; Table 3). Prior studies of these compounds in our laboratory had shown they have minimal to low activity in LuxR-type receptors [54], so this activity profile in SdiA was unexpected. The *meta*-iodo PPHL derivative **F45** displayed the strongest antagonism of this structure class: 87% inhibition with an IC_{50} of 28.5 μM. Finally, itc-derivative **11** had the highest efficacy and potency of any SdiA antagonist reported herein. Compound **11** inhibited all AHL-dependent SdiA activity (and all of the AHL-independent SdiA (or background) activity; 130% effective inhibition) with a sub-micromolar IC_{50} (318 nM). Compound **11** was originally designed by the Meijler lab to react with a cysteine in the AHL-binding pocket of LasR, thereby acting as an irreversible inhibitor [44]. SdiA does have a cysteine in the binding pocket (Cys45, see Figure 1D), but it is positioned near carbons 3 and 4 of the acyl tail in OOHL (**2**) in the SdiA crystal structure, rather than near the terminus of the alkyl tail [22]. We examine the possibility of **11** covalently modifying SdiA as part of the additional biological assays described next.

Heterologous SdiA reporter system and competition assay data. We submitted the most efficacious antagonists from above (**11**, **16**, **R8**, and **F45**) to an *E. coli* SdiA reporter (JLD271-pJN105SE-pSC11SE) to further characterize their active profiles (see Experimental section for full assay details). Specifically, we sought to determine whether their apparent activities were due to directly inhibiting SdiA activity, indirectly inhibiting the *Salmonella* reporter by altering the level of SdiA produced, inhibiting the activity of the enzymatic reporter, luciferase, or some combination of these pathways. The assay results in the *E. coli* SdiA reporter are summarized in Table 4 and full dose–response curves are in Supporting Information File 2. Compounds **F45** and **16** failed to display antagonistic activity in the *E. coli* strain, while **11** and **R8** were able to fully inhibit SdiA activity (with **11** inhibiting most of the AHL-independent activity as well). Compound **11** retained its high potency in the *E. coli* reporter (IC_{50} = 380 nM); the IC_{50} for **R8** could not be determined due to solubility limitations at high concentrations. These results suggest that **R8** and **11** inhibit both the *E. coli* and *S.* Typhimurium reporters at the level of SdiA transcriptional activity, not by changing the expression of SdiA or by inhibiting the luminescence reporter. Conversely, the inability of **F45** and **16** to even partially inhibit SdiA in the *E. coli* reporter system indicates that the means by which they inhibit SdiA activity in the *S.* Typhimurium reporter is dependent on either the expression of SdiA, the luminescence reporter system, or other *Salmonella* specific targets that could alter SdiA activity. None of these possible mechanisms of action would be ideal for probing AHL-mediated SdiA activity, and these follow-up studies underscore the value of using a heterologous strain to validate the activity of possible LuxR-type receptors modulators.

Table 4: SdiA antagonism assay data for select compounds in the *E. coli* reporter.[a]

compound	inhibition (%)	IC_{50} (nM)	95% CI (nM)[b]
11	130[c]	380	175–822
R8	106	–[d]	–
16	NA[e]		
F45	NA		

[a]All assays are biological triplicates of technical triplicates using the *E. coli* JLD271-pJN105SE-pSC11SE reporter system (see Experimental section). [b]CI = confidence interval for the IC_{50} value. [c]Inhibition greater than 100% suggests inhibition of AHL-independent SdiA activity. [d]– = Non-linear fit to the data could not be completed. [e]NA = not active.

We also submitted compounds **11**, **R8**, and **F45** to competition-type assays in the *S.* Typhimurium SdiA reporter to further characterize their activity profiles. (Because thiolactone **16** displayed multimodal, or non-monotonic [59] activity in the *S.* Typhimurium SdiA reporter (agonism at low concentrations and antagonism at high concentrations; see Supporting Information File 2) and did not display any activity in the *E. coli* reporter, we chose not to include it in this initial competition analysis.) In the competition assay, varied concentrations of the antagonist were competed against OOHL (**2**) in a dose–response-type analysis. If the EC_{50} of OOHL increased with increasing concentration of antagonist, yet its maximal activity was maintained, these results would be supportive of the compound acting as a competitive antagonist of SdiA in the reporter assay. However, if the maximal activity of OOHL decreased with the concentration of added antagonist, these results would be supportive of the compound acting as a non-competitive antagonist of SdiA. The results are shown in Figure 5 (EC_{50} and maximal activity values listed in Supporting Information File 3). The glycine ethyl ester **F45** showed a non-competitive inhibition profile in these competition assays (decreasing the maximal activity to 20% in the presence of 100 μM **F45**, Figure 5A), and as highlighted above, failed to inhibit SdiA in the *E. coli* reporter. These results support a reporter de-

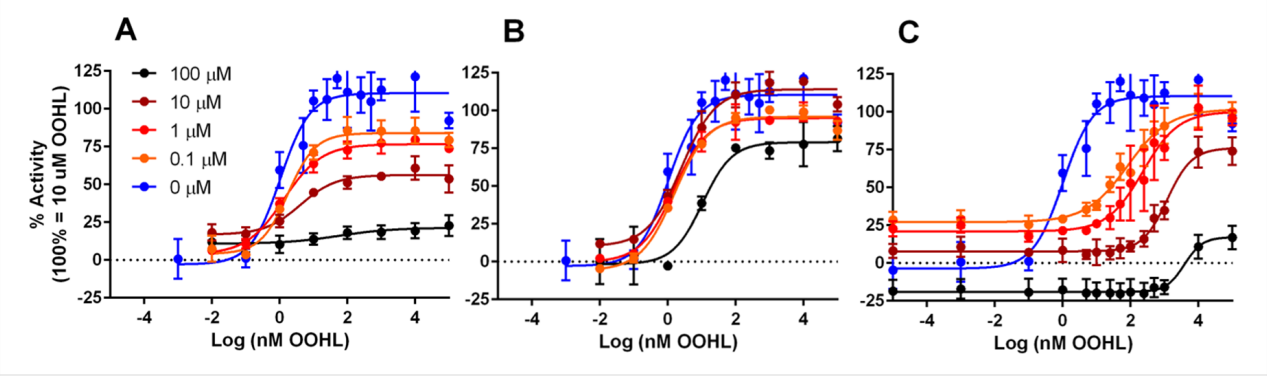

Figure 5: Dose–response activity curves for OOHL (**2**) in competition against various concentrations of synthetic compounds in the *S.* Typhimurium SdiA reporter. (A) Data for compound **F45**, (B), **R8**, and (C) **11**. Figure legend in panel A applies to panels B and C. All assays are biological triplicates of technical triplicates. See Experimental section for full assay details.

pendent, rather than SdiA dependent, inhibitory activity for **F45**. BHL **R8**, which was an SdiA antagonist in both reporter systems, yielded dose–response curves against OOHL (**2**) largely supportive of competitive SdiA inhibition in the *S.* Typhimurium reporter, increasing the EC_{50} of OOHL from 1.03 nM to 10.6 nM with only a small decrease in maximal activity to 80% (Figure 5B). These results support the conclusion that **R8** inhibits SdiA activity by targeting SdiA directly.

Itc-derivative **11** showed both competitive and non-competitive inhibition of OOHL (**2**) in the competition assay (Figure 5C): the EC_{50} increased from 1.03 nM to 4.67 μM while the maximal activity decreased to 20%. This activity trend is consistent with **11** interacting with SdiA both reversibly (by presumably outcompeting OOHL in the ligand binding site) and irreversibly (by covalently modifying SdiA). Such a dual-activity mechanism was previously reported by the Meijler lab for **11** in LasR [44]. Because AHL-dependent and AHL-independent inhibition was observed in both reporter systems, it is likely that **11** targets SdiA for covalent modification rather than some other target that affects the reporter system. To further probe the hypothesis that **11** binds competitively to the SdiA ligand-binding site, we examined the structurally homologous, yet unreactive azide analog of **11**, **Az-11** (structure shown in Figure 3), in the *S.* Typhimurium SdiA reporter. **Az-11** was found to fully agonize SdiA with an EC_{50} of 125 nM (Table 1), in contrast to the full antagonism and 318 nM IC_{50} of **11** in SdiA, providing indirect support that **11** could bind in the AHL-binding site. Further experiments are needed to characterize the mechanism of SdiA inhibition by **11**, and are on-going.

Conclusion

In summary, a focused library of non-native AHL analogs was screened in a cell-based reporter strain for agonism and antagonism of the LuxR homolog, SdiA, from *S.* Typhimurium. This AHL library contained many scaffolds with demonstrated agonism and antagonism activity in other LuxR-type receptors. Despite the relative structural diversity of the library, nearly 80% of the compounds were able to activate SdiA by more than 50% at 100 μM. This level of promiscuity in terms of agonist ligand is extreme in comparison to other well-studied receptors, such as LasR. The most potent agonists of SdiA were found to be AHLs with medium length acyl tails (7–8 carbons), PHLs with *meta* substituents, and almost all of the POHLs tested. This study further underscores the "privileged" nature of the PHL structural class as potent ligands for LuxR-type receptors, and provides strong support for further analysis of the POHL class. In almost every case, the substitution of a thiolactone for the lactone head group increased the potency of the compound either as an agonist or as an antagonist of SdiA.

The SdiA antagonists uncovered herein all had relatively bulky acyl tails, suggestive that sufficient bulk on the AHL ligand can deactivate SdiA activity. In fact, the majority of these compounds were actually partial agonists of SdiA, but three types of antagonists had the ability to fully inhibit SdiA in the *S.* Typhimurium reporter system: BHLs with large alkyl substituents exemplified by **R8**, glycine ethyl ester head groups exemplified by **F45**, and the itc-functionalized compound **11**. Analyses of these antagonists in a heterologous SdiA reporter system and additional competition assays against OOHL (**2**) supported the conclusion that **R8** and **11** directly inhibit SdiA activity. **R8** acts by a competitive inhibition mechanism, while **11** displays a pattern of activity suggestive of both reversible and irreversible inhibition of SdiA.

There were several important outcomes of this study. First, this work provides the first set of chemical probes for SdiA, with a broad range of agonistic and antagonistic activities, which will provide a new entry into the study of QS in *S.* Typhimurium and its role in infections. Second, we have found that many of

the ligands identified herein as active in SdiA are also potent agonists and antagonists of other LuxR-type receptors. In view of the heightened stability of SdiA in vitro relative to these other receptors, coupled with this overlap of active ligands, we believe that the biophysical bases of these agonistic and antagonistic activities can now be explored in vitro using SdiA, for the first time, to improve the fundamental understanding of the modes by which ligand binding modulates LuxR-type receptor activity. Third, several tactics have been identified that can be used for developing second-generation AHL-type ligands with enhanced potencies in SdiA: using electrophilic groups to target the cysteine in the SdiA binding pocket (taking a possible cue from **11**); delineating the SARs for activity by the POHL class, with an eye toward examining bulky substituents that should engender antagonism; and the incorporation of thiolactone head groups into lead compounds. Fourth and finally, in view of the close homology of the known SdiA receptors in *Escherichia, Klebsiella, Enterobacter*, and *Citrobacter* genera, the compounds and tactics reported herein should be exportable to these other bacteria, thereby significantly expanding their utility as chemical approaches to study QS.

Experimental

Bacterial strains and growth conditions. The strains, plasmids, and primers used in this study are summarized in Table 5. All biological media and reagents were obtained from commercial sources and used according to the manufacturers' instructions. All strains were grown in lysogeny broth (LB) at 37 °C with shaking (at 200 rpm). Bacterial growth was assessed by measuring cell culture density by absorbance at 600 nm (OD_{600}). *S.* Typhimurium-pJNS25 was grown in 20 μg/mL tetracycline. *E. coli* JLD271-pJN105SE-pSC11SE was grown in 10 μg/mL gentamicin and 100 μg/mL ampicillin.

Construction of *E. coli* JLD271-pJN105SE-pSC11SE. The same promoter region used by Smith and Ahmer [27] to construct pJNS25 was used for the promoter region in pSC11SE [66]. 477 base pairs of the *srgE* (STM1554) promoter region (−330 to +147) from *S.* Typhimurium (14028) were cloned into pSC11, using the *psrgE* primers listed in Table 5 (cut sites are lowercase). 723 base pairs of *sdiA* from *S.* Typhimurium were cloned into pJN105, using the *sdiA* primers listed in Table 5 (cut sites are lowercase) [66]. PCR-generated fragments were digested, ligated with cut vector, and transformed into *E. coli* DH5α using standard restriction digest cloning methods as we have reported previously [67]. These plasmids were then transformed into *E. coli* JLD271.

Chemistry and compound handling. The compounds tested were either synthesized as previously described [44,45,53,54,57,64] or purchased. Compounds **1**, **2**, **3** and **A1** were purchased from Sigma-Aldrich. The *E. coli* reporter assay substrate, *ortho*-nitrophenyl-β-D-galactopyranoside (ONPG), was purchased from DOT Scientific. Stock solutions of compounds were prepared at 10 mM in DMSO and stored at −20 °C in sealed vials.

***Salmonella* SdiA reporter assay.** *S.* Typhimurium-pJNS25 was grown 16–18 h overnight in LB, diluted 1:100 in fresh LB medium, and then incubated for 6 h at 37 °C with shaking at 200 rpm in the presence of compounds (1% DMSO). For antagonism assays, OOHL (**2**) at its EC_{90} (10 nM, 0.1% DMSO) was added to the subculture immediately prior to adding the compound for testing. All compounds were screened at 100 μM and 1 μM in triplicate in agonism and antagonism assays. Raw luminescence values were divided by the OD_{600} and then normalized to the controls; negative (DMSO) and positive (10 μM

Table 5: Bacterial strains, plasmids, and primers used in this study.[a]

strain, plasmid, or primer	description	reference
E. coli DH5α	F^-, Δ80d*lacZ* Δ M15 Δ (*lacZYA-argF*)U169 *deoR recA*1 *endA*1 *hsdR*17(rk^-, mk^+) *phoA supE*44 λ^- *thi*-1 *gyrA*96 *relA*1	Invitrogen
E. coli JLD271	K-12 Δ*lacX74 sdiA271*::Cam; Cm^R	[60]
S. Typhimurium 14028	wild type *S. enterica* serovar Typhimurium	ATCC
pJNS25	*psrgE-luxCDABE* transcriptional fusion reporter plasmid; Tet^R	[27]
pJN105SE	arabinose-inducible expression plasmid for *sdiA*; Gm^R	this study
pSC11SE	*psrgE-lacZ* transcriptional fusion reporter plasmid; Ap^R	this study
psrgE forward primer	CATgtcgacCTGGTTAATGACGCGTGATACAGTCG	this study
psrgE reverse primer	CATggatccGGGAGAGCTAATTAGCTCTTTCAGG	this study
sdiA forward primer	CATgaattcATGCAGGAAAATGATTTCTTCACC	this study
sdiA reverse primer	CATgaattcATGCAGGAAAATGATTTCTTCACC	this study

[a]Abbreviations: Cm^R, chloramphenicol resistance; Gm^R, gentamicin resistance; Ap^R, ampicillin resistance; Tet^R, tetracycline resistance.

OOHL) control samples were included in every assay plate and used to normalize assay results, setting the positive control to 100% and the negative control to 0%. Luminescence was measured using a Biotek Synergy 2 plate reader and Gen 5 software (version 1.05). Dose–response analyses were performed by preparing dilutions of compounds in DMSO and testing each concentration in the agonism or antagonism assays. Competition dose–response assays (data in Figure 5) were performed in the same manner as the antagonism assays, except instead of OOHL being added to the subculture, the antagonist being tested was added. Non-linear regression curve fits were generated using GraphPad Prism software (version 6) using variable slope (four parameter) dose–response analysis.

***E. coli* SdiA reporter assay.** The β-galactosidase assay using the *E. coli* SdiA reporter was performed as reported previously, with minor modifications [56,61]. The reporter strain was grown 16–18 h overnight in LB, diluted 1:10 in fresh LB medium, and incubated at 37 °C with shaking at 200 rpm until it reached an OD_{600} of 0.25. Expression of SdiA was induced by the addition of 4 mg/mL arabinose, and the culture was incubated in the presence of compounds (1% DMSO) for 4 h at 37 °C with shaking at 200 rpm. For antagonism assays, the subculture was supplemented with OOHL (**2**) at its EC_{50} (1.5 nM, 0.1% DMSO) before addition of the compound for testing. A 50 μL aliquot of culture from each well was lysed in 200 μL of Z-buffer and 8 μL of chloroform, and a 100 μL aliquot of this lysate was incubated with 25 μL of 4 mg/mL ONPG for 20 min at 30 °C before reading absorption at 420 nm and 550 nm using a Biotek Synergy 2 plate reader. Non-linear regression curve fits were generated using GraphPad Prism software (version 6) using variable slope (four parameter) dose–response analysis.

Supporting Information

Supporting Information File 1

Compound library structures and screening results.
[https://www.beilstein-journals.org/bjoc/content/supplementary/1860-5397-14-243-S1.pdf]

Supporting Information File 2

Full dose–response curves.
[https://www.beilstein-journals.org/bjoc/content/supplementary/1860-5397-14-243-S2.pdf]

Supporting Information File 3

Competition assay efficacy and potency data.
[https://www.beilstein-journals.org/bjoc/content/supplementary/1860-5397-14-243-S3.pdf]

Acknowledgements

Financial support for this work was provided by the NIH under Award Number R01 GM109403. M.J.S. was supported in part by the National Institute of General Medical Sciences of the NIH under Award Number T32 GM008349. We gratefully acknowledge Prof. Brian Ahmer (The Ohio State University) and Prof. Sigrid C. J. De Keersmaecker (Scientific Institute of Public Health in Belgium) for donating reporter strains and plasmids.

ORCID® iDs

Matthew J. Styles - https://orcid.org/0000-0003-3236-0425
Helen E. Blackwell - https://orcid.org/0000-0003-4261-8194

References

1. Wright, G. D. *Nat. Rev. Microbiol.* **2007,** *5,* 175–186. doi:10.1038/nrmicro1614
2. Wright, G. D. The Origins of Antibiotic Resistance. In *Antibiotic Resistance. Handbook of Experimental Pharmacology;* Coates, A., Ed.; Springer: Berlin, Heidelberg, 2012; Vol. 211, pp 13–30. doi:10.1007/978-3-642-28951-4_2
3. Bush, K.; Courvalin, P.; Dantas, G.; Davies, J.; Eisenstein, B.; Huovinen, P.; Jacoby, G. A.; Kishony, R.; Kreiswirth, B. N.; Kutter, E.; Lerner, S. A.; Levy, S.; Lewis, K.; Lomovskaya, O.; Miller, J. H.; Mobashery, S.; Piddock, L. J. V.; Projan, S.; Thomas, C. M.; Tomasz, A.; Tulkens, P. M.; Walsh, T. R.; Watson, J. D.; Witkowski, J.; Witte, W.; Wright, G.; Yeh, P.; Zgurskaya, H. I. *Nat. Rev. Microbiol.* **2011,** *9,* 894–896. doi:10.1038/nrmicro2693
4. Clatworthy, A. E.; Pierson, E.; Hung, D. T. *Nat. Chem. Biol.* **2007,** *3,* 541–548. doi:10.1038/nchembio.2007.24
5. Maura, D.; Ballok, A. E.; Rahme, L. G. *Curr. Opin. Microbiol.* **2016,** *33,* 41–46. doi:10.1016/j.mib.2016.06.001
6. Cegelski, L.; Marshall, G. R.; Eldridge, G. R.; Hultgren, S. J. *Nat. Rev. Microbiol.* **2008,** *6,* 17–27. doi:10.1038/nrmicro1818
7. Whiteley, M.; Diggle, S. P.; Greenberg, E. P. *Nature* **2017,** *551,* 313–320. doi:10.1038/nature24624
8. Sintim, H. O.; Smith, J. A.; Wang, J.; Nakayama, S.; Yan, L. *Future Med. Chem.* **2010,** *2,* 1005–1035. doi:10.4155/fmc.10.185
9. Njoroge, J.; Sperandio, V. *EMBO Mol. Med.* **2009,** *1,* 201–210. doi:10.1002/emmm.200900032
10. Schuster, M.; Sexton, D. J.; Diggle, S. P.; Greenberg, E. P. *Annu. Rev. Microbiol.* **2013,** *67,* 43–63. doi:10.1146/annurev-micro-092412-155635
11. Rutherford, S. T.; Bassler, B. L. *Cold Spring Harbor Perspect. Med.* **2012,** *2,* a012427. doi:10.1101/cshperspect.a012427
12. Parker, C. T.; Sperandio, V. *Cell. Microbiol.* **2009,** *11,* 363–369. doi:10.1111/j.1462-5822.2008.01272.x
13. Waters, C. M.; Bassler, B. L. *Annu. Rev. Cell Dev. Biol.* **2005,** *21,* 319–346. doi:10.1146/annurev.cellbio.21.012704.131001
14. Dyszel, J. L.; Soares, J. A.; Swearingen, M. C.; Lindsay, A.; Smith, J. N.; Ahmer, B. M. M. *PLoS One* **2010,** *5,* e8946. doi:10.1371/journal.pone.0008946
15. Venturi, V.; Ahmer, B. M. M. *Front. Cell. Infect. Microbiol.* **2015,** *5,* No. 89. doi:10.3389/fcimb.2015.00089
16. Michael, B.; Smith, J. N.; Swift, S.; Heffron, F.; Ahmer, B. M. M. *J. Bacteriol.* **2001,** *183,* 5733–5742. doi:10.1128/JB.183.19.5733-5742.2001

17. Smith, J. N.; Dyszel, J. L.; Soares, J. A.; Ellermeier, C. D.; Altier, C.; Lawhon, S. D.; Adams, L. G.; Konjufca, V.; Curtiss, R., III; Slauch, J. M.; Ahmer, B. M. M. *PLoS One* **2008,** *3,* e2826. doi:10.1371/journal.pone.0002826
18. Dyszel, J. L.; Smith, J. N.; Lucas, D. E.; Soares, J. A.; Swearingen, M. C.; Vross, M. A.; Young, G. M.; Ahmer, B. M. M. *J. Bacteriol.* **2010,** *192,* 29–37. doi:10.1128/JB.01139-09
19. Habyarimana, F.; Sabag-Daigle, A.; Ahmer, B. M. M. *J. Bacteriol.* **2014,** *196,* 2301–2312. doi:10.1128/JB.01602-14
20. Janssens, J. C.; Metzger, K.; Daniels, R.; Ptacek, D.; Verhoeven, T.; Habel, L. W.; Vanderleyden, J.; De Vos, D. E.; De Keersmaecker, S. C. *Appl. Environ. Microbiol.* **2007,** *73,* 535–544. doi:10.1128/AEM.01451-06
21. Kim, T.; Duong, T.; Wu, C. A.; Choi, J.; Lan, N.; Kang, S. W.; Lokanath, N. K.; Shin, D.; Hwang, H.-Y.; Kim, K. K. *Acta Crystallogr., Sect. D: Biol. Crystallogr.* **2014,** *70,* 694–707. doi:10.1107/S1399004713032355
22. Nguyen, Y.; Nguyen, N. X.; Rogers, J. L.; Liao, J.; MacMillan, J. B.; Jiang, Y.; Sperandio, V. *mBio* **2015,** *6,* No. e02429. doi:10.1128/mBio.02429-14
23. Wang, X. D.; de Boer, P. A.; Rothfield, L. I. *EMBO J.* **1991,** *10,* 3363–3372. doi:10.1002/j.1460-2075.1991.tb04900.x
24. García-Lara, J.; Shang, L. H.; Rothfield, L. I. *J. Bacteriol.* **1996,** *178,* 2742–2748. doi:10.1128/jb.178.10.2742-2748.1996
25. Kanamaru, K.; Kanamaru, K.; Tatsuno, I.; Tobe, T.; Sasakawa, C. *Mol. Microbiol.* **2000,** *38,* 805–816. doi:10.1046/j.1365-2958.2000.02171.x
26. Ahmer, B. M. M.; van Reeuwijk, J.; Timmers, C. D.; Valentine, P. J.; Heffron, F. *J. Bacteriol.* **1998,** *180,* 1185–1193.
27. Smith, J. N.; Ahmer, B. M. M. *J. Bacteriol.* **2003,** *185,* 1357–1366. doi:10.1128/JB.185.4.1357-1366.2003
28. Ahmer, B. M. M. *Mol. Microbiol.* **2004,** *52,* 933–945. doi:10.1111/j.1365-2958.2004.04054.x
29. Hughes, D. T.; Terekhova, D. A.; Liou, L.; Hovde, C. J.; Sahl, J. W.; Patankar, A. V.; Gonzalez, J. E.; Edrington, T. S.; Rasko, D. A.; Sperandio, V. *Proc. Natl. Acad. Sci. U. S. A.* **2010,** *107,* 9831–9836. doi:10.1073/pnas.1002551107
30. Van Houdt, R.; Aertsen, A.; Moons, P.; Vanoirbeek, K.; Michiels, C. W. *FEMS Microbiol. Lett.* **2006,** *256,* 83–89. doi:10.1111/j.1574-6968.2006.00103.x
31. Sharma, V. K.; Bearson, S. M. D.; Bearson, B. L. *Microbiology (London, U. K.)* **2010,** *156,* 1303–1312. doi:10.1099/mic.0.034330-0
32. Abed, N.; Grépinet, O.; Canepa, S.; Hurtado-Escobar, G. A.; Guichard, N.; Wiedemann, A.; Velge, P.; Virlogeux-Payant, I. *Mol. Microbiol.* **2014,** *94,* 254–271. doi:10.1111/mmi.12738
33. Bouwman, C. W.; Kohli, M.; Killoran, A.; Touchie, G. A.; Kadner, R. J.; Martin, N. L. *J. Bacteriol.* **2003,** *185,* 991–1000. doi:10.1128/JB.185.3.991-1000.2003
34. Heffernan, E. J.; Wu, L.; Louie, J.; Okamoto, S.; Fierer, J.; Guiney, D. G. *Infect. Immun.* **1994,** *62,* 5183–5186.
35. Rosselin, M.; Virlogeux-Payant, I.; Roy, C.; Bottreau, E.; Sizaret, P.-Y.; Mijouin, L.; Germon, P.; Caron, E.; Velge, P.; Wiedemann, A. *Cell Res.* **2010,** *20,* 647–664. doi:10.1038/cr.2010.45
36. Yang, Y.; Zhou, M.; Hardwidge, P. R.; Cui, H.; Zhu, G. *Front. Cell. Infect. Microbiol.* **2018,** *8,* No. 155. doi:10.3389/fcimb.2018.00155
37. Yao, Y.; Martinez-Yamout, M. A.; Dickerson, T. J.; Brogan, A. P.; Wright, P. E.; Dyson, H. J. *J. Mol. Biol.* **2006,** *355,* 262–273. doi:10.1016/j.jmb.2005.10.041
38. Welsh, M. A.; Blackwell, H. E. *FEMS Microbiol. Rev.* **2016,** *40,* 774–794. doi:10.1093/femsre/fuw009
39. O'Connor, C. J.; Laraia, L.; Spring, D. R. *Chem. Soc. Rev.* **2011,** *40,* 4332–4345. doi:10.1039/c1cs15053g
40. Galloway, W. R. J. D.; Hodgkinson, J. T.; Bowden, S.; Welch, M.; Spring, D. R. *Trends Microbiol.* **2012,** *20,* 449–458. doi:10.1016/j.tim.2012.06.003
41. Morkunas, B.; Galloway, W. R. J. D.; Wright, M.; Ibbeson, B. M.; Hodgkinson, J. T.; O'Connell, K. M. G.; Bartolucci, N.; Della Valle, M.; Welch, M.; Spring, D. R. *Org. Biomol. Chem.* **2012,** *10,* 8452–8464. doi:10.1039/c2ob26501j
42. Hodgkinson, J. T.; Galloway, W. R. J. D.; Wright, M.; Mati, I. K.; Nicholson, R. L.; Welch, M.; Spring, D. R. *Org. Biomol. Chem.* **2012,** *10,* 6032–6044. doi:10.1039/c2ob25198a
43. Rabin, N.; Delago, A.; Inbal, B.; Krief, P.; Meijler, M. M. *Org. Biomol. Chem.* **2013,** *11,* 7155–7163. doi:10.1039/c3ob41377b
44. Amara, N.; Mashiach, R.; Amar, D.; Krief, P.; Spieser, S. A. H.; Bottomley, M. J.; Aharoni, A.; Meijler, M. M. *J. Am. Chem. Soc.* **2009,** *131,* 10610–10619. doi:10.1021/ja903292v
45. Geske, G. D.; O'Neill, J. C.; Miller, D. M.; Mattmann, M. E.; Blackwell, H. E. *J. Am. Chem. Soc.* **2007,** *129,* 13613–13625. doi:10.1021/ja074135h
46. Palmer, A. G.; Streng, E.; Blackwell, H. E. *ACS Chem. Biol.* **2011,** *6,* 1348–1356. doi:10.1021/cb200298g
47. Stacy, D. M.; Welsh, M. A.; Rather, P. N.; Blackwell, H. E. *ACS Chem. Biol.* **2012,** *7,* 1719–1728. doi:10.1021/cb300351x
48. Welsh, M. A.; Eibergen, N. R.; Moore, J. D.; Blackwell, H. E. *J. Am. Chem. Soc.* **2015,** *137,* 1510–1519. doi:10.1021/ja5110798
49. Welsh, M. A.; Blackwell, H. E. *Cell Chem. Biol.* **2016,** *23,* 361–369. doi:10.1016/j.chembiol.2016.01.006
50. O'Loughlin, C. T.; Miller, L. C.; Siryaporn, A.; Drescher, K.; Semmelhack, M. F.; Bassler, B. L. *Proc. Natl. Acad. Sci. U. S. A.* **2013,** *110,* 17981–17986. doi:10.1073/pnas.1316981110
51. Geske, G. D.; O'Neill, J. C.; Miller, D. M.; Wezeman, R. J.; Mattmann, M. E.; Lin, Q.; Blackwell, H. E. *ChemBioChem* **2008,** *9,* 389–400. doi:10.1002/cbic.200700551
52. Geske, G. D.; Mattmann, M. E.; Blackwell, H. E. *Bioorg. Med. Chem. Lett.* **2008,** *18,* 5978–5981. doi:10.1016/j.bmcl.2008.07.089
53. McInnis, C. E.; Blackwell, H. E. *Bioorg. Med. Chem.* **2011,** *19,* 4820–4828. doi:10.1016/j.bmc.2011.06.071
54. McInnis, C. E.; Blackwell, H. E. *Bioorg. Med. Chem.* **2011,** *19,* 4812–4819. doi:10.1016/j.bmc.2011.06.072
55. Gerdt, J. P.; Wittenwyler, D. M.; Combs, J. B.; Boursier, M. E.; Brummond, J. W.; Xu, H.; Blackwell, H. E. *ACS Chem. Biol.* **2017,** *12,* 2457–2464. doi:10.1021/acschembio.7b00458
56. Eibergen, N. R.; Moore, J. D.; Mattmann, M. E.; Blackwell, H. E. *ChemBioChem* **2015,** *16,* 2348–2356. doi:10.1002/cbic.201500357
57. Mattmann, M. E.; Geske, G. D.; Worzalla, G. A.; Chandler, J. R.; Sappington, K. J.; Greenberg, E. P.; Blackwell, H. E. *Bioorg. Med. Chem. Lett.* **2008,** *18,* 3072–3075. doi:10.1016/j.bmcl.2007.11.095
58. Palmer, A. G.; Streng, E.; Jewell, K. A.; Blackwell, H. E. *ChemBioChem* **2011,** *12,* 138–147. doi:10.1002/cbic.201000551
59. Moore, J. D.; Rossi, F. M.; Welsh, M. A.; Nyffeler, K. E.; Blackwell, H. E. *J. Am. Chem. Soc.* **2015,** *137,* 14626–14639. doi:10.1021/jacs.5b06728
60. Lindsay, A.; Ahmer, B. M. M. *J. Bacteriol.* **2005,** *187,* 5054–5058. doi:10.1128/JB.187.14.5054-5058.2005

61. Miller, J. H. *Experiments in Molecular Genetics;* Cold Spring Press: Plainview, NY, 1972.
62. We note that, within the screening and dose-response curve results, several maximum activation values are listed as >100%, but not significantly different than the positive control. The variance in the signal for the positive control, and for fully activated SdiA in general, was observed to be relatively large (e.g., 95% CI of 88–112% for a sample of 9 sets of triplicate positive controls). Accordingly, 10 μM was not always where OOHL would reaches its maximum activity; therefore, normalization to this activity level would then yield > or < 100% activation values depending on where the average for one day would fall within the average over several days.
63. Sabag-Daigle, A.; Ahmer, B. M. M. *PLoS One* **2012,** *7,* e47720. doi:10.1371/journal.pone.0047720
64. Mattmann, M. E.; Shipway, P. M.; Heth, N. J.; Blackwell, H. E. *ChemBioChem* **2011,** *12,* 942–949. doi:10.1002/cbic.201000708
65. O'Reilly, M. C.; Dong, S.-H.; Rossi, F. M.; Karlen, K. M.; Kumar, R. S.; Nair, S. K.; Blackwell, H. E. *Cell Chem. Biol.* **2018,** *25,* 1128–1139. doi:10.1016/j.chembiol.2018.06.007
66. Lequette, Y.; Lee, J.-H.; Ledgham, F.; Lazdunski, A.; Greenberg, E. P. *J. Bacteriol.* **2006,** *188,* 3365–3370. doi:10.1128/JB.188.9.3365-3370.2006
67. Gerdt, J. P.; McInnis, C. E.; Schell, T. L.; Rossi, F. M.; Blackwell, H. E. *Chem. Biol.* **2014,** *21,* 1361–1369. doi:10.1016/j.chembiol.2014.08.008

License and Terms

BEILSTEIN JOURNAL OF ORGANIC CHEMISTRY

Synthesis and biological evaluation of 1,2-disubstituted 4-quinolone analogues of *Pseudonocardia* sp. natural products

Stephen M. Geddis[1], Teodora Coroama[1], Suzanne Forrest[2], James T. Hodgkinson[*3], Martin Welch[*2] and David R. Spring[*1]

Letter

Open Access

Address:
[1]Department of Chemistry, University of Cambridge, Lensfield Road, Cambridge, CB2 1EW, UK, [2]Department of Biochemistry, University of Cambridge, 80 Tennis Road, Cambridge, CB2 1GA, UK and [3]Leicester Institute of Structural and Chemical Biology, and Department of Chemistry, University of Leicester, George Porter Building, University Road, Leicester, LE1 7RH, UK

Email:
James T. Hodgkinson[*] - jthodgkinson@leicester.ac.uk; Martin Welch[*] - mw240@cam.ac.uk; David R. Spring[*] - spring@ch.cam.ac.uk

* Corresponding author

Keywords:
antibiotics; cross-coupling; heterocycles; quorum-sensing; structure–activity relationships

Beilstein J. Org. Chem. **2018,** *14,* 2680–2688.
doi:10.3762/bjoc.14.245

Received: 31 July 2018
Accepted: 10 October 2018
Published: 19 October 2018

This article is part of the thematic issue "Antibacterials, bacterial small molecule interactions and quorum sensing".

Associate Editor: I. R. Baxendale

Abstract

A series of analogues of *Pseudonocardia* sp. natural products were synthesized, which have been reported to possess potent antibacterial activity against *Helicobacter pylori* and induce growth defects in *Escherichia coli* and *Staphylococcus aureus*. Taking inspiration from a methodology used in our total synthesis of natural products, we applied this methodology to access analogues possessing bulky N-substituents, traditionally considered to be challenging scaffolds. Screening of the library provided valuable insights into the structure–activity relationship of the bacterial growth defects, and suggested that selectivity between bacterial species should be attainable. Furthermore, a structurally related series of analogues was observed to inhibit production of the virulence factor pyocyanin in the human pathogen *Pseudomonas aeruginosa*, which may be a result of their similarity to the *Pseudomonas* quinolone signal (PQS) quorum sensing autoinducer. This provided new insights regarding the effect of N-substitution in PQS analogues, which has been hitherto underexplored.

Introduction

The quinolone core has long been implemented in structures possessing formidable activity in a broad range of fields, including antibiotics, bacterial signalling and iron metabolism [1]. Structural optimisation of quinolones possessing intriguing properties can lead to the discovery of important drug classes, as demonstrated by the fluoroquinolone antibiotics, which were

inspired by the observation of an antibacterial quinolone side-product generated during the synthesis of the antimalarial chloroquine [2].

Given this high potential for the discovery of useful chemical entities, we have recently been engaged in research regarding a family of quinolone natural products which are produced by the actinomycete *Pseudonocardia* sp. CL38489, and were first isolated by Dekker et al. (**1**–**8**, Figure 1) [3]. The authors noted the potent antibacterial activity of these compounds against *Helicobacter pylori*, which is responsible for the generation of numerous digestive disorders [4]. Furthermore, with the presence of a lipophilic chain in the 2-position, there is a structural resemblance to the *Pseudomonas* quinolone signal (PQS), and its biosynthetic precursor 2-heptyl-4(1*H*)-quinolone (HHQ), which are vital to the cooperative behaviour of the human pathogen *Pseudomonas aeruginosa* via quorum sensing (QS). This is a means by which bacteria alter their phenotype in response to changes in population density, regulating virulence and biofilm formation when most impactful to the host organism [5]. This process is mediated by signalling molecules such as PQS, and natural product structures **1**–**8** analogous to PQS may provide interspecies QS-modulator chemical probes. It has been proposed that such a strategy may perturb bacterial virulence and pathogenicity associated with QS, thus conferring a therapeutic benefit, without applying a selection pressure for resistance [6]. Whilst recent experiments suggest that resistance may still emerge, it has been proposed that this development should be limited under certain conditions [7].

We wished to investigate the potential of **1**–**8** to modulate QS in *P. aeruginosa*, however, the compounds are available in only trace amounts from natural sources [3], and so we embarked on the total synthesis of the compounds. We first developed a strategy which constructed natural products **1**–**4** by uniting the quinolone cores with the side chain by means of an sp^2–sp^3 Suzuki–Miyaura coupling reaction [8]. Whilst these compounds unfortunately provided no modulation of PQS quorum

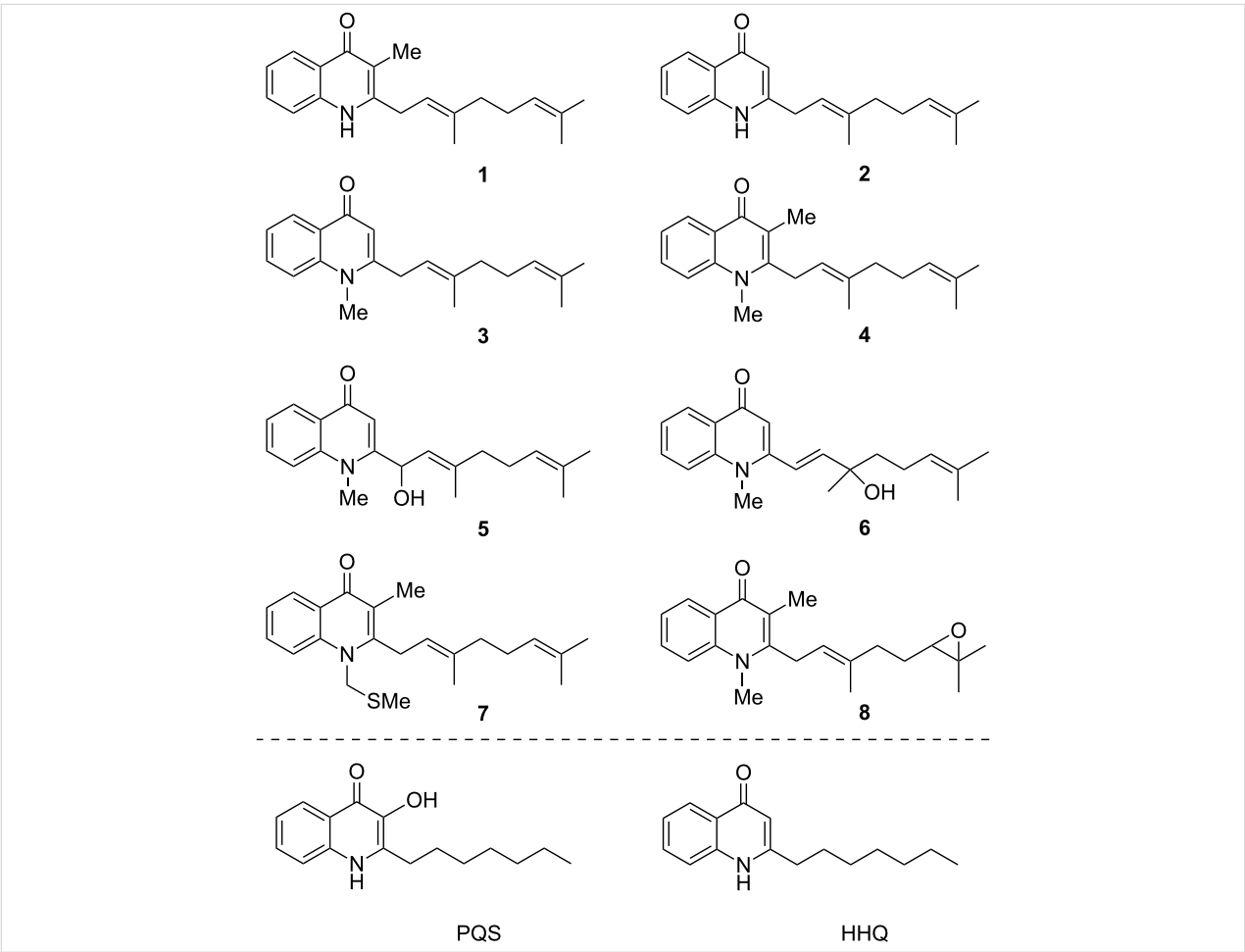

Figure 1: A family of quinolone natural products **1**–**8**, which were first isolated from *Pseudonocardia* sp. CL38489 by Dekker et al. [3], shown alongside the structure of the *Pseudomonas* quinolone signal (PQS), a key autoinducer used in quorum sensing signalling by the human pathogen *Pseudomonas aeruginosa*, and 2-heptyl-4(1*H*)-quinolone (HHQ), the biosynthetic precursor of PQS.

screening (as determined using a heterologous *Escherichia coli* reporter system [9]), an intriguing effect upon the growth of *E. coli* and *Staphylococcus aureus* was noted, which showed an extended lag phase in response to the compounds (except **4**, which was inactive towards *E. coli*. It should be noted that in this previous publication, the graphical data for compounds **3** and **4** was erroneously switched). It is tentatively proposed that this is as a result of disruption of electron transport, as the compounds bear resemblance to the menaquinones which are used by bacteria for this purpose [10]. Following on from this, we recently reported a divergent strategy which granted access to remainder of the natural products **5**–**8**, alongside offering more efficient synthesis of **1** and **4** [11]. Allylic alcohols **5** and **6** were accessed from a mutual precursor (constructed using methodology adapted from that reported by Bernini et al. [12]) using an acid-catalysed transposition, whilst **4**, **7** and **8** were derivatised from **1**.

In this current work, we turn to the further elucidation of the biological activity of this class of compounds. In order to gain additional insight into the associated structure–activity relationships (SAR), it was desired to generate analogues of the natural products. The chemistry developed towards the allylic alcohols **5** and **6**, outlined in Scheme 1, seemed ideal to this end. A range of alkynes **10** could undergo Sonogashira coupling with the commercially available acid chloride **9**. The resultant ynones **11** could then undergo conjugate addition with primary amines **12**, which following metal-catalysed cyclisation would give 1,2-disubstituted quinolones **14**.

Upon the successful synthesis of analogues of the form **14**, biological evaluation of these and the natural products **1**, **4** and **5**–**7** (synthesised during our previous study [11]) would then be possible. In particular, it was desired to further probe the intriguing growth defects which had been observed for natural products **1**–**4** in *E. coli* and *S. aureus*. Furthermore, exploration of any effect on QS of the analogues **14** would be valuable, as to our knowledge studies on the SAR of PQS analogues have not yet thoroughly assessed substitution at the 1-position of the quinolone system [13]. This is perhaps as a result of direct alkylation at this position being very challenging, with low yields and poor O- vs N-selectivity being encountered, particularly with a sterically demanding substituent present in the 2-position [14,15].

As a measure of modulation of QS in *P. aeruginosa*, it was desired to measure the amount of pyocyanin produced by bacterial cultures after treatment with the compounds. This virulence factor is known to be under the regulation of PQS signalling system, and is capable of disrupting many important biochemical processes [16]. This leads to numerous deleterious effects on human cells, including inhibited respiration and ciliary action [17]. These effects allow pyocyanin to play a critical role in infection; indeed, mutant *P. aeruginosa* strains which are unable to produce pyocyanin have been shown to be unsuccessful in infecting the lungs of mice [18]. Being able to prevent the production of pyocyanin could therefore be of great therapeutic benefit.

Results and Discussion

In the implementation of the strategy outlined in Scheme 1, alkynes **10a** and **10b** were first subjected to Sonogashira coupling with commercially available acid chloride **9** according to the previously reported conditions (Scheme 2) [12]. These alkynes were chosen so as to allow access to valuable SAR data regarding the side chain of the natural products **1**–**8**. Commercially available alkyne **10a** would ultimately lead to a simple saturated side chain of the same length as that observed naturally, whilst **10b** (itself synthesised according to a literature procedure [19]) would provide analogues possessing a truncated

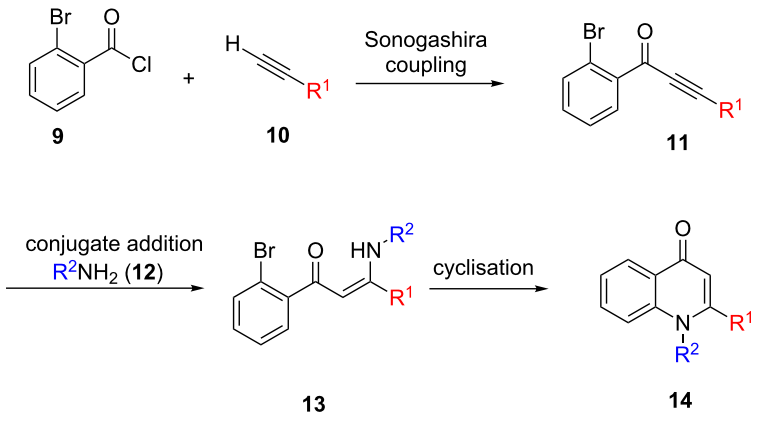

Scheme 1: Proposed use of the chemistry developed towards the total synthesis of **5** and **6** for generation of natural product analogues. Modular coupling of alkynes **10** and amines **12** with commercially available acid chloride **9** was proposed to give 1,2-disubstituted quinolones **14**.

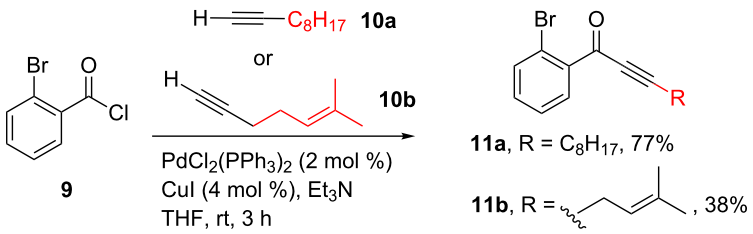

Scheme 2: Sonagashira coupling of alkynes **10a** and **10b** with commercially available acid chloride **9** to give ynones **11a** and **11b**.

prenyl-type substituent. In the event, ynone **11a** was obtained with good yield, however, a poorer yield resulted for **11b**, which was attributed to difficulties in obtaining its precursor **10b** with high purity which stemmed from its volatility.

These ynones were then subjected to a conjugate addition with an assortment of primary amines **12a–f** (Scheme 3). The reactions proceeded with excellent yield in all cases, with aliphatic and aromatic moieties well tolerated. Given the high volatility

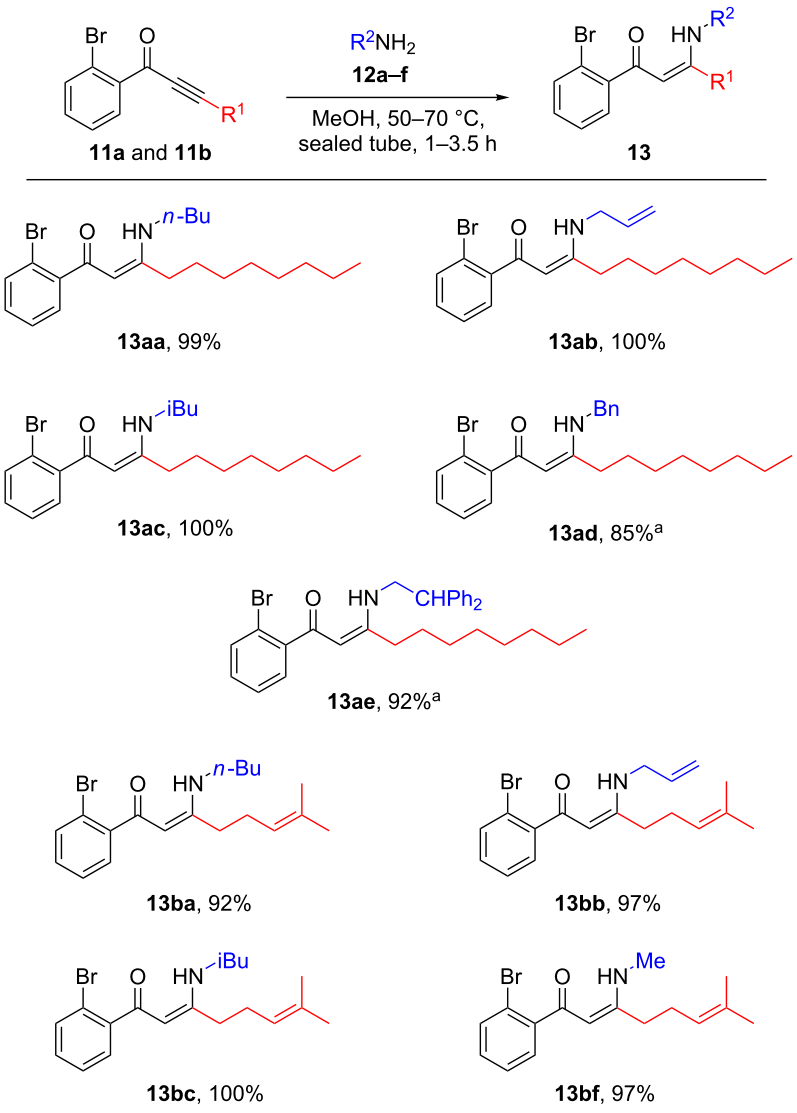

Scheme 3: Conjugate addition of primary amines **12a–f** with ynones **11a** and **11b**. [a]Following concentration in vacuo, further purification using silica gel flash chromatography was required.

of most of the amine starting materials, the products **13** were in general analytically pure following concentration in vacuo of the reaction mixture. However, use of higher boiling-point amines necessitated purification by flash column chromatography, which may account for the slightly lower yields in these cases (**13ad** and **13ae**).

With the compounds **13** now in hand, their cyclisation to the desired analogues **14** was explored. However, whilst the conditions which had proved successful in the total synthesis of natural products **5** and **6** proved satisfactory in most cases, some optimisation was required for substrates possessing unsaturated functionality attached to the amine (Table 1). When the palladium-catalysed conditions were employed [20], a complex mixture resulted, from which no product could be obtained (Table 1, entry 1). Meanwhile, use of base-induced S_NAr-type conditions allowed a small amount of product to be isolated (Table 1, entry 2) [21], but copper-catalysed conditions offered a higher yield (Table 1, entry 3) [12]. This behaviour stands in contrast to that noted for substrates bearing an alkyl substituent in our previous study, for which these copper-catalysed conditions resulted in dimerization [11].

Following the discovery of this substrate-dependent dichotomy with respect to optimal reaction conditions, the entire library of compounds was successfully cyclised. Whilst the yields ranged from low to moderate (Scheme 4), sufficient quantities were obtained to facilitate biological screening. It appeared that bulkier N-substituents (e.g., **14ae**) resulted in lower yields than less bulky derivatives (e.g., **14bf**), underlining the importance of steric factors during cyclisation. Interestingly, the allyl-substituted substrates **13ab** and **13bb** underwent an isomerisation under the reaction conditions, with the double bond moving into conjugation with the amine to give inseparable mixtures of enamine-type products **14ab** and **14bb**. Given the likely hydrolytic instability of synthetic precursors possessing an enamine moiety, these compounds would likely be highly challenging to synthesise by other means. However, it is proposed that the involvement of the nitrogen lone-pair in the aromaticity of the quinolone system attenuates the susceptibility of **14ab** and **14bb** towards hydrolysis.

Intriguingly, the employment of an excess of DMEDA in the Cu-catalysed cyclisation of **13bb** generated **14bg** as a side-product, which represents another interesting analogue for biological study (Scheme 5). This may putatively result from the displacement of the allylamine in **13bb** by the DMEDA ligand, followed by heterocyclisation with concomitant N–>N' methyl transfer.

With the library of natural products and analogues in hand, our attention turned to their biological activity. It was desired to further explore the growth defects which had been previously noted for natural products **1**–**4** against *E. coli* and *S. aureus*, and so these species were grown in the presence of the compounds. The results for *E. coli* ESS are shown in Figure 2, split into the natural product series, the series of analogues with a saturated side chain, and the truncated series of analogues. As can be seen in Figure 2A, natural product **1** resulted in slowed bacterial growth whilst **4** elicited no such effect, consistent with our previous observations (although the later recovery in population in the presence of **4** was less pronounced in the present case) [8]. Meanwhile, **5** appeared to show a moderate growth-slowing effect, which when compared to the stronger effect previously observed for **3**, demonstrates that oxidation of the geranyl side chain is deleterious to the biological effect under investigation. The regioisomeric **6** showed a very small effect, further showing the lack of tolerance of the effect towards side-

Table 1: Optimisation of conditions for the cyclisation of **13ad** to natural product analogue **14ad**.

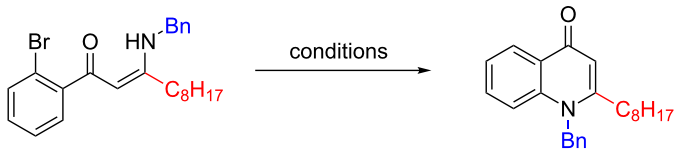

13ad **14ad**

entry	conditions	result
1	Cs_2CO_3, Pd_2dba_3, P(2-furyl)$_3$, toluene, 100 °C, 24 h [20]	complex mixture[a]
2	KO*t*-Bu, dioxane, 90 °C, 24 h [21]	13%[b]
3	CuI, DMEDA, NaO*t*-Bu, DMSO, 80 °C, 2 h [12]	22%[b]

[a]As determined by LCMS and ^{1}H NMR analysis of the crude reaction product. [b]Isolated yield.

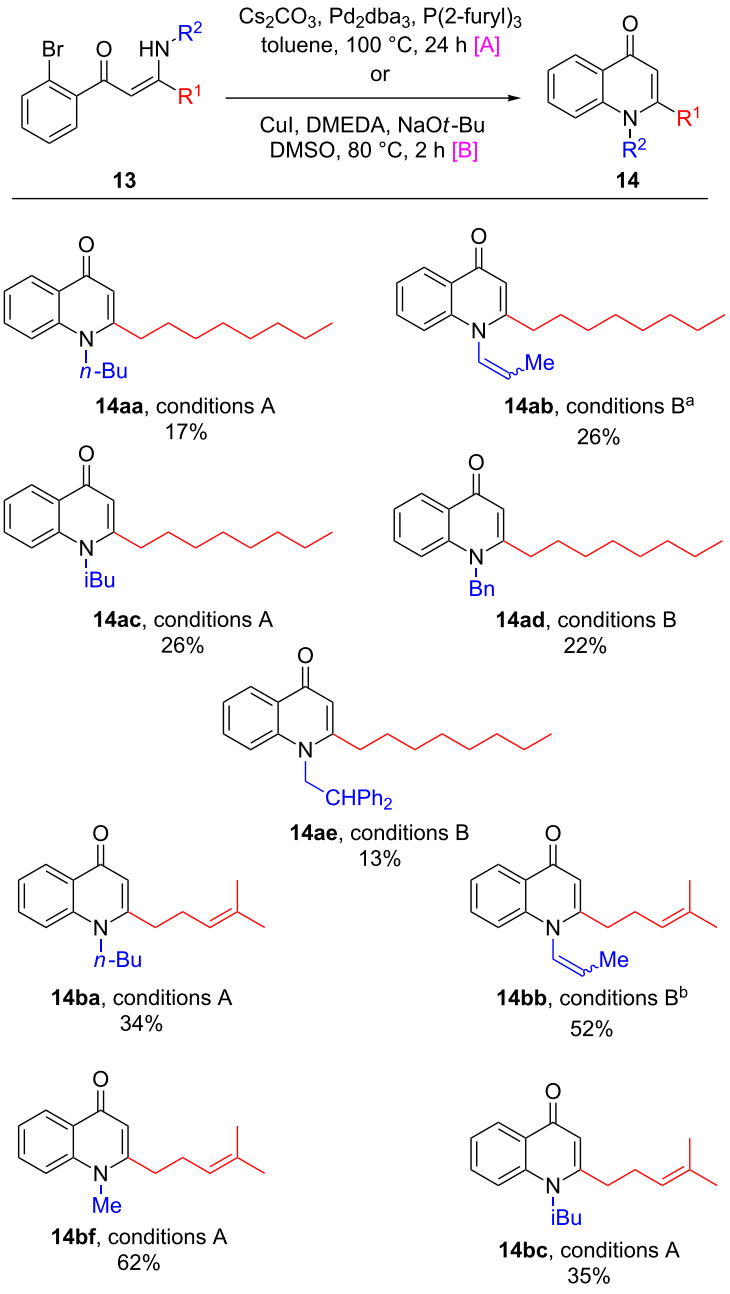

Scheme 4: Cyclisation of precursors **13** to natural product analogues **14** using palladium- or copper-catalysed conditions. Yields quoted are isolated. [a]**13ab** used as starting material, *E*/*Z* ratio = 29:71 based on ^{1}H NMR data. [b]**13bb** used as starting material, *E*/*Z* ratio = 15:85 based on ^{1}H NMR data.

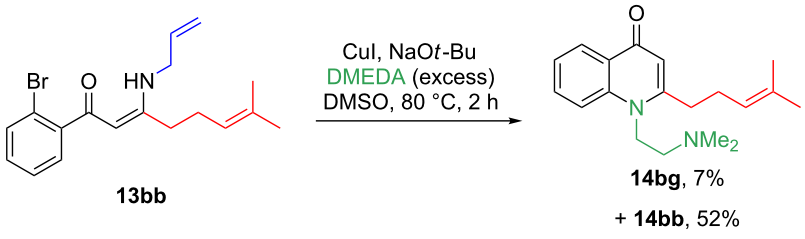

Scheme 5: Use of an excess of DMEDA in the Cu-catalysed cyclisation of **13bb** resulted in the generation of **14bg** as a side-product, alongside **14bb**.

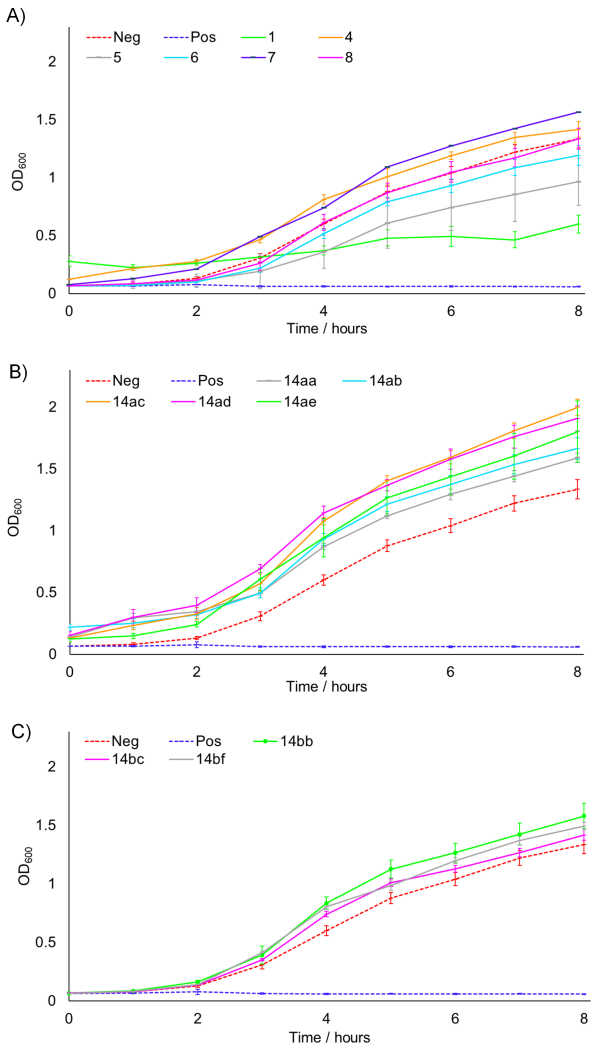

Figure 2: Growth of *E. coli* ESS with time in the presence of 200 μM of each compound. A) Natural product series. B) Saturated analogue series. C) Truncated analogue series. Neg = negative control (DMSO blank), Pos = positive control (gentamicin). Experiments were carried out in triplicate, with the exception of **7**, for which there was insufficient material for repeats. Error bars refer to standard deviation.

chain oxidation. Finally, neither replacement of the N-Me of **4** with the methylthiomethylene substituent of **7**, nor epoxidation of **4**'s side chain to give **8**, offered any improvement in the biological activity. The result for **8** is particularly intriguing, as this natural product was noted to have the strongest effect upon the growth of *H. pylori* in the study by Dekker et al., which may imply that these compounds are acting through different mechanisms upon each bacterial species. Next, considering Figure 2B and C, we see that none of the analogues were capable of affecting the growth of *E. coli*, further demonstrating the importance of the geranyl side for biological activity against this species. This observation is particularly striking for analogue **14bf**, which possesses an identical quinolone core structure to natural product **3**, which was previously shown to be active.

Meanwhile, Figure 3 shows the data for *S. aureus* 25923, which is split into the same three series as before. Considering the natural products (Figure 3A), we see that both **1** and **4** resulted in a slowing of growth consistent with that reported previously, although the effect for **1** was less pronounced in the present case, operating for only the first three hours [8]. Whilst most of the other natural products appeared to show only slight effects, moderate activity was observed for **7**, which stands in an interesting contrast to the inactivity of this compound against *E. coli*. This implies that the structural requirements for optimal activity differ between the species, a conclusion which is further bolstered by the results for the saturated series of analogues shown in Figure 3B. Whilst these compounds were completely inactive against *E. coli*, in this case a strong effect was observed, which for **14aa**, **14ab** and **14ac** was comparable to the

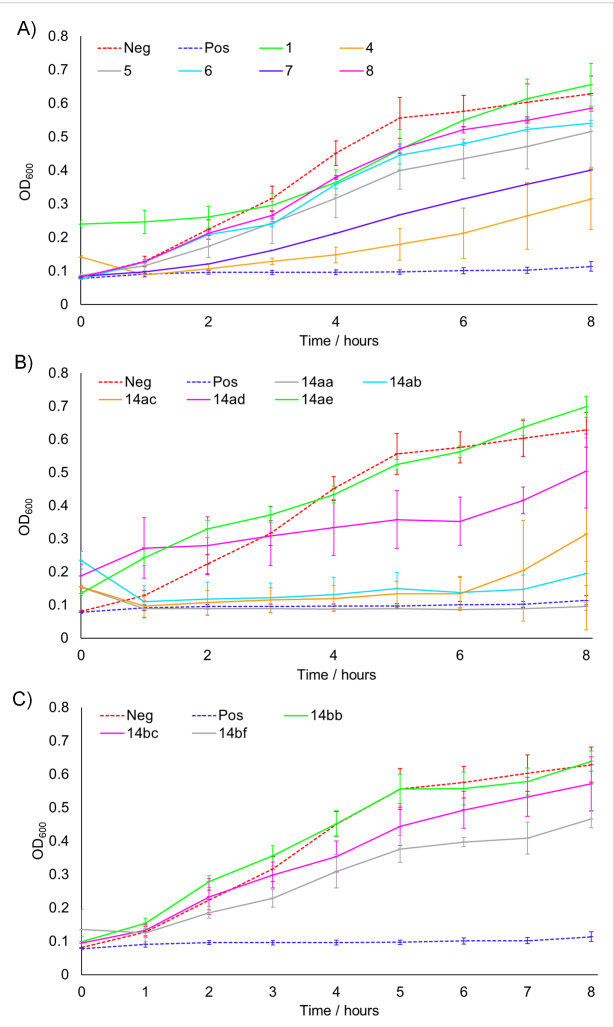

Figure 3: Growth of *S. aureus* 25923 with time in the presence of 200 μM of each compound. A) Natural product series. B) Saturated analogue series. C) Truncated analogue series. Neg = negative control (DMSO blank), Pos = positive control (gentamicin). Experiments were carried out in triplicate, with the exception of **7**, for which there was insufficient material for repeats. Error bars refer to standard deviation.

positive gentamicin control over the timescale of concern. These results show the high efficacy of the saturated side chain against *S. aureus*, however, considering the data for **14ad** and **14ae**, we can observe that adding bulky aromatic moieties to the N-substituent results in reduced activity, with smaller alkyl groups in this position instead being optimal. Finally, the truncated series of analogues appeared to show only small effects upon the growth of *S. aureus* (Figure 3C).

Attention then turned to the ability of the compounds to modulate *P. aeruginosa* PA01 QS, as measured by the production of the virulence factor pyocyanin. Bacterial cultures were grown for eight hours in the presence of each compound, followed by extraction of the pyocyanin under acidic conditions [22]. This was then quantified by measurement of the OD_{520}, which corresponds to absorption by the toxin. The results are shown in Figure 4, normalised by the bacterial density as measured by OD_{600} (no significant effect on the overall growth of the bacteria was observed for any of the compounds, see Supporting Information File 1 for details). The most promising results were replicated to ensure validity (due to the large amount of chemicals required for the assay, it was not practical to perform this for every compound). Of the natural products, only **4** seemed to show attenuation of pyocyanin production relative to the negative control. Meanwhile, whilst the truncated series of analogues appeared to lack activity, a marked reduction in pyocyanin production was noted for the compounds possessing a linear octanyl side chain. We speculate that this is due to the similarity to the heptanyl chain present in the native PQS ligand. This observation is highly intriguing, as HHQ (Figure 1), which differs from these analogues only by the lack of an N-substituent and a slightly shortened side chain, is known to activate *P. aeruginosa* QS (although it is incapable of inducing full pyocyanin expression) [23]. It would therefore appear that this inhibitory activity is likely due to the N-substitution, an avenue which has been to our knowledge underexplored in the SAR analysis of PQS and HHQ. In particular, analogues possessing smaller N-substituents (**14aa**, **14ab** and **14ac**) appeared to elicit a stronger effect than those possessing larger aromatic moieties (**14ad** and **14ae**).

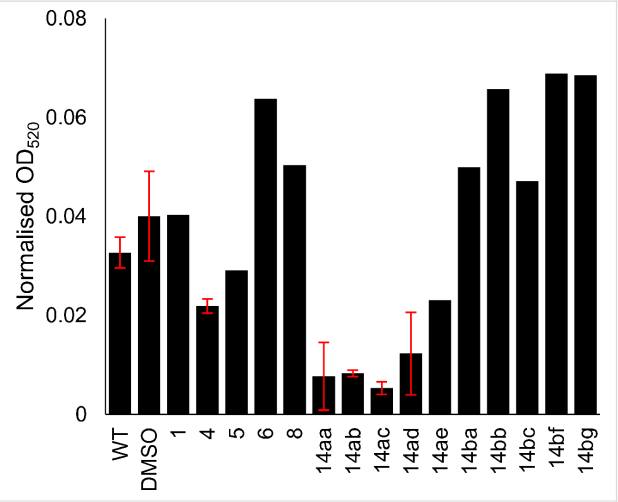

Figure 4: OD_{520} (absorption corresponding to pyocyanin) normalised by the culture population (measured by OD_{600}) for cultures of *P. aeruginosa* PA01 grown in the presence of concentrations of 200 μM of natural products and analogues after 8 hours. WT = wild type, no treatment added. DMSO = treated with DMSO blank. The experiment for **7** was not performed due to lack of material. The most promising results were replicated once to ensure validity, as shown by error bars.

Conclusion

We have reported the synthesis of structural analogues of a family of 4-quinolone *Pseudonocardia* sp. natural products, which encompassed variation of both the side chain and N-substituent. This represented an extension of the chemistry which we employed towards the natural products, utilising sequential Sonogashira coupling, high-yielding conjugate addition, and metal-catalysed cyclisation. A dichotomy in the optimal conditions for the final step was discovered, depending on the nature of the N-substituent. These analogues were then tested, together with a number of previously synthesised natural products, for their ability to bring about an intriguing "growth-slowing" effect towards certain species of bacteria. Whilst the presence of a geranyl side chain was shown to be vital for strong activity in *E. coli*, analogues possessing a saturated side chain exhibited marked inhibition of *S. aureus* growth. This intriguing result implies that slightly different mechanisms may be at work in each case, and suggests that it may be possible to attain selective therapeutic treatment of a specific species. Furthermore, the saturated series of analogues were demonstrated to inhibit the production of pyocyanin by *P. aeruginosa*, a virulence factor known to be under QS regulation, providing valuable new SAR insights regarding N-substitution of PQS and HHQ analogues.

Supporting Information

Supporting Information File 1

Experimental procedures and analytical data.
[https://www.beilstein-journals.org/bjoc/content/supplementary/1860-5397-14-245-S1.pdf]

Acknowledgements

SF was supported by a BBSRC studentship. DRS acknowledges support from the Engineering and Physical Sciences Research Council (EP/P020291/1) and Royal Society (Wolfson Research Merit Award). Data accessibility: all data supporting this study are provided as Supporting Information accompanying this paper.

ORCID® iDs

Suzanne Forrest - http://orcid.org/0000-0002-9605-7962
Martin Welch - http://orcid.org/0000-0003-3646-1733
David R. Spring - http://orcid.org/0000-0001-7355-2824

References

1. Heeb, S.; Fletcher, M. P.; Chhabra, S. R.; Diggle, S. P.; Williams, P.; Cámara, M. *FEMS Microbiol. Rev.* **2011,** *35,* 247–274. doi:10.1111/j.1574-6976.2010.00247.x
2. Bisacchi, G. S. *J. Med. Chem.* **2015,** *58,* 4874–4882. doi:10.1021/jm501881c
3. Dekker, K. A.; Inagaki, T.; Gootz, T. D.; Huang, L. H.; Kojima, Y.; Kohlbrenner, W. E.; Matsunaga, Y.; McGuirk, P. R.; Nomura, E.; Sakakibara, T.; Sakemi, S.; Suzuki, Y.; Yamauchi, Y.; Kojima, N. *J. Antibiot.* **1998,** *51,* 145–152. doi:10.7164/antibiotics.51.145
4. Rho, T. C.; Bae, E.-A.; Kim, D.-H.; Oh, W. K.; Kim, B. Y.; Ahn, J. S.; Lee, H. S. *Biol. Pharm. Bull.* **1999,** *22,* 1141–1143. doi:10.1248/bpb.22.1141
5. Whiteley, M.; Diggle, S. P.; Greenberg, E. P. *Nature* **2017,** *551,* 313–320. doi:10.1038/nature24624
6. Clatworthy, A. E.; Pierson, E.; Hung, D. T. *Nat. Chem. Biol.* **2007,** *3,* 541–548. doi:10.1038/nchembio.2007.24
7. Allen, R. C.; Popat, R.; Diggle, S. P.; Brown, S. P. *Nat. Rev. Microbiol.* **2014,** *12,* 300–308. doi:10.1038/nrmicro3232
8. Salvaggio, F.; Hodgkinson, J. T.; Carro, L.; Geddis, S. M.; Galloway, W. R. J. D.; Welch, M.; Spring, D. R. *Eur. J. Org. Chem.* **2016,** 434–437. doi:10.1002/ejoc.201501400
9. Cugini, C.; Calfee, M. W.; Farrow, J. M., III; Morales, D. K.; Pesci, E. C.; Hogan, D. A. *Mol. Microbiol.* **2007,** *65,* 896–906. doi:10.1111/j.1365-2958.2007.05840.x
10. Kurosu, M.; Begari, E. *Molecules* **2010,** *15,* 1531–1553. doi:10.3390/molecules15031531
11. Geddis, S. M.; Carro, L.; Hodgkinson, J. T.; Spring, D. R. *Eur. J. Org. Chem.* **2016,** 5799–5802. doi:10.1002/ejoc.201601195
12. Bernini, R.; Cacchi, S.; Fabrizi, G.; Sferrazza, A. *Synthesis* **2009,** 1209–1219. doi:10.1055/s-0028-1087990
13. Ó Muimhneacháin, E.; Reen, F. J.; O'Gara, F.; McGlacken, G. P. *Org. Biomol. Chem.* **2018,** *16,* 169–179. doi:10.1039/C7OB02395B
14. Abe, H.; Kawada, M.; Inoue, H.; Ohba, S.-i.; Nomoto, A.; Watanabe, T.; Shibasaki, M. *Org. Lett.* **2013,** *15,* 2124–2127. doi:10.1021/ol400587a
15. Mehra, M. K.; Tantak, M. P.; Arun, V.; Kumar, I.; Kumar, D. *Org. Biomol. Chem.* **2017,** *15,* 4956–4961. doi:10.1039/C7OB00940B
16. Lau, G. W.; Hassett, D. J.; Ran, H.; Kong, F. *Trends Mol. Med.* **2004,** *10,* 599–606. doi:10.1016/j.molmed.2004.10.002
17. Sorensen, R. U.; Klinger, J. D. *Basic Research and Clinical Aspects of Pseudomonas Aeruginosa. International Symposium on Pseudomonas Aeruginosa;* 1987; Vol. 39, pp 113–124.
18. Lau, G. W.; Ran, H.; Kong, F.; Hassett, D. J.; Mavrodi, D. *Infect. Immun.* **2004,** *72,* 4275–4278. doi:10.1128/IAI.72.7.4275-4278.2004
19. Smith, W. N.; Beumel, O. F., Jr. *Synthesis* **1974,** 441–443. doi:10.1055/s-1974-23341
20. Wolfe, J. P.; Rennels, R. A.; Buchwald, S. L. *Tetrahedron* **1996,** *52,* 7525–7546. doi:10.1016/0040-4020(96)00266-9
21. Janni, M.; Arora, S.; Peruncheralathan, S. *Org. Biomol. Chem.* **2016,** *14,* 8781–8788. doi:10.1039/C6OB01568A
22. Frank, L. H.; DeMoss, R. D. *J. Bacteriol.* **1959,** *77,* 776–782.
23. Xiao, G.; Déziel, E.; He, J.; Lépine, F.; Lesic, B.; Castonguay, M.-H.; Milot, S.; Tampakaki, A. P.; Stachel, S. E.; Rahme, L. G. *Mol. Microbiol.* **2006,** *62,* 1689–1699. doi:10.1111/j.1365-2958.2006.05462.x

License and Terms

BEILSTEIN JOURNAL OF ORGANIC CHEMISTRY

Synthesis of pyrrolidine-based hamamelitannin analogues as quorum sensing inhibitors in *Staphylococcus aureus*

Jakob Bouton[1], Kristof Van Hecke[2], Reuven Rasooly[3] and Serge Van Calenbergh[*1]

Full Research Paper

Open Access

Address:
[1]Laboratory for Medicinal Chemistry, Ghent University, Ottergemsesteenweg 460, 9000 Ghent, Belgium, [2]XStruct, Department of Chemistry, Ghent University, Krijgslaan 281 S3, 9000 Ghent, Belgium and [3]Western Regional Research Center, Foodborne Toxin Detection & Prevention Research Unit, Agricultural Research Service, United States Department of Agriculture, Albany, CA 94710, USA

Email:
Serge Van Calenbergh[*] - serge.vancalenbergh@ugent.be

* Corresponding author

Keywords:
hamamelitannin; iminosugar; pyrrolidine; quorum sensing; *Staphylococcus aureus*

Beilstein J. Org. Chem. **2018,** *14,* 2822–2828.
doi:10.3762/bjoc.14.260

Received: 01 August 2018
Accepted: 01 November 2018
Published: 12 November 2018

This article is part of the thematic issue "Antibacterials, bacterial small molecule interactions and quorum sensing".

Guest Editor: D. Spring

Abstract

Interfering with bacterial cell-to-cell communication is a promising strategy to combat antimicrobial resistance. The natural product hamamelitannin and several of its analogues have been identified as quorum sensing inhibitors. In this paper the synthesis of pyrrolidine-based analogues of a more lead-like hamamelitannin analogue is reported. A convergent synthetic route based on a key ring-closing metathesis reaction was developed and delivered the pyrrolidine analogue in 17 steps in high yield. Chemoselective derivatization of the pyrrolidine nitrogen atom resulted in 6 more compounds. The synthesized compounds were evaluated in a biofilm model, but were all inactive.

Introduction

Antimicrobial resistance is rapidly becoming a global threat [1,2]. It is estimated that worldwide, at least 700 000 people die every year from drug-resistant strains of common bacterial infections. Strategies to deal with the global antimicrobial resistance problem need to be multifactorial. Next to disease prevention and the development of new antibiotics, it is essential to investigate innovative strategies to combat bacterial infections [3,4]. Recently, targeting bacterial virulence has gained a lot of attention [5-7]. It has been hypothesized that by "disarming" the pathogen, rather than inhibiting its growth, selective pressure for resistance development will be much lower. Furthermore, reduction of bacterial virulence directly protects the host, and at the same time renders the bacteria more susceptible towards the host defense system and antibiotics.

The Centers for Disease Control and Prevention (CDC) have listed a number of bacteria that present serious, urgent and concerning threats [8]. One of these problematic bacteria is methicillin-resistant *Staphylococcus aureus* (MRSA), a human pathogen that causes a wide range of clinical infections. In *S. aureus*, virulence is mainly mediated by quorum sensing, a bacterial cell-to-cell communication system based on the secretion of signal molecules [9-11]. The natural product hamamelitannin (**1**) has been identified as a non-peptide analogue of RIP (RNAIII-inhibiting protein), an inhibitor of the RAP/TRAP (RNAIII-activating protein/target of RAP) quorum sensing system in *S. aureus* (Figure 1) [12-14]. Furthermore, hamamelitannin has been shown to inhibit biofilm formation and to potentiate the activity of antibiotics against staphylococcal biofilms in vitro and in vivo [12,15]. Structural optimization of hamamelitannin by our group resulted in several more potent and more druglike analogues of which compound **2** emerged as a promising starting point for further optimization and subsequent development (Figure 1) [16-19]. Our earlier work revealed that the optimal side chain substituents are an *o*-chlorobenzamide on the 5-position and a non-substituted benzamide on the 2'-position. In absence of any structural information of the inhibitor–target interaction, we were interested in replacing the core tetrahydrofuran scaffold by a pyrrolidine ring in order to further elucidate the structure–activity relationship. The pyrrolidine nitrogen atom provides an extra point of diversification, allowing further elaboration of the scaffold. Substituents on the ring nitrogen might lead to additional interactions with the target and therefore provide more potent analogues. Moreover, the O-to-N replacement is expected to increase solubility and possible polar interactions with the target. In this work we report the design, synthesis and biological evaluation of a number of pyrrolidine-based hamamelitannin analogues.

The envisioned strategy for the synthesis of the target pyrrolidine-based hamamelitannin analogues is depicted in Scheme 1. The synthesis of **4** as a key intermediate allows to gain access to a diverse set of analogues by chemoselective late-stage derivatization of the pyrrolidine nitrogen. Previously, we used the iminosugar **5** to prepare a series of 2'-homoazanucleosides. This possible precursor was synthesized convergently in 12 steps [20]. The pyrrolidine ring was constructed via alkylation of **6** and **7**, followed by ring-closing metathesis. Stereoselective dihydroxylation of the resulting alkene then furnished the protected iminosugar **5**. However, using intermediate **5** as a starting point for the hamamelitannin analogues would render the synthetic route very linear and impractical to produce sufficient amounts required to prepare a series of analogues.

Therefore, we envisioned a modification of the previously developed synthetic route, where the two fully functionalized side chains are introduced prior to coupling and ring closure to afford **8**. This new synthetic route would be more convergent and efficient for the preparation of **3**. Retrosynthetic analysis led to **9** and **10** as two key synthons, which would be assembled via a Mitsunobu–Fukuyama reaction, and subsequently the secondary amine converted to the pyrrolidine ring via a ring-closing metathesis reaction [21].

Results and Discussion

Chemistry

The synthesis of fragment **9** is depicted in Scheme 2 and proved to be challenging. It was essential to introduce the nosyl group only in the last step, since several previous attempts to synthesize **9** failed due to side reactions caused by the strongly electron-withdrawing properties of the nosyl group. The successful synthesis starts with a Pd-catalyzed dynamic kinetic asymmetric transformation of racemic butadiene monoepoxide to **12**, employing phthalimide as nucleophile [22,23]. Attempts to substitute the alcohol functionality of **12** via displacement of the derived mesylate with NaN_3 failed, similar to previously reported difficulties by Trost et al. [24]. The benzamide substituent was therefore introduced via Mitsunobu reaction with N-Boc-protected *ortho*-chlorobenzamide **13**. Removal of the

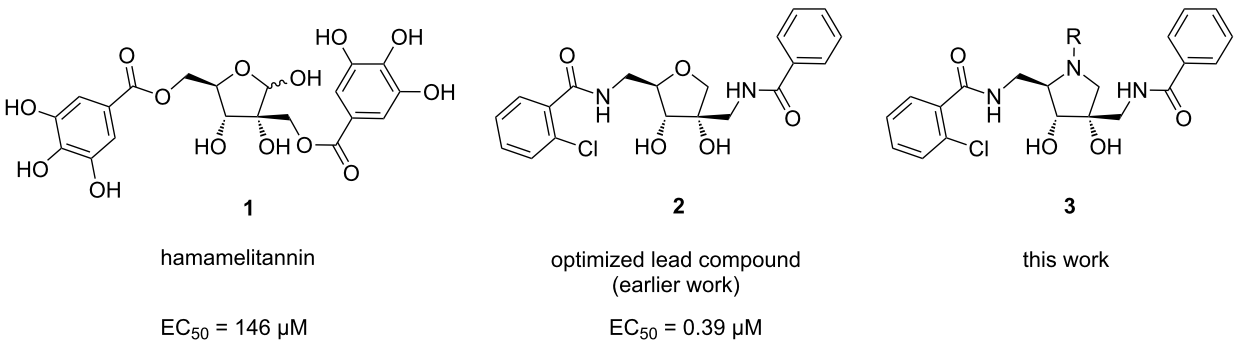

Figure 1: Structures of hamamelitannin (**1**), lead compound **2** and target compounds **3**.

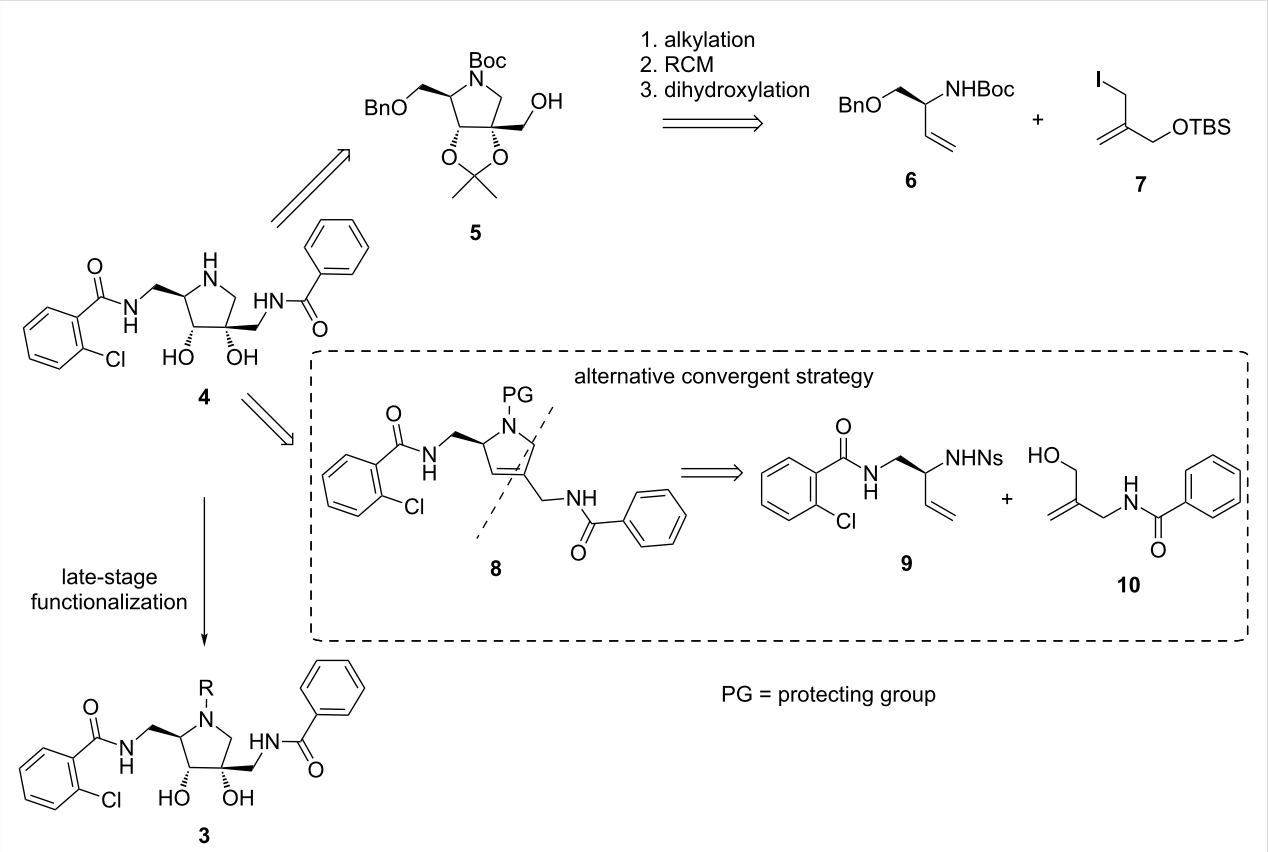

Scheme 1: Proposed strategy for the synthesis of the target analogues.

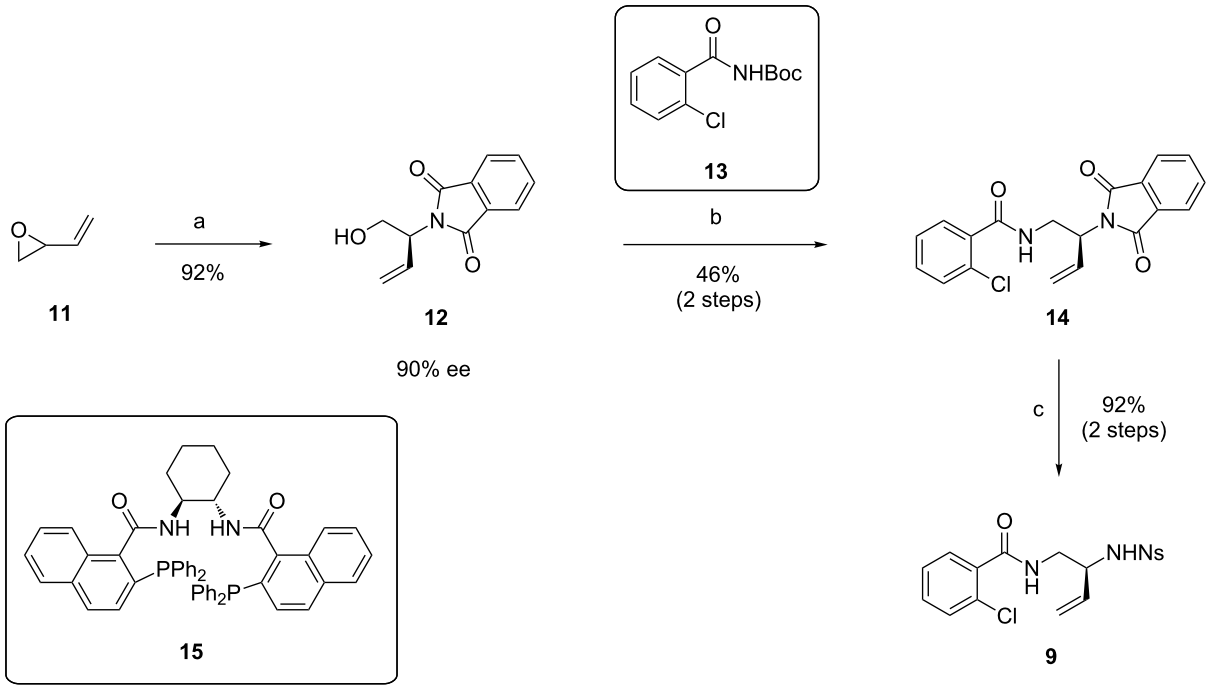

Scheme 2: Synthesis of fragment **9**. Reagents and conditions: a) phthalimide, $Pd_2(allyl)_2Cl_2$, ligand **15**, Na_2CO_3, CH_2Cl_2, rt; b) i) **13**, DEAD, PPh_3, toluene, 0 °C to rt; ii) TFA, CH_2Cl_2, H_2O, rt; c) i) ethylenediamine, EtOH/THF 7:3, reflux; ii) *p*-Ns-Cl, Et_3N, THF, 0 °C.

Boc-group with TFA resulted in **14**. Next, the phthalimide was removed via refluxing with ethylenediamine and the resulting amine protected as *para*-nitrobenzenesulfonamide to obtain the desired fragment **9**.

The synthesis of **10** starts from commercially available 2-methylene-1,3-propanediol (**16**), which was selectively monoprotected in high yield as TBS ether (Scheme 3) [25]. The remaining alcohol was then substituted for a phthalimide via Mitsunobu reaction. Phthalimide deprotection, acylation with benzoic acid, and removal of the silyl protecting group furnished **10**.

Fragments **9** and **10** were coupled under Mitsunobu conditions (Scheme 4), affording **20** contaminated with Mitsunobu byproducts. Unfortunately, attempted ring-closing metathesis of **20** using the Grubbs–Hoveyda II catalyst failed to produce any product, probably due to the insolubility of **20** in solvents suitable for metathesis reactions (1,2-DCE, toluene) and/or the coordinating ability of the three (sulfon)amide functionalities [26,27].

To circumvent this problem, we were forced to alter the initial synthetic strategy and used a different eastern fragment for the ring-closing metathesis reaction. The *ortho*-chlorobenzamide substituent would then be introduced in a later stage. We chose to protect alcohol **12** as TBS ether and used the derived nosyl-protected fragment **23** as the coupling partner (Scheme 5).

Fragments **23** and **10** were coupled via Mitsunobu reaction, yielding **24** in 49% yield (Scheme 6). Fortunately, ring-closing metathesis of **24** now smoothly afforded **25** in high yield.

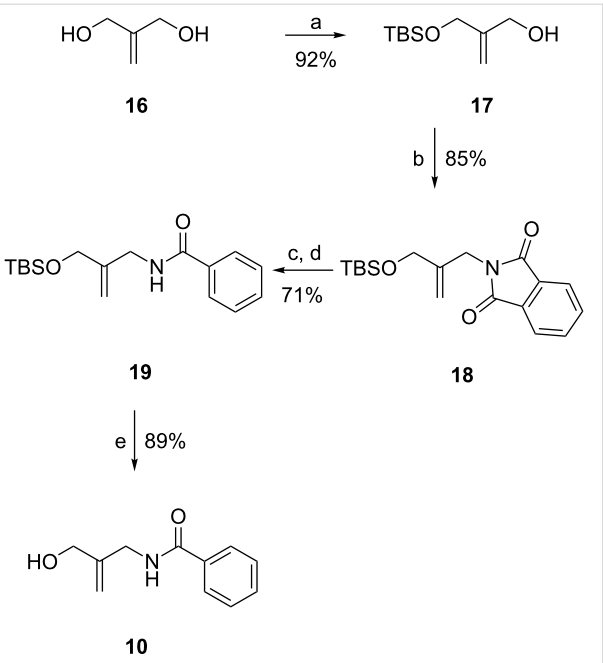

Scheme 3: Synthesis of fragment **10**. Reagents and conditions: a) TBSCl, NaH, THF, rt; b) phthalimide, PPh_3, DEAD, THF, 0 °C to rt; c) $H_2NNH_2{\cdot}H_2O$, MeOH, reflux; d) BzCl, Et_3N, CH_2Cl_2, 0 °C; e) TBAF, THF, rt.

Dihydroxylation selectively yielded the desired stereoisomer of diol **26**, which was subsequently protected as isopropylidene acetal. In the next step, after removal of the TBS group and mesylation, attempted substitution with NaN_3 resulted only in an elimination product. This led us to replace the electron-withdrawing nosyl protecting group with a Boc group. After removal of the TBS ether and mesylation of the resulting alcohol, substitution with NaN_3 now smoothly provided azide

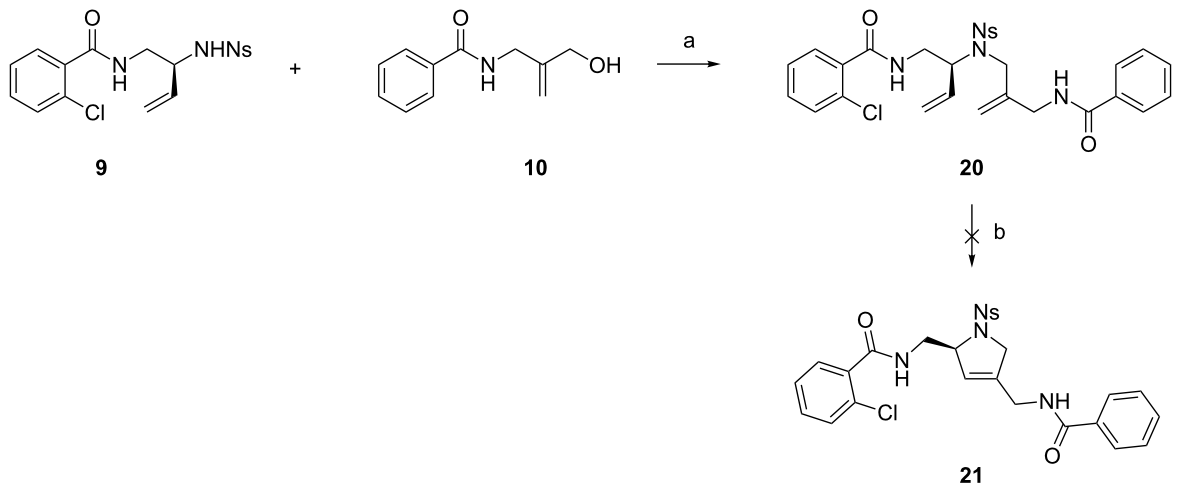

Scheme 4: Coupling of **9** and **10** and attempted ring-closing metathesis. Reagents and conditions: a) PPh_3, DEAD, THF/DMF 2:1, 0 °C to rt; b) 5 mol % Grubbs–Hoveyda II, 1,2-DCE, 50 °C.

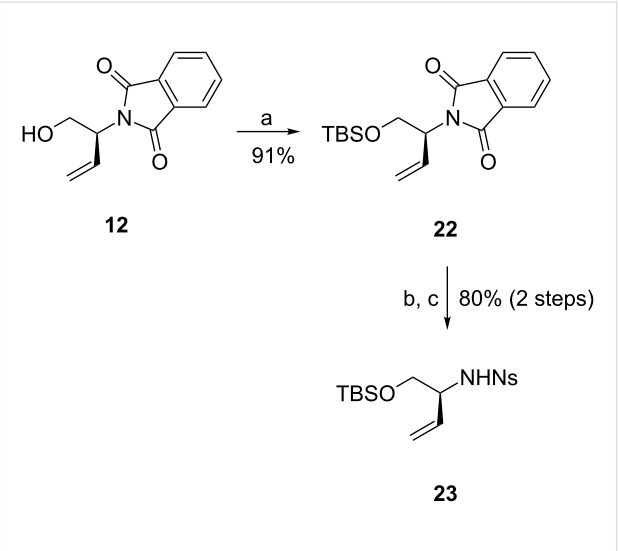

Scheme 5: Synthesis of alternative eastern fragment **23**. Reagents and conditions: a) TBSCl, imidazole, CH_2Cl_2, rt; b) $H_2NNH_2{\cdot}H_2O$, MeOH, reflux; c) *p*-Ns-Cl, Et_3N, CH_2Cl_2, 0 °C.

29. The azide was then reduced under classical Staudinger conditions, followed by amide formation with *ortho*-chlorobenzoic acid and a final acidic deprotection step to provide the desired analogue **4**. Despite the change of the initial strategy and resulting elongation of the synthetic route, the overall synthesis still proved to be very efficient, delivering **4** in 6% yield in 17 steps from **16**.

The pyrrolidine nitrogen was then further derivatized with several small substituents (Scheme 7). Reductive amination with several aldehydes resulted in **3a**–**c**. The N-methyl analogue **3d** was synthesized via methylation with MeI. The methanesulfonamide **3e** and acetamide **3f**, in which the cationic character of the pyrrolidine nitrogen is removed, were also synthesized.

The correct stereochemistry of the synthesized analogues was unequivocally proven via X-ray structural analysis of compound **3a** (Figure 2).

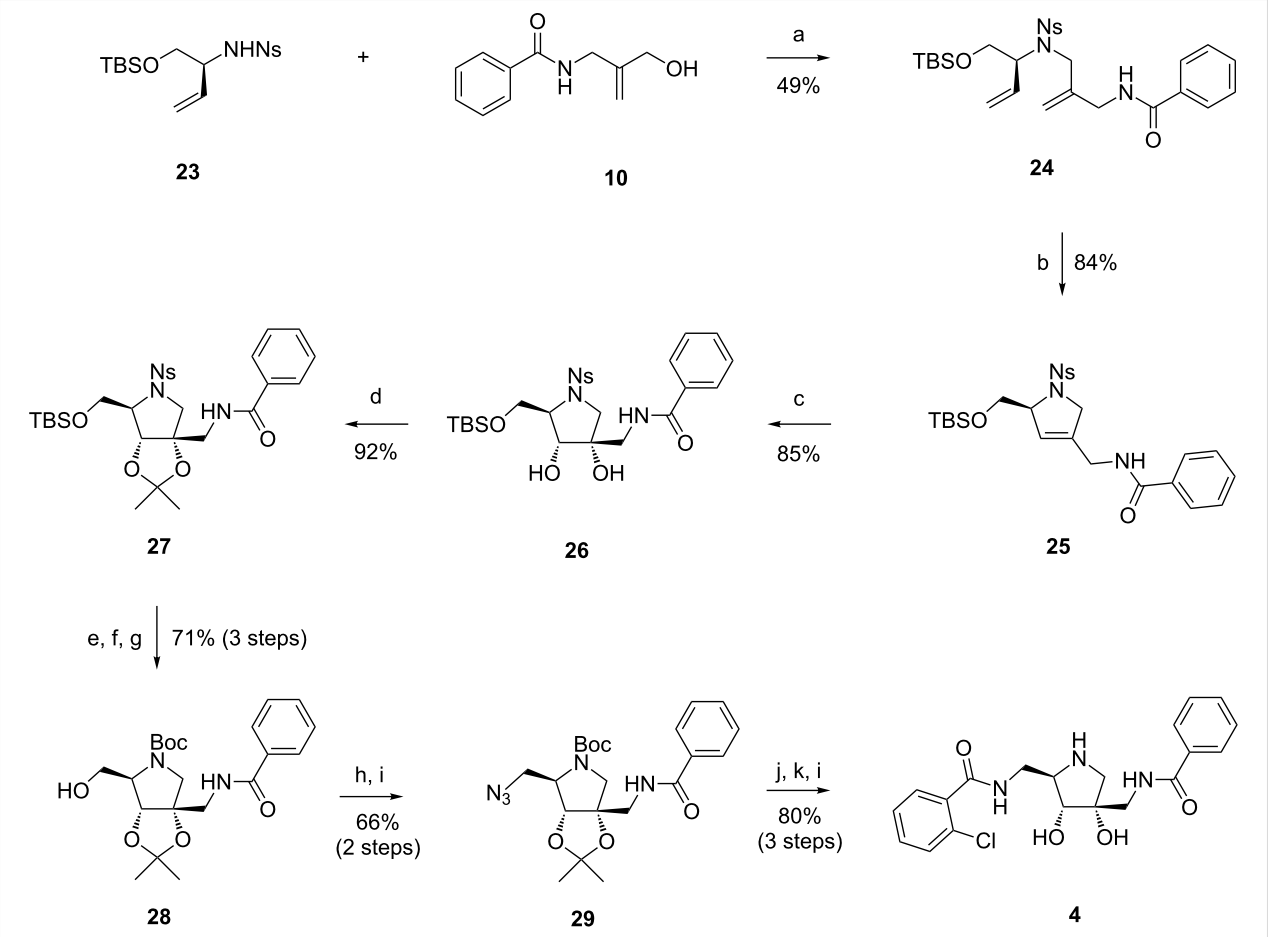

Scheme 6: Synthesis of **4**. Reagents and conditions: a) PPh_3, DEAD, THF, 0 °C to rt; b) Grubbs–Hoveyda II (5 mol %), 1,2-DCE, 50 °C; c) $K_2OsO_4{\cdot}2H_2O$, NMO, acetone/H_2O 3:1, rt; d) 2-methoxypropene, CSA (cat.), THF, rt; e) PhSH, K_2CO_3, MeCN, 50 °C; f) Boc_2O, Et_3N, CH_2Cl_2, rt; g) TBAF, THF, rt; h) Ms-Cl, Et_3N, CH_2Cl_2, 0 °C; i) NaN_3, DMF, 60 °C; j) PMe_3, H_2O, THF, rt; k) 2-chlorobenzoyl chloride, Et_3N, CH_2Cl_2, 0 °C; l) conc. HCl, MeOH/H_2O 1:1, reflux.

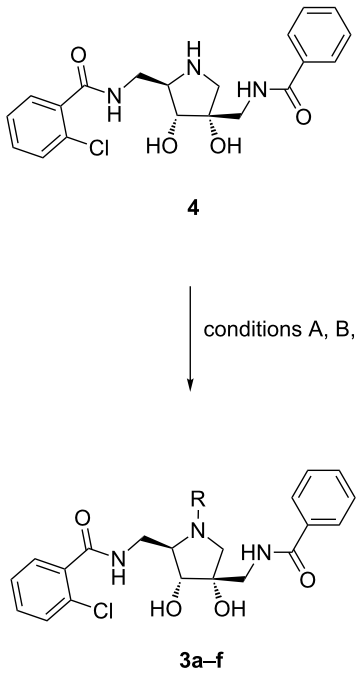

compound	R =	reaction conditions (yield)
3a		A (93%)
3b		A (46%)
3c		A (83%)
3d		B (52%)
3e		C (35%)
3f		D (70%)

Scheme 7: Late stage functionalization of the pyrrolidine nitrogen. Reagents and conditions: A) (masked) aldehyde, $NaBH_3CN$, AcOH, MeOH, 60 °C; B) MeI, DIPEA, THF, 0 °C; C) Ms-Cl, Et_3N, THF, 0 °C; D) AcOH, DIPEA, HATU, DMF, rt.

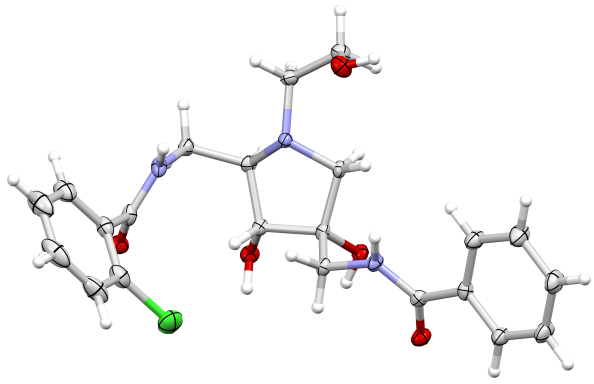

Figure 2: Molecular X-ray structure of **3a**, showing thermal displacement ellipsoids at the 50% probability level. Positional disorder of the chlorophenyl ring and the water solvent molecule are not shown.

Biological evaluation

The synthesized analogues were tested in a *S. aureus* biofilm model, but were all inactive (see Supporting Information File 1).

Conclusion

A convergent synthetic route for the synthesis of pyrrolidine-based hamamelitannin analogues was developed. The originally envisioned strategy failed due to difficulties in the ring-closing metathesis reaction, but modification of one of the coupling partners solved this issue. The desired pyrrolidine-based analogue was synthesized in 17 steps and chemoselective modification of the nitrogen atom provided 6 analogues. Unfortunately, these analogues were inactive in inhibiting *S. aureus* biofilm formation.

Supporting Information

Supporting Information File 1

Experimental details.
[https://www.beilstein-journals.org/bjoc/content/supplementary/1860-5397-14-260-S1.pdf]

Acknowledgements

Izet Karalic is gratefully acknowledged for technical assistance. KVH thanks the Hercules Foundation (project AUGE/11/029

"3D-SPACE: 3D Structural Platform Aiming for Chemical Excellence") and the Special Research Fund (BOF) – UGent (project 01N03217) for funding.

ORCID® iDs

Jakob Bouton - https://orcid.org/0000-0003-4193-7644
Kristof Van Hecke - https://orcid.org/0000-0002-2455-8856
Serge Van Calenbergh - https://orcid.org/0000-0002-4201-1264

References

1. Tackling drug-resistant infections globally: final report and recommendations. *The review on antimicrobial resistance;* 2016.
2. Ventola, C. L. *P T* **2015,** *40,* 277–283.
3. Czaplewski, L.; Bax, R.; Clokie, M.; Dawson, M.; Fairhead, H.; Fischetti, V. A.; Foster, S.; Gilmore, B. F.; Hancock, R. E. W.; Harper, D.; Henderson, I. R.; Hilpert, K.; Jones, B. V.; Kadioglu, A.; Knowles, D.; Ólafsdóttir, S.; Payne, D.; Projan, S.; Shaunak, S.; Silverman, J.; Thomas, C. M.; Trust, T. J.; Warn, P.; Rex, J. H. *Lancet Infect. Dis.* **2016,** *16,* 239–251. doi:10.1016/S1473-3099(15)00466-1
4. Brown, E. D.; Wright, G. D. *Nature* **2016,** *529,* 336–343. doi:10.1038/nature17042
5. Rasko, D. A.; Sperandio, V. *Nat. Rev. Drug Discovery* **2010,** *9,* 117–128. doi:10.1038/nrd3013
6. Heras, B.; Scanlon, M. J.; Martin, J. L. *Br. J. Clin. Pharmacol.* **2015,** *79,* 208–215. doi:10.1111/bcp.12356
7. Escaich, S. *Curr. Opin. Chem. Biol.* **2008,** *12,* 400–408. doi:10.1016/j.cbpa.2008.06.022
8. *Antibiotic resistance threats in the united states;* U.S. Department of Health and Human Services - Centers for Disease Control and Prevention 2013.
9. Assis, L. M.; Nedeljković, M.; Dessen, A. *Drug Resist. Updates* **2017,** *31,* 1–14. doi:10.1016/j.drup.2017.03.001
10. Khan, B. A.; Yeh, A. J.; Cheung, G. Y.; Otto, M. *Expert Opin. Invest. Drugs* **2015,** *24,* 689–704. doi:10.1517/13543784.2015.1019062
11. Gordon, C. P.; Williams, P.; Chan, W. C. *J. Med. Chem.* **2013,** *56,* 1389–1404. doi:10.1021/jm3014635
12. Kiran, M. D.; Adikesavan, N. V.; Cirioni, O.; Giacometti, A.; Silvestri, C.; Scalise, G.; Ghiselli, R.; Saba, V.; Orlando, F.; Shoham, M.; Balaban, N. *Mol. Pharmacol.* **2008,** *73,* 1578–1586. doi:10.1124/mol.107.044164
13. Giacometti, A.; Cirioni, O.; Gov, Y.; Ghiselli, R.; Del Prete, M. S.; Mocchegiani, F.; Saba, V.; Orlando, F.; Scalise, G.; Balaban, N.; Dell'Acqua, G. *Antimicrob. Agents Chemother.* **2003,** *47,* 1979–1983. doi:10.1128/AAC.47.6.1979-1983.2003
14. Balaban, N.; Cirioni, O.; Giacometti, A.; Ghiselli, R.; Braunstein, J. B.; Silvestri, C.; Mocchegiani, F.; Saba, V.; Scalise, G. *Antimicrob. Agents Chemother.* **2007,** *51,* 2226–2229. doi:10.1128/AAC.01097-06
15. Brackman, G.; Breyne, K.; De Rycke, R.; Vermote, A.; Van Nieuwerburgh, F.; Meyer, E.; Van Calenbergh, S.; Coenye, T. *Sci. Rep.* **2016,** *6,* No. 20321. doi:10.1038/srep20321
16. Vermote, A.; Brackman, G.; Risseeuw, M. D. P.; Vanhoutte, B.; Cos, P.; Van Hecke, K.; Breyne, K.; Meyer, E.; Coenye, T.; Van Calenbergh, S. *Angew. Chem.* **2016,** *55,* 6551–6555. doi:10.1002/anie.201601973
17. Vermote, A.; Brackman, G.; Risseeuw, M. D. P.; Coenye, T.; Van Calenbergh, S. *Bioorg. Med. Chem.* **2016,** *24,* 4563–4575. doi:10.1016/j.bmc.2016.07.058
18. Vermote, A.; Brackman, G.; Risseeuw, M. D. P.; Cappoen, D.; Cos, P.; Coenye, T.; Van Calenbergh, S. *ACS Med. Chem. Lett.* **2017,** *8,* 38–42. doi:10.1021/acsmedchemlett.6b00315
19. Vermote, A.; Brackman, G.; Risseeuw, M. D. P.; Coenye, T.; Van Calenbergh, S. *Eur. J. Med. Chem.* **2017,** *127,* 757–770. doi:10.1016/j.ejmech.2016.10.056
20. Bouton, J.; Van Hecke, K.; Van Calenbergh, S. *Tetrahedron* **2017,** *73,* 4307–4316. doi:10.1016/j.tet.2017.05.083
21. Fukuyama, T.; Jow, C.-K.; Cheung, M. *Tetrahedron Lett.* **1995,** *36,* 6373–6374. doi:10.1016/0040-4039(95)01316-A
22. Xiong, H.; Chen, B.; Durand-Réville, T. F.; Joubran, C.; Alelyunas, Y. W.; Wu, D.; Huynh, H. *ACS Med. Chem. Lett.* **2014,** *5,* 1143–1147. doi:10.1021/ml500284k
23. Trost, B. M.; Horne, D. B.; Woltering, M. J. *Angew. Chem.* **2003,** *42,* 5987–5990. doi:10.1002/anie.200352857
24. Trost, B. M.; Bunt, R. C.; Lemoine, R. C.; Calkins, T. L. *J. Am. Chem. Soc.* **2000,** *122,* 5968–5976. doi:10.1021/ja000547d
25. McDougal, P. G.; Rico, J. G.; Oh, Y. I.; Condon, B. D. *J. Org. Chem.* **1986,** *51,* 3388–3390. doi:10.1021/jo00367a033
26. Adjiman, C. S.; Clarke, A. J.; Cooper, G.; Taylor, P. C. *Chem. Commun.* **2008,** 2806–2808. doi:10.1039/b802921k
27. Fürstner, A.; Langemann, K. *J. Am. Chem. Soc.* **1997,** *119,* 9130–9136. doi:10.1021/ja9719945

License and Terms

BEILSTEIN JOURNAL OF ORGANIC CHEMISTRY

Protein–protein interactions in bacteria: a promising and challenging avenue towards the discovery of new antibiotics

Laura Carro

Review

Open Access

Address:
School of Pharmacy, University of East Anglia, Norwich Research Park, Norwich NR4 7TJ, UK

Email:
Laura Carro - l.carro-santos@uea.ac.uk

Keywords:
new antibiotics; protein–protein interactions; resistance

Beilstein J. Org. Chem. **2018,** *14,* 2881–2896.
doi:10.3762/bjoc.14.267

Received: 31 July 2018
Accepted: 02 November 2018
Published: 21 November 2018

This article is part of the thematic issue "Antibacterials, bacterial small molecule interactions and quorum sensing".

Guest Editor: D. Spring

Abstract

Antibiotics are potent pharmacological weapons against bacterial infections; however, the growing antibiotic resistance of microorganisms is compromising the efficacy of the currently available pharmacotherapies. Even though antimicrobial resistance is not a new problem, antibiotic development has failed to match the growth of resistant pathogens and hence, it is highly critical to discover new anti-infective drugs with novel mechanisms of action which will help reducing the burden of multidrug-resistant microorganisms. Protein–protein interactions (PPIs) are involved in a myriad of vital cellular processes and have become an attractive target to treat diseases. Therefore, targeting PPI networks in bacteria may offer a new and unconventional point of intervention to develop novel anti-infective drugs which can combat the ever-increasing rate of multidrug-resistant bacteria. This review describes the progress achieved towards the discovery of molecules that disrupt PPI systems in bacteria for which inhibitors have been identified and whose targets could represent an alternative lead discovery strategy to obtain new anti-infective molecules.

Introduction

Bacterial infections are not only one of the most frequent diseases in humans and livestock, but also one of the top ten causes of death according to the World Health Organization [1]. The serendipitous discovery of penicillin and its introduction into the clinic in the first half of the 20th century gave rise to the “Golden Age” of antibiotics discovery and have unquestionably represented one of the most important achievements in medicine. Unfortunately, since their use is intrinsically linked to the appearance of resistance, threatening antibiotic-resistant bacteria levels are being observed, compromising the efficacy of nearly all available antibiotics to cure infectious diseases [2-4].

The rise in the percentage of antibiotic-insensitive strains, the steady decline in the number of new antibacterial drugs and the insufficient investment in antimicrobial research and development (R&D) by the major pharmaceutical companies have led to a global health crisis in which the prospect of a future without a safe and effective anti-infective compound is a very real and alarming possibility [5,6]. Consequently, new antibacterial drugs and treatment strategies are urgently needed to tackle the increasing multidrug-resistance in bacteria [7].

To further accelerate antibiotics development numerous approaches have been put in place. For example, the WHO recently published a list of global priority antibiotic-resistant bacteria to help prioritizing the research and development of new and effective antibiotic treatments [8]. In this list the pathogens were ranked in three priority levels according to the species and type of resistance:

1. Priority 1 – Critical:

- *Acinetobacter baumannii*, carbapenem-resistant
- *Pseudomonas aeruginosa*, carbapenem-resistant
- *Enterobacteriaceae*, carbapenem-resistant, 3rd generation cephalosporin-resistant

2. Priority 2 – High:

- *Enterococcus faecium*, vancomycin-resistant
- *Staphylococcus aureus*, methicillin-resistant, vancomycin intermediate and resistant
- *Helicobacter pylori*, clarithromycin-resistant
- *Campylobacter*, fluoroquinolone-resistant
- *Salmonella* spp., fluoroquinolone-resistant
- *Neisseria gonorrhoeae*, 3rd generation cephalosporinresistant, fluoroquinolone-resistant

3. Priority 3 – Medium:

- *Streptococcus pneumoniae*, penicillin-non-susceptible
- *Haemophilus influenzae*, ampicillin-resistant
- *Shigella* spp., fluoroquinolone-resistant

Given the prevalence of antibacterial drug-resistant pathogens, one viable and promising strategy to combat these multidrug-resistant bacteria is the development of antibiotic therapies with novel unconventional targets [9], such as protein–protein interactions [10,11].

This review covers the recent medicinal chemistry efforts towards the discovery of antibacterial molecules that disrupt protein–protein interactions (PPIs) by interacting directly to the protein–protein binding interface in both Gram-negative and Gram-positive microorganisms. In order to encourage prospective drug discovery endeavours in this field, this study focuses on four examples of bacterial PPIs for which inhibitors with promising activities have been reported. For each of the targets the structural features of the ligands, the discovery strategy, the characterization assay, the biological activity, and, if applicable, the SAR are discussed.

Review

Protein–protein interactions

Due to the fact that protein–protein interactions (PPIs) play a pivotal role in many cellular processes, they have increasingly become an attractive target over the past two decades [12-14].

PPIs are challenging targets because of their flat, large and hydrophobic binding surface, in comparison with the well-defined binding sites of more classical targets such as GPCRs, enzymes or ion channels (Figure 1). Moreover, PPIs, unlike the previous examples, do not have a small natural ligand which can be used as a lead in a standard drug development programme [15,16]. Despite the binding surfaces being large, it is well known that not all the amino acid residues at the interface contribute equally to the binding, but in fact there are focal points (i.e., hot spots or hot segments) that contribute to the majority of the binding energy [17,18]. Targeting these "druggable" sites can therefore be used for the rational design of new therapeutic compounds that can disrupt those critical interactions. However, their identification requires detailed structure elucidation, which in the end makes the design of an effective PPI modulator both difficult and challenging [19-22]. PPI modulation can be achieved through two opposite but complementary approaches: stabilization or inhibition (Figure 1). Although so far the vast majority of protein–protein interaction modulators execute their activity through inhibition, stabilization of specific protein complexes could also be therapeutically beneficial [23,24].

Even though historically PPIs have been considered to be "undruggable", recent remarkable medicinal chemistry efforts, mainly due to the development and implementation of more sophisticated screening methods and synthetic procedures, have led to the identification and clinical development of chemical entities that disrupt protein–protein interactions [15,25,26].

A selection of a few PPI modulators that have recently been approved or reached clinical validation can be found in Figure 2. If we analyze their mechanism of action, nearly all of them are currently being investigated as oncological treatments. For example, navitoclax (**1**, Figure 2), a Bcl-2/Bcl-X_L inhibitor developed by Abbot Laboratories is currently in phase II for the

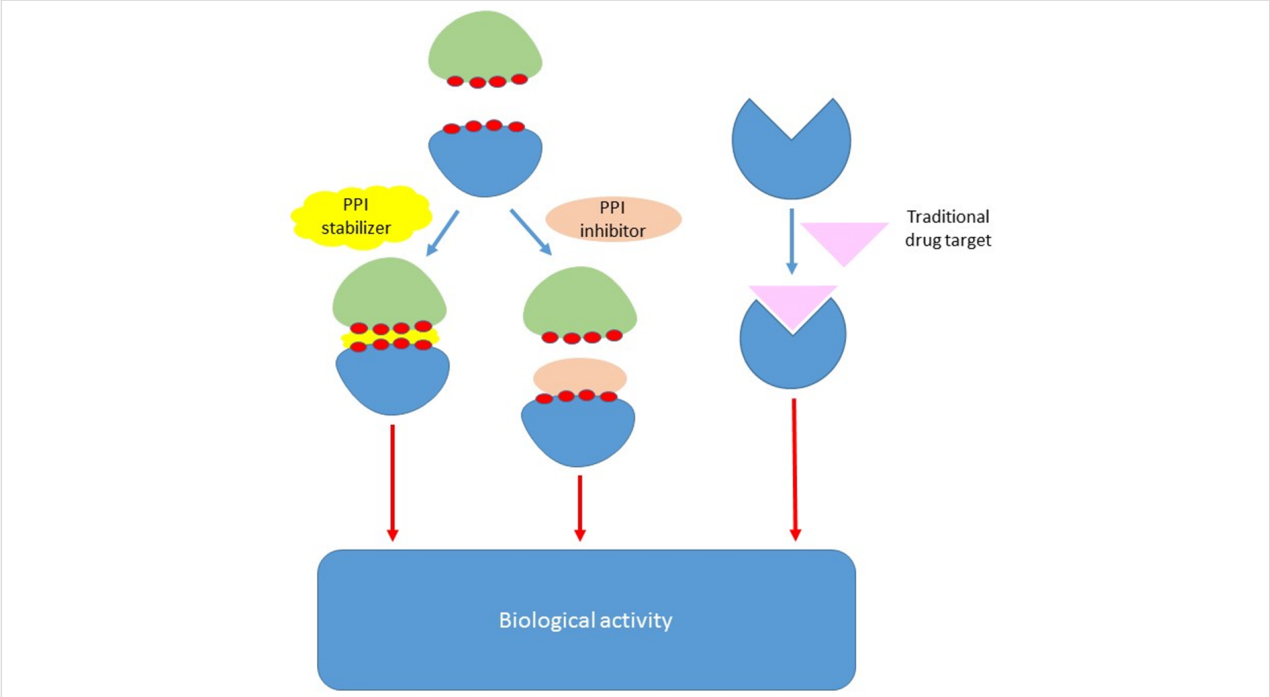

Figure 1: Illustration of a PPI modulator (stabilizer or inhibitor) vs a traditional drug target.

treatment of several types of cancers [27]. Idasanutlin (**2**, Figure 2) from Hoffmann-La Roche, targets the extensively studied interaction between MDM2/p53 and is currently in phase III for the treatment of refractory acute myeloid leukemia in combination with cytarabine [28]. LCL-161 (**3**, Figure 2), an inhibitor of the interaction between Smac (second mitochondria-derived activator of caspases) and IAP (inhibitor of apoptosis proteins) developed by Novartis, has recently entered phase II for the treatment of leukaemia [29]. Another example is the inhibitor of the BET (bromodomain and extra terminal) molibresib (**4**, Figure 2), developed by GSK and currently in phase I for the treatment of several carcinomas [30]. It is also worth highlighting two PPI inhibitors that have recently been approved: lifitegrast (**5**, Figure 2) is an anti-inflammatory integrin antagonist that disrupts the LFA-1/ICAM-1 interaction used for the treatment of dry eye disease [31,32], and tirofiban (**6**, Figure 2), a platelet glycoprotein IIb/IIIa inhibitor indicated in acute coronary syndrome [33]. In addition to small molecules, natural products have been shown to be able to modulate protein–protein interactions and have validated PPI stabilization as a biological target. One of the most prominent examples of PPI-stabilizing natural products that are currently used in the treatments of human diseases is rapamycin (**7**, Figure 2), an immunosuppressant that inhibits the protein kinase TOR (target of rapamycin) [34]. This natural product, isolated from *Streptomyces hygroscopicus*, was one of the first protein–protein interaction stabilizers reported: it first binds to its receptor (i.e., FKBP12) with high affinity, after which the FKBP12-rapamycin complex will associate with TOR resulting in inhibition of the catalytic activity of the enzyme [23].

All these drug discovery successes have validated PPIs as a target and, in conjunction with the elucidation and reconstruction of protein–protein interaction networks in bacteria, have paved the way towards the development of novel and promising inhibitors of PPIs which may find application as anti-infective therapies.

Protein–protein interactions in bacteria

Like in eukaryotes, protein–protein interactions are essential in prokaryotic cells in which they also have a central role. They coordinate many bacterial physiological processes such as regulation of gene expression, DNA replication, signal transduction, virulence, etc. and therefore represent potential fruitful targets for antibacterial drug discovery.

Recently, scientific efforts have helped towards the understanding and the deciphering of the protein-interaction networks (PINs) that forge the bacterial interactome [35]. However, despite the potential of these bacterial PPI maps, they have only been studied in detail in a few microorganisms including *Escherichia coli* (one of the best-studied model organisms in this field) [36-39], *Mycobacterium tuberculosis* [40], *Helicobacter pylori* [41], *Pseudomonas aeruginosa* [42], *Campylobacter jejuni* [43], *Treponema pallidum* [44], the cyanobacterium *Synechocystis* spp. [45], *Mesorhizobium loti* [46] and

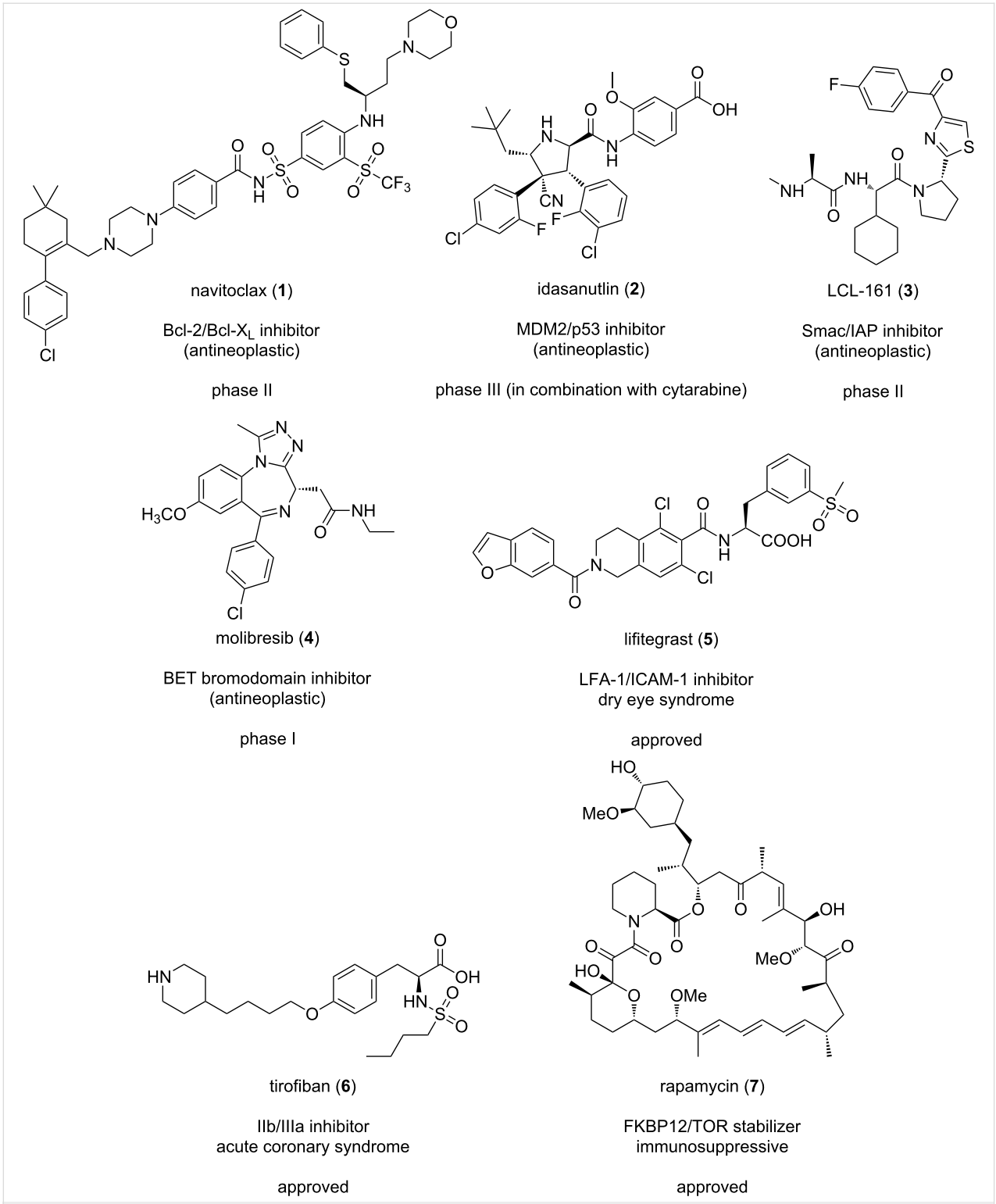

Figure 2: Examples of protein–protein interaction modulators in clinical trials or in clinical use.

Mycoplasma pneumoniae [47]. Furthermore, partial PINs for *Bacillus subtilis* [48] and *Streptococcus pneumoniae* [49] have been reported recently, and many more are near completion [50].

These hundreds of thousands of known interactions, and those which are yet to be discovered, have been and will be essential for identifying potential points of intervention in clinically relevant pathogens that can serve as drug targets for antibacterial

therapy. There are several reasons that support this argument: they are essential for not only the growth but the reproduction of the cells, they are conserved across many strains of pathogens and, most importantly, they are specific to the prokaryotic kingdom, meaning that either these interactions are non-existent or substantially different from their corresponding processes in eukaryotic cells [51].

Four examples of protein–protein interaction systems in bacteria for which inhibitors have been discovered and that could represent an alternative lead-discovery strategy to obtain new antimicrobial molecules are presented below.

β-Sliding clamp

Sliding clamps are prokaryotic ring-shaped proteins that secure DNA polymerases to the DNA template and slide along the double helix, enabling enzyme activity at a specific region of the DNA and increasing the rapid and processive DNA synthesis [52-54]. The β-clamp interacts with many different proteins such as several polymerases (e.g. I, II, III, IV, V and DnaE) and other proteins involved in DNA replication including DNA ligase and the replication regulatory protein Hda, all of which contain the conserved binding pentapeptide motif QL(S/D)LF (**8**, Figure 3) [55,56].

There are several reasons that make the bacterial clamp a promising and attractive target for the development of new antibiotics: it is essential for DNA replication and repair, it is highly conserved across the different bacterial pathogens and, most importantly from a drug discovery perspective, its structure differs significantly from the eukaryotic equivalent clamp (PCNA, proliferating cell nuclear activity) [51,57].

O'Donnell et al. first identified the structure of an inhibitor of the *E. coli* sliding clamp (ECSC) [58]. In the search for a molecule that binds to the peptide-binding pocket of the β-clamp, they carried out a fluorescence anisotropy titration screening of the Rockefeller University chemical library containing 30,600 polar organic compounds which led to the discovery of RU7 (**9**, Figure 3) with an inhibition constant of 10 μM. Pleasingly, it was also found that RU7 selectively disrupts the *E. coli* β-clamp without affecting its eukaryotic counterpart in *Saccharomyces cerevisiae*. In this same study, the co-crystal structure of RU7 with the sliding clamp revealed that the inhibitor occupies the deepest subsite (i.e., 1) of the two subsites that form the binding pocket (Figure 4) [58,59].

Utilizing a virtual screening of two different databases (i.e., the National Cancer Institute [60] and an in-house collection of 32,000 compounds), Wijfells et al. were able to identify a small-molecule mimic of the *des*-amino-Leu-Phe (dLF) component of the ECSC **10** (Figure 3), which displayed an IC_{50} in the low micromolar range (IC_{50} = 40 μM). X-ray crystallography studies revealed that this biphenyl oxime derivative **10** also occupies subsite I of the β-clamp [61].

In 2014, the Zenobia's First Pass Screen fragment library containing more than 350 fragments was screened by X-ray crystallography leading to the identification of four fragment hits. In an attempt to improve their binding affinities, another library was searched for compounds displaying similarity to these initial hits. After a docking-based screening followed by a fluorescence polarization (FP) assay of the selected candidates, the substituted tetrahydrocarbazole **11** (Figure 3) was found to not only completely occupy *E. coli* SC subsite I with the highest affinity (IC_{50} = 115 μM) and to inhibit in vitro DNA replication, but also to have antibacterial activity against several Gram-positive and Gram-negative pathogens, namely *Bacillus subtilis*, *Staphylococcus aureus, Escherichia coli and Acinetobacter baylyi* with MICs ranging from 39 to 78 μM [62]. A year later, further SAR investigations from the same research group led to the identification of another tetrahydrocarbazole derivative **12** (Figure 3) which displayed a >4-fold increase in its affinity for *E. coli* SC [63].

Recent evidence suggests that non-steroidal anti-inflammatory drugs (NSAIDs) have antimicrobial activity. Oakley et al. studied the *E. coli* β-clamp binding affinity of commercially available NSAIDs with the help of a FP competition assay. Of the twenty compounds evaluated, five showed K_i values in the high micromolar range, but only vedaprofen, bromfenac and carprofen (**13**–**15**, Figure 3) displayed the strongest effects (K_i < 300 μM) [64]. Similarly to the preliminary study by Yin et al. [62] the antibacterial activity of the selected NSAIDs was determined on four clinically relevant species, two Gram-negative bacteria (*E. coli* and *A. baylyi*) and two Gram-positive (*S. aureus* and *B. subtilis*). In opposition to Yin's studies, the latter species showed higher susceptibility than the Gram-negative bacteria with minimal inhibitory concentrations as low as 44 μg/mL in the case of vedaprofen (**13**). Again, and in agreement with previous studies, the compounds that most potently inhibited *E. coli* β-clamp binding also showed the highest level of antibacterial activity, supporting the correlation between inhibition of the sliding clamp and the antibacterial effects.

In addition to small molecules, peptides have also been investigated as disruptors of protein–protein interactions in the sliding clamp.

A structure-based approach, using the natural pentapeptide QL(S/D)LF (**8**, Figure 3) as a template, led to the identification of the short peptide P6 (**16**, Figure 5) with enhanced affinity for

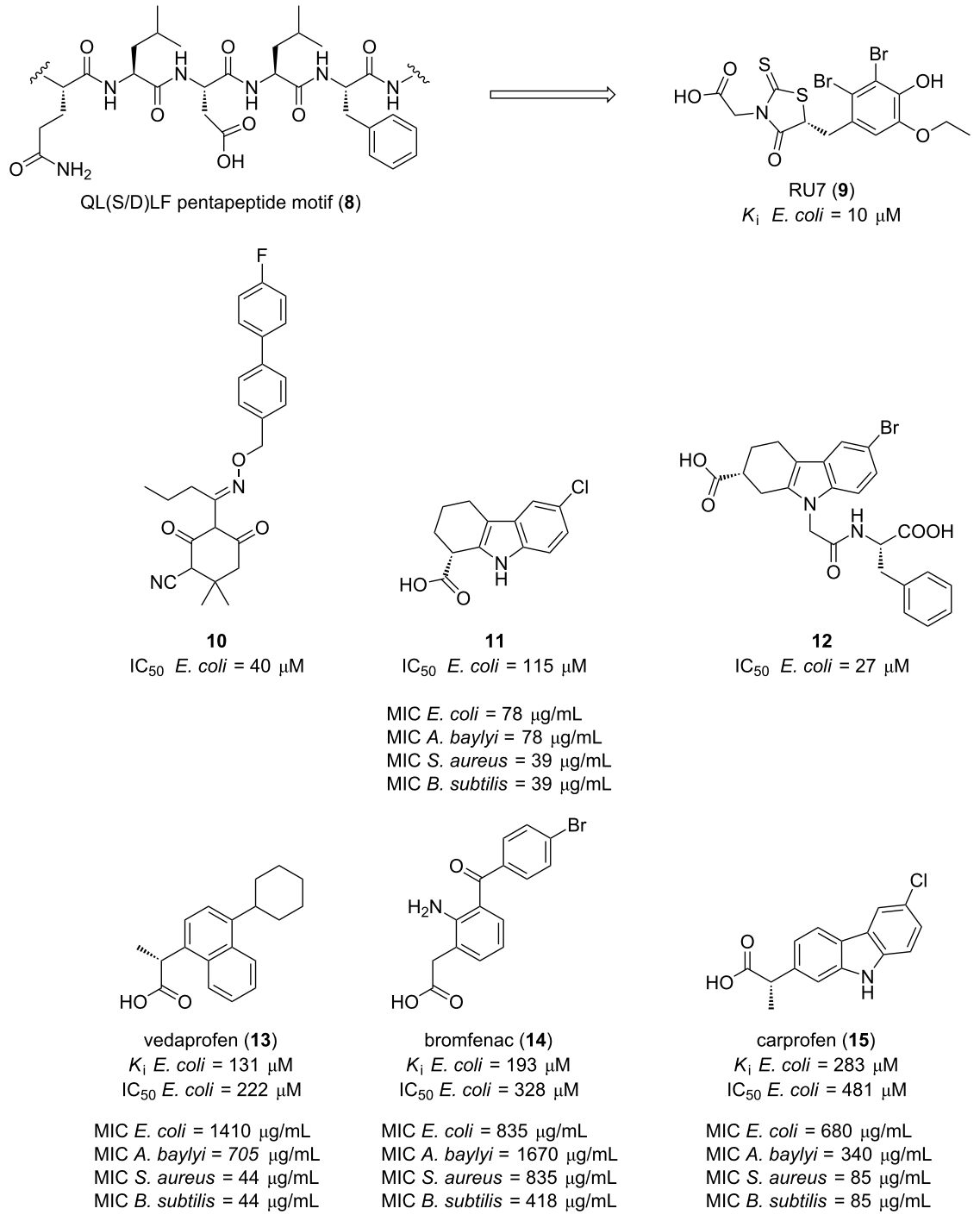

Figure 3: Small-molecule inhibitors of PPIs in the β-sliding clamp.

the β-clamp (IC_{50} = 1.12 μM, measured by surface plasmon resonance). This acetylated peptide was used as a lead and further modified at the second position, where the leucine residue was replaced by a cyclohexyl-L-alanyl group (Cha), and also on the terminal phenylalanine benzyl ring, in which two chlorine atoms where incorporated in the benzene ring to achieve P14 (**17**, Figure 5) with a 15-fold increase of its binding affinity for the sliding clamp and reaching the 10^{-8} M range (IC_{50} = 0.077 μM) [65].

Recently, Løbner-Olesen and co-workers screened a library of peptides for their ability to disrupt PPIs in the β-sliding clamp of *Staphylococcus aureus*. In this elegant study, from a library of 900,000 cyclic peptides, which was intracellularly generated

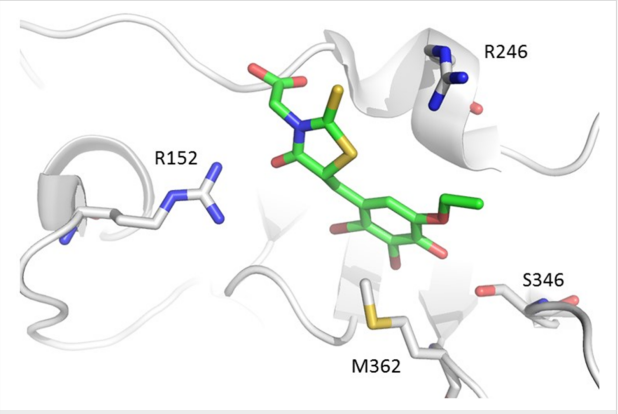

Figure 4: Crystal structure of the RU7 (**9**)-sliding clamp complex (PDB code 3D1G; adapted from Georgescu et al. [58]). Essential residues R152, M362, S346 and R246 are highlighted (sticks).

using the split-intein circular ligation of peptides and proteins (SICLOPPS) technology [66], three hits, peptides III-5, III-6 and III-7 (**18**–**20**, Figure 5), were identified to be able to disrupt the DnaN–DnaN (β-clamp–β-clamp) interaction. Interestingly, III-5 (**18**) and III-6 (**19**) were able to inhibit the growth of *Staphylococcus aureus* with MIC values of approximately 50 μg/mL while their linear counterparts displayed no activity [67].

Historically, natural products have been one of the most fruitful sources to obtain antibacterial lead compounds [5,68,69]. Griselimycin, a cyclic depsidecapeptide isolated from *Streptomyces* sp., was discovered fifty years ago, nonetheless, due to its poor pharmacokinetic properties and the availability of other drugs such as rifampicin, the optimization programme was abandoned [70]. Recently, the interest in neglected antibiotics with anti-tuberculosis potential resurged and led to further optimization and development studies around the griselimycin structure (**21**, Figure 5) [71]. Müller et al. discovered that griselimycin and its metabolically more stable analogues (methyl-griselimycin, MGM, **22** and cyclohexyl-griselimycin, CGM, **23**) were active against *M. tuberculosis* in the low micromolar range with MICs of 1, 0.6 and 0.06 μg/mL, respectively. To characterize the target protein of griselimycins, surface plasmon resonance (SPR) was used, analysis that demonstrated that they bound with high affinity to the sliding clamps of *M. tuberculosis* (K_d ranging from 1.0×10^{-10} M to 2.0×10^{-10} M). Encouragingly, no binding was detected between griselimycins and the human sliding clamp, and, hence, exhibiting an excellent selectivity profile. Crystal structures revealed that GM (**21**) and CGM (**23**) bind to a hydrophobic pocket between domains II and III, the protein–protein interaction site responsible for the recruitment of DNA enzymes by the sliding clamp, and therefore promisingly validating the sliding clamp as a feasible antibacterial target.

Single-stranded DNA-binding protein (SSB)

SSB is a class of proteins that coordinates fundamental cell processes including DNA replication, recombination and repair, and is, consequently, vital for cell survival. In addition, it also mediates the binding to more than fourteen genome maintenance proteins of the SSB interactome [72]. This latter activity enables SSB to act as a conserved hub of proteins which recruits their binding partners (e.g., exonuclease I, the DNA primase DnaG and the DNA helicase PriA) to their site of action [73].

Similarly to the aforementioned sliding clamp, the structural arrangement of most bacterial SSBs differs significantly to its homolog in eukaryotic cells (replication protein A, RPA) [74]. This dissimilarity could be beneficial from a drug discovery perspective because it would enable selective targeting of the bacterial interactome without impacting the eukaryotic cell processes.

Keck and co-workers identified four small molecules that disrupt the *Escherichia coli* SSB interaction with one of its well-studied binding partners, exonuclease I (ExoI) [75]. The screening by means of a high-throughput fluorescence polarization assay of 50,400 compounds from the Chemical Diversity, Maybridge and Chembridge chemical libraries, and subsequent dose-dependent evaluation of the disruption of the SSB/ExoI complex, led to the discovery of four inhibitors, CFAM, BCBP, BOTP and MPTA (**24**–**27**, Figure 6), with IC_{50} values ranging from 8–80 μM. Afterwards, the scientists were able to successfully obtain the crystal structures of the complexes of ExoI with both CFAM (**24**) and BCBP (**25**). From the crystallography studies it was revealed that, even though both compounds bind to the B site of ExoI, only CFAM (**24**) is able to interact with the crucial residues in the basic ridge which are known to be essential for the in vitro complex formation of ExoI with SSB [73], a finding that supports the low IC_{50} value exhibited by this molecule. Remarkably, these four compounds were also able to disrupt the complex formation of SSB with some other binding partners such as the DNA helicases RecQ and PriA but, unfortunately, less potently.

In an attempt to prove the hypothesis that direct targeting of PPIs, particularly SSB, could be an effective strategy for the development of novel broad-spectrum antibacterial agents, the colony formation evaluation of three of the previously mentioned hits (namely **24**, **25** and **27**) was assessed against a panel of bacterial strains that included Gram-positive microorganisms *Listeria monocytogenes*, *Staphylococcus aureus*, *Mycobacterium smegmatis*, *Mycobacterium tuberculosis*, *Mycobacterium avium paratuberculosis* and *Mycobacterium bovis*, and Gram-negative pathogens *Escherichia coli* (wt and

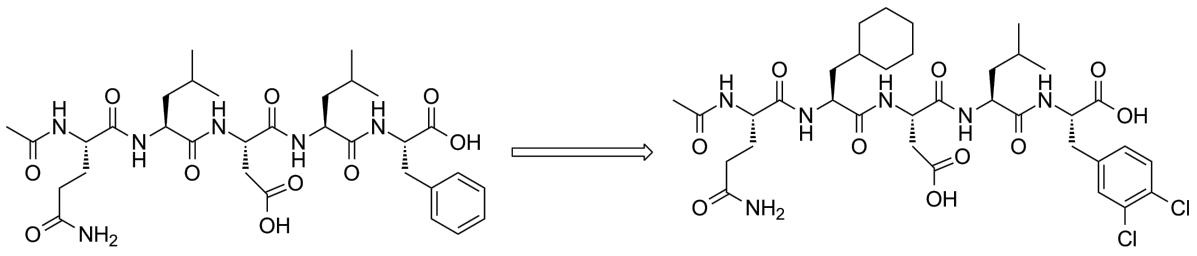

AcQLDLF P6 (**16**)
IC_{50} *E. coli* = 1.12 μM

AcQ1ChaD3L4diClF P14 (**17**)
IC_{50} *E. coli* = 0.077 μM

peptide	III-5 (**18**)	III-6 (**19**)	III-7 (**20**)
linear peptide sequence	VFLCGC	SQGLFK	GHVWVD
MIC (*S. epidermidis*)	683 mM	1228 mM	673 mM
peptide synthesized as	**CR**VFLCGC	**CR**SQGLFK	**CR**GHVWVD
MIC (*S. aureus*)	50 μM	50 μM	20 μM

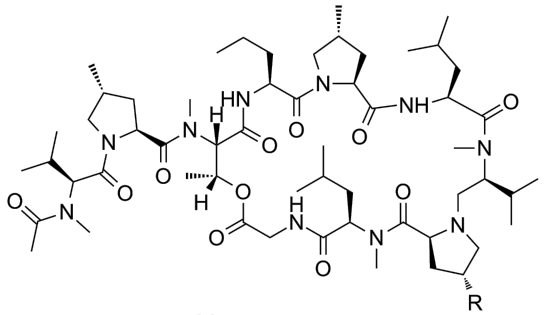

R = H, griselimycin (GM) (**21**)
K_d *M. tuberculosis* = 1 × 10^{-10} M - MIC *M. tuberculosis* = 1 μg/mL

R = Me, methyl-griselimycin (MGM) (**22**)
K_d *M. tuberculosis* = 1.1 × 10^{-10} M - MIC *M. tuberculosis* = 0.6 μg/mL

R = cyclohexyl, cyclohexyl-griselimycin (CGM) (**23**)
K_d *M. tuberculosis* = 2 × 10^{-10} M - MIC *M. tuberculosis* = 0.06 μg/mL

Figure 5: Peptidic inhibitors of PPIs in the sliding clamp.

imp4213), *Bacillus subtilis*, *Neisseria gonorrhoeae*, *Neisseria meningitidis* and *Neisseria lactamica* [76]. As a result, the compounds were able to successfully inhibit the growth of some of the bacteria tested. The authors also determined the growth suppressive effects on model Gram-positive (*B. subtilis*) and Gram-negative (*E. coli* imp4213) bacteria. The MIC values against *B. subtilis* were found to be 40, 11, 16 μM for CFAM, BCBP and MPTA, respectively, while the MIC values against the membrane-compromised *E. coli* were found to be 36, 62 and 10 μM, respectively.

High-throughput screening initiatives have gained popularity in the past two decades and have become the prevailing approach to identify leads in medicinal chemistry research [77,78]. However, due to the intrinsic features of PPIs, these are not amenable to the HTS approaches used to identify small molecules which will typically target enzymes (e.g., kinases and proteases) or extracellular receptors [79].

Recently, a HTS strategy to identify inhibitors of the *Klebsiella pneumonia* SSB PPI was reported. Starting from a library of

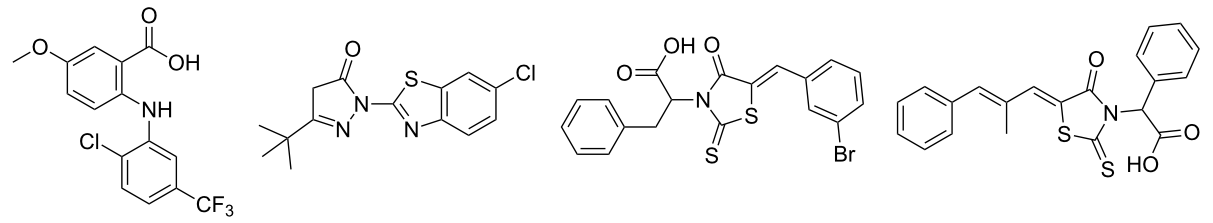

Figure 6: SSB protein–protein interaction inhibitors identified by HTS.

more than 72,000 compounds from Life Chemicals Inc. (Munich, Germany), nine selective inhibitors of the SSB/PriA interaction with IC_{50} values of <40 μM were identified by orthogonal fluorescence polarization assays. Of these nine initial hits, two were observed to interact with PriA by thermal stabilisation in a differential scanning fluorimetry (DSF) assay [80]. Regrettably, no data was presented on the chemical structures of these compounds or the antibacterial activity. Nevertheless, this study reinforces the usefulness of integrating biophysical techniques with HTS approaches in order to detect and investigate SSB protein–protein interactions in bacterial systems.

In the same year, Oakley et al. implemented a fragment-based drug discovery (FBDD) approach in order to identify disruptors to the interaction of SSB with another of its partners, the DNA primase DnaG [81]. In this study, a SPR competition assay and a saturation-transfer difference NMR (STD-NMR) led to the identification of thirty fragments. Subsequent 2D-^{15}N–^{1}H HSQC NMR returned four fragment hits **28**–**31** (Figure 7), with binding affinities, determined by NMR titration, in the low millimolar range.

Of all of the fragments, tetrazole **31** was chosen for further optimization due to its physicochemical properties and its potential for fragment growth. After virtual screening and binding studies by STD-NMR studies, the authors were able to find tetrazole **32** (Figure 7) which had a three-fold improved affinity (K_d = 1.3 mM) compared to the initial hit **31**. Later, the ZINC

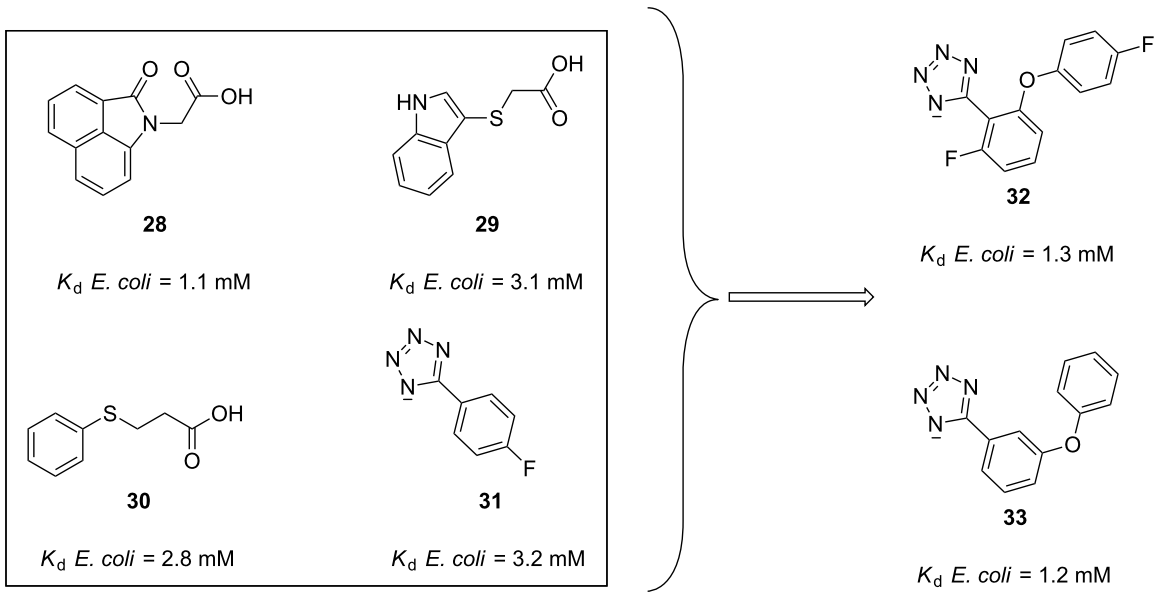

Figure 7: SSB protein–protein interaction inhibitors identified by FBDD.

database [82] was searched for structurally similar compounds leading to the identification of the *meta*-substituted tetrazole **33** (Figure 7), which was found to have a similar dissociation constant. Moreover, in order to predict the orientation of the fragments in the binding site, molecular docking of **33** to DnaG was predicted.

Finally, the fragments were also assessed against other SSB partner proteins by means of STD-NMR. Although the affinity values were not determined, all of them were satisfactorily found to bind to *E. coli* PriA, *E. coli* RNAse HI and the χ subunit of *E. coli* and *A. Baumannii* DNA polymerase III, and thus represent promising leads in the search for PPI inhibitors in bacteria.

Filamenting temperature-sensitive protein Z (FtsZ)

FtsZ is a prokaryotic tubulin-like protein which plays a crucial role in cell division in both Gram-positive and Gram-negative bacteria [83]. This protein polymerizes into a ring structure (the Z-ring) early at the division site and operates as a focal point for the assembly of the other division proteins [84].

There are several advantages of cell-division proteins as an antibacterial target: first, their intrinsic characteristics and essentiality for the multiplication and viability of bacteria, and second, they are highly conserved in many bacterial species [85].

Various studies have shown that Z interaction protein A (ZipA) is one of the essential components that stabilize the Z-ring formation and that it binds to FtsZ with high affinity. The interaction between FtsZ and ZipA is essential for cell division in *E. coli* and other Gram-negative bacteria, and therefore, it has been suggested that disruption of the ZipA/FtsZ interaction can be exploited to develop potential antibacterial molecules [83,86].

The development of a small-molecule antibiotic that targeted the ZipA/FtsZ protein–protein interaction was first investigated by scientists at Wyeth Research. In this study, a fluorescence polarization-based high-throughput screening of 250,000 corporate compounds led to the identification of pyridylpyrimidine **34** (Figure 8), which was shown to be the most potent with a K_i of 12 μM as measured by a FP competition assay [87]. Kenny et

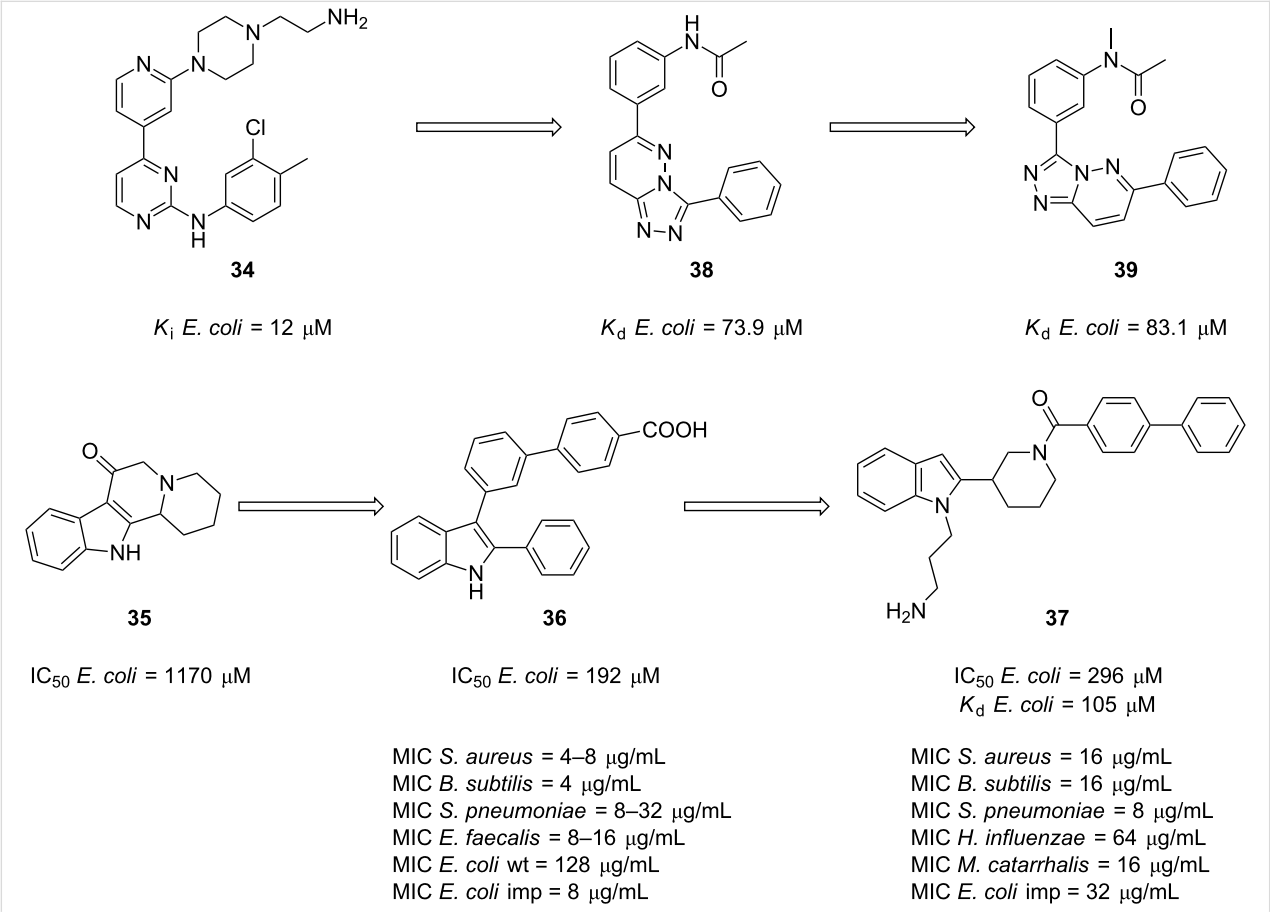

Figure 8: Examples of molecules that disrupt the ZipA/FtsZ interaction.

al. succeeded in obtaining a crystal structure of **34** bound to ZipA which provided detailed knowledge of the basis of the binding mode. Interestingly, it was found that, although **34** occupies only half of the ZipA/FtsZ binding pocket, the phenyl, the pyridine and the pyrimidine rings make critical hydrophobic interactions with residues in the shallow groove of the pocket [87].

Nearly simultaneously, the same group reported the SAR studies of a family of biphenylindole derivatives as inhibitors of the same PPI. A structure-based design built on the indoloquinolizinone **35** (Figure 8), afforded the chimeric molecule indole **36** (Figure 8) as an inhibitor of the ZipA/FtsZ interaction with an improved, but still modest, IC_{50} of 192 μM. The antibacterial activity of all the target compounds was also evaluated against a panel of microorganisms which included Gram-positive pathogens *Staphylococcus aureus*, *Streptococcus pneumoniae*, *Bacillus subtilis*, *Enterococcus faecalis* and the Gram-negative bacterium *Escherichia coli* (wt and an outer membrane permeable strain). Gratifyingly, the antibacterial screening showed that improved IC_{50} values correlated with improved minimal inhibitory concentrations and that Gram-positive microorganisms are more susceptible, likely due to the inability of molecules to permeate the outer membrane of Gram-negative pathogens [88].

In a follow-up study, a combinatorial synthesis approach was utilized to generate a library of small molecules whose inhibition properties were measured by a fluorescence polarization competition assay [89]. Derivatization of the indole nitrogen atom of lead compound **36** (Figure 8) returned the interesting indole analogue **37** (Figure 8). The authors then confirmed that the compounds were binding to the *E. coli* Zip A in the FtsZ binding site by means of 2D-HSQC NMR experiments and later submitted the selected compounds to cell division inhibition assays and MIC determination against a broad panel of bacterial strains which included *S. aureus*, *B. subtilis*, *S. pneumoniae*, *H. influenzae*, *M. catarrhalis*, and *E. coli* (imp). Unfortunately, the most active compound, indole **37**, exhibited an IC_{50} = 296 μM and a dissociation constant of 105 μM which undoubtedly make it a too weak inhibitor. Excitingly, the results are consistent with the inhibition of the ZipA/FtsZ interaction measured by FP and therefore indole **37** exhibited the best profile of in vitro cell growth inhibition with MICs ranging from 8–64 μg/mL.

Computational studies were also undertaken in an attempt to identify new inhibitors of the interaction between ZipA and FtsZ [90]. Utilizing the structure of the pyridylpyrimidine **34** (Figure 8) as a template, Rush et al. applied a shape-comparison program (rapid overlay of chemical structures, ROCS). This study led to the identification of three lead-like scaffolds among which compound **38** (Figure 8) was the most active with a K_d of 73.9 μM. In spite of the fact that this molecule was less active than the original lead, the authors argued that it had less development issues. Finally, in order to confirm the binding mode of these new structures, the crystal structure of **39** (K_d = 83.1 μM) in complex with ZipA was solved. Excitingly, the X-ray analysis revealed that ROCS very accurately predicted the binding mode and therefore validated its use as an alternative approach to identify new promising leads as inhibitors of this protein–protein interaction.

Despite the reported advances, these compounds were not found to be therapeutically relevant inhibitors of the ZipA/FtsZ protein–protein interaction, nonetheless considering the challenges involved in targeting PPIs, it is significant that the authors demonstrated by NMR that compounds from this library bind to ZipA at the FtsZ binding site and that small molecule disruptors of the ZipA/FtsZ interaction could inhibit cell division in both Gram-positive and Gram-negative microorganisms, findings that could be of value in the development of optimized antagonists for potential use as antibacterials.

N-Utilization substances (Nus) B and E

Another point of therapeutic intervention to develop new anti-infectives that target cell viability is bacterial transcription, a process that is executed by the enzyme RNA polymerase (RNAP) and regulated by several transcription factors.

Similarly to the previously described targets, bacterial transcription represents a promising antibacterial drug target for several reasons: it is essential to cell viability, RNAP and its transcription factors are considerably conserved across many important bacterial strains and both of them differ from their eukaryotic homologs [91,92].

The transcription factors NusB and NusE and their interaction is vital for the efficient transcription in all bacteria [93] and have recently attracted interest as a potential target for a new antibiotic class.

In 2017, McCluskey and co-workers carried out the virtual screening of 56,000 compounds from the mini-Maybridge library which led to the identification of five synthetically accessible hits [94]. In order to validate these in silico screened hits, their ability to inhibit the *Bacillus subtilis* NusB/NusE PPI was examined. Gratifyingly, compounds **40** and **41** (Figure 9) exhibited an inhibition of the NusB/NusE interaction at 25 μM higher than 50% and IC_{50} values in the low micromolar range (6.1 and 19.8 μM, respectively). A subsequent antibacterial screening showed that the lead pyrimidine **40** was also a moder-

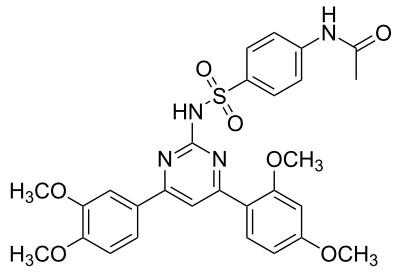

40

IC_{50} *B. subtilis* = 6.1 μM

growth inhibition (200 μM)
B. subtilis = 9%
E. coli = 21%

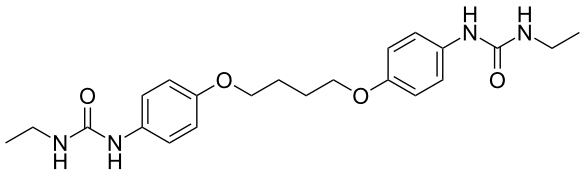

41

IC_{50} *B. subtilis* = 19.8 μM

growth inhibition (200 μM)
B. subtilis = inactive
E. coli = 17%

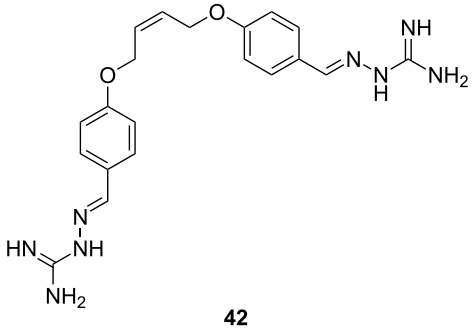

42

NusB/NusE PPI inhibition = 55% (25 μM)

MIC *S. aureus USA300* (methicillin resistant) <3 μg/mL
MIC *S. pneumoniae* <3 μg/mL
MIC *P. aeruginosa* <51 μg/mL
MIC *A. baumannii ATCC19606* <51 μg/mL

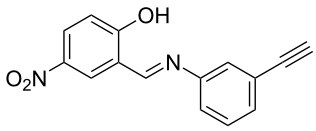

MC4 (**43**)

IC_{50} *B. subtilis* = 34.7 μM

MIC *S. aureus USA300* (methicillin resistant) = 64 μg/mL
MIC *S. aureus 25923* = 8 μg/mL
MIC *S. aureus ST239* (methicillin resistant) = 16 μg/mL

Figure 9: Inhibitors of the NusB/NusE interaction.

ate inhibitor of the growth of the Gram-positive pathogen *B. subtilis* and the Gram-negative microorganism *E. coli*.

The same research group developed further SAR studies using compound **41** (Figure 9) as lead of interest [95]. To this end, four focused compound libraries based on this bis-ether were developed leading to the identification of the rigidified *cis*-butene aminoguanidine analogue **42** (Figure 9) as both a good inhibitor of the NusB/NusE PPI (>50% at 25 μM) and a potent antibacterial against not only Gram-positive pathogens such as methicillin-resistant *S. aureus* and *S. pneumoniae* but also Gram-negative bacteria strains such as *P. aeruginosa* and *A. baumannii* (MIC ≤ 3 μg/mL and ≤51 μg/mL, respectively) [95]. In spite of the efficiency of the bis-aminoguanidine derivative **42**, unfortunately, its toxicity was an issue. Nonetheless, this study represents a step forward towards the potential development of next-generation anti-transcription antibiotics and validates the correlation between the NusB/NusE PPI and the in vitro antibiotic effect.

The first specific inhibitor against *S. aureus*, including MRSA, was reported very recently by Ma et al. [96]. After an in silico screening of a combination of the previously mentioned mini-Maybridge library and the Enamine antibacterial library, seven hits were identified. Among all of them, the nitrophenol derivative MC4 (**43**, Figure 9) was able to inhibit NusB/NusE binding with an IC_{50} of 34.7 μM. Its antimicrobial properties were also evaluated against a panel of clinically relevant microorganisms such as *Enterococcus faecalis*, *Klebsiella pneumonia*, *Acinetobacter baumannii*, *Pseudomonas aeruginosa*, *Enterobacter cloacae*, *Escherichia coli*, *Proteus vulgaris* and *Staphylococcus aureus*. However, in spite of the fact that NusB and NusE are highly conserved in bacteria, the compound exhibited preferred antibacterial activity against *S. aureus* strains (including

MRSA) with minimum inhibitory values as low as 8 μg/mL. Pleasingly, unlike the aminoguanidine **42**, compound **43** did not display toxicity to mammalian cells.

Even though the NusB/NusE interaction is still in its infancy, and further investigations are needed to both elucidate off-target effects and apparent preferential inhibitory activity against Gram-positive pathogens, the identification of promising small molecules against these PPI (or other interactions involved in bacterial transcription yet to be discovered and validated) may have something to offer in the ongoing research towards the development of new anti-infectives with novel mechanisms of action.

Conclusion

Pathogenic bacteria are a leading cause of human mortality, particularly in Third World countries. Due to the fact that new resistant microorganisms continue to emerge, combating these infections has become a global challenge for which the discovery and development of new antibacterial drugs is of critical importance.

Although progress has been made in order to address and overcome drug resistance, there is an urgent need to develop new antibacterial drug leads that operate through a novel mechanism of action.

On the other hand, the past two decades have observed the emergence of protein–protein interactions as a drug design target. During this time, many important studies have been conducted towards the identification and characterization of protein–protein interactions which have successfully resulted in several modulators reaching the clinical stage (Figure 1). These achievements would not have been possible without the utilization of appropriate design and screening approaches to determine the interactions at a molecular level and hence the development of PPIs as tractable targets.

To this end, interrogating interaction systems in prokaryotic cells that are critical for bacterial survival have recently become an attractive target which may offer therapeutically promising perspectives for infectious diseases.

In this review, the most significant compounds which have been found to disrupt protein–protein interactions in bacteria have been highlighted. These chemical scaffolds target different bacterial processes such as replication (SSB and sliding clamp), division (FtsZ) and transcription (NusB/NusE interaction). It is hoped that the knowledge acquired in both discovering and developing these inhibitors will lay the foundation for future antibacterial drug development pipelines. Given that the protein interactions systems described are conserved in prokaryotes but not present in eukaryotes, it may be feasible to develop inhibitors that selectively target the microorganism systems, and therefore avoiding mechanism-related side effects. However, these large sets of interactions remain poorly characterized and targeting them is a challenge.

Thus far, extensive in silico and high throughput screening campaigns of libraries of compounds, combinatorial synthesis and structure-based design approaches, biophysical screening techniques (i.e., fluorescence polarization, surface plasmon resonance and differential scanning fluorimetry) in combination with structural elucidation by combination of NMR and X-ray crystallography have played a pivotal role in identifying and deciphering the crucial target–inhibitor interactions with the aim of treating disease.

Although this review covers the description of PPI in bacteria, there are other strategies that are being explored towards the discovery of new antibiotics with novel mechanisms of action such as for example inhibitors of host–pathogen interactions and of the type 3 secretion system (T3SS) in Gram-negative bacteria, nonetheless, the specific targets remain unknown or ambiguous [97,98].

The challenge for new drug discovery efforts in the field of PPIs, which is still in the early stage, is to learn their real potential in combating infectious diseases. It is expected that enhanced understanding of the biology of bacteria and the nature of the PPI interfaces, in combination with medicinal chemistry efforts, may result in an opportunity to obtain antibacterial molecules whose mechanisms do not overlap with those of existing anti-infective drugs and consequently reduce the burden of multidrug-resistant pathogens.

Acknowledgements

The author gratefully acknowledges the helpful comments and suggestions provided by Professor A. Ganesan and Dr. Amalia Ruiz Estrada.

ORCID® iDs

Laura Carro - https://orcid.org/0000-0002-2093-2222

References

1. The top 10 causes of death. http://www.who.int/news-room/fact-sheets/detail/the-top-10-causes-of-death (accessed June 22, 2018).
2. Davies, J. *Can. J. Infect. Dis. Med. Microbiol.* **2006,** *17,* 287–290. doi:10.1155/2006/707296
3. Bartlett, J. G.; Gilbert, D. N.; Spellberg, B. *Clin. Infect. Dis.* **2013,** *56,* 1445–1450. doi:10.1093/cid/cit070
4. Ventola, C. L. *P T* **2015,** *40,* 277–283.

5. O'Connell, K. M. G.; Hodgkinson, J. T.; Sore, H. F.; Welch, M.; Salmond, G. P. C.; Spring, D. R. *Angew. Chem., Int. Ed.* **2013,** *52,* 10706–10733. doi:10.1002/anie.201209979
6. Fair, R. J.; Tor, Y. *Perspect. Med. Chem.* **2014,** *6,* 25–64. doi:10.4137/pmc.s14459
7. Simpkin, V. L.; Renwick, M. J.; Kelly, R.; Mossialos, E. *J. Antibiot.* **2017,** *70,* 1087–1096. doi:10.1038/ja.2017.124
8. Global priority list of antibiotic-resistant bacteria to guide research, discovery, and development of new antibiotics. http://www.who.int/medicines/publications/WHO-PPL-Short_Summary_25Feb-ET_NM_WHO.pdf?ua=1 (accessed June 22, 2018).
9. Brown, E. D.; Wright, G. D. *Nature* **2016,** *529,* 336–343. doi:10.1038/nature17042
10. Hurley, K. A.; Santos, T. M. A.; Nepomuceno, G. M.; Huynh, V.; Shaw, J. T.; Weibel, D. B. *J. Med. Chem.* **2016,** *59,* 6975–6998. doi:10.1021/acs.jmedchem.5b01098
11. Cossar, P. J.; Lewis, P. J.; McCluskey, A. *Med. Res. Rev.* **2018,** 1–26. doi:10.1002/med.21519
12. Modell, A. E.; Blosser, S. L.; Arora, P. S. *Trends Pharmacol. Sci.* **2016,** *37,* 702–713. doi:10.1016/j.tips.2016.05.008
13. Zinzalla, G.; Thurston, D. E. *Future Med. Chem.* **2009,** *1,* 65–93. doi:10.4155/fmc.09.12
14. Petta, I.; Lievens, S.; Libert, C.; Tavernier, J.; De Bosscher, K. *Mol. Ther.* **2016,** *24,* 707–718. doi:10.1038/mt.2015.214
15. Arkin, M. R.; Tang, Y.; Wells, J. A. *Chem. Biol.* **2014,** *21,* 1102–1114. doi:10.1016/j.chembiol.2014.09.001
16. Wells, J. A.; McClendon, C. L. *Nature* **2007,** *450,* 1001–1009. doi:10.1038/nature06526
17. Clackson, T.; Wells, J. A. *Science* **1995,** *267,* 383–386. doi:10.1126/science.7529940
18. London, N.; Raveh, B.; Schueler-Furman, O. *Curr. Opin. Chem. Biol.* **2013,** *17,* 952–959. doi:10.1016/j.cbpa.2013.10.011
19. Scott, D. E.; Bayly, A. R.; Abell, C.; Skidmore, J. *Nat. Rev. Drug Discovery* **2016,** *15,* 533–550. doi:10.1038/nrd.2016.29
20. Makley, L. N.; Gestwicki, J. E. *Chem. Biol. Drug Des.* **2013,** *81,* 22–32. doi:10.1111/cbdd.12066
21. Thompson, A. D.; Dugan, A.; Gestwicki, J. E.; Mapp, A. K. *ACS Chem. Biol.* **2012,** *7,* 1311–1320. doi:10.1021/cb300255p
22. Arkin, M. R.; Wells, J. A. *Nat. Rev. Drug Discovery* **2004,** *3,* 301–317. doi:10.1038/nrd1343
23. Thiel, P.; Kaiser, M.; Ottmann, C. *Angew. Chem., Int. Ed.* **2012,** *51,* 2012–2018. doi:10.1002/anie.201107616
24. Andrei, S. A.; Sijbesma, E.; Hann, M.; Davis, J.; O'Mahony, G.; Perry, M. W. D.; Karawajczyk, A.; Eickhoff, J.; Brunsveld, L.; Doveston, R. G.; Milroy, L.-G.; Ottmann, C. *Expert Opin. Drug Discovery* **2017,** *12,* 925–940. doi:10.1080/17460441.2017.1346608
25. Sheng, C.; Dong, G.; Miao, Z.; Zhang, W.; Wang, W. *Chem. Soc. Rev.* **2015,** *44,* 8238–8259. doi:10.1039/c5cs00252d
26. Higueruelo, A. P.; Jubb, H.; Blundell, T. L. *Curr. Opin. Pharmacol.* **2013,** *13,* 791–796. doi:10.1016/j.coph.2013.05.009
27. Tse, C.; Shoemaker, A. R.; Adickes, J.; Anderson, M. G.; Chen, J.; Jin, S.; Johnson, E. F.; Marsh, K. C.; Mitten, M. J.; Nimmer, P.; Roberts, L.; Tahir, S. K.; Xiao, Y.; Yang, X.; Zhang, H.; Fesik, S.; Rosenberg, S. H.; Elmore, S. W. *Cancer Res.* **2008,** *68,* 3421–3428. doi:10.1158/0008-5472.can-07-5836
28. Ding, Q.; Zhang, Z.; Liu, J.-J.; Jiang, N.; Zhang, J.; Ross, T. M.; Chu, X.-J.; Bartkovitz, D.; Podlaski, F.; Janson, C.; Tovar, C.; Filipovic, Z. M.; Higgins, B.; Glenn, K.; Packman, K.; Vassilev, L. T.; Graves, B. *J. Med. Chem.* **2013,** *56,* 5979–5983. doi:10.1021/jm400487c
29. Ma, W. W.; Zhang, H.; Hylander, B.; LeVea, C.; Repasky, E.; Weng, D.; Burns, J.; Chunduru, S.; Graham, M.; Fetterly, G.; McKinlay, M.; Adjei, A. *Cancer Res.* **2012,** *72* (Suppl. 8), 1939. doi:10.1158/1538-7445.am2012-1939
30. Mirguet, O.; Gosmini, R.; Toum, J.; Clément, C. A.; Barnathan, M.; Brusq, J.-M.; Mordaunt, J. E.; Grimes, R. M.; Crowe, M.; Pineau, O.; Ajakane, M.; Daugan, A.; Jeffrey, P.; Cutler, L.; Haynes, A. C.; Smithers, N. N.; Chung, C.-w.; Bamborough, P.; Uings, I. J.; Lewis, A.; Witherington, J.; Parr, N.; Prinjha, R. K.; Nicodème, E. *J. Med. Chem.* **2013,** *56,* 7501–7515. doi:10.1021/jm401088k
31. Gadek, T. R.; Burdick, D. J.; McDowell, R. S.; Stanley, M. S.; Marsters, J. C., Jr.; Paris, K. J.; Oare, D. A.; Reynolds, M. E.; Ladner, C.; Zioncheck, K. A.; Lee, W. P.; Gribling, P.; Dennis, M. S.; Skelton, N. J.; Tumas, D. B.; Clark, K. R.; Keating, S. M.; Beresini, M. H.; Tilley, J. W.; Presta, L. G.; Bodary, S. C. *Science* **2002,** *295,* 1086–1089. doi:10.1126/science.295.5557.1086
32. Zhong, M.; Gadek, T. R.; Bui, M.; Shen, W.; Burnier, J.; Barr, K. J.; Hanan, E. J.; Oslob, J. D.; Yu, C. H.; Zhu, J.; Arkin, M. R.; Evanchik, M. J.; Flanagan, W. M.; Hoch, U.; Hyde, J.; Prabhu, S.; Silverman, J. A.; Wright, J. *ACS Med. Chem. Lett.* **2012,** *3,* 203–206. doi:10.1021/ml2002482
33. Hartman, G. D.; Egbertson, M. S.; Halczenko, W.; Laswell, W. L.; Duggan, M. E.; Smith, R. L.; Naylor, A. M.; Manno, P. D.; Lynch, R. J. *J. Med. Chem.* **1992,** *35,* 4640–4642. doi:10.1021/jm00102a020
34. Putyrski, M.; Schultz, C. *FEBS Lett.* **2012,** *586,* 2097–2105. doi:10.1016/j.febslet.2012.04.061
35. Bouveret, E.; Brun, C. *Methods Mol. Biol. (N. Y., NY, U. S.)* **2012,** *804,* 15–33. doi:10.1007/978-1-61779-361-5_2
36. Rajagopala, S. V.; Sikorski, P.; Kumar, A.; Mosca, R.; Vlasblom, J.; Arnold, R.; Franca-Koh, J.; Pakala, S. B.; Phanse, S.; Ceol, A.; Häuser, R.; Siszler, G.; Wuchty, S.; Emili, A.; Babu, M.; Aloy, P.; Pieper, R.; Uetz, P. *Nat. Biotechnol.* **2014,** *32,* 285–290. doi:10.1038/nbt.2831
37. Butland, G.; Peregrín-Alvarez, J. M.; Li, J.; Yang, W.; Yang, X.; Canadien, V.; Starostine, A.; Richards, D.; Beattie, B.; Krogan, N.; Davey, M.; Parkinson, J.; Greenblatt, J.; Emili, A. *Nature* **2005,** *433,* 531–537. doi:10.1038/nature03239
38. Hu, P.; Janga, S. C.; Babu, M.; Díaz-Mejía, J. J.; Butland, G.; Yang, W.; Pogoutse, O.; Guo, X.; Phanse, S.; Wong, P.; Chandran, S.; Christopoulos, C.; Nazarians-Armavil, A.; Nasseri, N. K.; Musso, G.; Ali, M.; Nazemof, N.; Eroukova, V.; Golshani, A.; Paccanaro, A.; Greenblatt, J. F.; Moreno-Hagelsieb, G.; Emili, A. *PLoS Biol.* **2009,** *7,* e1000096. doi:10.1371/journal.pbio.1000096
39. Arifuzzaman, M.; Maeda, M.; Itoh, A.; Nishikata, K.; Takita, C.; Saito, R.; Ara, T.; Nakahigashi, K.; Huang, H.-C.; Hirai, A.; Tsuzuki, K.; Nakamura, S.; Altaf-Ul-Amin, M.; Oshima, T.; Baba, T.; Yamamoto, N.; Kawamura, T.; Ioka-Nakamichi, T.; Kitagawa, M.; Tomita, M.; Kanaya, S.; Wada, C.; Mori, H. *Genome Res.* **2006,** *16,* 686–691. doi:10.1101/gr.4527806
40. Wang, Y.; Cui, T.; Zhang, C.; Yang, M.; Huang, Y.; Li, W.; Zhang, L.; Gao, C.; He, Y.; Li, Y.; Huang, F.; Zeng, J.; Huang, C.; Yang, Q.; Tian, Y.; Zhao, C.; Chen, H.; Zhang, H.; He, Z.-G. *J. Proteome Res.* **2010,** *9,* 6665–6677. doi:10.1021/pr100808n

41. Häuser, R.; Ceol, A.; Rajagopala, S. V.; Mosca, R.; Siszler, G.; Wermke, N.; Sikorski, P.; Schwarz, F.; Schick, M.; Wuchty, S.; Aloy, P.; Uetz, P. *Mol. Cell. Proteomics* **2014,** *13,* 1318–1329. doi:10.1074/mcp.o113.033571
42. Zhang, M.; Su, S.; Bhatnagar, R. K.; Hassett, D. J.; Lu, L. J. *PLoS One* **2012,** *7,* e41202. doi:10.1371/journal.pone.0041202
43. Parrish, J. R.; Yu, J.; Liu, G.; Hines, J. A.; Chan, J. E.; Mangiola, B. A.; Zhang, H.; Pacifico, S.; Fotouhi, F.; DiRita, V. J.; Ideker, T.; Andrews, P.; Finley, R. L., Jr. *Genome Biol.* **2007,** *8,* R130. doi:10.1186/gb-2007-8-7-r130
44. Titz, B.; Rajagopala, S. V.; Goll, J.; Häuser, R.; McKevitt, M. T.; Palzkill, T.; Uetz, P. *PLoS One* **2008,** *3,* e2292. doi:10.1371/journal.pone.0002292
45. Sato, S.; Shimoda, Y.; Muraki, A.; Kohara, M.; Nakamura, Y.; Tabata, S. *DNA Res.* **2007,** *14,* 207–216. doi:10.1093/dnares/dsm021
46. Shimoda, Y.; Shinpo, S.; Kohara, M.; Nakamura, Y.; Tabata, S.; Sato, S. *DNA Res.* **2008,** *15,* 13–23. doi:10.1093/dnares/dsm028
47. Kühner, S.; van Noort, V.; Betts, M. J.; Leo-Macias, A.; Batisse, C.; Rode, M.; Yamada, T.; Maier, T.; Bader, S.; Beltran-Alvarez, P.; Castaño-Diez, D.; Chen, W.-H.; Devos, D.; Güell, M.; Norambuena, T.; Racke, I.; Rybin, V.; Schmidt, A.; Yus, E.; Aebersold, R.; Herrmann, R.; Böttcher, B.; Frangakis, A. S.; Russell, R. B.; Serrano, L.; Bork, P.; Gavin, A.-C. *Science* **2009,** *326,* 1235–1240. doi:10.1126/science.1176343
48. Marchadier, E.; Carballido-López, R.; Brinster, S.; Fabret, C.; Mervelet, P.; Bessières, P.; Noirot-Gros, M.-F.; Fromion, V.; Noirot, P. *Proteomics* **2011,** *11,* 2981–2991. doi:10.1002/pmic.201000791
49. Wuchty, S.; Rajagopala, S. V.; Blazie, S. M.; Parrish, J. R.; Khuri, S.; Finley, R. L., Jr.; Uetz, P. *mSystems* **2017,** *2,* e00019–17. doi:10.1128/msystems.00019-17
50. Zoraghi, R.; Reiner, N. E. *Curr. Opin. Microbiol.* **2013,** *16,* 566–572. doi:10.1016/j.mib.2013.07.010
51. Robinson, A.; Causer, R. J.; Dixon, N. E. *Curr. Drug Targets* **2012,** *13,* 352–372. doi:10.2174/138945012799424598
52. Johnson, A.; O'Donnell, M. *Annu. Rev. Biochem.* **2005,** *74,* 283–315. doi:10.1146/annurev.biochem.73.011303.073859
53. Waga, S.; Stillman, B. *Annu. Rev. Biochem.* **1998,** *67,* 721–751. doi:10.1146/annurev.biochem.67.1.721
54. Indiani, C.; O'Donnell, M. *Nat. Rev. Mol. Cell Biol.* **2006,** *7,* 751–761. doi:10.1038/nrm2022
55. Dalrymple, B. P.; Kongsuwan, K.; Wijffels, G.; Dixon, N. E.; Jennings, P. A. *Proc. Natl. Acad. Sci. U. S. A.* **2001,** *98,* 11627–11632. doi:10.1073/pnas.191384398
56. Wijffels, G.; Dalrymple, B. P.; Prosselkov, P.; Kongsuwan, K.; Epa, V. C.; Lilley, P. E.; Jergic, S.; Buchardt, J.; Brown, S. E.; Alewood, P. F.; Jennings, P. A.; Dixon, N. E. *Biochemistry* **2004,** *43,* 5661–5671. doi:10.1021/bi036229j
57. Warbrick, E. *BioEssays* **2000,** *22,* 997–1006. doi:10.1002/1521-1878(200011)22:11<997::aid-bies6>3.0.co;2-#
58. Georgescu, R. E.; Yurieva, O.; Kim, S.-S.; Kuriyan, J.; Kong, X.-P.; O'Donnell, M. *Proc. Natl. Acad. Sci. U. S. A.* **2008,** *105,* 11116–11121. doi:10.1073/pnas.0804754105
59. Burnouf, D. Y.; Olieric, V.; Wagner, J.; Fujii, S.; Reinbolt, J.; Fuchs, R. P. P.; Dumas, P. *J. Mol. Biol.* **2004,** *335,* 1187–1197. doi:10.1016/j.jmb.2003.11.049
60. Ihlenfeldt, W.-D.; Voigt, J. H.; Bienfait, B.; Oellien, F.; Nicklaus, M. C. *J. Chem. Inf. Model.* **2002,** *42,* 46–57. doi:10.1021/ci010056s
61. Wijffels, G.; Johnson, W. M.; Oakley, A. J.; Turner, K.; Epa, V. C.; Briscoe, S. J.; Polley, M.; Liepa, A. J.; Hofmann, A.; Buchardt, J.; Christensen, C.; Prosselkov, P.; Dalrymple, B. P.; Alewood, P. F.; Jennings, P. A.; Dixon, N. E.; Winkler, D. A. *J. Med. Chem.* **2011,** *54,* 4831–4838. doi:10.1021/jm2004333
62. Yin, Z.; Whittell, L. R.; Wang, Y.; Jergic, S.; Liu, M.; Harry, E. J.; Dixon, N. E.; Beck, J. L.; Kelso, M. J.; Oakley, A. J. *J. Med. Chem.* **2014,** *57,* 2799–2806. doi:10.1021/jm500122r
63. Yin, Z.; Whittell, L. R.; Wang, Y.; Jergic, S.; Ma, C.; Lewis, P. J.; Dixon, N. E.; Beck, J. L.; Kelso, M. J.; Oakley, A. J. *J. Med. Chem.* **2015,** *58,* 4693–4702. doi:10.1021/acs.jmedchem.5b00232
64. Yin, Z.; Wang, Y.; Whittell, L. R.; Jergic, S.; Liu, M.; Harry, E.; Dixon, N. E.; Kelso, M. J.; Beck, J. L.; Oakley, A. J. *Chem. Biol.* **2014,** *21,* 481–487. doi:10.1016/j.chembiol.2014.02.009
65. Wolff, P.; Oliéric, V.; Briand, J. P.; Chaloin, O.; Dejaegere, A.; Dumas, P.; Ennifar, E.; Guichard, G.; Wagner, J.; Burnouf, D. Y. *J. Med. Chem.* **2011,** *54,* 4627–4637. doi:10.1021/jm200311m
66. Tavassoli, A. *Curr. Opin. Chem. Biol.* **2017,** *38,* 30–35. doi:10.1016/j.cbpa.2017.02.016
67. Kjelstrup, S.; Hansen, P. M. P.; Thomsen, L. E.; Hansen, P. R.; Løbner-Olesen, A. *PLoS One* **2013,** *8,* e72273. doi:10.1371/journal.pone.0072273
68. Clardy, J.; Fischbach, M. A.; Walsh, C. T. *Nat. Biotechnol.* **2006,** *24,* 1541–1550. doi:10.1038/nbt1266
69. Wright, G. D. *Nat. Prod. Rep.* **2017,** *34,* 694–701. doi:10.1039/c7np00019g
70. Dong, M.; Pfeiffer, B.; Altmann, K.-H. *Drug Discovery Today* **2017,** *22,* 585–591. doi:10.1016/j.drudis.2016.11.015
71. Kling, A.; Lukat, P.; Almeida, D. V.; Bauer, A.; Fontaine, E.; Sordello, S.; Zaburannyi, N.; Herrmann, J.; Wenzel, S. C.; König, C.; Ammerman, N. C.; Barrio, M. B.; Borchers, K.; Bordon-Pallier, F.; Brönstrup, M.; Courtemanche, G.; Gerlitz, M.; Geslin, M.; Hammann, P.; Heinz, D. W.; Hoffmann, H.; Klieber, S.; Kohlmann, M.; Kurz, M.; Lair, C.; Matter, H.; Nuermberger, E.; Tyagi, S.; Fraisse, L.; Grosset, J. H.; Lagrange, S.; Müller, R. *Science* **2015,** *348,* 1106–1112. doi:10.1126/science.aaa4690
72. Shereda, R. D.; Kozlov, A. G.; Lohman, T. M.; Cox, M. M.; Keck, J. L. *Crit. Rev. Biochem. Mol. Biol.* **2008,** *43,* 289–318. doi:10.1080/10409230802341296
73. Lu, D.; Keck, J. L. *Proc. Natl. Acad. Sci. U. S. A.* **2008,** *105,* 9169–9174. doi:10.1073/pnas.0800741105
74. Pokhrel, N.; Origanti, S.; Davenport, E. P.; Gandhi, D.; Kaniecki, K.; Mehl, R. A.; Greene, E. C.; Dockendorff, C.; Antony, E. *Nucleic Acids Res.* **2017,** *45,* 9413–9426. doi:10.1093/nar/gkx598
75. Lu, D.; Bernstein, D. A.; Satyshur, K. A.; Keck, J. L. *Proc. Natl. Acad. Sci. U. S. A.* **2010,** *107,* 633–638. doi:10.1073/pnas.0909191107
76. Marceau, A. H.; Bernstein, D. A.; Walsh, B. W.; Shapiro, W.; Simmons, L. A.; Keck, J. L. *PLoS One* **2013,** *8,* e58765. doi:10.1371/journal.pone.0058765
77. Broach, J. R.; Thorner, J. *Nature* **1996,** *384,* 14–16.
78. Hughes, J. P.; Rees, S.; Kalindjian, S. B.; Philpott, K. L. *Br. J. Pharmacol.* **2011,** *162,* 1239–1249. doi:10.1111/j.1476-5381.2010.01127.x
79. Heeres, J. T.; Hergenrother, P. J. *Chem. Soc. Rev.* **2011,** *40,* 4398–4410. doi:10.1039/b923660k
80. Voter, A. F.; Killoran, M. P.; Ananiev, G. E.; Wildman, S. A.; Hoffmann, F. M.; Keck, J. L. *SLAS Discovery* **2018,** *23,* 94–101. doi:10.1177/2472555217712001

81. Chilingaryan, Z.; Headey, S. J.; Lo, A. T. Y.; Xu, Z.-Q.; Otting, G.; Dixon, N. E.; Scanlon, M. J.; Oakley, A. J. *Antibiotics* **2018,** *7,* No. 14. doi:10.3390/antibiotics7010014
82. Irwin, J. J.; Shoichet, B. K. *J. Chem. Inf. Model.* **2005,** *45,* 177–182. doi:10.1021/ci049714+
83. Hale, C. A.; de Boer, P. A. J. *Cell* **1997,** *88,* 175–185. doi:10.1016/s0092-8674(00)81838-3
84. Bi, E.; Lutkenhaus, J. *Nature* **1991,** *354,* 161–164. doi:10.1038/354161a0
85. Lock, R. L.; Harry, E. J. *Nat. Rev. Drug Discovery* **2008,** *7,* 324–338. doi:10.1038/nrd2510
86. Mosyak, L.; Zhang, Y.; Glasfeld, E.; Haney, S.; Stahl, M.; Seehra, J.; Somers, W. S. *EMBO J.* **2000,** *19,* 3179–3191. doi:10.1093/emboj/19.13.3179
87. Kenny, C. H.; Ding, W.; Kelleher, K.; Benard, S.; Dushin, E. G.; Sutherland, A. G.; Mosyak, L.; Kriz, R.; Ellestad, G. *Anal. Biochem.* **2003,** *323,* 224–233. doi:10.1016/j.ab.2003.08.033
88. Sutherland, A. G.; Alvarez, J.; Ding, W.; Foreman, K. W.; Kenny, C. H.; Labthavikul, P.; Mosyak, L.; Petersen, P. J.; Rush, T. S., III; Ruzin, A.; Tsao, D. H. H.; Wheless, K. L. *Org. Biomol. Chem.* **2003,** *1,* 4138–4140. doi:10.1039/b312016c
89. Jennings, L. D.; Foreman, K. W.; Rush, T. S., III; Tsao, D. H. H.; Mosyak, L.; Kincaid, S. L.; Sukhdeo, M. N.; Sutherland, A. G.; Ding, W.; Kenny, C. H.; Sabus, C. L.; Liu, H.; Dushin, E. G.; Moghazeh, S. L.; Labthavikul, P.; Petersen, P. J.; Tuckman, M.; Haney, S. A.; Ruzin, A. V. *Bioorg. Med. Chem.* **2004,** *12,* 5115–5131. doi:10.1016/j.bmc.2004.07.031
90. Rush, T. S.; Grant, J. A.; Mosyak, L.; Nicholls, A. *J. Med. Chem.* **2005,** *48,* 1489–1495. doi:10.1021/jm040163o
91. Chopra, I. *Curr. Opin. Invest. Drugs (BioMed Cent.)* **2007,** *8,* 600–607.
92. Ho, M. X.; Hudson, B. P.; Das, K.; Arnold, E.; Ebright, R. H. *Curr. Opin. Struct. Biol.* **2009,** *19,* 715–723. doi:10.1016/j.sbi.2009.10.010
93. Baniulyte, G.; Singh, N.; Benoit, C.; Johnson, R.; Ferguson, R.; Paramo, M.; Stringer, A. M.; Scott, A.; Lapierre, P.; Wade, J. T. *Nat. Commun.* **2017,** *8,* No. 2027. doi:10.1038/s41467-017-02124-9
94. Cossar, P. J.; Ma, C.; Gordon, C. P.; Ambrus, J. I.; Lewis, P. J.; McCluskey, A. *Bioorg. Med. Chem. Lett.* **2017,** *27,* 162–167. doi:10.1016/j.bmcl.2016.11.091
95. Cossar, P. J.; Abdel-Hamid, M. K.; Ma, C.; Sakoff, J. A.; Trinh, T. N.; Gordon, C. P.; Lewis, P. J.; McCluskey, A. *ACS Omega* **2017,** *2,* 3839–3857. doi:10.1021/acsomega.7b00273
96. Yang, X.; Luo, M. J.; Yeung, A. C. M.; Lewis, P. J.; Chan, P. K. S.; Ip, M.; Ma, C. *Biochemistry* **2017,** *56,* 5049–5052. doi:10.1021/acs.biochem.7b00349
97. Duncan, M. C.; Linington, R. G.; Auerbuch, V. *Antimicrob. Agents Chemother.* **2012,** *56,* 5433–5441. doi:10.1128/aac.00975-12
98. Costa, T. R. D.; Felisberto-Rodrigues, C.; Meir, A.; Prevost, M. S.; Redzej, A.; Trokter, M.; Waksman, G. *Nat. Rev. Microbiol.* **2015,** *13,* 343–359. doi:10.1038/nrmicro3456

License and Terms

The definitive version of this article is the electronic one which can be found at:
doi:10.3762/bjoc.14.267

BEILSTEIN JOURNAL OF ORGANIC CHEMISTRY

Repurposing the anticancer drug cisplatin with the aim of developing novel *Pseudomonas aeruginosa* infection control agents

Mingjun Yuan[‡1], Song Lin Chua[‡1,2], Yang Liu[1], Daniela I. Drautz-Moses[1], Joey Kuok Hoong Yam[1], Thet Tun Aung[3,4], Roger W. Beuerman[4,5,6], May Margarette Santillan Salido[1], Stephan C. Schuster[1,3], Choon-Hong Tan[7], Michael Givskov[1,8], Liang Yang[*1,3,§] and Thomas E. Nielsen[*1,8,§]

Full Research Paper

Open Access

Address:
[1]Singapore Centre for Environmental Life Sciences Engineering (SCELSE), Nanyang Technological University, Singapore 637551, [2]Lee Kong Chian School of Medicine, Nanyang Technological University, Singapore 639798, [3]School of Biological Sciences, Nanyang Technological University, Singapore 639798, [4]Singapore Eye Research Institute, Singapore 169879, [5]SRP Neuroscience and Behavioural Disorders and Emerging Infectious Diseases, Duke-NUS, Singapore 169857, [6]Ophthalmology, Yong Loo Lin School of Medicine, National University of Singapore, Singapore 168751, [7]Division of Chemistry & Biological Chemistry, School of Physical & Mathematical Sciences, Nanyang Technological University, Singapore 637371 and [8]Costerton Biofilm Center, Department of Immunology and Microbiology, University of Copenhagen, 2200 København N, Denmark

Email:
Liang Yang[*] - yangliang@ntu.edu.sg; Thomas E. Nielsen[*] - ten@sund.ku.dk

* Corresponding author ‡ Equal contributors
§ Tel: (65) 6592-3085, Fax: (65) 6515-6751

Keywords:
biofilm; cisplatin; *Pseudomonas aeruginosa*; resistance; type III secretion

Beilstein J. Org. Chem. **2018,** *14,* 3059–3069.
doi:10.3762/bjoc.14.284

Received: 07 August 2018
Accepted: 02 November 2018
Published: 14 December 2018

This article is part of the thematic issue "Antibacterials, bacterial small molecule interactions and quorum sensing".

Guest Editor: D. Spring

Abstract

Antibiotic resistance threatens effective treatment of microbial infections globally. This situation has spurred the hunt for new antimicrobial compounds in both academia and the pharmaceutical industry. Here, we report how the widely used antitumor drug cisplatin may be repurposed as an effective antimicrobial against the nosocomial pathogen *Pseudomonas aeruginosa*. Cisplatin was found to effectively kill strains of *P. aeruginosa*. In such experiments, transcriptomic profiling showed upregulation of the *recA* gene, which is known to be important for DNA repair, implicating that cisplatin could interfere with DNA replication in *P. aeruginosa*. Cisplatin treatment significantly repressed the type III secretion system (T3SS), which is important for the secretion of

exotoxins. Furthermore, cisplatin was also demonstrated to eradicate in vitro biofilms and in vivo biofilms in a murine keratitis model. This showed that cisplatin could be effectively used to eradicate biofilm infections which were otherwise difficult to be treated by conventional antibiotics. Although cisplatin is highly toxic for humans upon systemic exposure, a low toxicity was demonstrated with topical treatment. This indicated that higher-than-minimal inhibitory concentration (MIC) doses of cisplatin could be topically applied to treat persistent and recalcitrant *P. aeruginosa* infections.

Introduction

Pseudomonas aeruginosa is a leading nosocomial pathogen which causes, among others, corneal, chronic otitis media, urinary tract (UTI) and respiratory tract infections [1]. *P. aeruginosa* is also the main cause of fatal infections in patients with cystic fibrosis (CF) [2] and cancer patients [3,4]. The success of *P. aeruginosa* as a leading pathogen is attributed to its ability to form resilient biofilms, resist antimicrobials and secrete virulence products.

Microbial cells resident in biofilms are encased by an extracellular matrix, which protects them from antimicrobial treatment and the host's immune clearance [5]. Clinical *P. aeruginosa* isolates are mostly multidrug-resistant (MDR) strains [6], with robust ability to form biofilms [7]. *P. aeruginosa* also secretes virulence factors targeting important components of the immune system, such as the type III secretion systems (T3SS), which was shown to be associated with poor clinic outcomes in patients with lower respiratory infections [8] and ventilator-associated pneumonia [9]. Identifying antimicrobial compounds which actively target bacteria in the biofilm mode including virulence mechanisms that cripple immune defenses, may offer novel antimicrobial therapies against a variety of otherwise persistent *P. aeruginosa* infections.

Here, we screened our in-house collection of FDA-approved drugs and found that cisplatin was the most potent among several other Pt(II)-based compounds to kill *P. aeruginosa*. It was previously reported that cisplatin had antimicrobial effects on nosocomial pathogens, such as *Escherichia coli*, *Klebsiella pneumonia* and *Staphylococcus aureus* [10] and persister cells [11]. Transcriptomic analysis was employed to reveal the molecular mechanisms on how cisplatin inhibits the growth and production of virulence factors of *P. aeruginosa*. We also examined the effects of cisplatin treatment on in vitro *P. aeruginosa* biofilms and in a mouse model of corneal infection (keratitis). We showed that cisplatin is more effective than the clinically used antibiotic tobramycin in eradicating biofilms. Although cisplatin is highly toxic for intravenous applications, we showed that it has low toxicity when applied topically to wounds, as 25 mM (0.75 mg mL^{-1}) did not have adverse effect on wound healing. This meant that higher doses (5–10 × MIC) of cisplatin could be safely used for topical applications. Given the low topical toxicity of cisplatin, it may be utilized as an attractive therapeutic agent for prevention and treatment of *P. aeruginosa* biofilm infections.

Materials and Methods

Bacterial strains and culture media

The bacterial strains used in this study are listed in Supporting Information File 1, Table S3. Luria–Bertani (LB) medium was used to maintain the bacterial strains. Growth assay and static biofilm cultivation were carried out at 37 °C in ABTGC (ABT minimal medium [12] supplemented with 0.4 g/L glucose and 0.4 g/L casamino acids). For marker selection in *P. aeruginosa*, 30 μg mL^{-1} gentamycin (Gm), 50 μg mL^{-1} tetracycline (Tc), 100 μg mL^{-1} streptomycin (Strep) or 200 μg mL^{-1} carbenicillin (Cb) were used, as appropriate.

Platinum complexes and solution preparation for MIC assay

Cisplatin, transplatin, cDPCP, oxaliplatin, K_2PtCl_4 and *cis*-$PtCl_2(CH_3CN)_2$ were purchased from Sigma-Aldrich were used as received. Platinum complexes *cis*-$PtCl_2(Py)_2$ [13,14] and *cis*-$PtCl_2(PPh_3)_2$ [15] were prepared according to the reported procedure. For minimal inhibitory concentration (MIC) assays, cisplatin, cDPCP, oxaliplatin, K_2PtCl_4 and *cis*-$PtCl_2(CH_3CN)_2$ were dissolved in saline solution (0.85% w/v) at 2.5 mM concentration, while transplatin, *cis*-$PtCl_2(Py)_2$ and *cis*-$PtCl_2(PPh_3)_2$ were dissolved in DMF (v/v) at 2.5 mM concentration.

Determination of minimal inhibitory concentration (MIC)

The MIC assays were performed using a microtiter broth dilution method as previously described (≈1 × 10^5 cells) in the NACLAR guidelines [16]. Overnight cultures of bacterial strains were diluted in ABTGC medium. Cisplatin and other Pt-containing compounds were diluted from a stock solution with ABTGC medium at a concentration 10 times higher than the required range. 10 μL of each diluted solution of Pt compounds were added to each corresponding well of a 96-well microtiter plate (polypropylene, Costar) and 90 μL of diluted bacterial culture in ABTGC medium were added before serial dilutions. The plate was incubated at 37 °C for 16–18 h. MIC was taken as the lowest concentration where no visual growth (based on OD600) of bacteria was detected. The experiments

were performed in triplicate and representative results were shown.

RNA preparation

Bacterial cells were collected using the method described previously [17] with some modifications. Generally, PAO1 cells were cultivated either with (1.5 μM) or without cisplatin. The cells were harvested at the early-stationary phase (after approximately 8 h cultivation). Total RNA was extracted with an RNeasy Protect Bacteria Mini Kit with on-column DNase digestion (Qiagen). A Turbo DNA-free vigorous protocol was used for a second round of DNase treatment (Ambion). The 16S, 23S and 5S rRNA was removed using the Ribo-Zero Magnetic Kit (Bacteria) (Epicentre).

RNA sequencing and data analysis

Gene expression analysis was conducted via Illumina RNA sequencing (RNA-Seq technology). RNA-Seq was conducted for two biological replicates of each sample. The rRNA-depleted RNA was fragmented to 150–200 bp fragments, then first and second strand cDNA were synthesized with a cDNA-synthesis kit (ThermoScientific), followed by end repair and adapter ligation. After 12 cycles of PCR enrichment, the quality of the libraries was assessed using the Bioanalyzer (Agilent Technologies, USA). The libraries were sequenced using the Illumina HiSeq 2500 platform with a paired-end protocol and read lengths of 100 nt.

The sequencing data was analyzed as described previously [12]. Sequence reads were mapped onto PAO1 reference genome using the CLC genomics Workbench 8.0 (CLC Bio-Qiagen, Aarhus, Denmark). The differentially expressed genes were identified by performing a negative binomial test using the DESeq [18] package of R/Bioconductor [19], using the cut off of fold-change larger than 2 and a BH (Benjamini-Hochberg) adjusted P-value smaller than 0.05. The raw sequence reads were normalized by size factors, then $Log_2(N + 1)$ transformed. Hierarchical clustering analysis was performed using the transformed reads, and a heat-map was drawn for the differentially expressed genes between the cisplatin treated cells and control cells, using the heatmap.2 [19] package of R. Function enrichment analysis was conducted based on PseudoCAP Function Class (http://www.pseudomonas.com), and a dot plots figure was generated using the ggplot2 [20] package of R.

The RNA-Seq datasets are available at the NCBI Sequence Read Archives: SRS1038085 and SRS1038089.

qRT-PCR analysis

Total RNA was extracted using RNeasy Mini Kit (Qiagen) with on-column DNase digestion. The integrity, purity and concentration of the RNA were determined by NanoDrop spectrophotometry and Agilent 2200 TapeStation system.

Quantitative reverse transcriptase PCR (qRT-PCR) was performed using a two-step method. First-strand cDNA was synthesized from total RNA using SuperScript III First-Strand Synthesis SuperMix kit (Cat. No. 18080-400, Invitrogen). The cDNA was used as a template for qRT-PCR with a SYBR Select Master Mix kit (Cat. No. 4472953, Applied Biosystems by Life Technologies) on an Applied Biosystems StepOnePlus Real-Time PCR System with the specific primers (see Supporting Information File 1, Table S4). The three genes of GAPDH, *gyrB*, *rpoD* were used as endogenous control. Melting curve analyses were employed to verify the specific single-product amplification.

P. aeruginosa killing assay

The OD_{600} of overnight cultures of PAO1, Δ*recA* and Δ*recA* complementation strains were measured and adjusted to 0.3 in ABTGC medium with 0, 3.125, 6.25 and 12.5 μM cisplatin, respectively. The strains were incubated at 37 °C with shaking at 200 rpm for 4 h. The cultures were then harvested, serially diluted and plated on LB agar plates for incubation at 37 °C overnight. Colonies on the plate were enumerated and colony forming units (CFU) mL^{-1} were tabulated as follows: CFU mL^{-1} = average number of colonies X dilution factor X volume used to spread on LB agar plate. Experiments were conducted in triplicate, and the results are shown as the mean ± s.d.

P. aeruginosa biofilm killing assay by cisplatin and tobramycin

Biofilms were grown in 24-well plates (Nunc, Denmark) at 37 °C, as previously described [21]. Biofilms were washed 3 times with 0.9% NaCl and treated with ABTGC medium with 0, 3.125, 6.25 and 12.5 μM cisplatin, respectively. For tobramycin treatment, biofilms were treated with ABTGC medium with 5.3, 10.6 and 21.2 μM tobramycin, respectively. The treated biofilms were incubated at 37 °C for 4 h. The biofilms were harvested by scraping with a cell scraper, homogenized in 1 mL 0.9% NaCl, serially diluted and plated on LB agar plates for incubation at 37 °C overnight. Colonies on the plate were counted and CFU mL^{-1} was tabulated. Experiments were conducted in triplicate, and results are shown as the mean ± s.d.

RAW264.7 macrophage cytotoxicity assay

The murine macrophages (RAW264.7) were maintained in Dulbecco's modified Eagle's medium (DMEM) (Life Technologies), supplemented with 10% fetal bovine serum (FBS) (Gibco), in 75 cm^2 cell culture flasks at a density of 1.0×10^6 cells mL^{-1} at 37 °C, 5% CO_2 for 72 h. The 5.0×10^6 macrophages per well were seeded in 24-well plate

(Nunc, Denmark) and grown at 37 °C, 5% CO_2 overnight. As previously described [12], macrophages were washed once with PBS and treated with PAO1 in DMEM medium with 0, 3.125, 6.25 and 12.5 μM cisplatin at a multiplicity of infection of 100 bacteria cells: 1 macrophage. As control, the macrophages were treated with the T3SS deficient Δ*pscJ* mutant in DMEM medium. The co-culture was incubated at 37 °C, 5% CO_2 for 2 h. The extracellular bacterial cells in DMEM were removed and the infected macrophages were washed 3 times with PBS. Fresh DMEM was added to the infected macrophages and a further incubation of the macrophages at 37 °C, 5% CO_2 for 4 h was ensued. A solution containing 20 μM propidium iodide (PI) was added to the macrophages to stain for dead macrophages killed by PAO1 treated with cisplatin or Δ*pscJ*. Live and dead macrophages were imaged by fluorescence microscopy (Zeiss, Germany) at 200× and tabulated under % of dead macrophages. Experiments were conducted in triplicate, and the results are shown as the mean ± s.d.

Rabbit corneal wound healing model

New Zealand White Rabbits (n = 4, weighing 2 to 3 kg) purchased from National University of Singapore, were used for this study. All animal experiments were conducted in compliance with the ARVO statement for the Use of Animals in Ophthalmic and Vision Research, the guide for the Care and Use of laboratory animals (National Research Council) and under the supervision of Singhealth Experimental Medical Centre (SEMC).

Four rabbits were randomly grouped into two groups of two rabbits each, comprising of the PBS control treated group and 0.75 mg mL^{-1} cisplatin treated group. Intra peritoneal injection of 1 mL of ketamine (100 mg mL^{-1}) and 0.5 mL of xylazil (20 mg mL^{-1}) had been used to anesthetize the rabbits. Corneas were then anesthetized by topical administration of xylocaine 1%. A corneal wound was made by using a 5 mm trephine and mechanical removal of epithelial cells was carried out by sterile mini blade (BD-Beaver) leaving the basal lamina intact [22,23]. All the groups were treated by topical administration of the respective drug 3 times per day. Cornea wound was visualized by the aid of cobalt-blue filter equipped slit lamp biomicroscopy (New-generation Zoom clinical Slit Lamp, NS-2D, Righton), staining with Minims fluorescein sodium eye drops (Bausch and Lomb, 2% w/v) which is used in ophthalmology clinic for disclosure of wound on the ocular surface [24,25]. Residual wound area (pixel square) was measured during the wound healing process by Image-J 1.44o version. Mann-Whitney U Test was employed to determine if a difference in re-epithelialization existed among the different groups by using GraphPad Prism 6.02. A probability value of $p \leq 0.05$ was considered statistically significant.

Murine model for corneal infection

The corneas of the C57BL/6 mice were scratched with a scraper to create wounds. 10 μL of PAO1 planktonic cells (≈1 × 10^6 cells) were dripped onto each cornea and incubated for 24 h on the mice to allow the biofilms to form on the scratched corneas as previously described [26,27]. About 10 μL of cisplatin (final concentration 25 μM) or 0.9% NaCl as control were dripped onto the cornea 3 times per day at 4 h interval on the second day. The mice were kept for 72 h and then sacrificed.

The corneas were harvested, and the biofilm was disrupted from the corneas by crushing with mortar and pestle, followed by vortexing with glass beads for 15 min. The homogenized biofilm cells were serially diluted, plated on LB agar plates and incubated at 37 °C overnight. The number of colonies was counted, and CFU ml^{-1} was tabulated. Experiments were performed in triplicate, and the results are shown as the mean ± s.d.

Results and Discussion

Cisplatin inhibits *P. aeruginosa* planktonic growth

During our screening of in-house collection of FDA-approved drugs against *P. aeruginosa* growth, we identified that cisplatin had a minimal inhibitory concentration (MIC) of 6.25 μM against the *P. aeruginosa* PAO1 lab strain (Figure 1). We further tested the growth inhibitory effect of cisplatin against another *P. aeruginosa* lab strain PA14 and a *P. aeruginosa* mucoid multiple-drug resistant (MDR) CF clinical isolate 57388A and found that cisplatin had equivalent MIC at 6.25 μM against these two strains (Supporting Information File 1, Table S3). We next evaluated several other Pt(II)-based compounds for their growth inhibitory effects on *P. aeruginosa*, but these tested compounds had higher MIC against *P. aeruginosa* as compared to cisplatin (Figure 1).

Mode of action

The growth inhibitory effects of cisplatin on both eukaryotic cells and microbial cells are attributed to the interactions of Pt(II) in cisplatin with DNA [28-30]. To reveal the growth arresting mechanisms and overall impact of cisplatin on the physiology of *P. aeruginosa*, we performed an RNA-sequencing (RNA-seq) based transcriptomic analysis on *P. aeruginosa* PAO1 after cultivation in sub-lethal concentration (1.5 μM) of cisplatin for 8 hours and compared the transcriptome with control transcriptomes of bacteria present in cisplatin-free medium. Using a negative binomial test with a BH adjusted P-value cut-off of 0.05 and a fold-change cut-off of 2, we found that sub-MIC cisplatin treatment induced the expression of 315 genes (Supporting Information File 1, Table S1) while repressed the expression of 72 genes (Support-

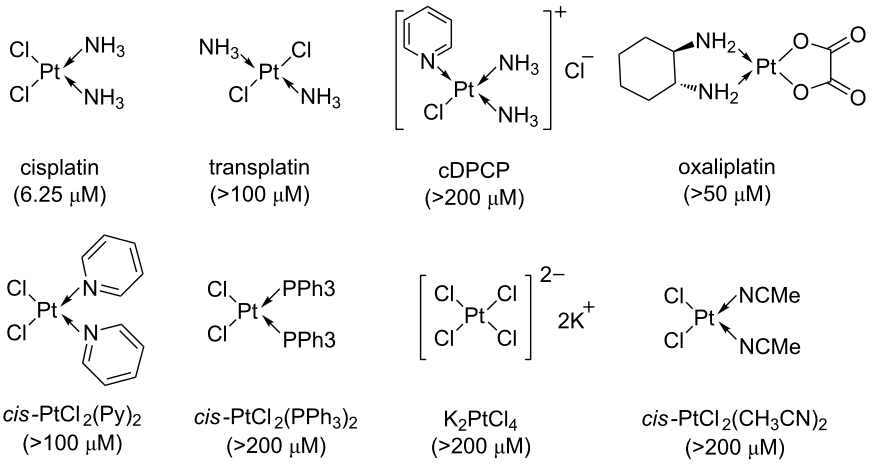

Figure 1: Structures and MICs of Pt-based compounds against *P. aeruginosa* PAO1.

ing Information File 1, Table S2) in *P. aeruginosa*. The heatmap and function enrichment of the genes that were differently expressed between cisplatin-treated and control *P. aeruginosa* samples were illustrated in Figure 2 and Figure 3, respectively.

The cisplatin treatment triggered the expression of a large fraction of the LexA-controlled SOS regulon [31], including genes involved in DNA replication, recombination, modification and repair (*dnaE2*, *imuB*, *imuA*, *dinG*, *recA*, *recN*, *recX*) and genes involved in pyocin synthesis (*PA0614-PA0648*), whose expression were previously reported to be induced by ciprofloxacin [31] and hydrogen peroxide treatments [32]. In addition, cisplatin treatment induced the expression of a series of genes involved in energy metabolism, which corroborated with previous proteomics work showing that cisplatin could interfere with stress response and energy metabolism in *E. coli* [33].

To further validate the impact of cisplatin on DNA replication, we compared the cisplatin sensitivity of the *P. aeruginosa* wild-type PAO1 strain and its DNA recombination-deficient *recA* mutant and found that the *rec* recombination pathway was essential for the cisplatin resistance in *P. aeruginosa* (Figure 4). Together with the transcriptome profiling, this result confirmed that cisplatin was able to interact with the *P. aeruginosa* DNA, resulting in up-regulation of stress response genes. This mechanism was also similar to the mechanism of action by another DNA crosslinker, mitomycin C which kills bacterial persister cells [34].

Anti-T3SS effect of cisplatin

Our transcriptomic analysis also revealed the expression of a large number of the secretion related genes, including those of the type III secretion system (T3SS), which were downregulated in PAO1 by cisplatin exposure (Table S2), which was similar to that by ciprofloxacin exposure [31]. Our qRT-PCR analysis confirmed that the expression of two selected T3SS genes, *exoS* and *pscG*, were downregulated by cisplatin treatment compared to control (Figure 5a). The downregulation of T3SS by the LexA-controlled SOS response [35] could be attributed to the induced expression of *ptrB*, a repressor of T3SS by cisplatin treatment (Supporting Information File 1, Table S3).

The T3SS is one of the major virulence mechanisms employed by *P. aeruginosa* and other microbial pathogens to impair the host immune systems during infection [36,37]. T3SS activity of *P. aeruginosa* was correlated with acute cytotoxicity to host epithelial cells and immune cells such as macrophages and neutrophils [38]. As we demonstrated that cisplatin treatment was able to reduce the T3SS of *P. aeruginosa*, we further tested the ability of cisplatin in attenuating the acute cytotoxicity of *P. aeruginosa* to macrophages. Cisplatin treatment of *P. aeruginosa* in the *P. aeruginosa*-macrophage co-cultures caused significant less death of the mouse macrophages compared to control samples (Figure 5b), suggesting the effectiveness of cisplatin against *P. aeruginosa* infection.

Antibiofilm effect of cisplatin

P. aeruginosa is notorious for its biofilm formation capacity, which might lead to persistent or recalcitrant infections. SOS response and DNA recombination are required for development of *P. aeruginosa* biofilm resistance [39-41]. Given cisplatin treatment was able to interfere with DNA repair, we hypothesized that cisplatin treatment could eradicate *P. aeruginosa* biofilm cells. We compared the biofilm killing effects of cisplatin and tobramycin at various concentrations. The MIC of cisplatin and tobramycin against planktonic *P. aeruginosa* cells were 6.25 μM and 2.65 μM, respectively. However, tobra-

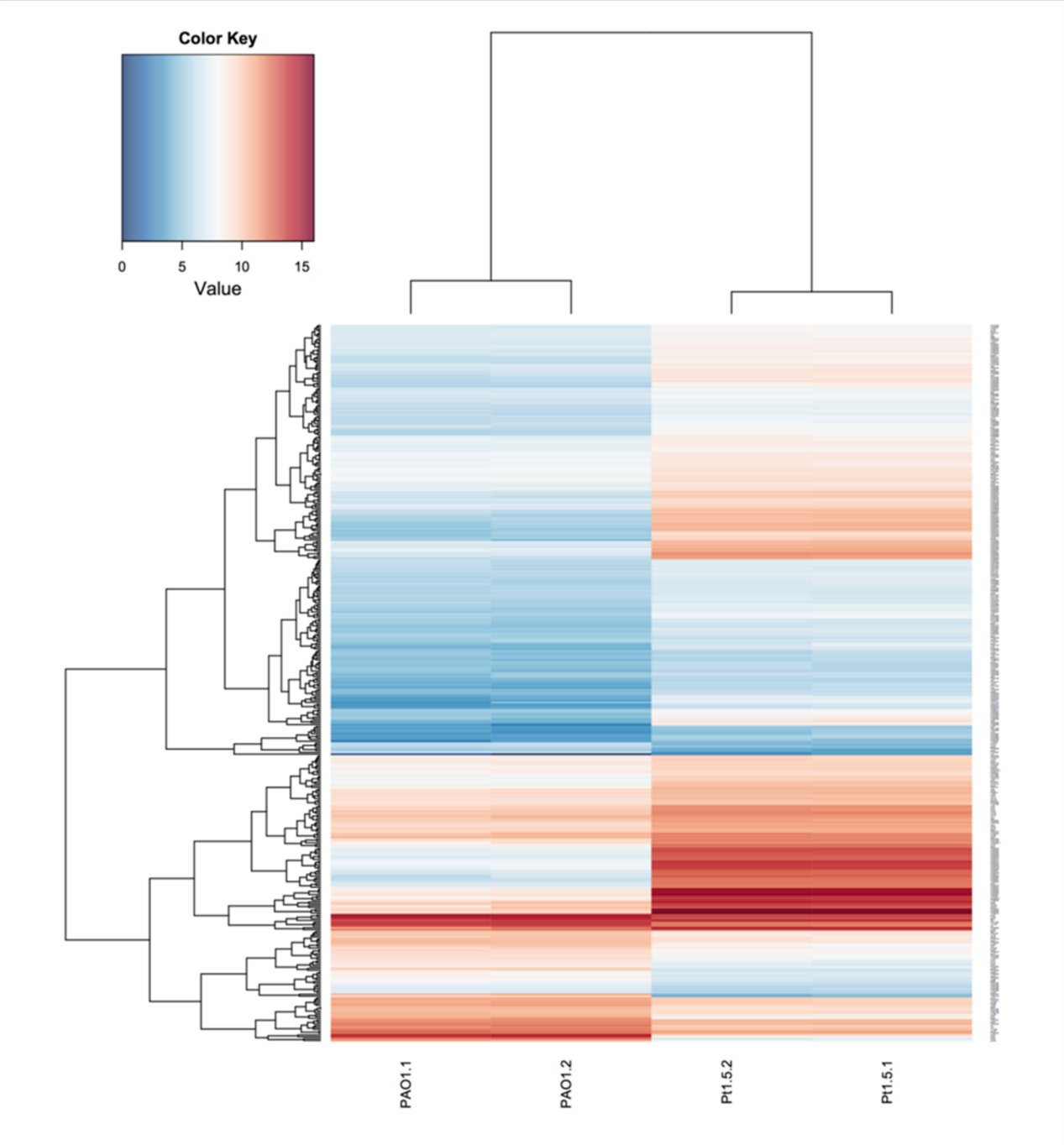

Figure 2: Transcriptomic analysis of control and cisplatin-treated PAO1 cultures. Heatmap comparing the transcriptomes of control and cisplatin-treated PAO1 cultures.

mycin could not kill the biofilm cells at 2 × MIC due to its limitation in biofilm penetration [42], while cisplatin was able to kill substantial amount of biofilm cells with nearly 100 times reduction of *P. aeruginosa* biofilm cells (Figure 6). This result suggested that cisplatin might penetrate the biofilms better than the otherwise eDNA trapped tobramycin to kill the *P. aeruginosa* cells [42]. The 4 × MIC and 8 × MIC of tobramycin treatment showed dose-dependent increase of biofilm killing capacity (Figure 6). Interestingly, cisplatin had combinatory effects with tobramycin in killing the PAO1 biofilms, as combinatorial treatment of 2 × MIC of cisplatin with 4 × MIC or 8 × MIC tobramycin killed the biofilm cells at a higher rate compared to the mono-compound treatment (Figure 6). These results suggest that combination of cisplatin and other conventional antimicrobials could be a useful strategy for eradicating persistent biofilm-associated infections.

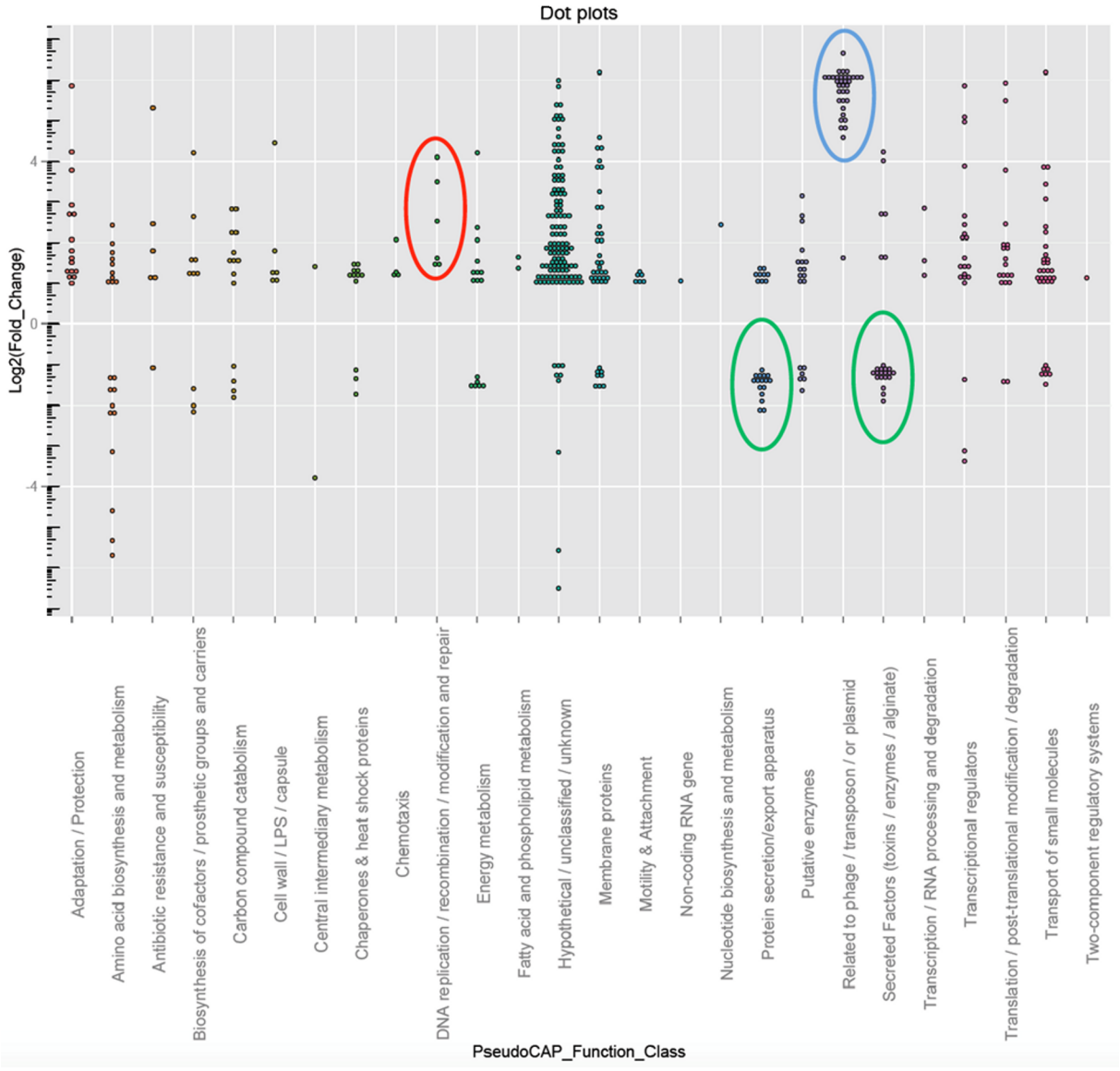

Figure 3: Function enrichment of differentially expressed genes from the transcriptomic analysis. A dot-lot figure was generated using ggplot2 the package of R. Red circle highlights the genes involved in DNA replication and repair; blue circle highlights the genes involved in pyocin synthesis; green circle highlights the genes involved in protein secretion (T3SS).

Cisplatin treatment attenuates *P. aeruginosa* infection

As cisplatin could reduce the synthesis of T3SS-mediated virulent products and kill biofilms of *P. aeruginosa*, we further tested if cisplatin treatment was able to eradicate in vivo *P. aeruginosa* infections using a mouse model of keratitis, where *P. aeruginosa* cells have biofilm-like morphology [26,27] and employ type III secretion during infections [43]. We firstly confirmed that cisplatin was not toxic and did not interfere with wound healing, with no observable inflammation or adverse effects, when applied topically on scratched corneas with no bacterial infection (Supporting Information File 1, Figure S1). We then allowed *P. aeruginosa* PAO1 to colonize and establish infection in the scratched corneas of mice for 24 h. 10 µL of 1 × MIC (6.25 µM) of cisplatin and control 0.9% NaCl were dripped at the site of *P. aeruginosa* infection 3 times (4 hour interval) on the second day. The mice were sacrificed on the third day and their corneas were harvested for CFU count. Cisplatin showed efficient killing capacity on *P. aeruginosa* cells from infected mouse corneas and there was a significant reduction in the bacterial loads from the cisplatin treated corneas as compared to the control corneas (Figure 7).

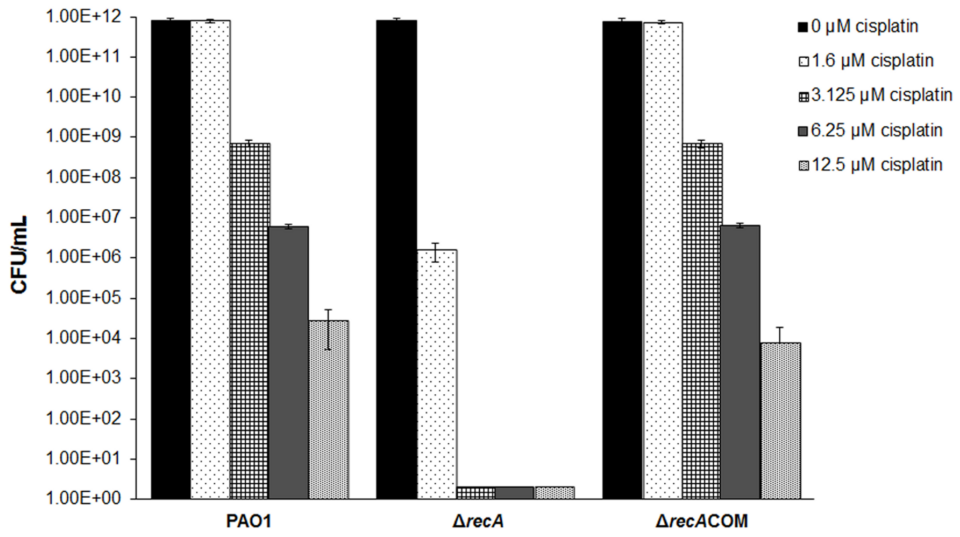

Figure 4: Cisplatin fast-kill assay against the *P. aeruginosa* PAO1, Δ*recA* mutant and the Δ*recA*COM strain. *P. aeruginosa* strains were treated by ABTGC medium with varies concentrations of cisplatin for 4 h. CFUs were determined for cisplatin-treated *P. aeruginosa* cultures. Means and s.d. from triplicate experiments are shown.

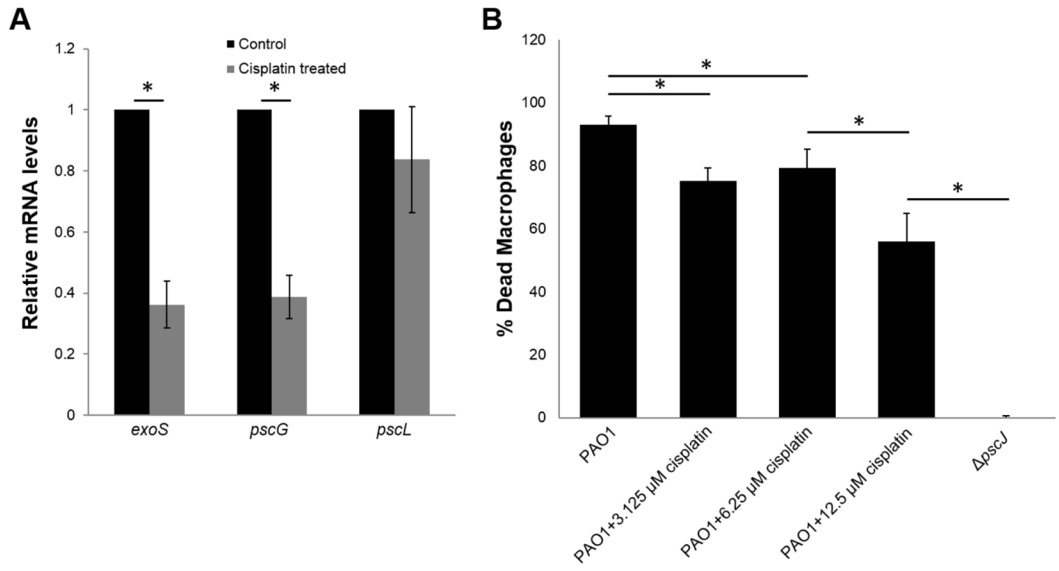

Figure 5: Cisplatin treatment represses T3SS associated virulence. (A) Cisplatin treatment downregulated the expression of T3SS gene revealed by qRT-PCR analysis. Means and s.d. from triplicate experiments are shown. Student's t-test was performed for testing differences between groups. *$P \leq 0.05$. (B) Cisplatin treatment reduced cytotoxicity of *P. aeruginosa* PAO1 against mouse macrophage cells. Means and s.d. from triplicate experiments are shown. Student's t-test was performed for testing differences between groups. *$P \leq 0.05$.

Conclusion

Here, we have demonstrated how cisplatin displays antivirulence and antibiofilm effects against the opportunistic pathogen *P. aeruginosa*. Since biofilms are notoriously difficult to be cleared by conventional antibiotics, cisplatin possesses the additional advantage of killing biofilms. This makes cisplatin a more attractive antimicrobial for treating biofilm infections clinically. Even though cisplatin is known for its toxic side effects on cancer patients when administered intravenously, we showed indications that cisplatin could be applied topically to infection sites with low toxicity and minimal negative impact on wound repair. Transcriptomic analysis revealed that the working mechanism of cisplatin towards *P. aeruginosa* is rather unique and distinct from other conventional antibiotics, which may offer alternative therapeutic approaches towards persistent infections.

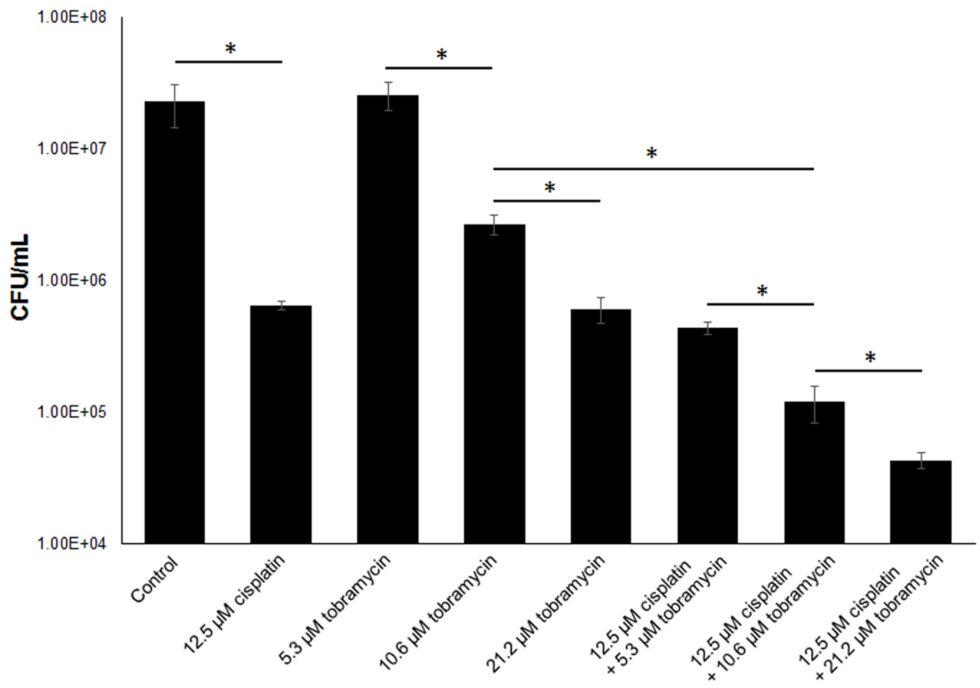

Figure 6: *P. aeruginosa* biofilm killing assay by cisplatin, tobramycin and their combinations. *P. aeruginosa* biofilms were treated by ABTGC medium with varies concentrations of cisplatin and or tobramycin for 4 h. CFUs were determined for cisplatin and or tobramycin-treated *P. aeruginosa* biofilms. Means and s.d. from triplicate experiments are shown. Student's t-test was performed for testing differences between groups. *$P \leq 0.05$.

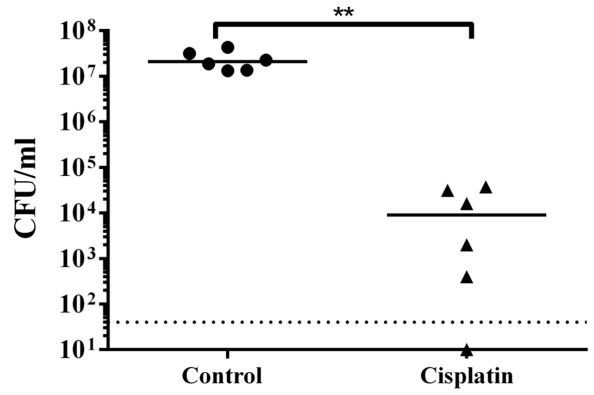

Figure 7: Cisplatin treatment attenuates *P. aeruginosa* infections. CFU mL^{-1} of PAO1 obtained from corneas with and without cisplatin treatment. Dotted horizontal lines represent limit of detection. The mean and s.d. from six experiments were shown for in vivo biofilms. Student's t-test was performed for testing differences between groups. *$P < 0.01$.

In recent years, metal-containing compounds have been identified as antimicrobial agents. Gallium was shown to disrupt the iron metabolism of *P. aeruginosa* and efficiently kill established biofilm [44]. In addition, the gold-containing drug, auranofin, was found to be a broad-spectrum bactericidal compound, that targets the thiol-redox homeostasis of a range of Gram-positive bacteria [45]. Further studies will be carried out to better understand the resistance mechanism and structural requirements of the Pt-based compounds as an alternative to the conventional antibiotics. Such compounds could also be used synergistically with specific enzymes that degrade the biofilm matrix [46] or biofilm-dispersal agents to boost the eradication of biofilms, to provide better treatment options for chronic and persistent infections.

Supporting Information

Supporting Information File 1

Additional information.
[https://www.beilstein-journals.org/bjoc/content/supplementary/1860-5397-14-284-S1.pdf]

Disclosure of Financial and Competing Interests

This research is supported by the National Research Foundation and Ministry of Education Singapore under its Research Centre of Excellence Programme and AcRF Tier 2 (MOE2016-T2-1-010) from Ministry of Education, Singapore. S.L. Chua is supported by the Lee Kong Chian School of Medicine (LKCMedicine) Postdoctoral Fellowship 2015. The authors declare no other conflict of interest. No writing assistance was utilized in the writing of the manuscript.

Ethical Conduct of Research

All animal experiments were conducted in compliance with the guide for the Care and Use of laboratory animals (National Research Council) under Nanyang Technological University Institutional Animal Care and Use Committee (IACUC) protocol number ARF SBS/NIE-A0192, which was approved by the Nanyang Technological University-IACUC.

Acknowledgements

We thank Ms. Yicai Chen for her help with the RNA experiments.

ORCID® iDs

Liang Yang - https://orcid.org/0000-0002-2362-0128

References

1. Lyczak, J. B.; Cannon, C. L.; Pier, G. B. *Microbes Infect.* **2000,** *2,* 1051–1060. doi:10.1016/s1286-4579(00)01259-4
2. Govan, J. R.; Deretic, V. *Microbiol. Rev.* **1996,** *60,* 539–574.
3. Markou, P.; Apidianakis, Y. *Front. Cell. Infect. Microbiol.* **2014,** *3,* 115. doi:10.3389/fcimb.2013.00115
4. Rolston, K. V. I.; Bodey, G. P. *Cancer Invest.* **1992,** *10,* 43–59. doi:10.3109/07357909209032787
5. Yang, L.; Liu, Y.; Wu, H.; Song, Z.; Høiby, N.; Molin, S.; Givskov, M. *FEMS Immunol. Med. Microbiol.* **2012,** *65,* 146–157. doi:10.1111/j.1574-695x.2011.00858.x
6. Zavascki, A. P.; Carvalhaes, C. G.; Picão, R. C.; Gales, A. C. *Expert Rev. Anti-Infect. Ther.* **2010,** *8,* 71–93. doi:10.1586/eri.09.108
7. Sanchez, C. J., Jr.; Mende, K.; Beckius, M. L.; Akers, K. S.; Romano, D. R.; Wenke, J. C.; Murray, C. K. *BMC Infect. Dis.* **2013,** *13,* 47. doi:10.1186/1471-2334-13-47
8. Roy-Burman, A.; Savel, R. H.; Racine, S.; Swanson, B. L.; Revadigar, N. S.; Fujimoto, J.; Sawa, T.; Frank, D. W.; Wiener-Kronish, J. P. *J. Infect. Dis.* **2001,** *183,* 1767–1774. doi:10.1086/320737
9. Hauser, A. R.; Cobb, E.; Bodí, M.; Mariscal, D.; Vallés, J.; Engel, J. N.; Rello, J. *Crit. Care Med.* **2002,** *30,* 521–528. doi:10.1097/00003246-200203000-00005
10. Joyce, K.; Saxena, S.; Williams, A.; Damurjian, C.; Auricchio, N.; Aluotto, S.; Tynan, H.; Demain, A. L. *J. Antibiot.* **2010,** *63,* 530–532. doi:10.1038/ja.2010.64
11. Chowdhury, N.; Wood, T. L.; Martínez-Vázquez, M.; García-Contreras, R.; Wood, T. K. *Biotechnol. Bioeng.* **2016,** *113,* 1984–1992. doi:10.1002/bit.25963
12. Chua, S. L.; Liu, Y.; Yam, J. K. H.; Chen, Y.; Vejborg, R. M.; Tan, B. G. C.; Kjelleberg, S.; Tolker-Nielsen, T.; Givskov, M.; Yang, L. *Nat. Commun.* **2014,** *5,* 4462. doi:10.1038/ncomms5462
13. Rajput, J.; Moss, J. R.; Hutton, A. T.; Hendricks, D. T.; Arendse, C. E.; Imrie, C. *J. Organomet. Chem.* **2004,** *689,* 1553–1568. doi:10.1016/j.jorganchem.2004.01.034
14. Griffith, D.; Bergamo, A.; Pin, S.; Vadori, M.; Müller-Bunz, H.; Sava, G.; Marmion, C. J. *Polyhedron* **2007,** *26,* 4697–4706. doi:10.1016/j.poly.2007.03.011
15. Ramos-Lima, F. J.; Quiroga, A. G.; Pérez, J. M.; Font-Bardía, M.; Solans, X.; Navarro-Ranninger, C. *Eur. J. Inorg. Chem.* **2003,** 1591–1598. doi:10.1002/ejic.200390209
16. Wiegand, I.; Hilpert, K.; Hancock, R. E. W. *Nat. Protoc.* **2008,** *3,* 163–175. doi:10.1038/nprot.2007.521
17. Tan, S. Y.-Y.; Liu, Y.; Chua, S. L.; Vejborg, R. M.; Jakobsen, T. H.; Chew, S. C.; Li, Y.; Nielsen, T. E.; Tolker-Nielsen, T.; Yang, L.; Givskov, M. *Antimicrob. Agents Chemother.* **2014,** *58,* 6648–6659. doi:10.1128/aac.02620-13
18. Anders, S.; Huber, W. *Genome Biol.* **2010,** *11,* R106. doi:10.1186/gb-2010-11-10-r106
19. Gentleman, R. C.; Carey, V. J.; Bates, D. M.; Bolstad, B.; Dettling, M.; Dudoit, S.; Ellis, B.; Gautier, L.; Ge, Y.; Gentry, J.; Hornik, K.; Hothorn, T.; Huber, W.; Iacus, S.; Irizarry, R.; Leisch, F.; Li, C.; Maechler, M.; Rossini, A. J.; Sawitzki, G.; Smith, C.; Smyth, G.; Tierney, L.; Yang, J. Y.; Zhang, J. *Genome Biol.* **2004,** *5,* R80. doi:10.1186/gb-2004-5-10-r80
20. Wickham, H. *ggplot2: Elegant Graphics for Data Analysis;* Springer Publishing Company, Inc.: New York City, NY, U.S.A., 2009; p 216. doi:10.1007/978-0-387-98141-3
21. Chua, S. L.; Hultqvist, L. D.; Yuan, M.; Rybtke, M.; Nielsen, T. E.; Givskov, M.; Tolker-Nielsen, T.; Yang, L. *Nat. Protoc.* **2015,** *10,* 1165–1180. doi:10.1038/nprot.2015.067
22. Koh, J.-J.; Lin, S.; Aung, T. T.; Lim, F.; Zou, H.; Bai, Y.; Li, J.; Lin, H.; Pang, L. M.; Koh, W. L.; Salleh, S. M.; Lakshminarayanan, R.; Zhou, L.; Qiu, S.; Pervushin, K.; Verma, C.; Tan, D. T. H.; Cao, D.; Liu, S.; Beuerman, R. W. *J. Med. Chem.* **2015,** *58,* 739–752. doi:10.1021/jm501285x
23. Aung, T. T.; Yam, J. K. H.; Lin, S.; Salleh, S. M.; Givskov, M.; Liu, S.; Lwin, N. C.; Yang, L.; Beuerman, R. W. *Antimicrob. Agents Chemother.* **2016,** *60,* 24–35. doi:10.1128/aac.01509-15
24. Reidy, J. J.; Zarzour, J.; Thompson, H. W.; Beuerman, R. W. *Br. J. Ophthalmol.* **1994,** *78,* 377–380. doi:10.1136/bjo.78.5.377
25. Brazzell, R. K. S. M.; Aquavella, J. V.; Beuerman, R. W.; Baird, L. *Invest. Ophthalmol. Visual Sci.* **1991,** *32,* 336–340.
26. Saraswathi, P.; Beuerman, R. W. *The ocular surface;* 2015.
27. Yam, J. K. H.; Aung, T. T.; Chua, S. L.; Cheng, Y.; Kohli, G. S.; Zhou, J.; Constancias, F.; Liu, Y.; Cai, Z.; Salido, M. M. S.; Drautz-Moses, D. I.; Rice, S. A.; Schuster, S. C.; Boo, Z. Z.; Wu, B.; Kjelleberg, S.; Tolker-Nielsen, T.; Beuerman, R. W.; Givskov, M.; Yang, L. *Environ. Microbiol.* **2018,** in press.
28. Fichtinger-Schepman, A. M.; van Oosterom, A. T.; Lohman, P. H.; Berends, F. *Cancer Res.* **1987,** *47,* 3000–3004.
29. Onoa, G. B.; Cervantes, G.; Moreno, V.; Prieto, M. J. *Nucleic Acids Res.* **1998,** *26,* 1473–1480. doi:10.1093/nar/26.6.1473
30. Siddik, Z. H. *Oncogene* **2003,** *22,* 7265–7279. doi:10.1038/sj.onc.1206933
31. Cirz, R. T.; O'Neill, B. M.; Hammond, J. A.; Head, S. R.; Romesberg, F. E. *J. Bacteriol.* **2006,** *188,* 7101–7110. doi:10.1128/jb.00807-06
32. Chang, W.; Small, D. A.; Toghrol, F.; Bentley, W. E. *BMC Genomics* **2005,** *6,* 115. doi:10.1186/1471-2164-6-115
33. Stefanopoulou, M.; Kokoschka, M.; Sheldrick, W. S.; Wolters, D. A. *Proteomics* **2011,** *11,* 4174–4188. doi:10.1002/pmic.201100203
34. Kwan, B. W.; Chowdhury, N.; Wood, T. K. *Environ. Microbiol.* **2015,** *17,* 4406–4414. doi:10.1111/1462-2920.12873
35. Wu, W.; Jin, S. *J. Bacteriol.* **2005,** *187,* 6058–6068. doi:10.1128/jb.187.17.6058-6068.2005
36. Hauser, A. R. *Nat. Rev. Microbiol.* **2009,** *7,* 654–665. doi:10.1038/nrmicro2199
37. Coburn, B.; Sekirov, I.; Finlay, B. B. *Clin. Microbiol. Rev.* **2007,** *20,* 535–549. doi:10.1128/cmr.00013-07

38. Finck-Barbançon, V.; Goranson, J.; Zhu, L.; Sawa, T.; Wiener-Kronish, J. P.; Fleiszig, S. M. J.; Wu, C.; Mende-Mueller, L.; Frank, D. W. *Mol. Microbiol.* **1997,** *25,* 547–557. doi:10.1046/j.1365-2958.1997.4891851.x
39. Poole, K. *Trends Microbiol.* **2012,** *20,* 227–234. doi:10.1016/j.tim.2012.02.004
40. Stewart, P. S.; Franklin, M. J.; Williamson, K. S.; Folsom, J. P.; Boegli, L.; James, G. A. *Antimicrob. Agents Chemother.* **2015,** *59,* 3838–3847. doi:10.1128/aac.00433-15
41. Boles, B. R.; Thoendel, M.; Singh, P. K. *Proc. Natl. Acad. Sci. U. S. A.* **2004,** *101,* 16630–16635. doi:10.1073/pnas.0407460101
42. Chiang, W.-C.; Nilsson, M.; Jensen, P. Ø.; Høiby, N.; Nielsen, T. E.; Givskov, M.; Tolker-Nielsen, T. *Antimicrob. Agents Chemother.* **2013,** *57,* 2352–2361. doi:10.1128/aac.00001-13
43. Zolfaghar, I.; Evans, D. J.; Ronaghi, R.; Fleiszig, S. M. J. *Infect. Immun.* **2006,** *74,* 3880–3889. doi:10.1128/iai.01891-05
44. Kaneko, Y.; Thoendel, M.; Olakanmi, O.; Britigan, B. E.; Singh, P. K. *J. Clin. Invest.* **2007,** *117,* 877–888. doi:10.1172/jci30783
45. Harbut, M. B.; Vilchèze, C.; Luo, X.; Hensler, M. E.; Guo, H.; Yang, B.; Chatterjee, A. K.; Nizet, V.; Jacobs, W. R., Jr.; Schultz, P. G.; Wang, F. *Proc. Natl. Acad. Sci. U. S. A.* **2015,** *112,* 4453–4458. doi:10.1073/pnas.1504022112
46. Yu, S.; Su, T.; Wu, H.; Liu, S.; Wang, D.; Zhao, T.; Jin, Z.; Du, W.; Zhu, M.-J.; Chua, S. L.; Yang, L.; Zhu, D.; Gu, L.; Ma, L. Z. *Cell Res.* **2015,** *25,* 1352–1367. doi:10.1038/cr.2015.129

License and Terms